MORPHOTECTONICS OF PASSIVE CONTINENTAL MARGINS: APPLICATION TO SOUTH-WESTERN AFRICA.

Thesis submitted in accordance with the requirements of the University of Liverpool for the degree of Doctor in Philosophy by Alan Robert Gilchrist.

July 1991

I declare that the work contained in this thesis and its appendices was done by me, the undersigned, and it has not been offered for any other degree.

24 July 1991

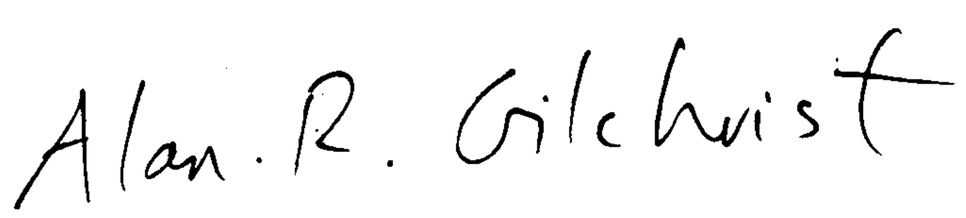

Alan Robert Gilchrist

ABSTRACT

A typical feature of mature (>60 Ma BP) high-elevation passive margins, such as south-western Africa, is a marginal topographic upwarp located parallel to, but generally 100 km or more inland of, the rift hinge. Marginal upwarps typically have a wavelength of 50-300 km and an amplitude of 300-900 m with respect to the continental interior. Such features cannot be adequately explained by dynamic models of rifting since their effects are localised to the rifted region. Magmatic underplating models, due to mantle plumes, are also incapable of accounting for marginal upwarps since the predicted domal uplifts have a diameter of 2000 km or more.

It is postulated that the link between onshore denudation, offshore sedimentation and isostasy is critical in determining the geomorphological evolution of passive margins and the origin of marginal topographic upwarps. A quantitative model, applicable to the south-west African rifted margin, has been formulated from a conceptual model of landform development.

The modelled results indicate that the isostatic effect of offshore sedimentation is only important in influencing the geomorphological evolution of rifted margins early on in their history. It is shown that the contrast in denudation rates between the evolving coastal flanks of rifted margins and their interior hinterlands is the major factor controlling the formation and evolution of

marginal topographic upwarps on mature rifted margins, if the lithosphere responds flexurally.

The generation of marginal upwarps as a result of differential denudational unloading not only explains their presence along mature rifted margins but also has important geomorphological and sedimentological implications. The presence of marginal upwarps up to 100 Ma or more after rifting may account for the deflection of drainage systems away from many rifted margins. The persistence of such a barrier to sediment transport across high-elevation rifted margins suggests that patterns of offshore deposition are likely to be controlled by a dual drainage system, comprising numerous small aggressively eroding coastal catchments and widely spaced outlets of large basins draining continental interiors well into the mature rifted margin phase. Moreover, the predicted inland migration of the axes of marginal upwarps in response to escarpment retreat are incompatible with existing cyclical denudation and surface uplift chronologies for the Gondwana continents.

Application of the model to south-west Africa has enabled the syn-break up palaeotopography of this region of Gondwana to be calibrated, which is otherwise unknown due to post-rift denudation. It is postulated that the origin of this landsurface was principally controlled by the isostatic response to magmatic crustal underplating by a mantle plume. Syn-rift drainage was probably essentially radial in nature, directed away from the dome centre.

The learned judge correctly that people of all ages have believed they *know* what is good and evil, praise- and blameworthy. But it is a prejudice of the learned that *we now know better* than any other age.

Friedrich Nietzsche.

CONTENTS AT A GLANCE

COMPREHENSIVE CONTENTS

LIST OF FIGURES

ACKNOWLEDGEMENTS

The pursuit of research during the last three years would have been much more difficult, and far less enjoyable, were it not for the following who I thank.

The Natural Environment Research Council for a PhD studentship.

My supervisors. Nick Kusznir in Liverpool whose perceptive observations have improved this thesis. Mike Summerfield in Edinburgh who has guided me down the 'rocky valley' of geomorphology, shown me its potential and acted as a user friendly encyclopedia of earth science literature. In particular I thank them for letting me find my own direction.

Keith Cox, Mike De Wit, Chris Hartnady, Harold Reading and John Ward for enlightening discussions.

The geodynamic modelling group at Liverpool, in particular Paul Caban, for helping with the maths and computing.

The postgrads in the Geography Department at Edinburgh for accepting a refugee and tolerating a geologist in their midst. I especially thank Neil Glasser for Strasbourg, Rik Kohnhorst for unravelling wordperfect, Jane Boygle for proof reading what follows and Loretta Lees for putting it into perspective.

Mum who never questions what I do but offers her wholehearted support.

1 INTRODUCTION

1.1 Research Aim

The research aim of this study is to explain the morphotectonic formation and evolution of the macroscale geomorphological features of mature passive margins.

1.2 Specific Objectives

The specific objectives are to; (1) derive a quantitative morphotectonic model of passive margin evolution, with particular emphasis upon how the sub-aerial denudational system develops in response to rifting; (2) apply the model to explain the evolution of the coupled onshore denudation/offshore sedimentation of passive margins; and (3) identify and quantify key mechanisms which control the development of topography on passive margins.

In this study the term denudation, as opposed to erosion, has been employed to define the general lowering of a landsurface and usually consists of the processes of weathering, transportation and erosion (Whitten and Brooks, 1972).

1.3 Research Background

1.3.1 Passive Margins

1.3.1.1 Definition

In plate tectonic theory there are three basic types of continental plate margins, which coincide with the ocean/crust boundary (Bally et al., 1981): (1) Active

margins, such as western South America, which are associated with intensive earthquake activity and are located where two tectonic plates are often in a convergent configuration; (2) extensional rifted margins, such as south-western Africa, eastern South America, eastern Australia, western India and the Red Sea Region where two tectonic plates are, or have been, in a divergent configuration; and (3) sheared margins, for example south-eastern Africa, where tectonic deformation is characterized by strike-slip plate motions.

Extensional and sheared margins can also be termed passive. This is because at present such margins generally show negligible seismic and volcanic activity. A passive margin is initially formed as an intra-plate region of structural weakness, due to a tensional stress field, which often exploits existing regions of crustal weakness. Penetrative tectonic deformation, often in the form of lithospheric extension, usually accompanies this initial phase. Subsequently, when plate divergence has ceased or has been accommodated by continental drift, tectonic deformation is dominated by vertical, or epeirogenic, plate motions in response to lithospheric loading events. Passive margins of the world are shown in Fig. 1.1.

1.3.1.2 Rifted Margin Features

In this case lithospheric extension by rifting causes thinning of the lithosphere which is accommodated by major normal faults in the upper crust. Crustal cross-sections of

several rifted margins are shown in Fig. 1.2. Three principal features are apparent. First, the stratigraphically oldest sediments, termed syn-rift sediments since they are deposited during rifting of the lithosphere, are located within fault-bounded sedimentary basins. These fault-bounded basins can be either half-graben, for example the Jeanne D'Arc basin (Fig. 1.2c), or full graben such as the Viking Graben (Fig. 1.2a). Secondly, above the syn-rift sediments there are younger and more uniform deposits, which often extend beyond syn-rift basins onto adjacent regions that have not undergone rifting. Thirdly, the Moho topography, imaged by seismic refraction or reconstructed from gravity data, is often shallower directly below the rift due to lithospheric thinning (Fig. 1.2a).

1.3.1.3 Sheared Margin Features

Crustal thinning does not usually take place on sheared margins and tectonic plate boundaries are strike-slip in nature. A typical example is the south-east African margin, where an oceanic spreading ridge was originally formed perpendicular to the present coastline in the Natal Valley. During the fragmentation of Gondwana (section 2.2.3.3) this spreading ridge migrated to the south-west into the region of the South Atlantic Ocean. Therefore, new oceanic crust was formed adjacent to a continental fragment which had not undergone extension, but was bounded to the south-east by a dextral shear zone. Two principal features

are shown on a profile across the margin (Fig. 1.3). First, the oceanic crust is thinner with comparison to the adjacent unextended continental crust. Secondly, the syn-rift fault-bounded phase of sedimentation, usually recognisable on rifted margins, is absent. Sedimentation is dominated by depositional cones adjacent to the continental margin due to alluvial systems, such as the Tugela River in Natal, South Africa, draining the continental landmass.

1.3.1.4 Geodynamic Models of Evolution

Many ideas concerning the nature of passive margins predate the general acceptance of plate tectonic theory in the early 1970s. For example Du Toit (1937) proposed that passive margins were the periphery edges of continents that had rifted and drifted apart. With the advent of plate tectonic theory, and the acquisition of more reliable data concerning crustal structure, it has become accepted that rifted regions have experienced lithospheric thinning as a result of extension.

A variety of geophysical models have been proposed to account for lithospheric thinning and the subsidence characteristics of rifted margin sedimentary basins. Perhaps the most influential of these has been the pure shear model of lithospheric stretching put forward by McKenzie (1978). This proposes that rapid stretching of the lithosphere causes thinning and upwelling of relatively hot asthenosphere (Fig 1.4). This phase is accompanied by normal faulting and subsidence. The lithosphere

subsequently thickens as the thermal perturbation re-equilibrates which causes further subsidence according to an exponential decay function (Fig. 1.5).

However, it has become apparent from improved seismic remote sensing techniques that extension on many rifted margins has occurred along low angle detachment zones (Wernicke, 1981). This realisation has led to the development of the simple shear end-member model (Fig. 1.6) of lithospheric extension (Wernicke, 1985), and a series of hybrid models which envisage that lithospheric extension is accommodated by simple shear in the upper crust and pure shear in the lower crust and underlying lithospheric mantle (Lister et al., 1986; Kusznir et al., 1987; Kusznir et al., 1990) [Fig. 1.7].

Such models can account for the principal characteristics of rifted margin sedimentary basins and lithospheric structural architecture. They also indicate the importance of mechanisms such as crustal thinning, magmatic underplating, thermal perturbations, lithospheric flexure and sediment loading in the formation and evolution of passive margins.

1.3.2 Macroscale Geomorphology of Passive Margins

1.3.2.1 Classification

Although the geomorphology of passive continental margins is highly variable, two main types can be identified: (1) Low-lying margins, such as southern Australia (Fig. 1.8), which rise gradually from the coast

to a low interior plain (low-elevation rifted margins); and (2) steeply rising margins in which the coastal plain is usually separated from the continental interior by a single major erosional escarpment (or in some cases multiple escarpments) which has probably retreated inland from the rift hinge (high-elevation rifted margins). Examples include such margins as south-western Africa (Fig. 1.9), eastern Australia (Fig. 1.10), eastern South America, western India and the Red Sea region. This study is concerned with high-elevation rifted margins.

1.3.2.2 Morphological Features

The morphology of high-elevation rifted margins can be thought to consist of several components, at different topographic wavelength scales or resolutions. In the case of the topography of south-western Africa (Fig. 1.11), it can be represented by an elevated plateau of regional extent at long wavelengths, inland of the coastal zone. Superimposed upon this landsurface is the gradual decline in mean elevation inland of the topographic discontinuity which is delineated by an erosional escarpment, or series of escarpments (Fig. 1.12). This gives rise to a rim of high terrain, or marginal topographic upwarp, typically 300-900 m high with respect to the continental interior and 50-300 km wide. The highest elevation of this feature usually coincides with the Great Escarpment, which is defined, for modelling purposes, as the most landward escarpment at the highest elevation, where more than one

exists. The Great Escarpment generally defines the drainage divide, which separates the coastal drainage from the adjacent interior drainage. The landsurface of high-elevation rifted margins therefore consists of two terrain types, the coastal and interior catchments, which are separated from each other by an erosional escarpment (Ollier and Marker, 1985).

In addition, a drainage network is incised into the landsurface giving it an irregular form. The drainage network which has incised the topographic profile in Fig. 1.13 can be characterised by the number of first magnitude streams draining through each point on the profile (Shreve, 1966). The horizontal wavelength of fluvial incision is highly variable and depends, probably to some degree, upon stream magnitude and drainage density. In Fig. 1.13 it is only a few kilometres in lateral extent to each drainage point on the profile, but the incision of the lower Orange and Fish Rivers, which have much higher stream magnitudes, forms a depression in the south-west African landscape with a scale of 10^{3} km (chapter 4).

Some high-elevation rifted margins, such as eastern Australia, show a slightly different morphology (Fig. 1.10). Whilst this area can still be thought to consist of two terrains, separated by an erosional escarpment, the drainage divide does not coincide with the escarpment as is generally the case in south-west Africa. Instead, the region landward of the escarpment is slightly domed, so that the drainage divide is generally located some distance

inland of the escarpment (Fig. 1.10).

1.3.2.3 Geomorphological Models of Evolution

The landscape of high-elevation rifted margins consists of a series of horizontal surfaces arranged stepwise, descending in elevation from the continental interior to the coastline, and separated by erosional escarpments. The most recent synthesis of the landscape evolution of southern Africa explains this observation in terms of periodic or 'cyclic' surface uplift of the continental margin (Partridge and Maud, 1987, 1988). In these studies it is assumed that each horizontal surface was formed at sea level by retreat of an erosional escarpment, that is, by pediplanation. The difference in elevation between two adjacent surfaces would therefore represent the amount of relative surface uplift that had occurred between the formation of these two surfaces.

1.3.3 Morphotectonics - A Key Research Theme

The study area for this thesis is south-western Africa, which is a mature (>60 Ma BP) rifted continental margin with an age of formation of ≈150 Ma BP (Gerrard and Smith, 1980). This margin has been chosen because of the wealth of literature concerning the region and its position at the centre of the break up of Gondwana. Cyclical theories of landscape evolution, which envisage periodic surface uplift throughout the development of the margin, were originally applied to this region by L.C. King and

most recently by Partridge and Maud (1987, 1988). However, such schemes appear to be incompatible with current geodynamic theory which, for passive margins at least, suggests that maximum active tectonic uplift generated by magmatic underplating, thermal perturbations or mechanical unloading linked to extension involve a single major event associated with continental rupture (Summerfield, 1988, 1989; Weissel and Karner, 1989; White and McKenzie, 1989; Steckler, 1990). Therefore, it is timely to reconcile the differences between geodynamic and geomorphological frameworks of passive margin evolution.

1.4 Thesis Organisation

A brief geological history of southern Africa is presented in chapter 2, with an emphasis upon the time since the break up of Gondwana. This provides a geological framework within which to consider models of passive margin evolution. A literature review of recent quantitative models of passive margin evolution is presented in chapter 3, in which the key mechanisms that have influenced the morphological evolution of such regions are identified, and an integrated conceptual morphotectonic model is developed. Field observations from southern Africa are discussed in chapter 4 and a conceptual denudational model, applicable to high-elevation passive margins, is formulated with reference to the dynamics of contemporary denudational systems. The theory of isostasy is outlined in chapter 5 and a numerical model, applicable to the macroscale

landform evolution of passive margins, is presented. The components of the quantitative morphotectonic model of passive margin evolution are integrated in chapter 6 and applied to a single profile across the south-west African rifted margin in order to explore the properties of the model. In chapter 7 the model is more generally applied to ten topographic profiles across the south-west African rifted margin. This is in order to suggest how the drainage of the margin might have evolved since before the fragmentation of Gondwana. Finally, in chapter 8, a synthesis of new knowledge reported in this thesis is presented, and the implications for passive margin evolution are discussed.

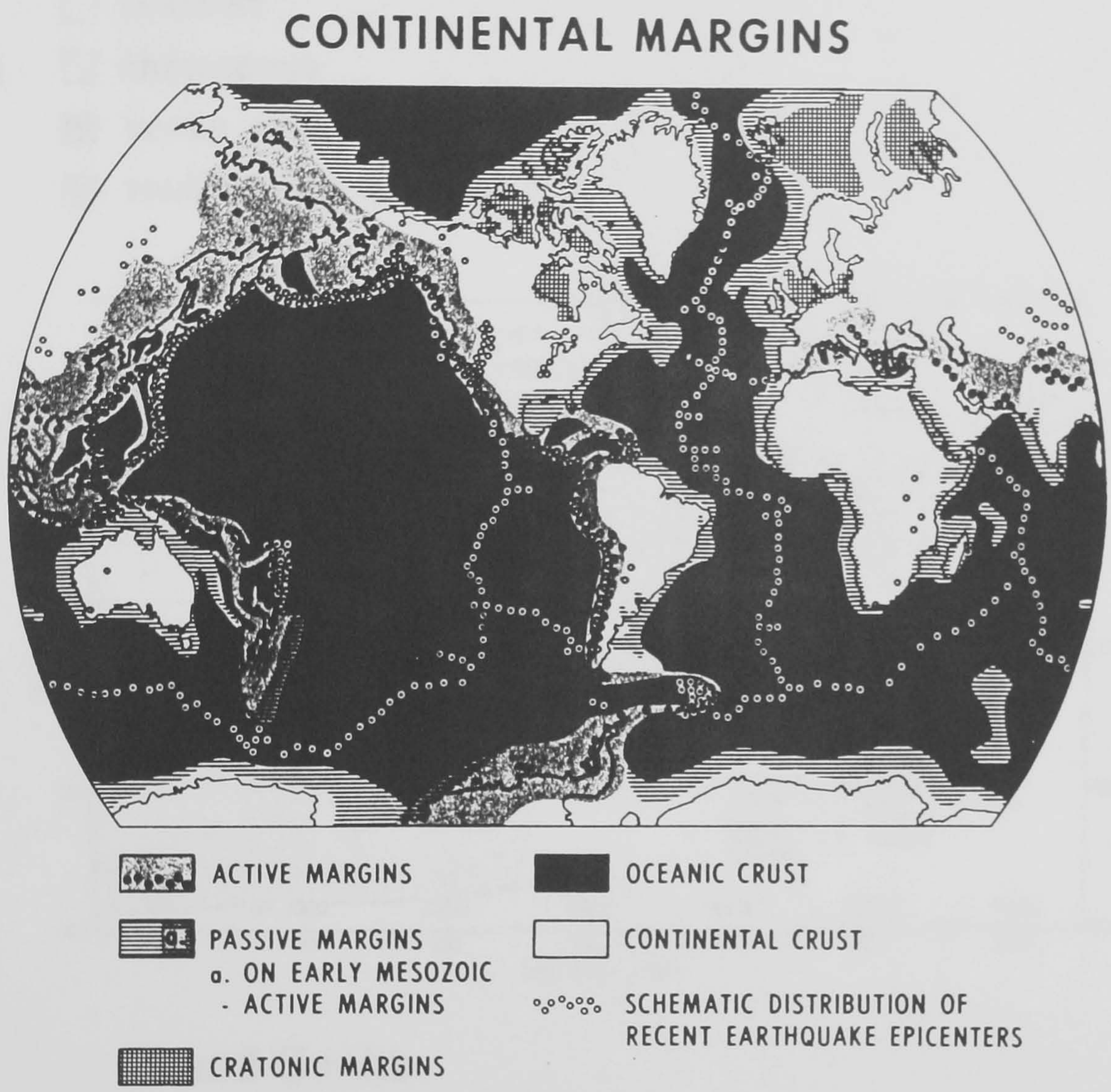

Fig. 1.1. Passive and active continental margins of the world, as determined from a variety of subsurface data (after Bally et al., 1981, Fig. 1.2).

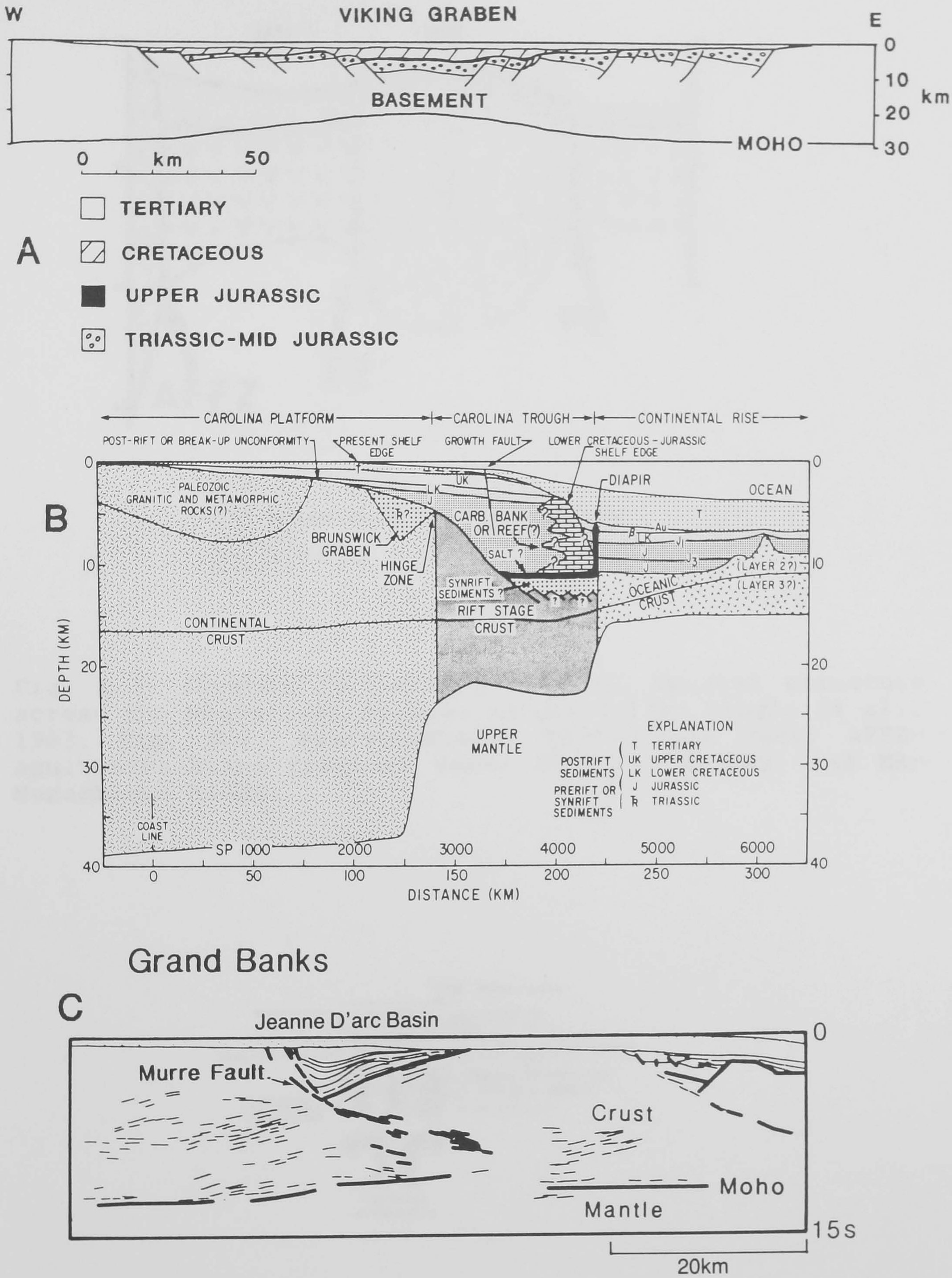

Fig. 1.2. Rifted continental margins: (a) Interpreted crustal profile across the Viking Graben in the northern North Sea (after Marsden et al., 1990, Fig. 12.2); (b) interpreted profile across the Carolina Trough (after Bally et al., 1981, Fig. 3.8); and (c) seismic profile across the Grand Banks (after Kusznir and Egan, 1989, Fig. 1).

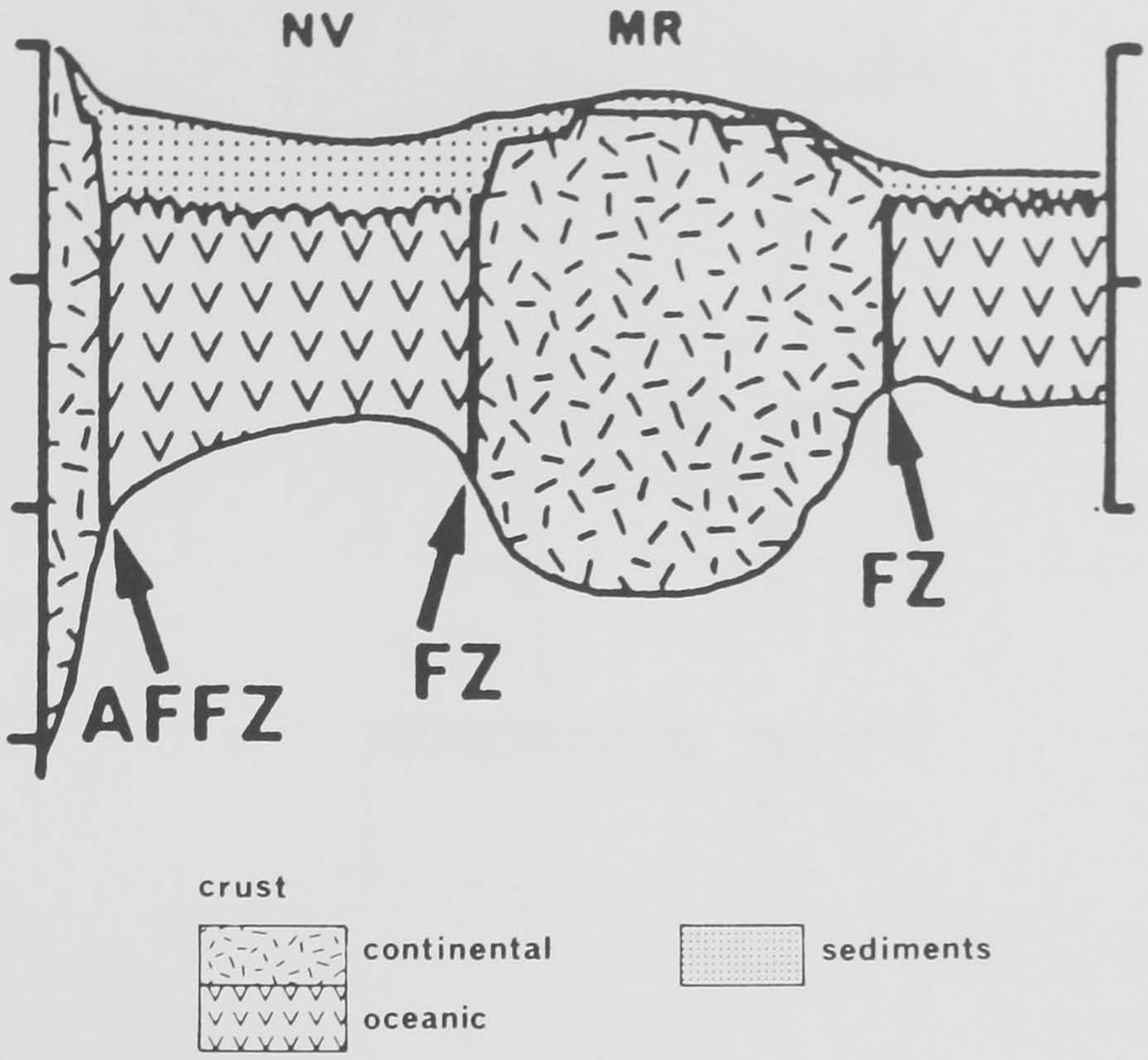

Fig. 1.3. Sheared continental margins. Crustal structure across the south-east African margin (after Dingle et al., 1983, Fig. 96). Abbreviations: FZ-fracture zone; AFFZ-Agulhas/Falkland fracture zone; NV-Natal Valley; and MR-Mozambique Ridge.

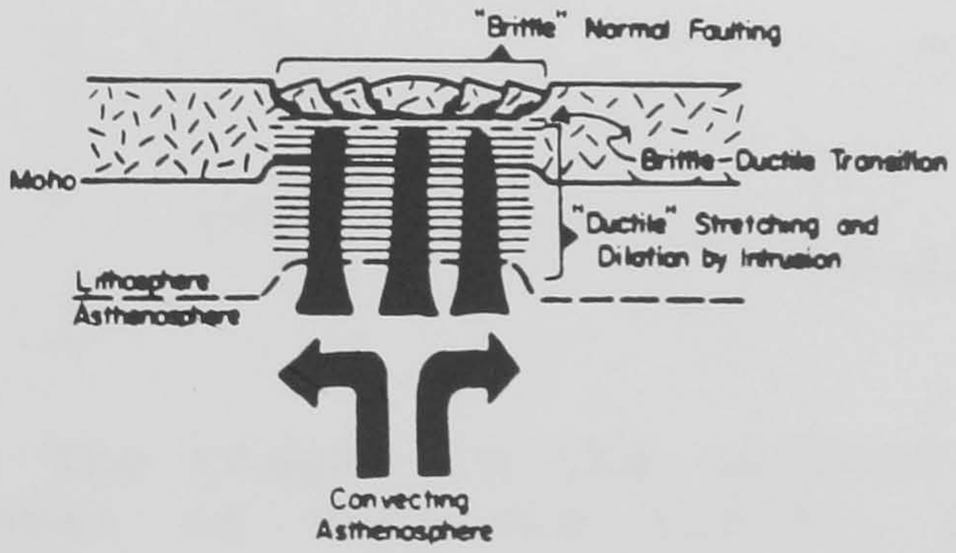

Fig. 1.4. Pure shear model of strain geometry in rifts, in which crust and mantle lithosphere are attenuated uniformly along any given vertical reference line (after Wernicke, 1985, Fig. 1).

A

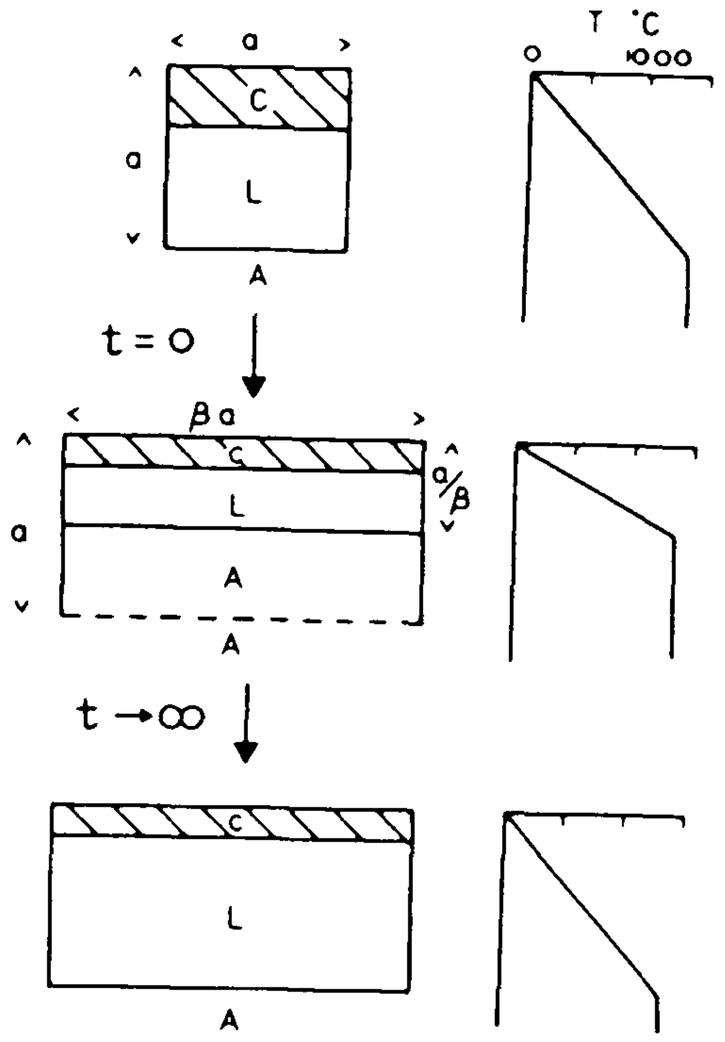

B

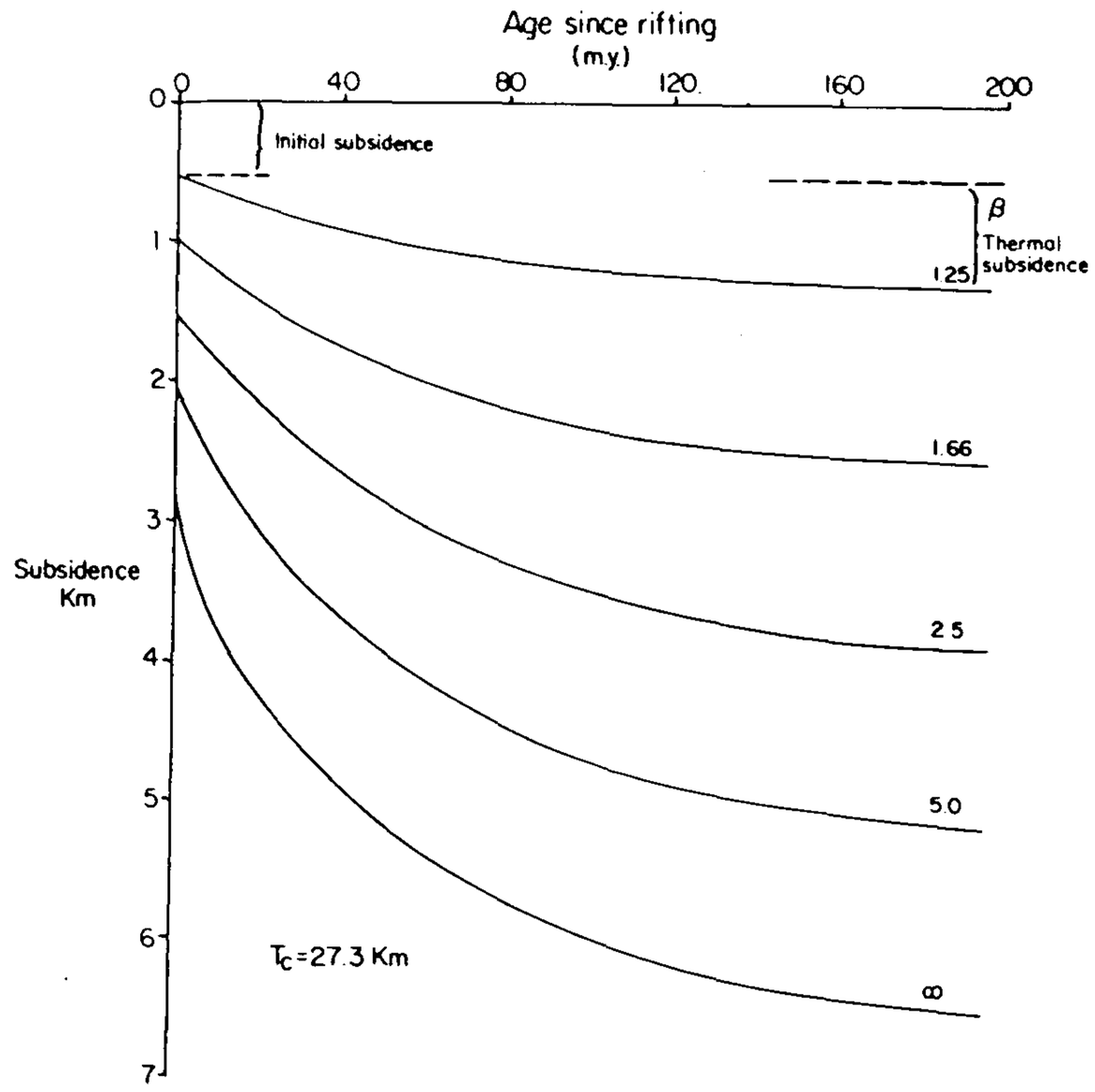

Fig. 1.5. (a) The stages in the uniform and instantaneous stretching model of McKenzie (1978). C is crust, L is lithosphere and A is asthenosphere. The lengths are unit dimensions. β is the amount of stretching. The crust and lithosphere are stretched, causing compression of the isotherms and passive heating of the lithosphere as shown in the schematic diagrams on the right.
(b) Subsidence curves calculated from the stretching model (after Bally et al., 1981, Fig. 2.16). Initial subsidence is the subsidence that occurs during rifting. T_c is the initial thickness of the crust.

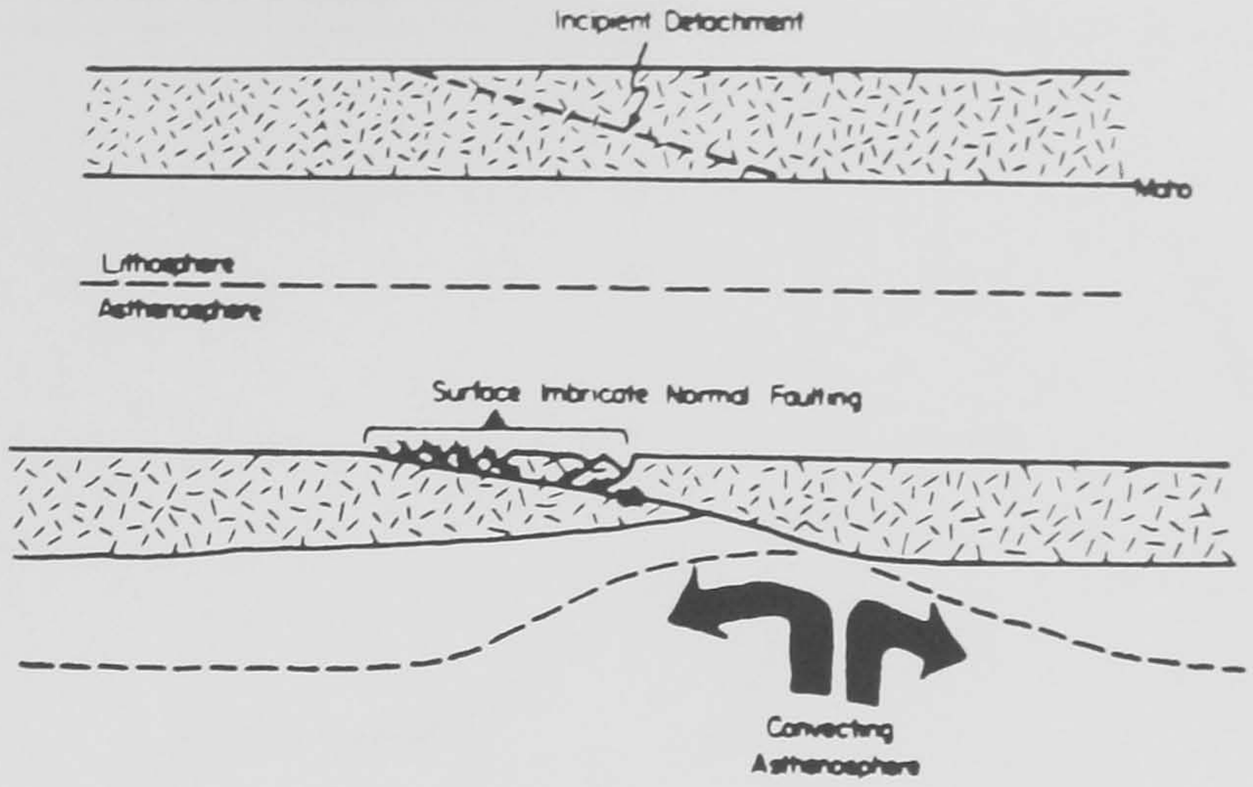

Fig. 1.6. Simple shear model of strain geometry in rifts, in which relative extension of crust and mantle lithosphere along any given vertical line is non-uniform (after Wernicke, 1985, Fig. 1).

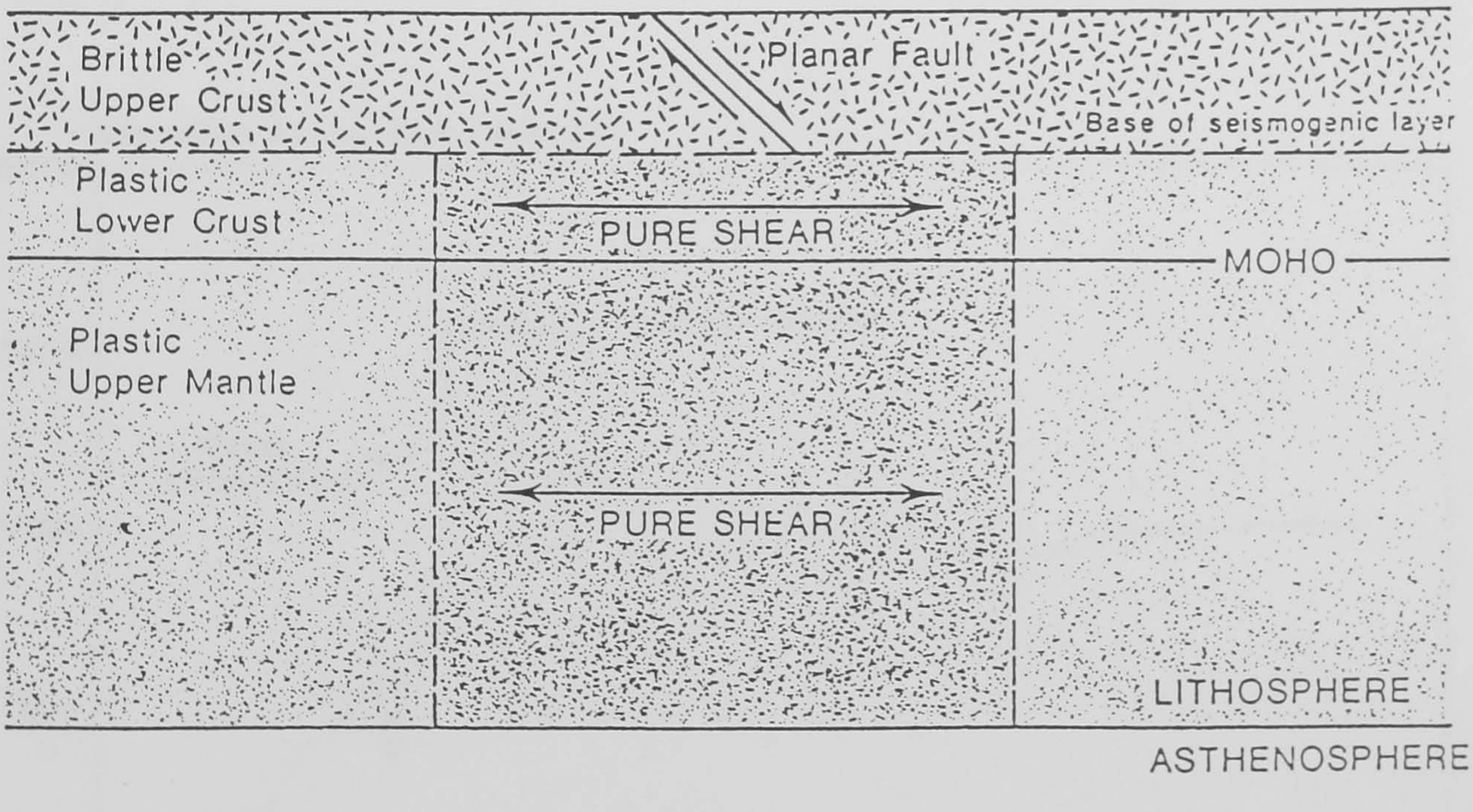

Fig. 1.7. A flexural cantilever simple shear/pure shear model of continental lithosphere extension (after Marsden et al., 1990, Fig. 12.5). Within the cool, brittle upper crust, lithosphere extension takes place by planar faulting (simple shear). Beneath the brittle/ductile transition, within the plastic lower crust and mantle, lithosphere extension takes place by distributed stretching (pure shear).

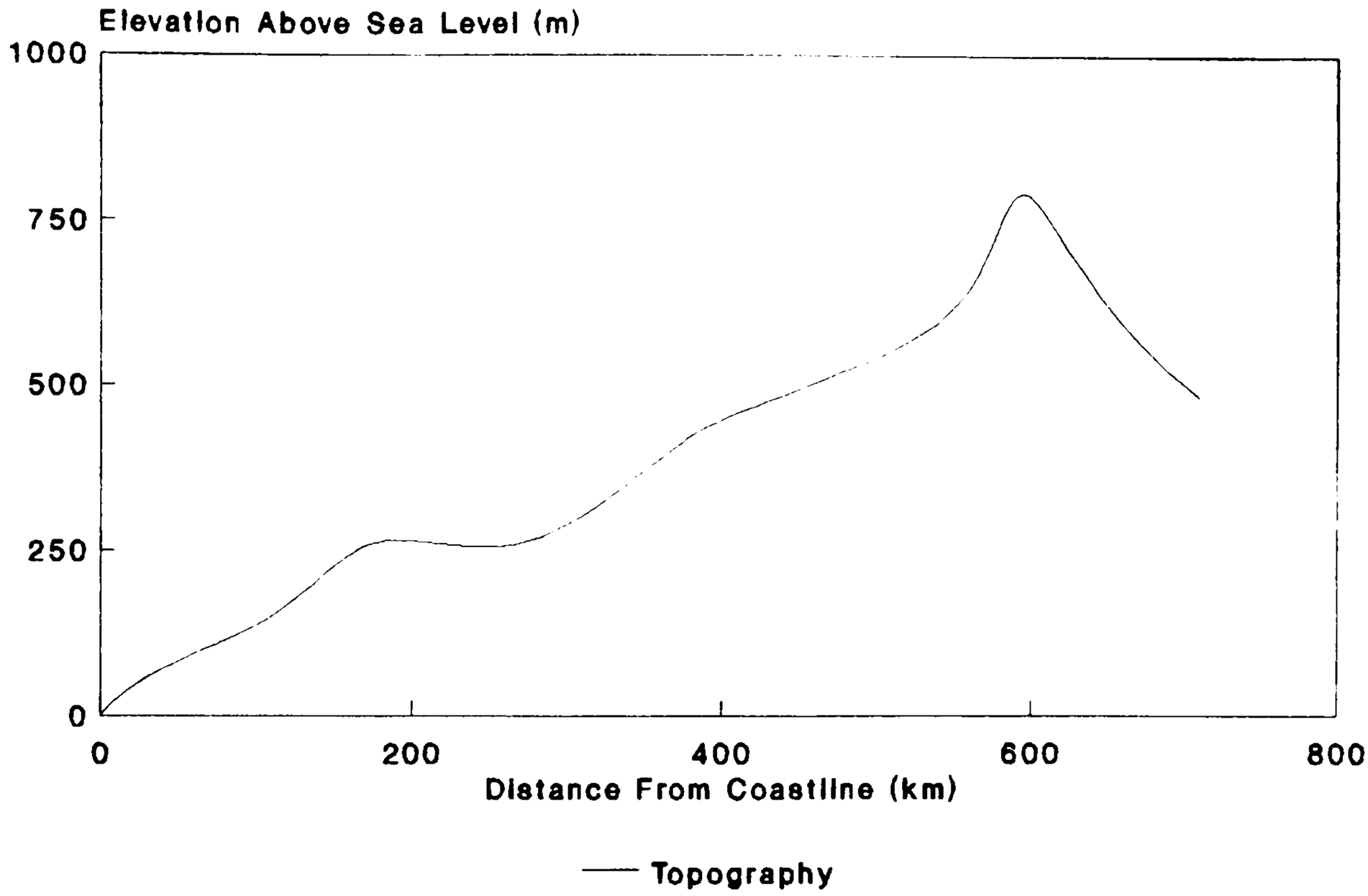

Fig. 1.8. Topographic profile across the south Australian rifted margin. Data from 1:1000000 operational navigation chart ONC Q-13, Aeronautical Information Section, Melbourne.

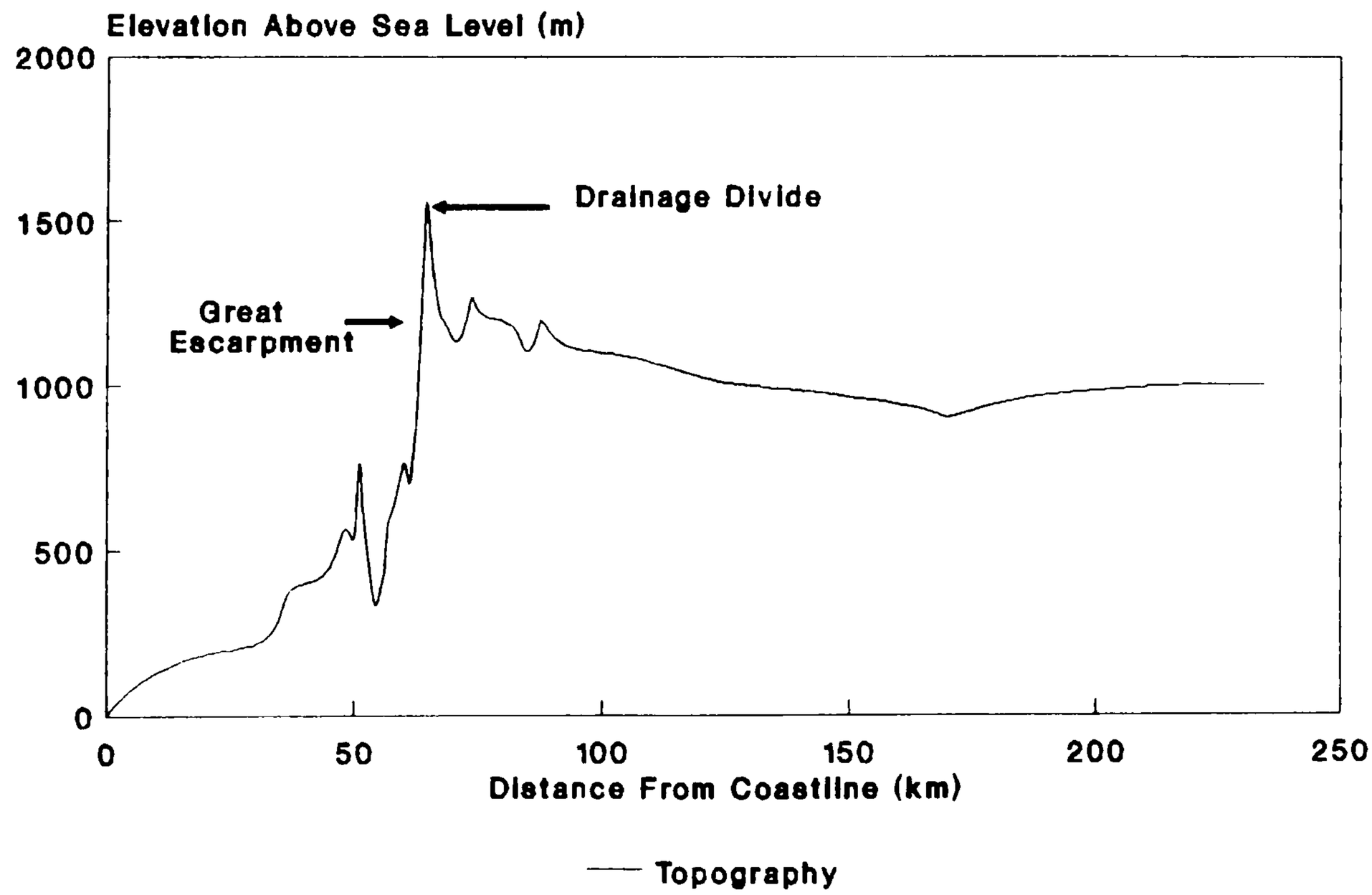

Fig. 1.9. Topographic profile across the south-west African rifted margin. Data from 1:500000 map of South Africa.

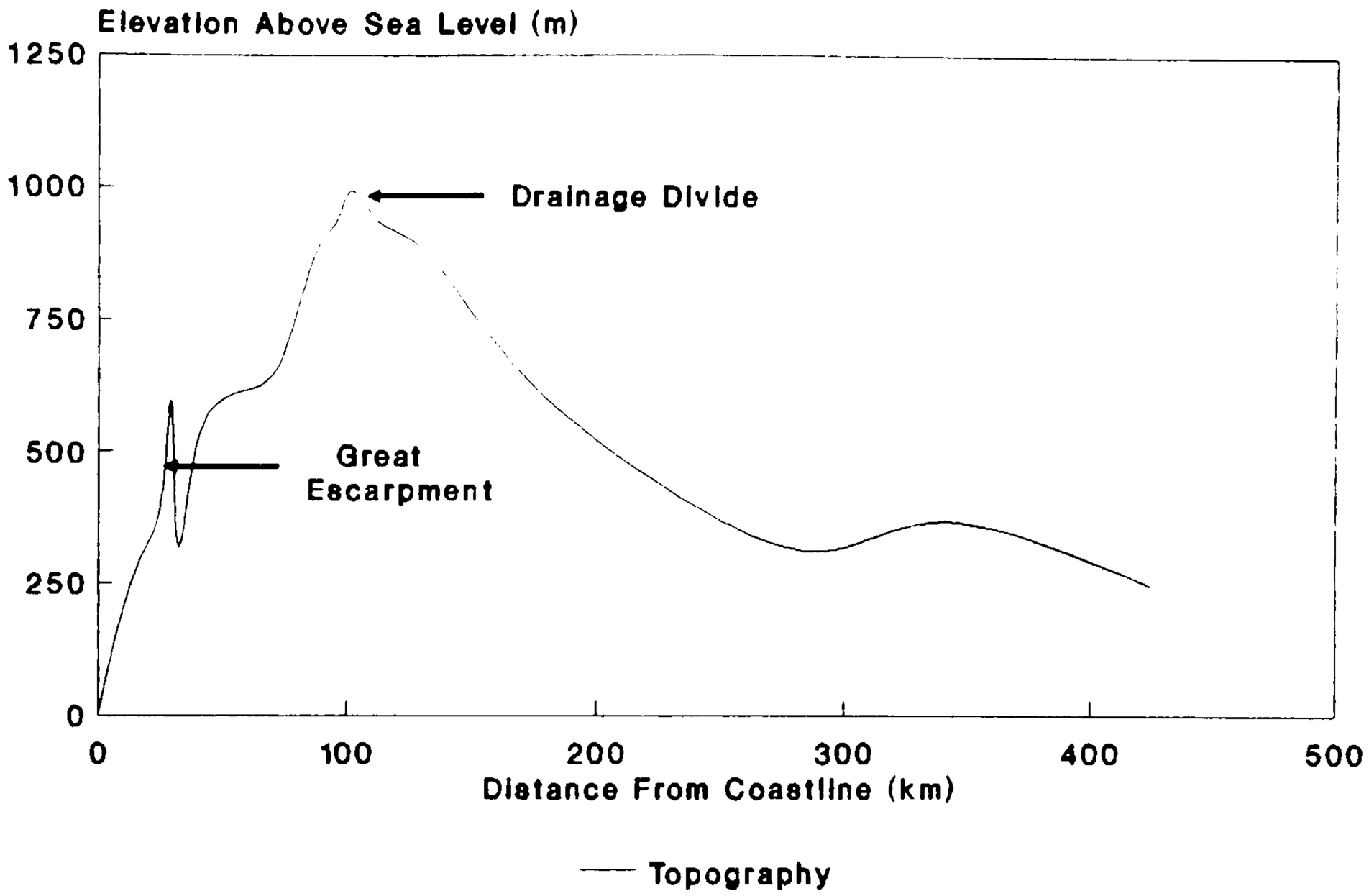

Fig. 1.10. Topographic profile across the east Australian rifted margin. Data from operational navigation chart R-13, scale 1:1000000, Aeronautical Information Section, Melbourne.

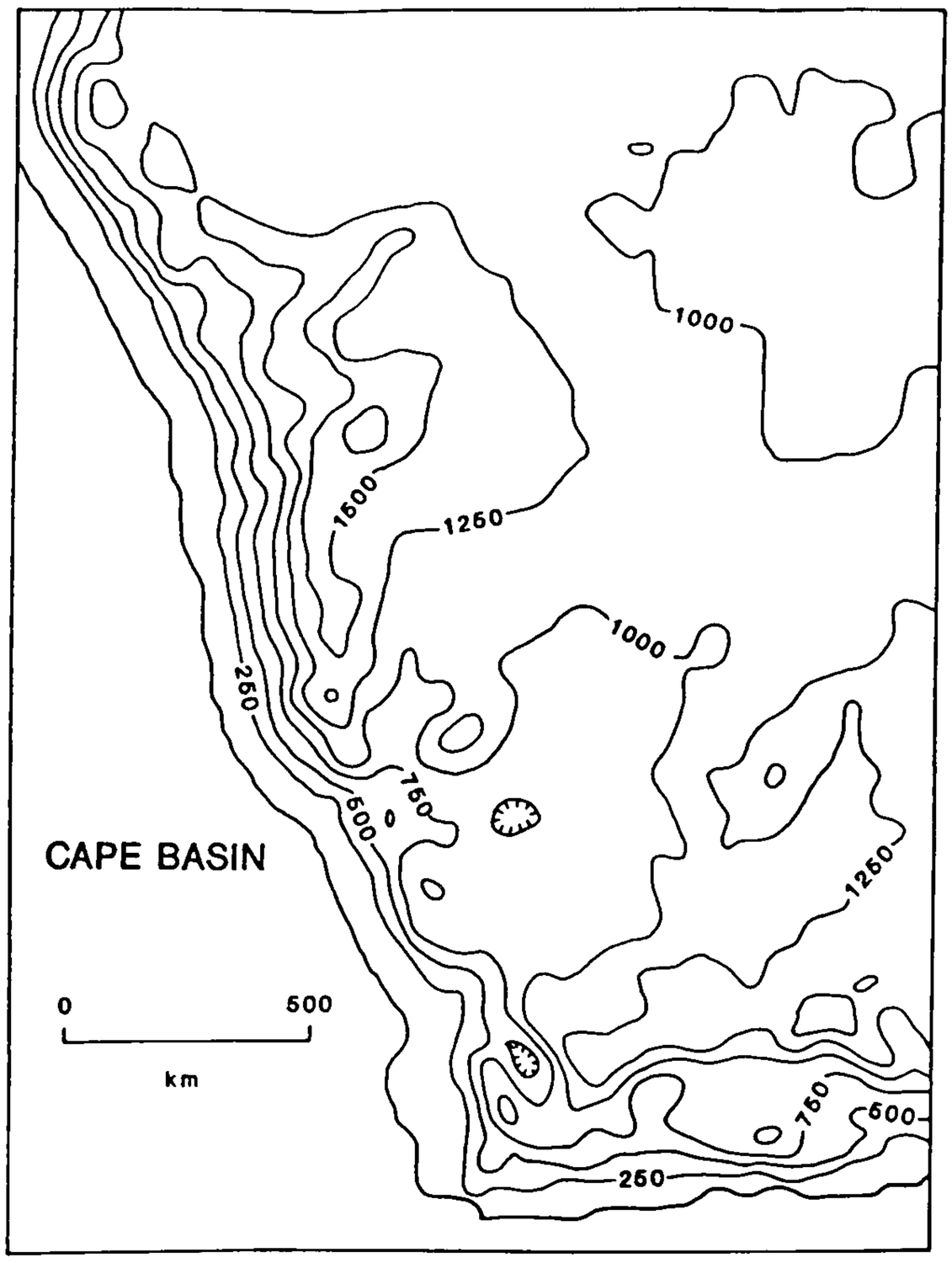

Fig. 1.11. Topography of south-western Africa. Data derived from the 10-min topographic data set from the National Geophysical Data Center, Boulder, Colorado, USA.

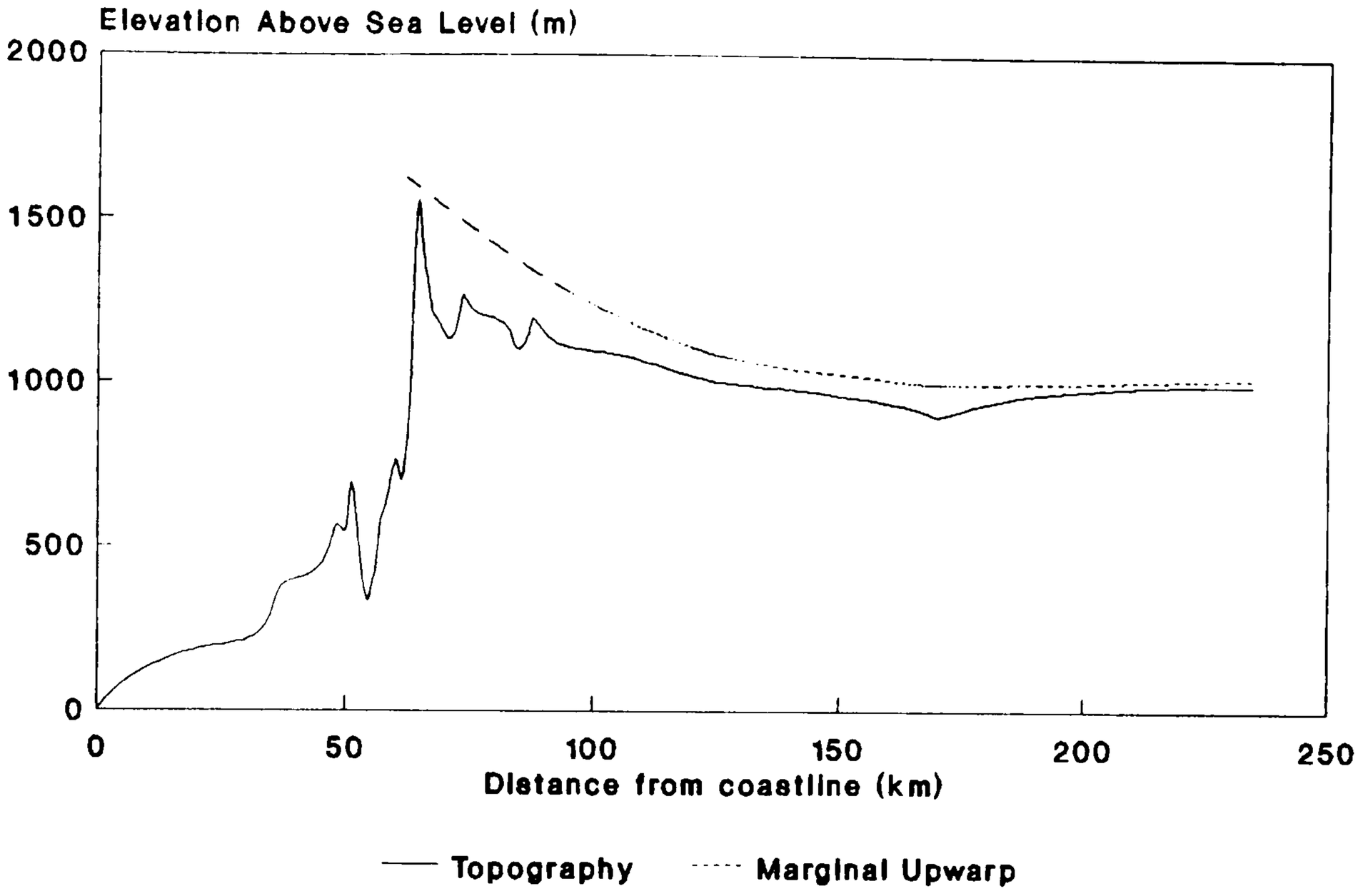

Fig. 1.12. Marginal topographic upwarp characteristic of high-elevation rifted margins, here shown on a topographic profile across the south-west African margin (Fig. 1.9).

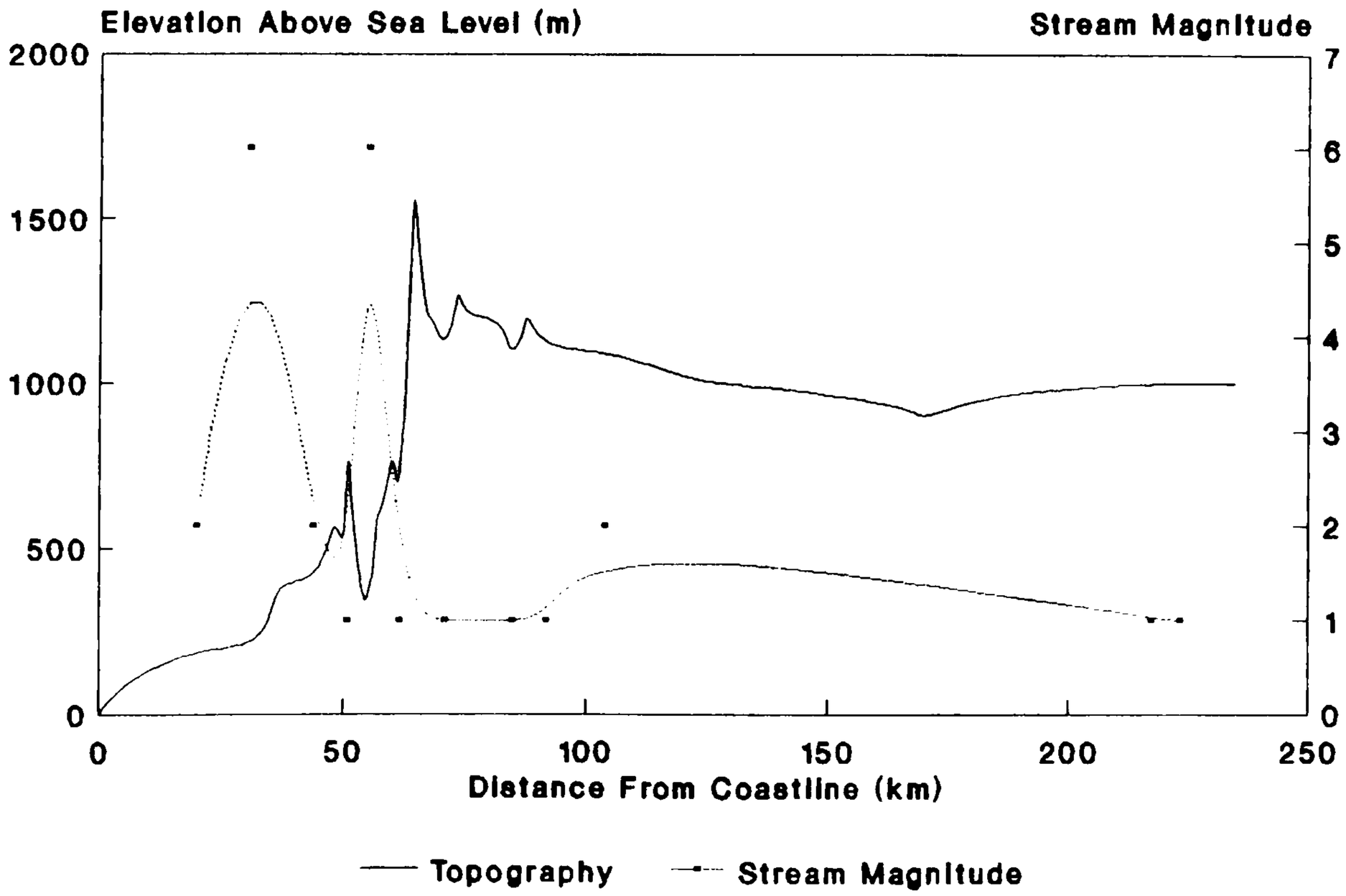

Fig. 1.13. Stream magnitude data for a topographic profile across the south-west African rifted margin (Fig. 1.9). Stream data from 1:500000 map of South Africa.

2 GEOLOGICAL FRAMEWORK OF SOUTHERN AFRICA

2.1 Introduction

The aim of this chapter is to review the geological history of southern Africa, which covers approximately 3.8 billion years, with particular emphasis on the period since the break up of the super-continent Gondwana. Such a task obviously draws heavily on existing syntheses, and the principle references by Tankard et al. (1982) and Dingle et al. (1983) are acknowledged here. A summary of the tectono-stratigraphy is presented in Fig. 2.1. The distribution of different types of lithology are then discussed as they are an important factor in controlling landform development (Hack, 1975, 1979) and drainage evolution (Deffontaine, 1991).

2.2 Geology

The geological framework of southern Africa will be considered as four phases: (1) Craton forming phase; (2) intra-cratonic deformation phase; (3) inter-cratonic deformation stage; and (4) epeirogenic deformation stage.

2.2.1 Craton Forming Phase (≈3800 - ≈500 Ma BP)

The centre of the southern African sub-continent consists of a craton composed entirely of Precambrian basement (Pretorius, 1979) and which is comprised of several Archean and Proterozoic terranes forming a stable

platform (Fig. 2.2). This craton was formed by the collision of island arcs (De Wit, 1986) and was part of the super-continent of Gondwana before its fragmentation during the Mesozoic. Later tectonic activity has been focused around the edge of the craton and although the craton itself has been largely undeformed, some zones of structural weakness have been reactivated during periods of intense tectonic activity.

2.2.2 Intra-Cratonic Deformation Phase (≈500 - ≈200 Ma BP)

This phase consists of three stages: (1) Cape Sedimentary Basin; (2) Karoo Sedimentary Basin; and (3) Cape Fold Belt.

2.2.2.1 Cape Sedimentary Basin

The Cape Sedimentary Basin was the product of sedimentary detritus filling an aborted Early Palaeozoic continental rift (Tankard and Hobday, 1979) and consists of the sediments of the Cape Supergroup (Fig. 2.3). The rift was reactivated several times during the Mesozoic fragmentation of Gondwana (Tankard et al. 1982).

2.2.2.2 Karoo Sedimentary Basin

This feature developed by post-Dwyka age subsidence to the north of the Cape Basin (Ryan, 1967). The Lower Permian to Jurassic succession (Fig. 2.4) was deposited during the migration of the super-continent Gondwana from polar to tropical latitudes (Creer, 1965).

The subsidence mechanism of such a large intracratonic basin, displaying little or no penecontemporaneous faulting, has remained an enigma (Bally and Snelson, 1980), and mechanisms which have been proposed include; (1) subcrustal erosion or asthenospheric deflation, (2) mantle phase changes, and (3) delay in the isostatic rebound associated with the melting of the Dwyka ice sheets. In later stages the basin was bounded to the south and southeast by elevated terrain, with surface uplift possibly related to activity in the Cape Fold Belt (Tankard et al., 1982). On the basis of faunal characteristics in the Karoo Basin and the contemporaneous Parana sedimentary basin in South America it has been postulated that the two basins were originally connected (Oelofsen, 1987).

2.2.2.3 Cape Fold Belt

Orogenic deformation affected deposits of the Cape Basin and adjacent regions of the Karoo Basin in three phases during the Permian and Triassic (Halbich et al., 1983). The principal shortening axes are now orientated north/south with subsidiary east/west shortening in the west and east (Fig. 2.3). These structural trends had an important controlling effect on rifted basin formation in this region during the break up of Africa and South America.

Du Toit (1937) first recognised that the Cape Fold Belt was part of a more extensive zone of deformation extending through much of Gondwana. However, the Cape Fold

Belt does not show features typical of a subduction generated orogen (Dingle et al., 1983). Reconstructions of Gondwana (Lawver et al., 1985) indicate that it was situated ≈1500 km from a convergent plate margin (Fig. 2.5). Lock (1980) has proposed that the Cape Fold Belt formed by flat slab subduction, whereas Dingle (1973) and Newton (1980) regard it as being the product of an intraplate orogeny. Halbich (1983) postulated that this could have occurred as a consequence of a short lived, rather small, mantle convection cell or plume.

2.2.3 Inter-Cratonic Deformation Phase (≈200 - ≈100 Ma BP)

2.2.3.1 Mechanism for Gondwana Fragmentation

W. Gondwana fragmentation occurred in two stages: (1) Between Africa and Antarctica; and (2) between Africa and South America at a later date. Cox (1978) has suggested that the opening of the South Atlantic was back-arc related to subduction along the western margin of the South American and west Antarctic plate margins. In contrast Dalziel et al. (1987) relate the fragmentation of Gondwana to a thermal effect, independent of plate margin geometry, which was initiated about 80 Ma prior to the commencement of seafloor spreading in the South Atlantic. In support of this idea Gurnis (1988) has predicted that the aggregation and dispersal of super-continents is periodic and related to large scale mantle convection, which was modelled using finite element techniques. It was proposed that continental crust insulates the mantle causing it to become hotter than

normal and to expand to give a geoid high. Subsequently, rifting occurs and the resulting super-continental fragments disperse towards geoid lows. Gurnis (1988) proposed that Gondwana was positioned over a geoid high prior to rifting during the Mesozoic. The production of large quantities of flood basalts, which are found on the south-western rifted and south-eastern sheared passive margins of southern Africa (Fig. 2.6), is predicted by a simple model of rifting above a thermal anomaly in the underlying mantle (White and McKenzie, 1989).

Although no comprehensive model of continental rifting exists, it is evident from the discussion above that the presence of a thermal anomaly in the mantle was probably an important component of the mechanism for Gondwana fragmentation.

2.2.3.2 Inter-plate Igneous Activity

The deposition of sediments in the Karoo basin was terminated by a violent episode of flood basalt volcanism, probably centred on Lesotho (Eales et. al., 1984). The first main phase started at ≈190 Ma BP with a second at ≈180 Ma BP (Fitch and Miller, 1984). These igneous episodes were related to the break up between east Gondwana [India, Australia and Antarctica] and west Gondwana [South America and Africa] (Scrutton, 1973). In north-western Namibia, spatially remote from the south-east African passive margin, intrusive igneous activity of the same age has also been recorded (Eales et al., 1984), as well as a later

phase of intrusive and extrusive igneous activity at about 120 Ma BP (Siedner and Mitchell, 1976). This later phase was probably related to rifting in the South Atlantic (White and McKenzie, 1989). Associated with the extrusion of the flood basalts were intrusive sill complexes, which were often emplaced between sedimentary horizons in the main Karoo basin (Eales et al., 1984). These igneous intrusions account for more than half the total thickness of the stratigraphic sequence in the centre of the Karoo basin (Winter and Venter, 1970).

2.2.3.3 Style of Gondwana Fragmentation

The style of Gondwana fragmentation is more complex than that originally proposed by Dietz and Holden (1970), who envisaged that separation between west and east Gondwana occurred as a result of extensional rifting. A more recent analysis (Lawver et al., 1985) indicates that separation of west and east Gondwana was along a transform fault which is now located along the eastern edge of the Mozambique Ridge (Fig. 2.7). Dating of the earliest known linear magnetic anomaly in the adjacent Mozambique Basin M22 (Simpson et al., 1979) indicates that sea floor spreading began 152 Ma BP according to the timescale of Larsen and Hilde (1975) or 142-3 Ma BP using that of Van Hinte (1976a, 1976b).

Opening of the South Atlantic was coincident with a sea floor spreading ridge in the Natal Valley, which was offset ≈1500 km along the Agulhas/Falkland Fracture Zone

(Fig. 2.7). This event has been dated by linear magnetic anomaly M12 (Larsen and Ladd, 1973) as 135 Ma BP or 127 Ma BP respectively using the time scales given above.

2.2.3.4 Syn-Fragmentation Sedimentation.

The complex tectonic style of Gondwana fragmentation is reflected in the different basin fill architecture at different sections of the emerging passive margin. In all areas extrusive volcanism accompanied, or occasionally excluded, sedimentation. Rifted basins on the south-west African margin were initiated ≈150 Ma BP (Gerrard and Smith, 1980). Crustal thinning was accommodated by normal faulting, which gave rise to a series of horst and graben approximately parallel to the present coastline. Sediment isopach maps show a great variation in thickness over these basement features (Fig. 2.8).

On the southern margin, basin formation was initiated 162 Ma BP (Hill, 1972). Extensional tectonics operated as a simple shearing couple that cut the Cape Fold Belt obliquely. Thus, sedimentary basins developed along pre-existing structural trends in the Cape Fold Belt as a series of half graben, later truncated by the Agulhas/Falkland Fracture Zone (Fig. 2.7).

The south-eastern margin is unusual in that it is defined by the Agulhas/Falkland fracture zone which defines the continental/oceanic lithosphere boundary. Therefore, it has oceanic crust to the south-east and is marked by a major bathymetric discontinuity. Sedimentary depocentres

are generally restricted to the area adjacent to the continental/oceanic lithosphere boundary and nearby oceanic crust. They have been formed by the outbuilding of sedimentary cones from rivers, such as the Tugela, draining the continental landmass.

2.2.4 Epeirogenic Deformation Phase (≈100 - 0 Ma BP)

2.2.4.1 Post Break up Dispersal of Gondwana Fragments

Syn-fragmentation faulting had ceased in the continental crust by 110-105 Ma BP (Kent, 1977). Dispersal of the Gondwana fragments continued in association with the production of new oceanic crust at spreading ridge sites in the South Atlantic, the Natal Valley and the Indian Ocean (Lawver et al., 1985). Thus, new oceanic sedimentary basins were created adjacent to the south-west African margin north of the Agulhas\Falkland Fracture Zone, while those next to the south-eastern margin were opened successively from the north-east to the south-west (Dingle and Scrutton, 1974).

The crustal evolution of southern Africa, therefore, entered its most recent phase with epeirogenic tectonic activity causing widespread intra-plate flexural deformation (Pretorius, 1979). This was in response to lithospheric loading events which influenced rifted sedimentary basin and continental landform evolution.

2.2.4.2 Post-Fragmentation Sedimentation.

Post-fragmentation sedimentation occurred in elongate

depocentres which prograded seawards beyond the boundaries of the previous syn-fragmentation basins (Fig. 2.9). Although borehole data for the south-western margin generally indicate decreasing rates of sedimentation during this period, the analysis of isopach data shows that the sediment mass accumulating offshore actually increased until the end of the Eocene (Rust and Summerfield, 1990). The decrease in sediment mass accumulating offshore since the mid-Tertiary (≈37 Ma BP) may be due to the development of an arid climate during this period (Ward et al., 1983).

2.2.4.3 Intra-plate Igneous Activity.

Continental mid-plate Cenozoic volcanism was concentrated in Pan-African basement areas (Fig. 2.2) and not in cratonic areas due to the absence of underlying fertile lithospheric mantle (Ashwal and Burke, 1989). In the cratonic interior of southern Africa regional plug shaped intrusions of kimberlite and alkaline magmas have shown three peaks of activity at ≈90, ≈65 and ≈35 Ma BP (Moore, 1976). Pretorius (1979) postulated that, on the basis of the analysis of the gravity field of southern Africa, there appears to be a close relationship between major crustal flexures and the distribution of magmatic intrusions.

2.3 Lithology Distribution

The present day surface geology can be characterised by two terranes (Fig. 2.10): (1) Horizontally bedded

sequences; and (2) crystalline basement.

2.3.1 Horizontally Bedded Sequences

Extensive areas are covered by flat-lying sediments of the Karoo depositional system, reflecting the stable tectonic conditions of accumulation. This sequence is intruded at various levels by igneous sill and dyke complexes associated with the fragmentation of Gondwana. These intrusive igneous complexes have a surface expression as flood basalts, which are presently seen around Lesotho and at Etendeka in north-western Namibia. However, these intrusives represent only a minor erosional remnant of a formerly much more widespread cover which may have extended over much of southern Africa (Cox, 1970, 1972).

Rift related deposits of the Cape Sedimentary Basin located on the Natal coast have been deformed into a monoclinal structure. Contemporaneous deposits in the Cape Province have been deformed by the Cape orogeny into a series of open folds whose axes are orientated perpendicular to the direction of crustal shortening (Fig. 2.3). Faulting in the Cape Fold Belt is characterized by a few major faults, with throws of up to ≈6000 m, which follow the fold trends (Dingle et al., 1983).

The Nama System of Late Proterozoic/Early Palaeozoic sediments, which outcrops extensively in southern Namibia, unconformably overlies Precambrian basement. The succession was deposited in a platform environment, and has been subsequently deformed by thrusting and folding in the

north-western and south-eastern fringes of the outcrop (Tankard et al., 1982).

2.3.2 Crystalline Basement

The Transvaal, central Namibia and western coastal fringe of South Africa are characterized by Precambrian crystalline basement. The structural features of these areas, encompassing over 3 billion years of geological history, are complex and consist of a variety of assembled terranes (Fig. 2.2). Discordant igneous bodies are important structural elements and post-Karoo age intrusive complexes are located in central Namibia.

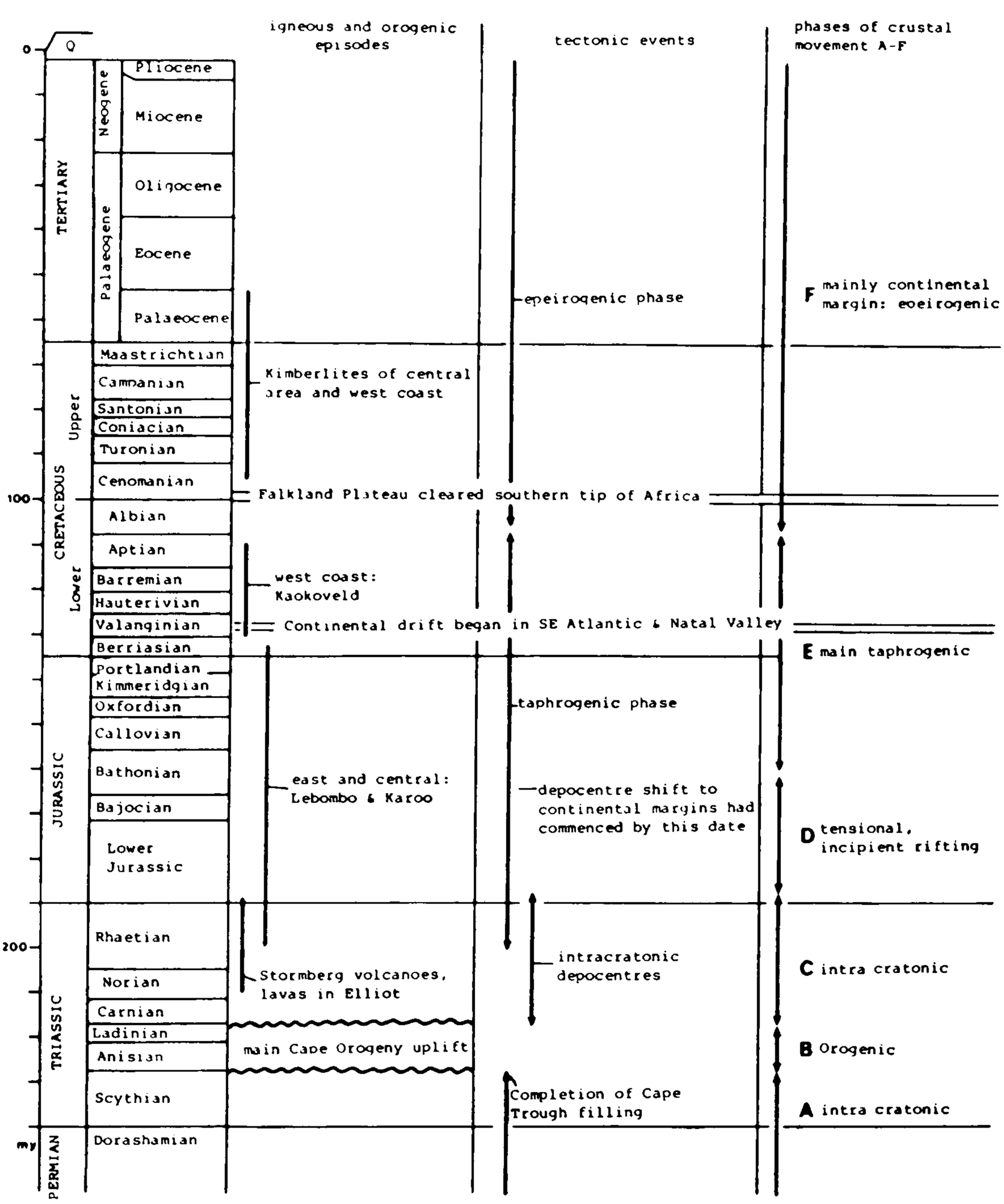

Fig. 2.1. Tectono-stratigraphy of southern Africa (after Dingle et al., 1983, Table 2).

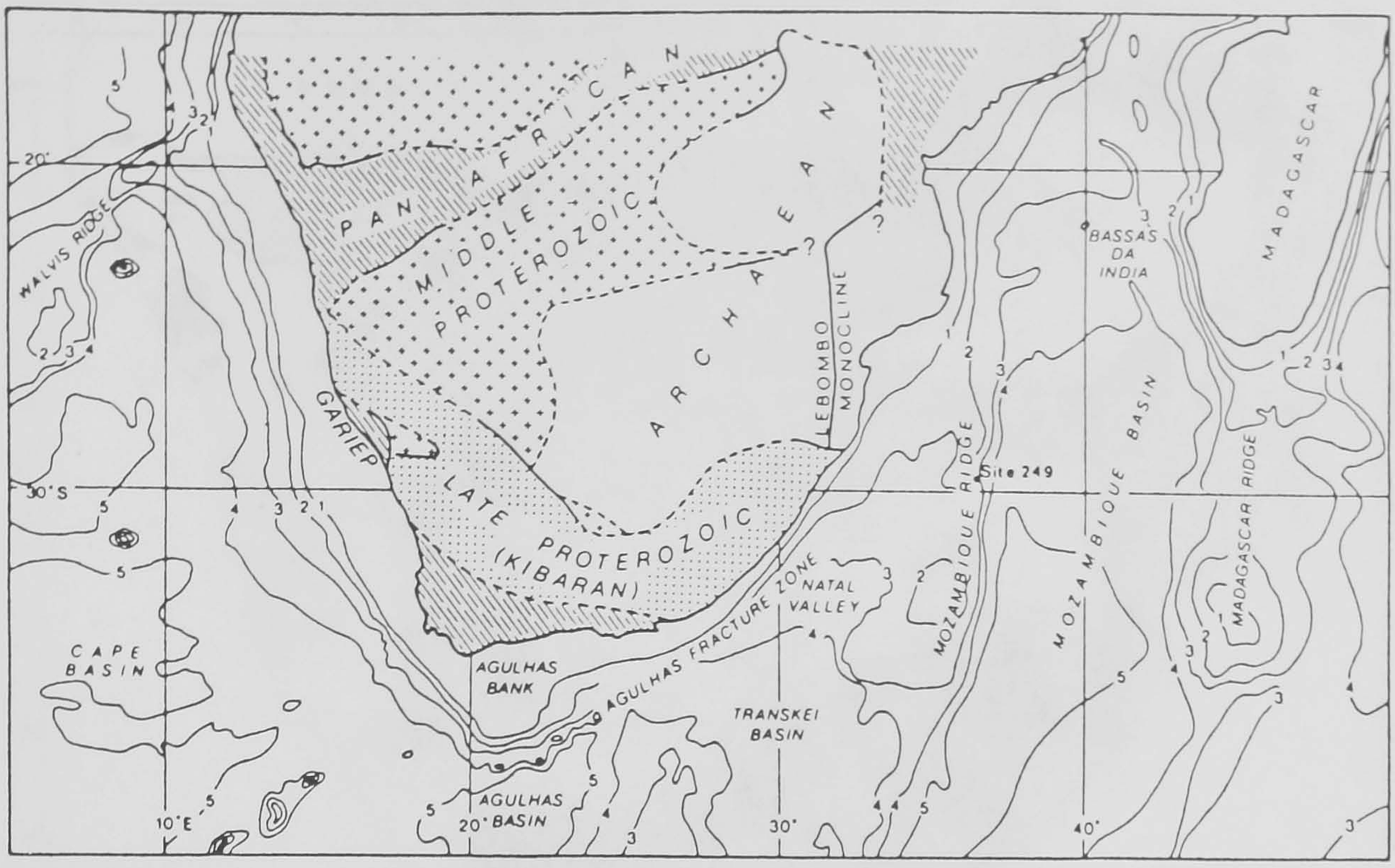

Fig. 2.2. Basement geology of southern Africa (after Eales et al., 1984, Fig. 3). Tectonic boundaries: Solid lines, observed; dashed lines, inferred and geophysical.

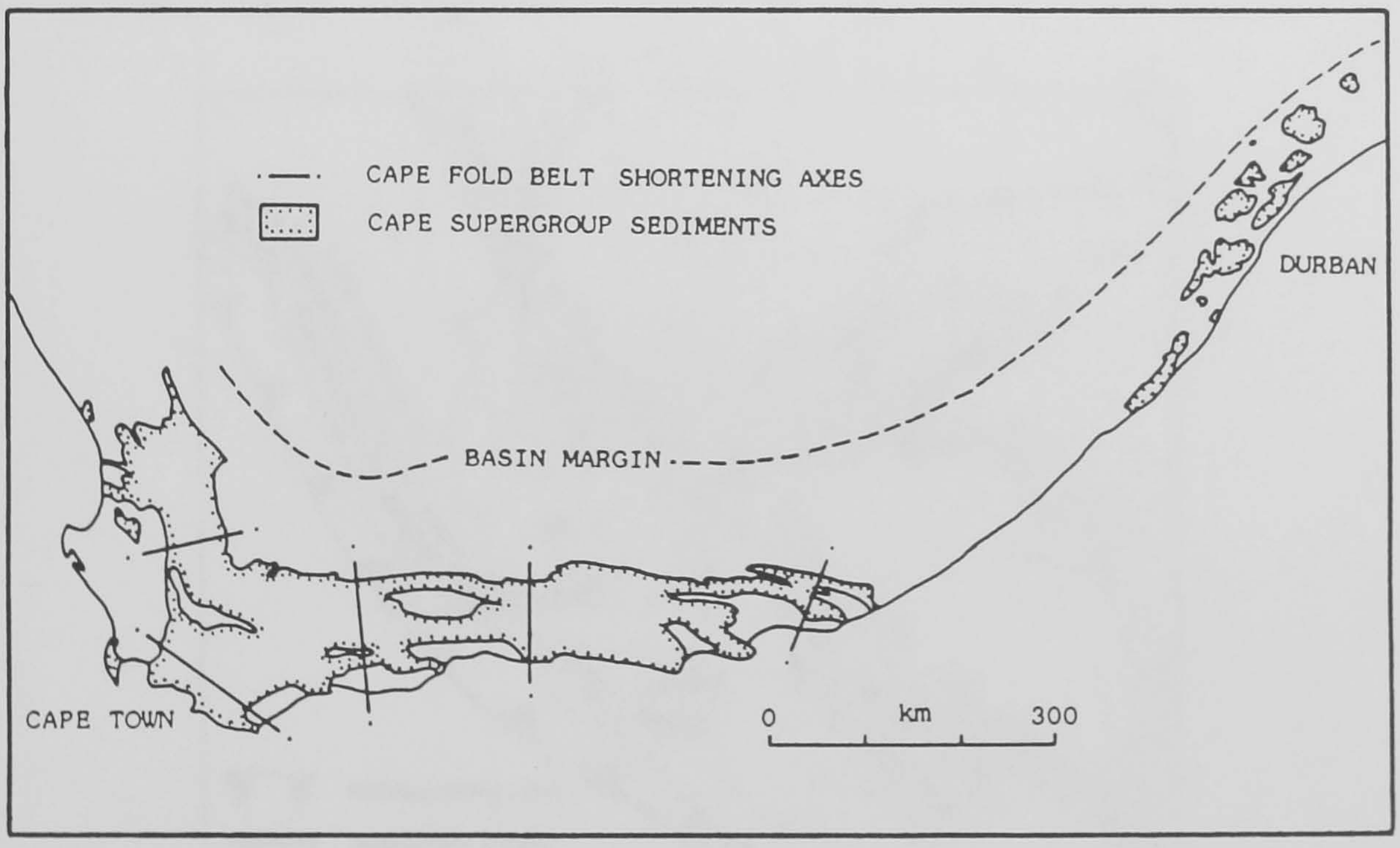

Fig. 2.3. Distribution of the Cape Supergroup sediments and Cape Fold Belt principal crustal shortening axes (after Tankard et al., 1982, Fig. 10-1 and Dingle et al., 1983, Fig. 47).

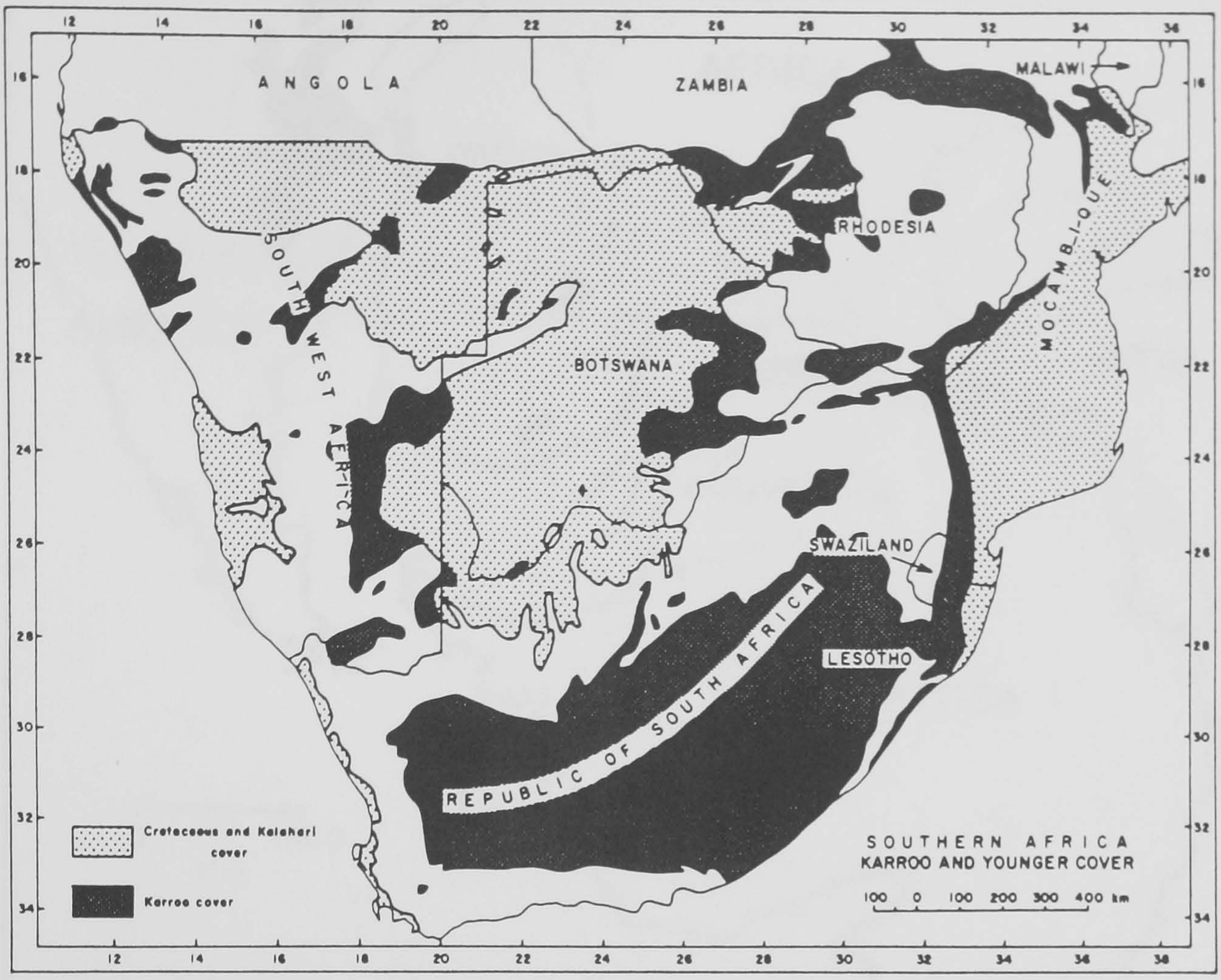

Fig. 2.4. Phanerozoic deposits in southern Africa (after Pretorius, 1979, Fig. 1).

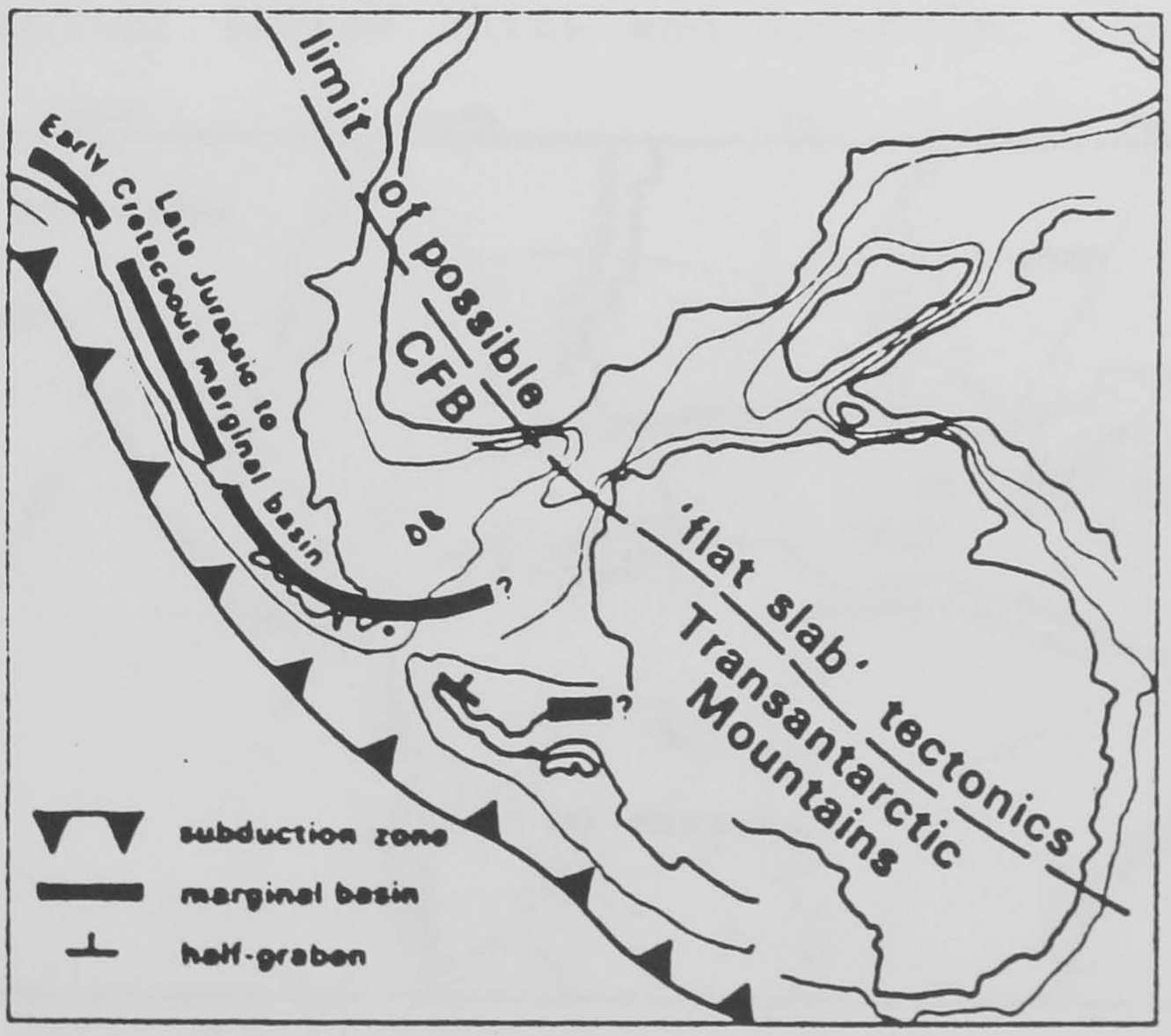

Fig. 2.5. Cape Fold Belt (CFB) age (≈225 Ma BP) compressional deformation in Gondwana (after Dalziel et al., 1987, Fig. 3).

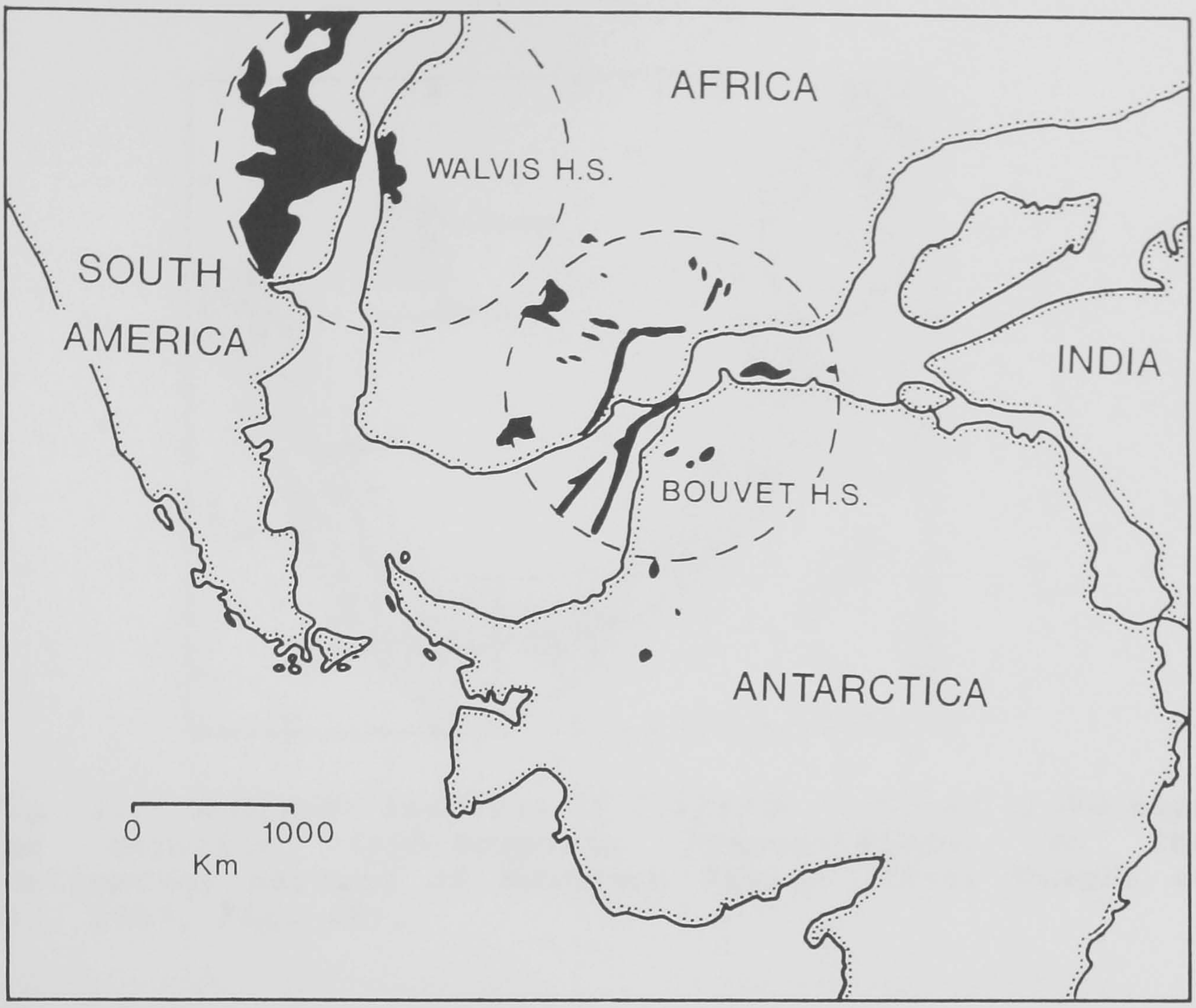

Fig. 2.6. Pre-break up reconstruction of Gondwana showing the postulated mantle plume locations thought to be responsible for continental flood basalts during rifting [solid shading] (after White and McKenzie, 1989, Figs. 15 and 21).

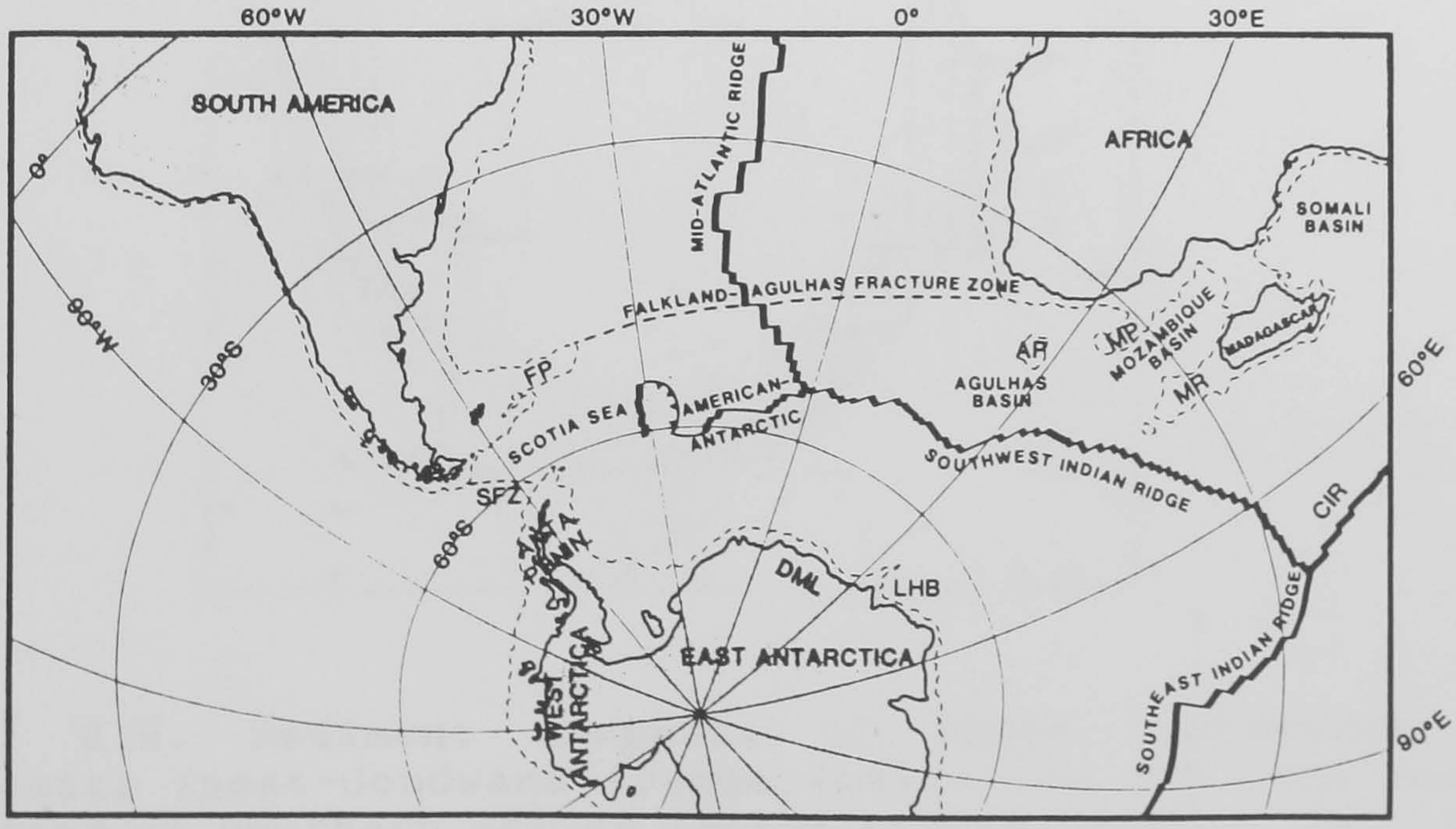

Fig. 2.7. Map of the South Atlantic and South-west Indian Oceans (after Lawver et al., 1985, Fig. 2). AP-Agulhas Plateau, FP-Falkand Plateau, CIR-Central Indian Ridge. The 3000 m bathymetry contour is shown as a dotted line.

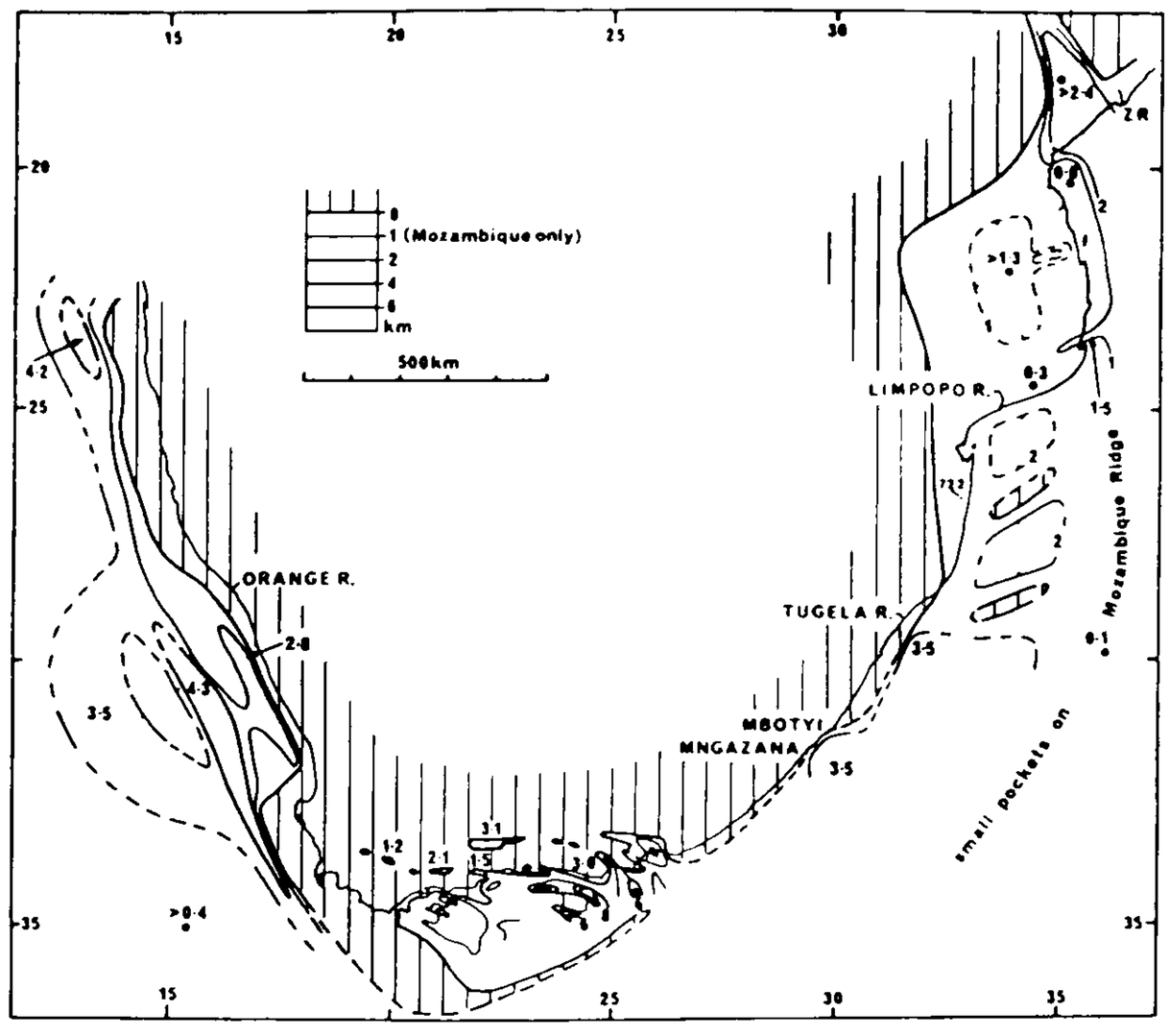

Fig. 2.8. Sediment isopachs of Jurassic to Lower Cretaceous age deposits (syn-Gondwana fragmentation) on the continental margins of southern Africa (after Dingle et al., 1983, Fig. 66).

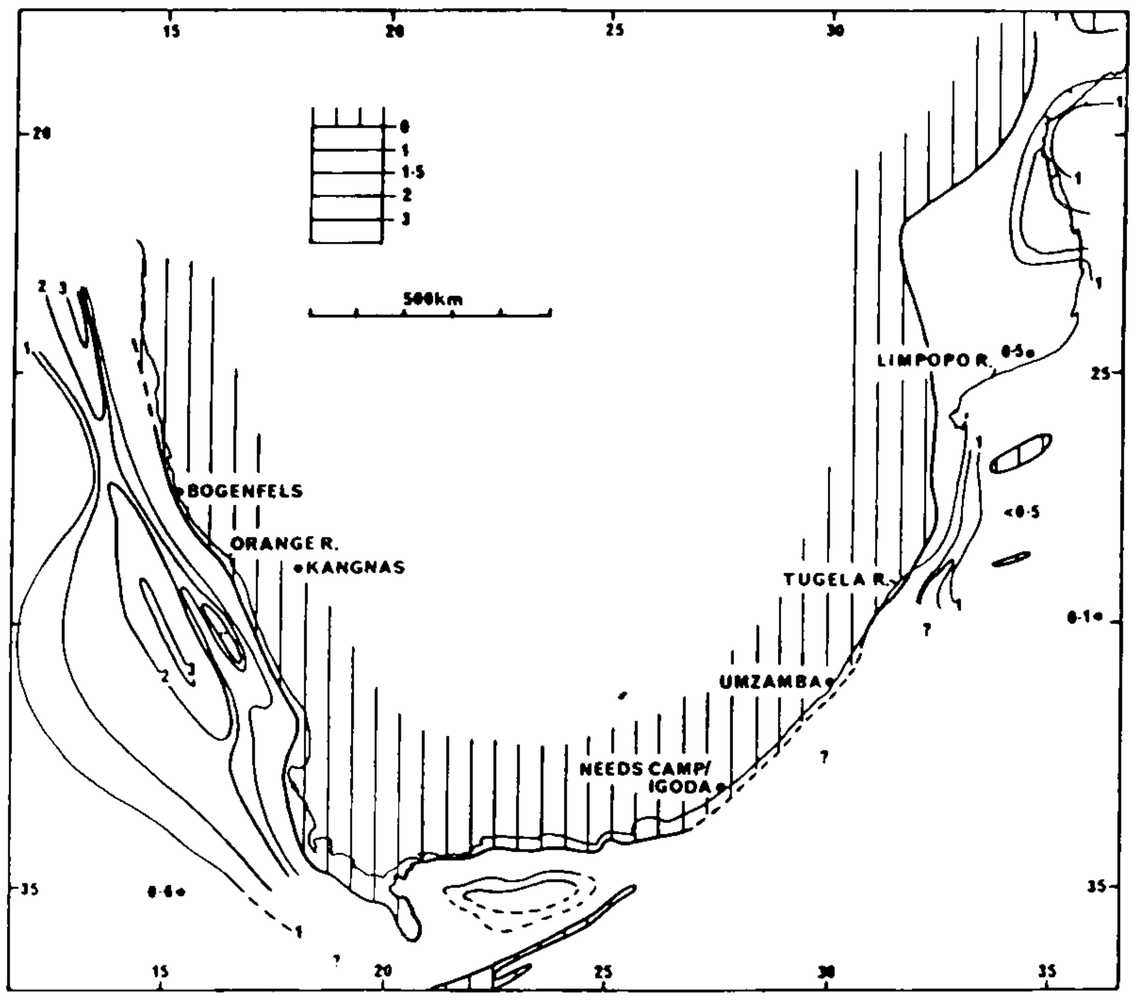

Fig. 2.9. Sediment isopachs of Upper Cretaceous age deposits (post-Gondwana fragmentation) on the continental margins of southern Africa (after Dingle et al., 1983, Fig. 124).

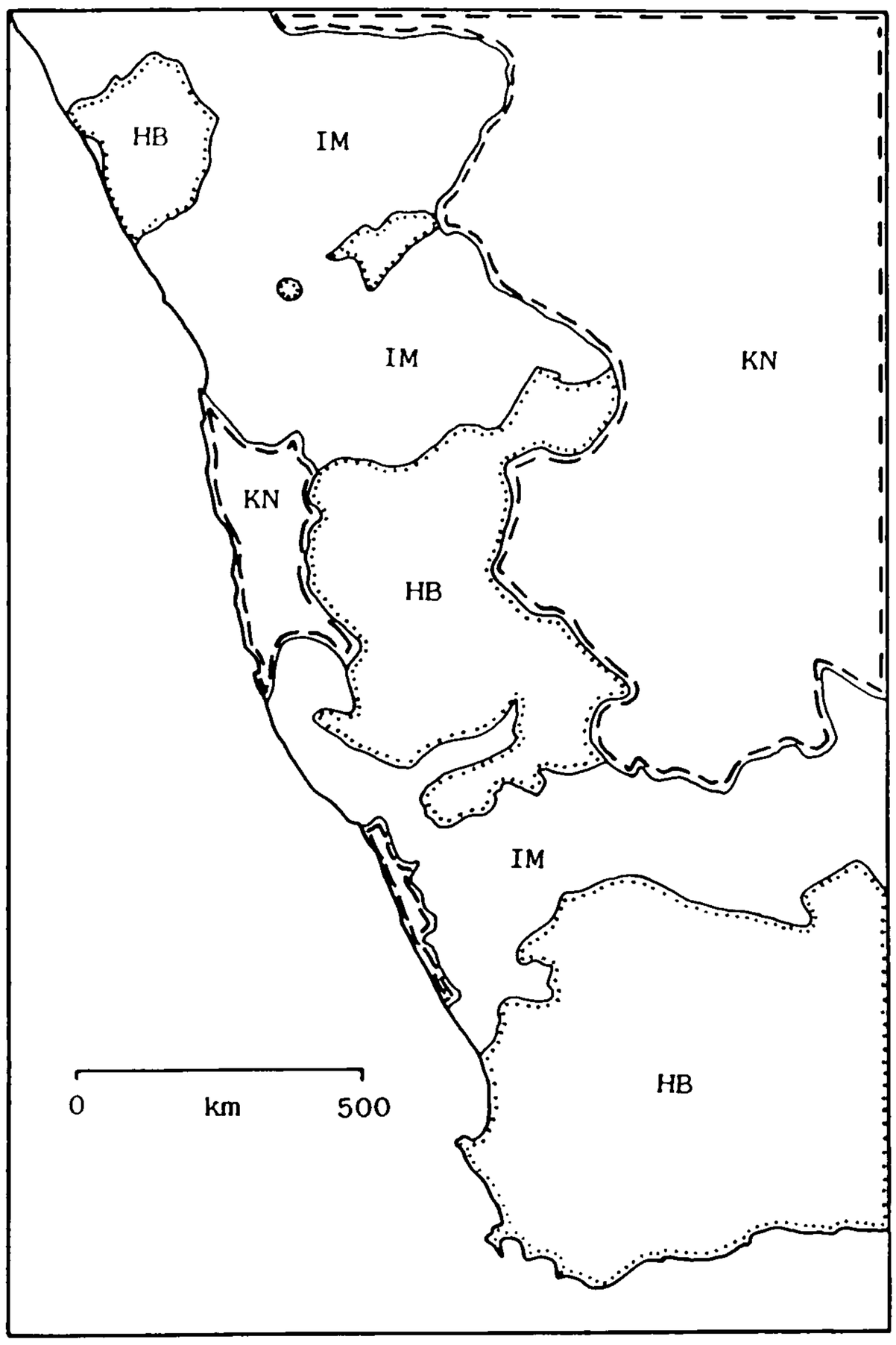

Fig. 2.10. Two terrane bedrock lithology distribution in south-western Africa: HB-horizontally bedded strata with frequent caprocks in the sequence; IM-igneous and metamorphic complexes; and KN-Kalahari/Namib deposits overlying bedrock. The approximate terrane boundaries are based on the 1:1000000 Geological Survey maps of South Africa,Namibia and field observations.

3 MORPHOTECTONIC EVOLUTION OF PASSIVE MARGINS

3.1 Introduction

This chapter will discuss current geophysical and geomorphological models which consider the origin and evolution of topography on passive margins. An integrated morphotectonic framework will then be presented which specifically addresses the origin of marginal topographic upwarps on mature rifted margins, but which is also applicable to the morphological evolution of passive margins in general.

3.2 Current Framework for Models of Landscape Evolution

3.2.1 Geophysical Models

There is an extensive literature on the extensional tectonic development of sedimentary basins on passive margins, presumably because of the economic importance of oil reserves in this environment. Many ideas date back to the beginning of the twentieth century, including the role of such subsidence mechanisms as crustal thinning, igneous underplating, thermal contraction, flexure and sediment loading (Bond and Kominz, 1988). Research has concentrated on the structural architecture and evolution of rifted margin sedimentary basins.

Quantitative models of rifted margin development have considered changes in lithospheric loading due to syn-rift lithospheric thinning and post-rift basin infill in

association with the thermal decay of the syn-rift thermal perturbation. Such load models have been integrated with an isostatic component in order to model sedimentary basin architecture and subsidence. However, the complementary morphological evolution of the subaerial portion of passive margins has largely been ignored by the earth science community, except as the onshore consequences of rift evolution. For example, surface uplift of the continental landsurface has been predicted as possibly being due to; (1) lateral heat flow; (2) depth-dependent (non-uniform) extension; and (3) regional (flexural) isostatic adjustment during rifting (Beaumont et al., 1982). The effect of a coupled denudational/isostatic system has generally been assumed to be negligible on young margins which have undergone relatively little denudation, or else totally ignored. In those studies that have included the effect of denudation and isostasy the simulation has usually been unrealistic in its approach, based upon mathematical simplicity rather than reality (section 4.6).

3.2.2 Geomorphological Models

Many researchers have considered the morphological evolution of southern Africa; especially notable have been the influential contributions of L.C. King. He developed a cyclical model of landscape evolution that was applied to the post-Gondwana break up of southern Africa. He suggested that major erosional escarpments, initiated during the fragmentation of Gondwana, retreated inland from the

coastal region and created a landscape of extensive pediment surfaces. Periodic surface uplift created new base levels and a new cycle of escarpment retreat was initiated (Fig. 3.1). As King states, "The successive landscape cycles are thus arranged stepwise from the interior plateau down towards the continental margin" (King, 1955). In this cyclical theory of landscape evolution King suggested that periodic surface uplift was due to a delayed isostatic response to denudational unloading by escarpment retreat (King, 1955). However, this idea rests on an incorrect interpretation of the work by Gunn (1949) concerning the elastic response of the lithosphere to loading events (section 5.3). Subsequently, King suggested the mechanism of cymatogeny with which to initiate new cycles of pediplanation. It was suggested that uplift and flexure of continental margins was as a consequence of sub-crustal processes, although these were not specified (King, 1967). It is worth noting that these landscape evolution models were developed before the advent of modern plate tectonic theory (although King was an early believer in the idea of continental drift) and the widespread application of quantitative models in the earth sciences.

There has been much debate about the validity of cyclical models of landscape evolution, in particular the methods of recognising coeval landsurfaces. King frequently modified his interpretation of the landscape evolution of southern Africa (Partridge and Maud, 1987). DeSwardt and Bennet (1974) have emphasised the problems of correlating

continental interior and coastal erosion surfaces because of the duality of the drainage in these two regions with different local base levels. The most recent synthesis of Partridge and Maud (1987, 1988) utilises a cyclical framework although the exact interpretation is different from that of King (Fig. 3.2). In their efforts to explain the periodic surface uplift of the margins of southern Africa they appeal to King's idea of a delayed isostatic response to denudational unloading (King, 1955), which is shown to be an incorrect interpretation of the then available literature in section 5.3. Dynamic mechanisms of surface uplift principally operate at the time of rifting, or soon after, due to the mechanics of continental lithosphere extension and are not periodic in nature.

3.3 Integrated Morphotectonic Framework

The previous discussion concerning geophysical and geomorphological models of rifted margin evolution indicates that an integrated geomorphological/tectonic framework is required to address the question of the morphological evolution of south-western Africa since the break up of Gondwana. Aspects of current tectonic theory of relevance to the morphological evolution of the southern African passive margins have been qualitatively explored by Summerfield (1985) and more generally to other passive margins by Summerfield (1988, 1989). This work suggests that some of the major factors controlling the geomorphological evolution of passive margins are; (1)

thermally-driven surface uplift; (2) isostatic uplift associated with regional denudation; and (3) subaerial surface uplift due to flexural coupling of thermal and sediment loading effects offshore (Fig. 3.3).

Lithosphere loading events causing surface uplift can be split into two types: (1) Thermal mechanisms of surface uplift; and (2) mass redistribution mechanisms of surface uplift.

3.3.1 Thermal Mechanisms of Surface Uplift

Marginal topographic upwarps are characteristic features of young rifted margins (age of formation < 60 Ma BP). In this setting they are usually referred to as rift-flank uplifts. Lithospheric thinning due to rifting elevates the geothermal gradient beneath the centre of the rift by the upwelling of hot asthenospheric material. Diffusion of this thermal perturbation allows lateral heat flow into the continental regions adjacent to the site of rifting, which causes surface uplift. However, this mechanism can only account for a few hundred metres of surface uplift (Beaumont et al., 1982). In the Red Sea region secondary convection, which can predict up to twice the amount of surface uplift in comparison to lateral heat flow (Buck, 1986; Buck et. al, 1988), has been used to explain surface uplift of the shoulders of the Suez rift (Steckler, 1985; Moretti and Chenet, 1987). Obviously such mechanisms affect the continental regions immediately adjacent to extensional rifts and significant surface

uplift generally occurs 50 km or less from the rift hinge (Fig. 3.4).

On passive margins characterized by the extrusion of continental flood basalts, as on the western and south-eastern margins of southern Africa, a simple model of rifting above a thermal anomaly in the underlying mantle (White and McKenzie, 1989) can account for the presence of volcanics (Fig. 2.5). If such a hot spot is present prior to rifting, it will cause surface uplift of around 1000 m at the centre of a region with a diameter of 1500-2000 km (Fig. 3.5). The gravitational potential of such an elevated region will greatly assist continental rifting (White and McKenzie, 1989).

There has been much speculation concerning the role of mantle thermal anomalies in generating significant surface uplift in intra-plate environments. The origin of the Drakensberg mountains of southern Africa, which rise to 3000 m or more above sea level within 200 km of the continental/oceanic lithosphere boundary on the south-east African passive margin, has been attributed to this mechanism by various researchers (Hartnady, 1985). Thiessen et al. (1979) suggested that the origin of the Drakensberg mountains was due to surface uplift associated with the rising limb of a convection cell in the upper mantle. However, in their model the continent was assumed to have remained stationary with respect to the underlying mantle. This view has been challenged by several more recent studies. Smith (1982) adopted an absolute reference frame

fixed to the South American tectonic plate and predicted extensive surface uplift of southern Africa during the late Tertiary. It was suggested that this surface uplift was associated with delayed phase changes in the mantle which were due to the continent passing over hot asthenosphere, originally situated beneath the north-west Indian Ocean spreading ridge (Smith, 1982). In contrast Morgan (1983) constructed an absolute plate motion model for Africa with respect to major hot spots in the region. This has been utilised by Hartnady (1985) to explain the origin of the Drakensberg mountains, and submarine volcanic features extending to the north-east across the seafloor of the Indian Ocean, as due to the migration of a hot spot. It was postulated that this hot spot is currently situated under the Drakensberg mountains and has caused significant surface uplift in this region during the Tertiary (Hartnady, 1985).

When considering thermal perturbations, due to lithospheric thinning during rifting, it should be noted that these decay with a time constant of ≈60 Ma (Sclater et al., 1980). Therefore, surface uplift will be greatest in the early phases of rifting and will have decayed on mature passive margins, such as those of southern Africa. The role of intra-plate thermal anomalies in the mantle, generating surface uplift, may be important on the south-eastern sheared margin of southern Africa. However, this region is spatially remote from the south-western margin with which this study is primarily concerned.

3.3.2 Mass Redistribution Mechanisms of Surface Uplift

Many models have been proposed for the generation of rift-flank surface uplift as a direct consequence of the rifting process. These include the flexural compensation of lithospheric unloading events, for example by lithospheric thinning accommodated by major faults (Weissel and Karner, 1989; Fig. 3.6) and lithospheric necking (Braun and Beaumont, 1989; Fig. 3.7). Other models which assume that the lithosphere has no lateral rigidity (Airy isostasy) can predict rift-flank surface uplift, such as by depth-dependent extension (Royden and Keen, 1980; White and McKenzie, 1988; Fig. 3.8). These models can generate 1000 m or more of surface uplift adjacent to the rift. However, in all of these cases the amplitude of residual surface uplift is reduced by sediment loading within the rift. More generally, marginal upwarps along mature passive margins cannot be adequately explained by dynamic models of rifting because the axis of maximum surface uplift along most mature passive margins is now located 100 km or more inland of the rift hinge, marking the boundary between rifted and unrifted continental lithosphere. Such models do not predict significant surface uplift so remote from the site of rifting (Figs. 3.6, 3.7, 3.8).

Magmatic underplating models associated with lithosphere extension (McKenzie, 1984; Lister et al., 1986; White and McKenzie, 1989; Etheridge et al., 1990) can account for the regionally high elevation of some rifted

margins. However, theoretical considerations indicate that little melt can probably be produced by the Lister et al. (1986) and Etheridge et al. (1990) simple shear models of lithospheric extension (Latin and White, 1990). Surface uplift is due to a combination of the intrusion of magmatic material into the lower crust and/or the extrusion of continental flood basalts at the surface (Fig. 3.9), which are of a lower density than the underlying asthenosphere. This mechanism can form domal topographic features on volcanic rifted margins up to ≈2000 km in diameter (Cox, 1989). However, this mechanism alone is unable to account for marginal topographic upwarps, which have a different form and a lower wavelength (≈50-300 km) than the domal features predicted by magmatic underplating models. The marginal upwarps on rifted margins such as south-western Africa are concave-upwards in profile (Fig. 1.3), whereas the domal upwarps predicted by magmatic underplating models are convex-up in profile (Fig. 3.9), although their primary form may not survive a prolonged period of denudation.

Rifted sedimentary basins are formed above lithosphere that has experienced thinning. Infilling of this structural depression loads the lithosphere causing subsidence. The sedimentary detritus is derived from denudation of the surrounding landmass, which leads to isostatic rebound as a result of denudational unloading. The flexural rotation due to such a denudation/sedimentation coupled system, pivoting around the rift hinge, has been viewed as an important factor in uplifting landmasses adjacent to

continental rifts (Kusznir et al., 1987; Summerfield, 1988). When considering uplift due to denudation it should be remembered, however, that the landsurface is being lowered by denudation at the same time as it is being isostatically uplifted and so two effects control the elevation of the landsurface.

3.3.3 Model Parameters

The preceding discussion indicates that thermal mechanisms of surface uplift are probably of minor importance in the origin of marginal topographic upwarps on mature rifted margins. Therefore, surface uplift is mainly by mass redistribution mechanisms coupled to isostasy which can form permanent topographic features, unless subsequently modified.

It would seem that mass redistribution mechanisms related to lithospheric thinning during rifting cannot generate significant marginal topographic upwarps greater than ≈100 km from the rift hinge, where marginal upwarps are often found on mature rifted margins. Many such models also take no account of sediment loading offshore and denudational loading onshore (Weissel and Karner, 1989).

Underplating models are unable to explain marginal topographic upwarps with wavelengths of ≈50-300 km. However, they do provide a mechanism for regionally elevating large continental areas, in the vicinity of rifts, into domal topographic features.

The roles of denudation and offshore sedimentation

have yet to be systematically assessed for mature rifted margins where their effects will be greatest. Denudation, in particular, has usually been assumed to be negligible in quantitative models of rifted margin evolution, or else the denudational models have been unrealistic in their assumptions (section 4.6). To assume that little denudation has occurred on the south-west African rifted margin would clearly be in error, since there has been an average depth of post-rift denudation of ≈1800 m over the present Atlantic draining catchments (Rust and Summerfield, 1990).

The conceptual morphotectonic model for the evolution of rifted margins is shown in Fig. 3.10. Dynamic models of rifting are unable to generate a marginal topographic upwarp more than 100 km inland of the rift hinge line, as on the south-west African rifted margin. Therefore, the relationship between denudation/sedimentation and isostasy provides the most likely explanation for the generation of marginal topographic upwarps on mature rifted margins. The next chapter will outline a denudational model applicable to south-western Africa, which is morphologically classified as a high-elevation rifted margin. It should be remembered that many of the tectonic mechanisms operating on rifted margins (Fig. 3.10) are probably not important in generating marginal topographic upwarps, but may control other temporal and spatial aspects of the morphological evolution of rifted margins.

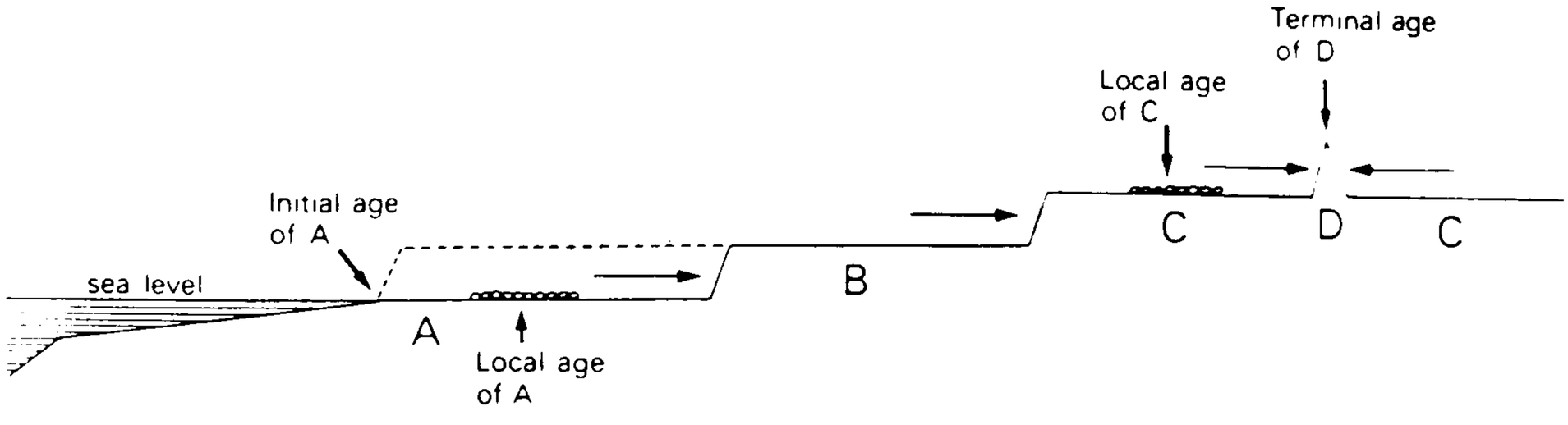

Fig. 3.1. Landscape evolution model according to the pediplanation (scarp retreat) theory proposed by L.C. King (after Summerfield, 1991a). The surfaces labelled A–D were initiated during four episodes of base level fall. Each is diachronous and deposits on the surface may be capable of yielding a minimum local age at that point. The final elimination of the last remnant of a particular surface (D) gives its terminal age.

Event	Geomorphic manifestation	Offshore sedimentation	Age
Climatic oscillations and glacio-eustatic sea-level changes (most pronounced during middle and late Pleistocene).	Low-level marine benches, coastal dune deposits, river terraces, Kalahari sands.	Accumulation of cones off mouths of major rivers. Widespread erosion elsewhere following development of near-shore current circulations. Renewed sedimentation in deep ocean basins.	Late Pliocene to Holocene
Post-African II cycle of major valley incision, especially in southeastern coastal hinterland.	Incision of coastal gorges, downcutting and formation of higher terraces along interior rivers, formation of Post-African II erosion surface (with planation restricted to eastern Lowveld region).		
Major uplift (up to 900 m in eastern marginal areas).	Asymmetrical uplift of the subcontinent and major westward tilting of previous landsurfaces of interior, with monoclinal warping along southern and eastern coastal margins.		Late Pliocene (~2,5 Ma)
Post-African I cycle of erosion.	Development of imperfectly planed Post-African I erosion surface. Major deposition in Kalahari Basin.	Renewed sedimentation giving rise to Uloa Fm. (southeastern coast), upper Alexandria Fm. (southern coast), Bredasdorp Fm. (southern and western coasts) and Elandsfontyn and Varswater Fms. (western coast). Major resurgence of sedimentation in deep ocean basins.	Early mid-Miocene to late Pliocene
Moderate uplift of 150–300 m.	Slight westward tilting of African surface with limited coastal monoclinal warping. Subsidence of Bushveld Basin.		End of early Miocene (~18 Ma)
African cycle of erosion (polycyclic).	Advanced planation throughout subcontinent. Surface at two levels above and below Great Escarpment. Development of deep-weathered laterite and silcrete profiles. Development of Kalahari basin with concomitant onset of sedimentation towards end of Cretaceous.	Widespread epeirogenic sedimentation in several pulses, as exemplified by offshore Alphard Fm., Mzinene and St Lucia Fms. of southeastern coast and lower Alexandria Fm. of southern coast. General slowing of shelf sedimentation from end-Cretaceous, culminating in major Oligocene uncomformity.	Late Jurassic/ early Cretaceous to end of early Miocene
Break up of Gondwanaland through rift faulting.	Initiation of Great Escarpment owing to high absolute elevation of southern African portion of Gondwanaland. Deposition of Enon Conglomerate Fm.	Rapid, localized taphrogenic sedimentation producing *inter alia* Uitenhage Group of southern coast.	Late Jurassic/ early Cretaceous

Fig. 3.2. Summary of postulated cyclic surface uplift events in southern Africa since the Mesozoic, based on geomorphological mapping (after Partridge and Maud, 1987, Table 1).

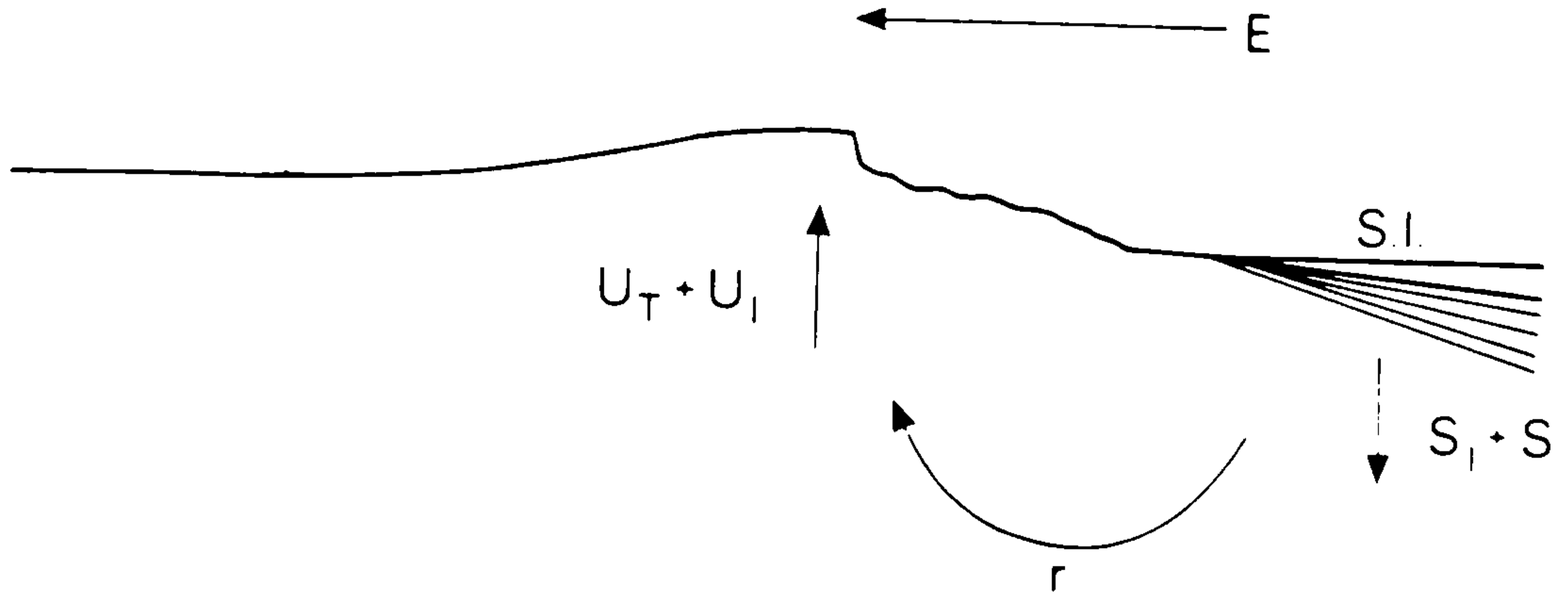

Fig. 3.3. Summary of some of the major factors controlling the morphological evolution of rifted passive margins (after Summerfield, 1991a): U_t=thermally driven uplift; U_I=isostatic uplift associated with denudational unloading; S_t=thermally driven subsidence; S_I=isostatic subsidence associated with sediment loading; r=rotation of the margin due to loading; E=erosion by escarpment retreat; and S.l.=sea level.

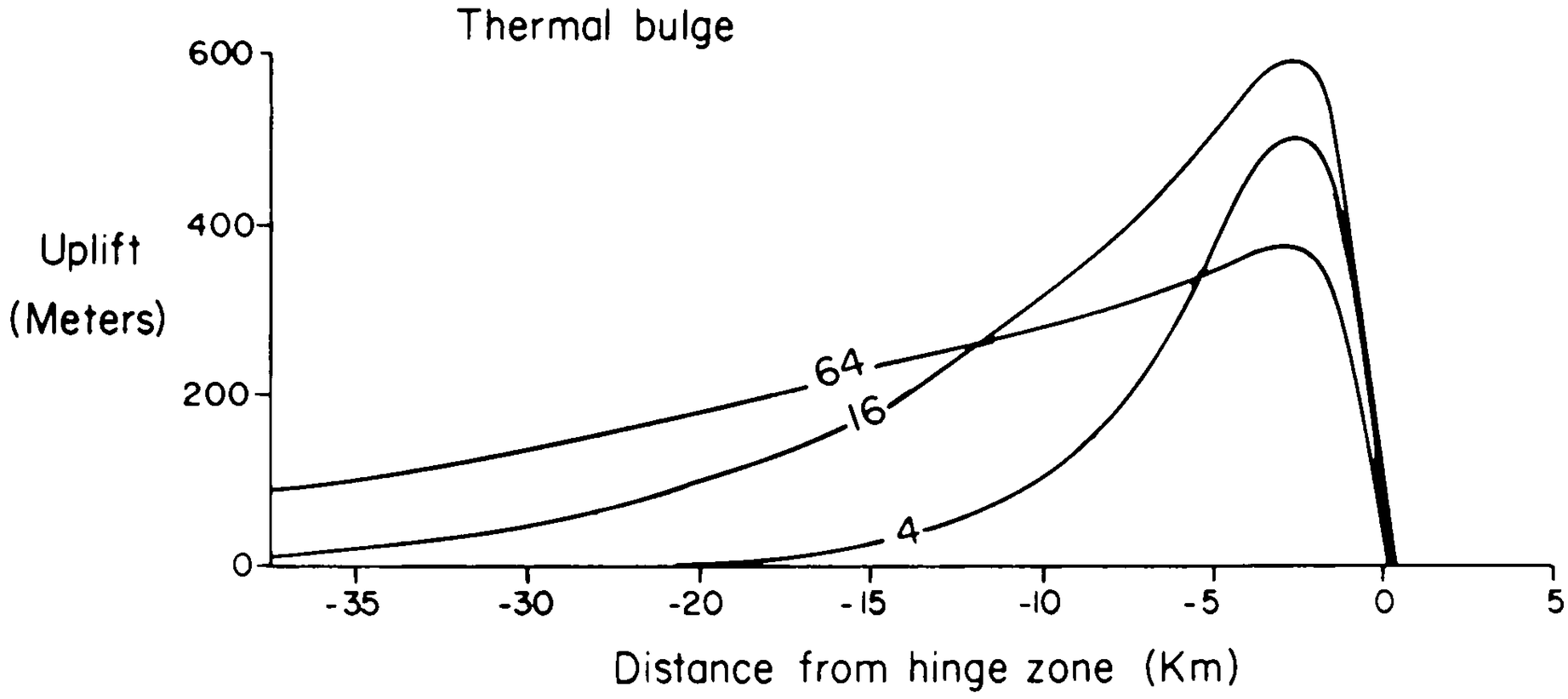

Fig. 3.4. Rifted margin surface uplift due to the effects of lateral heat flow (after Bally et al., 1981, Fig. 2.24). The section traverses the continental margin off New Jersey, USA, and the thermal model calculations for different times after rifting are shown.

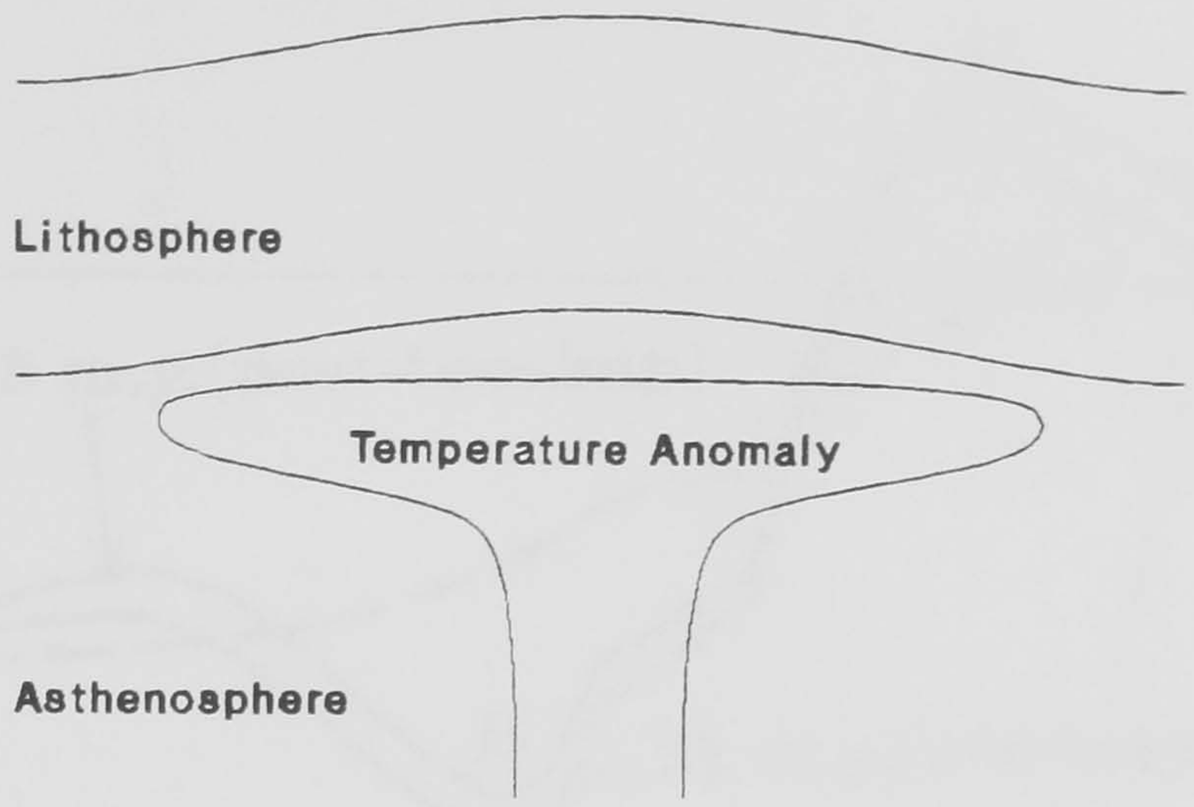

Fig. 3.5. Dynamic surface uplift due to a mantle thermal anomaly (after White and McKenzie, 1989, Fig. 2).

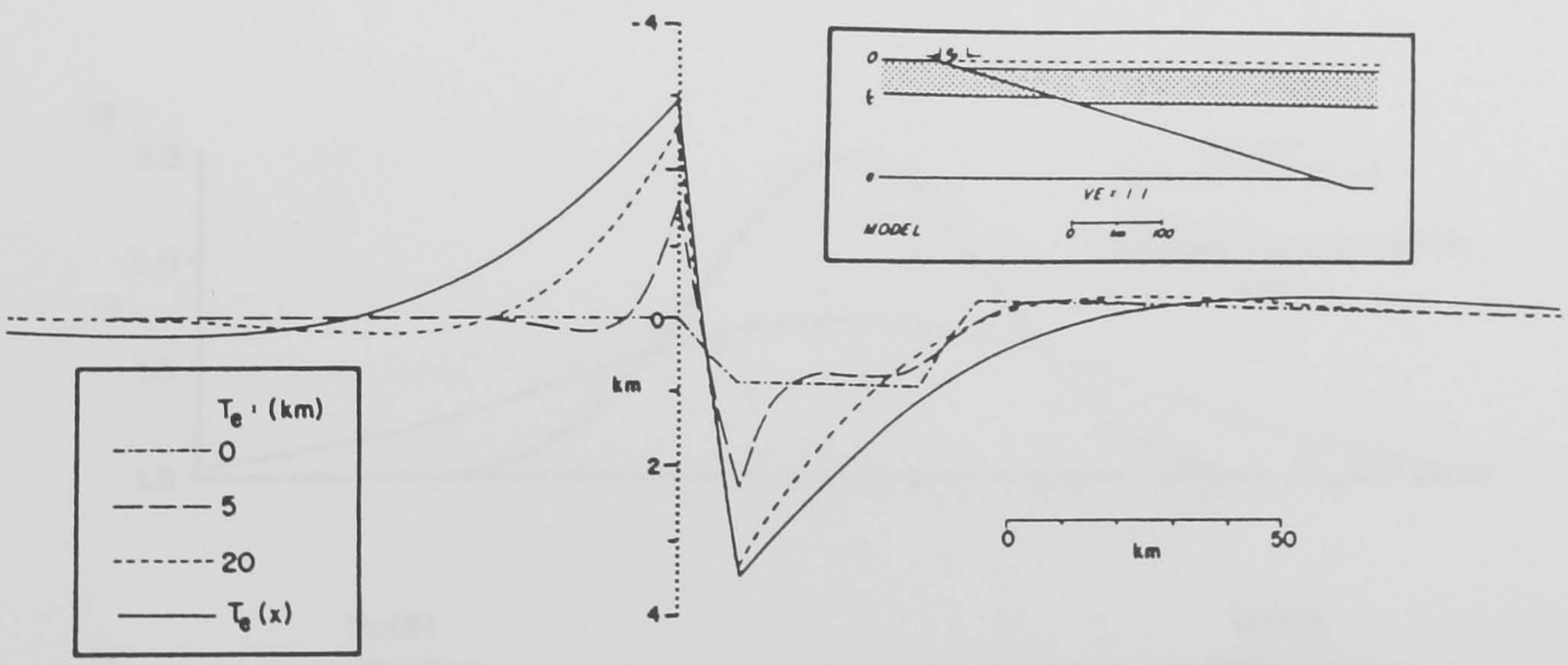

Fig. 3.6. Flexural uplift of rift-flanks due to mechanical unloading of the lithosphere during extension (after Weissel and Karner, 1989, Fig. 4). Resulting topography at time t=0 is due to normal faulting of the lithosphere. A fault dip of 20' and a horizontal offset of 10 km were used. The material overlying the plate is air. The topographic profiles were determined for different elastic thicknesses of the lithosphere (T_e). In the case of $T_e(x)$ the depth of the 450' C isotherm of the model defines the elastic thickness.

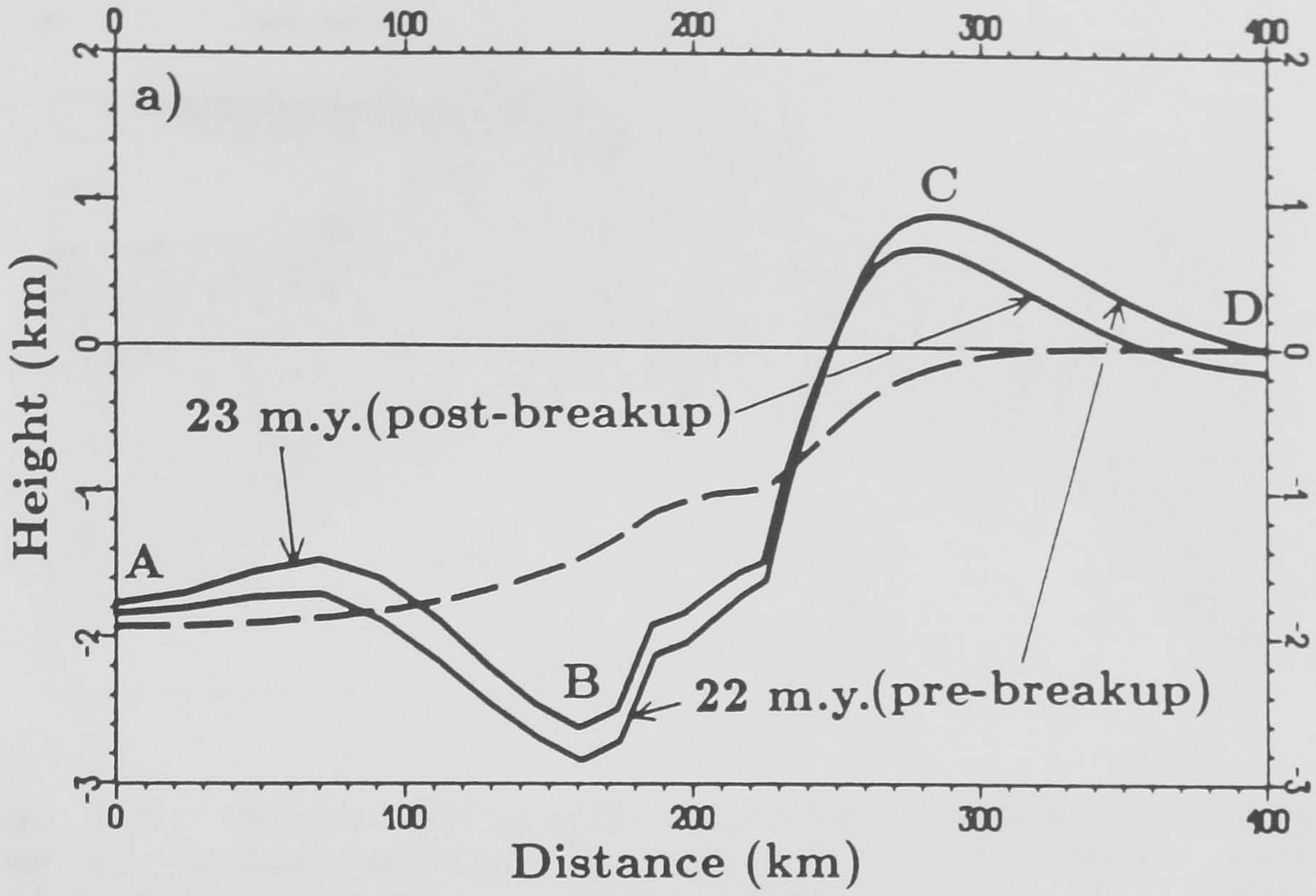

Fig. 3.7. Rift-flank uplift due to necking and rupture of the lithosphere during rifting (after Braun and Beaumont, 1989, Fig. 4a). Tectonic rift morphology has been predicted by a finite element model. Solid lines correspond to pre-rupture and post-rupture states. The material overlying the lithospheric plate is air.

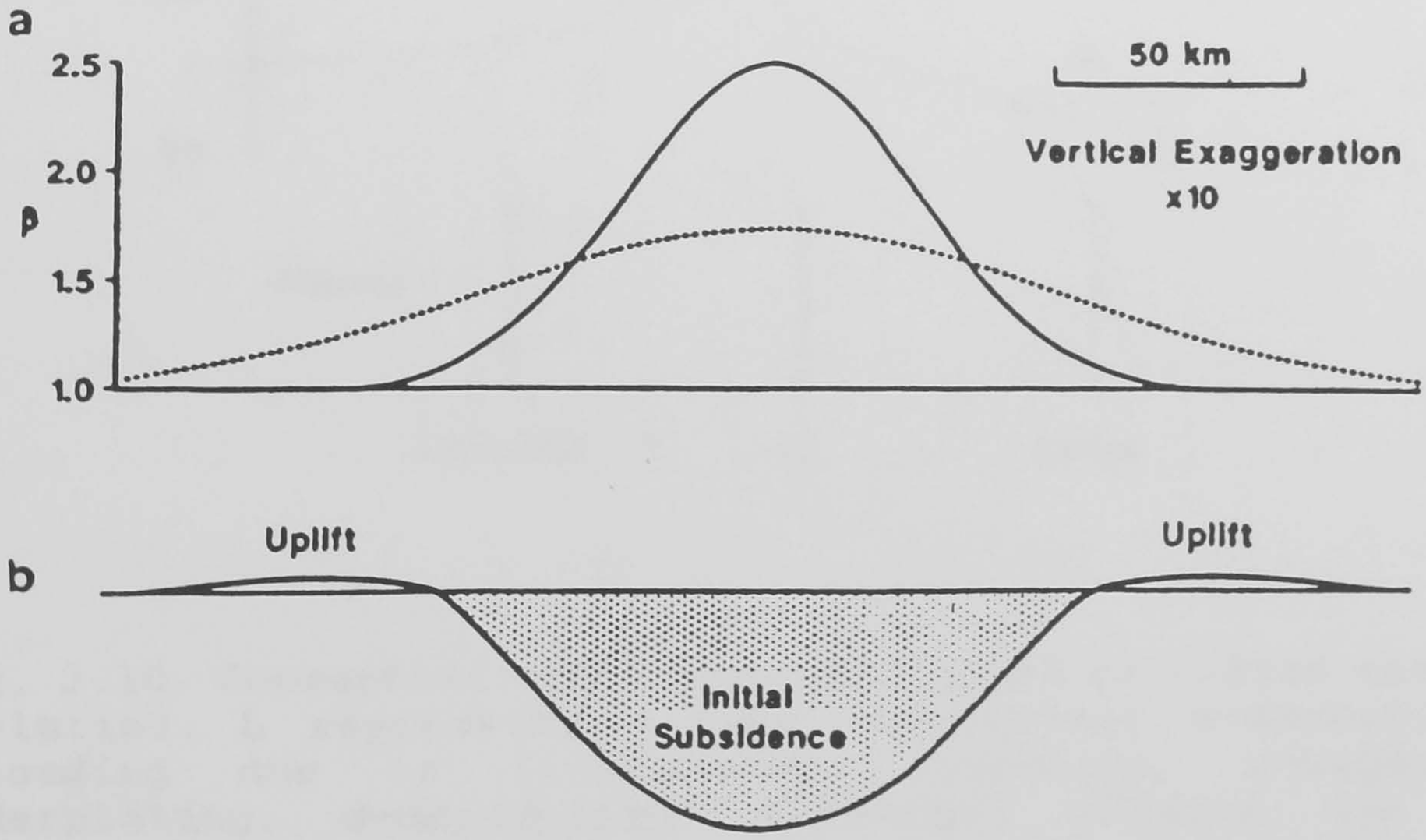

Fig. 3.8. Rift-flank uplift due to differential stretching of the crust and mantle (after White and McKenzie, 1988, Fig. 3). a: stretching factor in crust (solid line), and stretching factor in upper mantle (dotted line). b: initial subsidence and rift-flank uplift immediately after stretching.

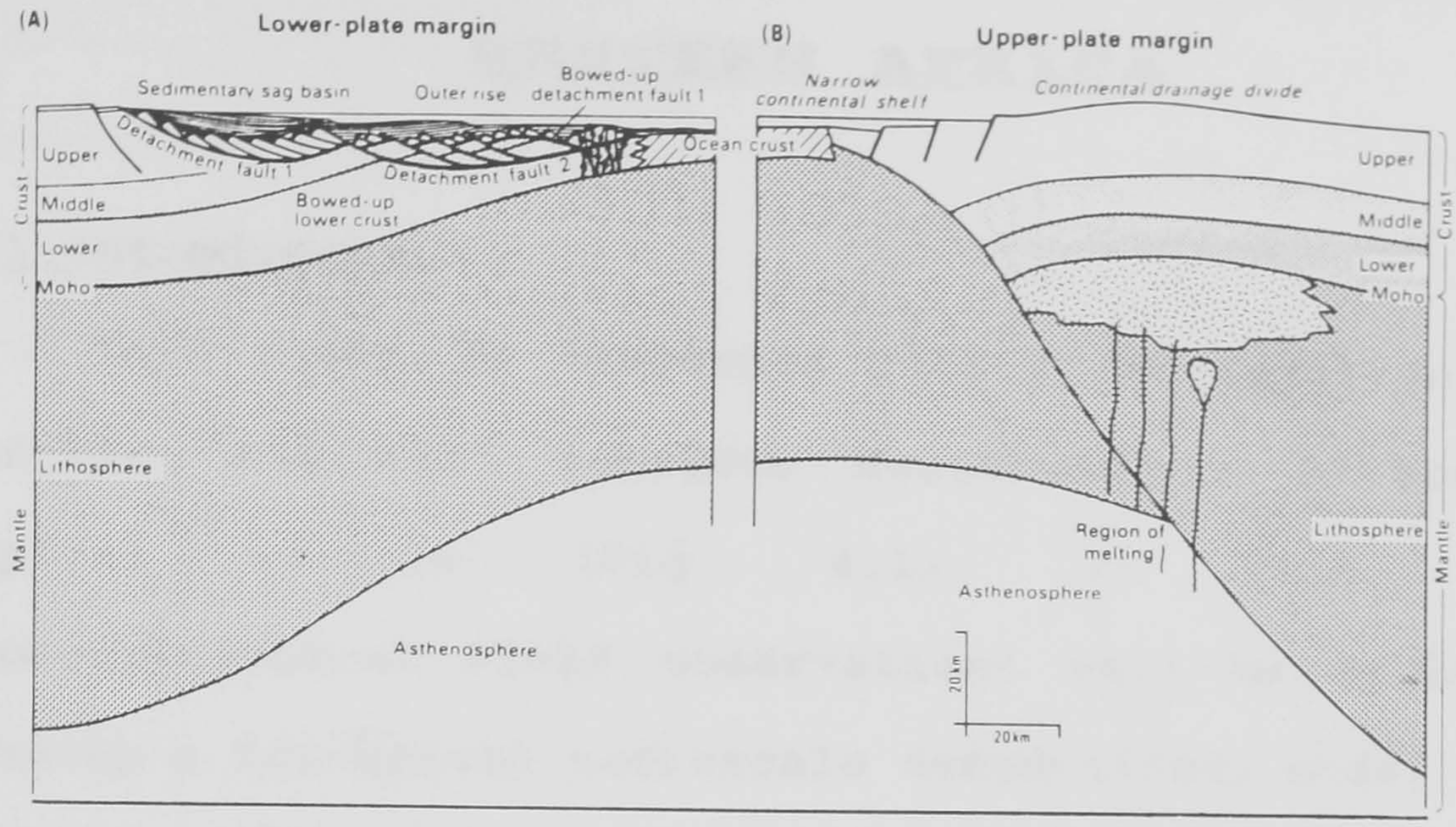

Fig. 3.9. Origin of passive margin mountains by magmatic crustal underplating, due to the detachment model of lithosphere extension (after Etheridge et. al., 1990, Fig. 1).

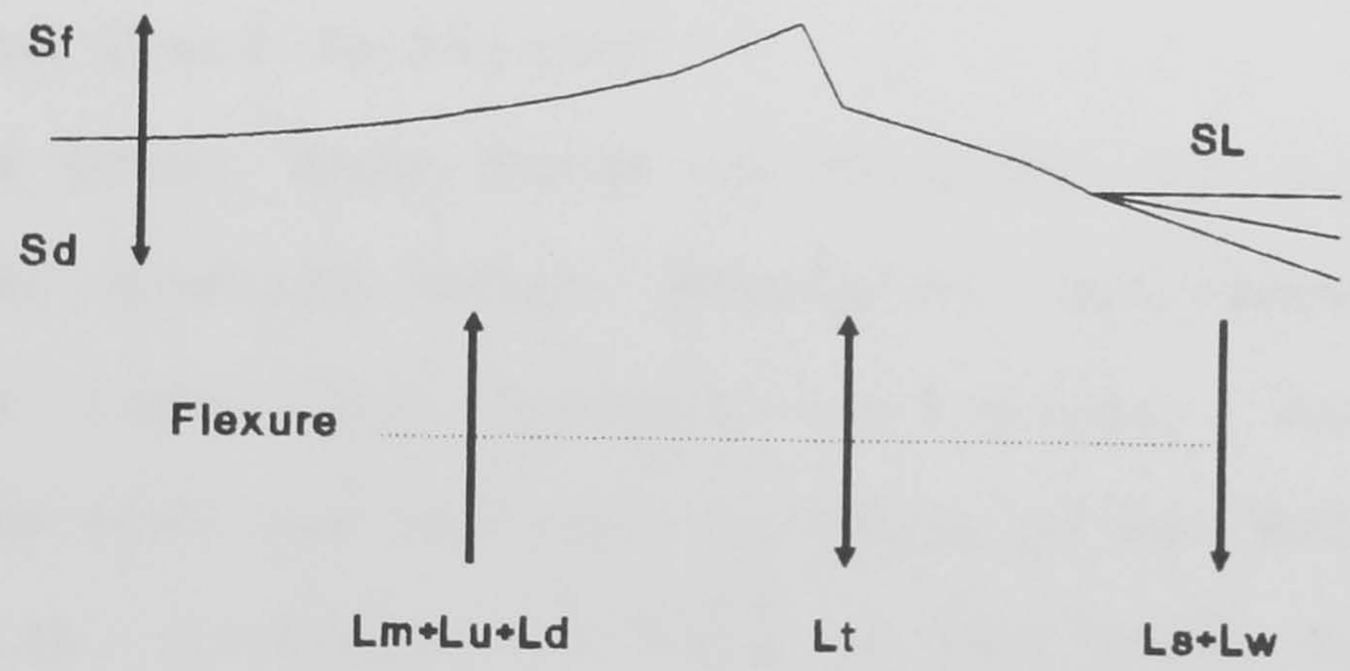

Fig. 3.10. Conceptual morphotectonic model of rifted margin evolution. L represents a load comprising; m-mechanical unloading due to lithospheric extension, u-magmatic underplating, d-denudation, t-thermal effects due to lithospheric thinning and mantle thermal anomalies, s-sediment infill of offshore rift basins, w-water infill to sea level (SL). These loads are isostatically compensated regionally by lithospheric flexure. S represents a surface elevation change due to; d-denudation, f-flood basalt extrusion associated with magmatic crustal underplating. The arrows indicate the general direction in which each mechanism acts.

4 DENUDATION MODEL FOR SOUTH-WESTERN AFRICA

4.1 Introduction

This study is concerned with high-elevation rifted margins, and will consider south-western Africa as a typical example (Fig. 4.1). In this chapter geomorphological field observations will be employed to develop a conceptual macroscale denudational model for the region. This will then be used in conjunction with empirical data to formulate a quantitative denudational model applicable to south-western Africa, and other margins with similar characteristics.

4.2 Morphological Field Observations

4.2.1 The Great Escarpment

The Great Escarpment of southern Africa is a major erosional feature which separates continental interior drainage from the coastal catchments, and generally coincides with the highest elevation of the marginal upwarp (Fig. 4.2). Although the form of the Great Escarpment is variable it can be recognised in two domains dominated by different bedrock geology (Fig. 2.10).

4.2.1.1 Form in Horizontally Bedded Lithology

Much of the southern African sub-continent is characterized by extensive areas of horizontally bedded strata with frequent lithological caprocks in the

succession. For example the Karoo sedimentary province is intruded by dolerite sills at various levels in the stratigraphic sequence which act as caprocks. The seaward edge of caprock units, which are relatively resistant to erosion, tends to define the escarpment and the rock mass strength of the lithological units controls the form of its equilibrium slope (Moon and Selby, 1983). Hence the exact form of the escarpment changes with location due to variations in caprock lithology. Examples include basalt lava flows in the Drakensberg mountains of south-eastern Africa, at the peripheral margins of the Orange catchment (Fig. 4.3), and the Table Mountain Sandstone in the region to the north and east of Cape Town, South Africa (Fig. 4.4).

In some areas the stratigraphic succession contains more than one dominant caprock and this can result in the formation of multiple escarpments. For example on the HAN profile through Calvinia, South Africa (Fig. 4.1) the lower escarpment is delineated by the Table Mountain Sandstone (Fig. 4.4), whereas the upper is defined by a dolerite sill (Fig. 4.5).

On the TIR profile to the north-east of Aus, Namibia, the Great Escarpment is often poorly defined in Proterozoic basement by very thin quartzite caprocks of the Late Proterozoic Nama system (Fig. 4.6), and in places caprocks are entirely absent. Their removal may have occurred recently as the topographic discontinuity representing the Great Escarpment is still present in basement rocks,

although there is no obvious caprock structural control maintaining the break in slope. An alternative explanation is that escarpment retreat may have occurred in a landscape composed entirely of the same lithology solely in response to surface or subsurface processes (Oberlander, 1989).

Studies of contemporary erosional escarpment development on the Colorado plateau, under similar semi-arid climatic conditions to present-day south-western Africa, indicate that escarpments experience a pattern of retreat which is controlled by the thickness and resistance to erosion of the caprocks (Schmidt, 1989). If horizontally bedded caprocks previously extended seawards of the present Great Escarpment, in south-western Africa, then this indicates that it has probably retreated some distance to its present position. If it is assumed that the Great Escarpment was initiated during rifting and has retreated from the rift hinge (King, 1955; Partridge and Maud, 1987), then it has probably done so in a regular style, as shown by its roughly linear trend parallel to the rift hinge (Fig. 4.1). Rogers (1920) suggested that escarpment retreat has occurred by the headward erosion of fluvial systems combined with structural control. Uniform retreat would then occur when stream spacing was equal and the caprocks had similar denudational properties, as on the TSA profile below the Tsarisberge mountains, Namibia (Fig. 4.7). When these conditions are not met then the Great Escarpment would have an irregular form, as in parts of the Drakensberg Mountains (Fig. 4.8).

4.2.1.2 Form in Crystalline Basement

The bedrock south of the Orange River towards Garies consists principally of Precambrian basement. Although there is no obvious horizontal stratification in the basement the Great Escarpment is still present in most areas but is often defined by structural planes, as on the ROO profile (Fig. 4.9). It should be noted that these structural planes may have developed due to pressure release associated with erosional unloading and therefore be a response, rather than a control, of the pattern of denudation. North of Usakos towards Fransfontein, Namibia, the Great Escarpment is defined by the seaward aspect of a series of inselbergs. For example the Great Escarpment is delineated by the edge of a granite intrusion in the case of the Brandberg inselberg on the BRA profile (Fig. 4.10), and a sequence of basalt lavas flows in the Erongo Mountains on the ERO profile (Fig. 4.11).

4.2.2 Interior Catchments

The continental interior plateau is essentially an extensive area of very low local relief (Fig. 4.12), at an average altitude of ≈1000 m (Ollier and Marker, 1985). Local relief is defined as the difference between the maximum and minimum elevation within a specified area, which in this study is based on 10-minute data (≈18x18 km). Parts of the interior plateau form depressions which have accumulated terrestrial sediments up to several hundred metres thick (Thomas and Shaw, 1987), for example the

Etosha (Fig. 4.13) and Kalahari basins which are separated by low drainage divides.

In the region of the marginal topographic upwarp fluvial systems have incised into the landsurface. For example at the headwaters of the Fish River in the Tsarisberge mountains, minor valleys a few hundred metres wide have been incised through the Quartzite caprock of Nama age deposits (Fig. 4.14). Downstream in the confluent zone of the Fish River the Fish River Canyon is up to 20 km wide and has been incised ≈500 m below the surrounding landsurface (Fig. 4.15). The marginal divide is breached by the Augrabies Falls on the Orange River (Fig. 4.16) although Augrabies lies some distance inland of the marginal upwarp axis. This may be because the greatest denudation in a fluvial system is often in the region of a waterfall (Young, 1985) and so the Augrabies Falls may represent knickpoint retreat. The Orange River provides an outlet for denuded material from the interior catchments to the offshore Cape Basin.

4.2.3 Coastal Catchment

This terrain drains the area seaward of the Great Escarpment by river systems that are orientated approximately perpendicular to the present coastline. The coastal catchment has generally been incised to a greater extent than the interior catchment behind the Great Escarpment (Fig. 4.17), which is to be expected given the much higher channel gradients in this region. This simple

drainage pattern is disrupted in the region between Oranjemund and Walvis Bay, Namibia, because of the presence of the Namib Sand Sea (Fig. 4.18). This feature consists of sand dunes up to ≈300 m high which act as a barrier to the coastal drainage so that ephemeral rivers, such as the Tsauchab, flow to drainage endpoints within the sand dunes (Fig. 4.18). Stratigraphic studies (Ward et al., 1983) indicate that a sand sea may have existed in the region of the present Namib since the Early to Middle Tertiary, when it was of a greater areal extent.

It has been suggested that drainage patterns are controlled by surface crustal structure (Deffontaines, 1991). There are many such examples in southern Africa, especially in the coastal catchment region. For example just north of Garies, South Africa, on the ROO profile (Fig. 4.19) a linear fault trace defines the orientation of the valley and different rock types can be seen on either side of the valley.

4.3 Conceptual Macroscale Denudational Model

In areas dominated by flat-lying lithology with frequent caprocks the escarpment is an erosional feature that is thought to have formed at the rift hinge during rifting and has retreated to its present position. Before rifting, the topography of a super-continent is probably one of predominantly low local relief owing to prolonged denudation. However, regional elevation may be relatively high in areas remote from pre-rifting coastlines where

local channel gradients, and hence denudation rates, are low. In addition, underplating associated with rifting may generate a regionally extensive increase in elevation along some passive margins soon after rifting begins (Cox, 1989). Continental rifting will create significantly lower base levels along newly formed high-elevation rifted margins. Consequently, two distinct denudational systems will be established, separated by a retreating major escarpment or multiple escarpments. Thus on the south-west African margin the high local relief along the coast (Fig. 4.20) is associated with relatively high slope and channel gradients (Fig. 4.17). This will promote relatively high denudation rates, whereas the very low relief inland of the Great Escarpment (Fig. 4.12) gives rise to low denudation rates, given the empirically derived linear relationship between mean local relief and mean drainage basin denudation rate (Ahnert, 1970). Thus the interior catchment, at a higher mean elevation than the coastal catchment area, will exhibit lower denudation rates.

The empirical study of Ahnert (1970) contrasts with the study of Pinet and Souriau (1988), who correlated mean mechanical denudation rate with mean basin elevation. The conceptual macroscale denudation model presented in the previous paragraph is in agreement with the analysis of Ahnert (1970). This is because it would be expected that higher denudation rates would be found adjacent to a newly formed rift due to the lowering of base levels in this region and the incision of the flanks of the rift. Other

studies consider that mean drainage basin denudation rates are related to climatic variables such as precipitation (Langbein and Schumm, 1958; Ohmori, 1983). However, the strong linear relationship between mean drainage basin denudation rates and mean local relief for mid-latitude catchments with a mean annual precipitation rate of 250-2500 mm (Ahnert, 1970), indicates that geomorphic variables have a greater effect in controlling denudation rates than climatic variables. In addition, it is thought that over the spatial and temporal scales under consideration in this study, climatic variables are not known with enough certainty to enable their inclusion in the model at present.

In areas without extensive horizontally bedded caprocks in the sequence, a more obscure landscape history is suggested since caprock controlled escarpment retreat did not probably occur. For example the inselbergs of central Namibia, as erosional remnants whose seaward aspect defines the Great Escarpment, have an unknown age of formation in the absence of datable material draping their morphological surfaces. In these areas the location of the Great Escarpment may not have changed significantly with time, since the Great Escarpment is generally controlled by sub-vertical structural discontinuities such as the edge of an igneous intrusion.

The basic conceptual macroscale denudational model, principally applicable to areas with extensive horizontal caprocks in the stratigraphic sequence, can be summarised

as follows. It consists of two terrains, characterized by high relief and high denudation rates in the coastal region, and low relief and low denudation rates in the continental interior. The two terrains are separated by a moving boundary, represented by the Great Escarpment, which was probably initiated at the rift hinge and has retreated to its present position.

4.4 Evidence to Support the Denudational Model

The mean local relief of continental catchments has been empirically found to be the controlling variable in regional denudation studies of contemporary systems (Ahnert, 1970). A comparison of the local relief data for a young rifted margin, such as the Gulf of Aden (Fig. 4.21), and a mature margin, such as south-western Africa (Fig. 4.20), indicates that the relief differential between coastal and interior catchments, and hence inferred denudation rates, would appear to be maintained throughout passive margin evolution. This suggests that post-rift denudation of a coastal catchment is greater than that of the interior catchment on a high-elevation passive margin. A palaeo-topographic reconstruction of eastern Australia agrees with this conclusion (Speight, 1987).

The overall depth of post-rift denudation, averaged over the present Atlantic-draining catchments in southern Africa, has been estimated to be ≈1800 m on the basis of offshore sediment volume data (Rust and Summerfield, 1990). Apatite fission track analysis (AFTA) of samples from south

of Luderitz, Namibia, show that several kilometres of denudation must have taken place over the area (Brown et al., 1990). The AFTA data also indicate that an accelerated phase of erosion most likely occurred during the Early Cretaceous, probably in response to new base levels created during the break up of Gondwana. It was suggested that this phase of denudation was regional in extent, both inland and seaward of the Great Escarpment. Employing a palaeo-geothermal gradient of 30 $^{\circ}Ckm^{-1}$ it was suggested that a minimum of ≈3000 m has been removed from the study area (Brown et al., 1990). This is higher than the estimate of the average amount of denudation that has occurred across the whole of the Atlantic draining catchments since the break up of Gondwana calculated from offshore sediment volume data. However, the AFTA data set only covers a small area of the Atlantic draining catchment and is sampled from the coastal region and the lower reaches of the Orange River. This is the area that is most likely to have been affected by new, lower, base levels after rifting and will probably have been denuded to a deeper level than the marginal reaches of the Orange River catchment. This area was probably extensively covered with Karoo strata at the time of Gondwana break up, and the rapid Early Cretaceous phase of erosion may also be accounted for by rapid escarpment retreat which stripped this cover prior to the development of the present major escarpment. AFTA data from other rifted margins such as the Red Sea (Bohannon et al., 1989) and eastern Australia (Moore et al., 1986) also

indicate significant post-rifting denudation in their coastal regions.

From faunal characteristics of the Karoo Basin of southern Africa and the contemporaneous Parana Basin of South America, which pre-date the fragmentation of Gondwana, it has been suggested that they were originally connected as a single depositional system (Oelofsen 1987). Therefore, the exposure of older Karoo strata and basement rocks along the south-west African margin also indicates significant depths of denudation in the coastal region, whereas the preservation of younger Karoo sediments and Cenozoic weathering profiles suggests generally low rates of post-rift denudation in the continental interior.

4.5 Quantitative Denudational Model Formulation

The basic conceptual model is derived from geomorphological field evidence and empirical estimates of the spatial patterns of denudation on high-elevation rifted margins. The model consists of an escarpment, initiated at the rift hinge during an assumed instantaneous rifting event, which is modelled as retreating at a constant rate to its present position. Since the former extent and mechanical properties of the dominant caprocks which control scarp retreat are unknown, this is the simplest assumption and is used in the absence of additional constraints. The present, or inferred, height of the Great Escarpment is assumed to have been maintained throughout the evolution of the margin, and so this value is assigned

as the vertical denudation rate of the retreating escarpment[1]. The ratio between the mean local relief of the interior and coastal drainage basins, derived from contemporary data, is maintained throughout the model run from rifting to the present day. The denudational model is diagrammatically represented in Fig. 4.22.

The denudational model can be numerically calibrated given constraints on the drainage evolution of the continental hinterlands and offshore sedimentation in the Cape Basin. Terrestrial sedimentation is ignored since it is volumetrically insignificant in comparison to offshore rift-basin sedimentation (Dingle et al., 1983). The area of the coastal catchment has been assumed to have increased linearly from zero, at the time of rifting, to its present area as the Great Escarpment has retreated. The total Atlantic-draining area has been assumed to have remained constant. However, the drainage history of the marginal reaches of the Orange Basin is unknown, and it is likely that some areas may have drained offshore to the east and south-east prior to the establishment of the current Atlantic draining catchment. There is also some evidence that the drainage of the continental interior of southern Africa was not fully integrated with the Atlantic drainage until ≈80 Ma after rifting (Rust and Summerfield, 1990). However, the simplest interpretation is adopted in view of the uncertainty of the detailed drainage history. If the mean depth of denudation for the total drainage area is known, which in the case of the study area has been

[1]Given that the time step of the model is 1 Ma.

estimated as ≈1800 m (Rust and Summerfield, 1990), then the two model unknowns, the denudation rates of the coastal and interior catchments, can be calculated. The denudational model calibration is shown in Fig. 4.23, from which the calibration equation is;

$$ADD = (\{T_t [A_{ic} Dd_{ic} + A_{cc} (Dd_{ic} \div 2 + Dd_{cc} \div 2)]\} + A_{cc} Dd_e) \div [A_{cc} + A_{ic}] \quad (4.1)$$

where;

ADD = mean depth of denudation of the total catchment (m)

T_t = model run time (Ma)

A_{ic} = present area of interior catchment (m^2)

A_{cc} = present area of coastal catchment (m^2)

Dd_{ic} = denudation rate of interior catchment (mMa^{-1})

Dd_e = denudation rate of escarpment (mMa^{-1})

Dd_{cc} = denudation rate of coastal catchment (mMa^{-1})

and given that from Ahnert (1970);

$$MLR_{cc} \div MLR_{ic} = Dd_{cc} \div Dd_{ic} \quad (4.2)$$

where;

MLR_{cc} = mean local relief of coastal catchment (m)

MLR_{ic} = mean local relief of interior catchment (m)

Dd_{cc} and Dd_{ic} can be calculated by the substitution of

equation 4.2 into 4.1.

At the coastal boundary the topography is graded to sea level, which is kept constant, as the escarpment retreats during the model evolution. Eustatic sea level change has not been incorporated into the model since the global sea level curve of Vail et al. (1977), and a sea level curve for around southern Africa (Siesser and Dingle, 1981), do not consider the influence of local tectonic movements and so do not represent true eustatic changes in sea level (Watts 1982). In any case the variation in sea level merely has the effect of shifting the modelled coastline slightly, since the landsurface dips relatively steeply into the sea, while the rest of the denudational system is unaffected since base level elevation is not a controlling variable in the model.

4.6 Justification of the Modelling Approach

Geomorphic process-response models, ignoring the effects of isostasy, have been developed to study landform evolution at small spatial scales and over short temporal scales under a variety of structural and climatic conditions (Culling, 1965; Kirkby, 1971; Ahnert, 1973; Kirkby, 1986; Anderson and Humphrey, 1989). While of undoubted interest, their approach is unsuitable for studying the role of denudation on passive margins because; (1) detailed input parameters required by such models, including structural and climatic data, are incompletely known; and (2) since the denudation rates in such models

are primarily a function of slope, the landscape evolution will be a direct function of the assumed initial topographic condition, which is also unknown due to post-rift denudation. Thus, the final topographic configuration of the model, and the spatial variation in denudation, is dependent upon data which is either incompletely known or unknown. At a more fundamental level process-response models attempt to represent real processes operating on a landsurface. Therefore, they consider such linked processes as soil creep, soil wash and fluvial activity (Kirkby, 1971), and aim to describe their actions on and interactions with a landsurface. In order to be realistic such process-response models have to be formulated at the microscale, with a resolution of no more than 1 m by 1 m (Parsons, 1988). Such a criterion is obviously impractical for modelling the landform evolution of a passive margin with a catchment area of the order of 10^6 km^2. The alternative is to formulate a conceptual model, based upon the observation of contemporary systems, which attempts to replicate the overall effects of weathering, erosion and transportation but does not consider the interaction of individual processes with each other and with a landsurface.

In previous attempts to assess the isostatic response to denudational unloading, using non process-response models, it has either been assumed that denudation rates are linearly proportional to mean regional elevation (Stephenson 1984; Lambeck and Stephenson 1986), or that

denudation can be represented by a simple diffusion equation in which it is assumed that flux of regolith is proportional to the slope gradient (Moretti and Turcotte 1985). Neither approach provides a valid basis for modelling denudation rates on high-elevation rifted margins. The relationship between regional elevation and denudation rate does not apply because low local relief (low slope and channel gradients) prevails on the high interior inland of the Great Escarpment, whereas high local relief typifies the lower elevation terrain on its seaward flank. The theoretical development of the diffusion equation as applicable to soil-covered slopes, where the rate of transport is the dominant denudational control, has been outlined by Culling (1965). In south-western Africa, where the topography is characterized by marked lithological control and denudation is weathering limited, there is no justification for the application of the diffusion equation to modelling regional denudation rates.

There are two crucial points to be aware of in forward modelling denudational processes: (1) The initial landsurface is unknown and has to be inferred; and (2) the subsequent evolution of the system is also unknown, except for the final topography, unless spatial elements can be defined in time. For example when dated deposits drape a geomorphological surface, giving it a minimum age of formation. In this respect geomorphological modelling is far more difficult than sedimentary basin modelling as there is no record of the evolution of the system, which in

basin modelling is provided by the basin stratigraphy. Therefore, researchers interested in denudational modelling have to develop their models with reference to present day systems, which behave in a similar fashion, and calibrate them using empirical data relevant to geological timescales.

In this thesis a simple conceptual denudation model, applicable to high-elevation rifted margins, has been developed using a set of reasoned assumptions and calibrated using offshore sediment volume data. Such a model is internally consistent over geological timescales since it is mass-balanced, although spatial and temporal variations in denudation not formulated by the model no doubt occur. However, the aim of this study is to explore the coupling between denudation and isostasy on high-elevation rifted margins and the implications for landscape evolution. Since the isostatic component is modelled flexurally (chapter 5) it is worth noting that this acts as a low pass filter to the denudational load and so the spatial resolution is not a critically important factor for assessing the isostatic response to the denudational model.

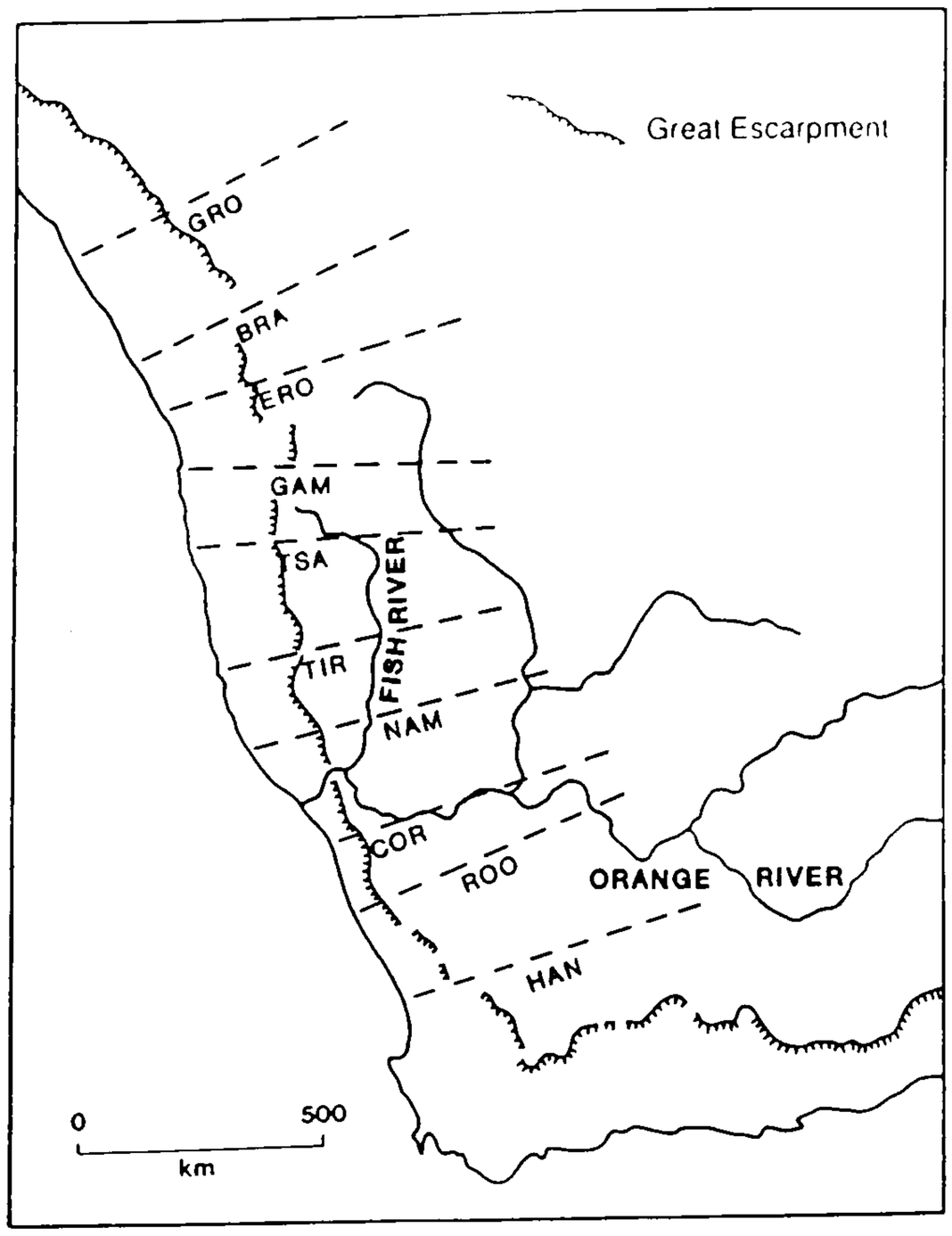

Fig. 4.1. The study area in south-western Africa showing the location of the Great Escarpment and the topographic profiles discussed in the text. The designation for each profile is derived from the first three letters of the marginal upwarp mountains which the profile traverses: GRO-Grootberg; BRA-Brandberg; ERO-Erongoberge; GAM-Gamsberg; TSA-Tsarisberge; TIR-Tirasberge; NAM-Namisberg; COR-Cornellberg; ROO-Rooiberg; HAN-Hantamsberg. The topographic profiles are used as scales in the following photographic figures.

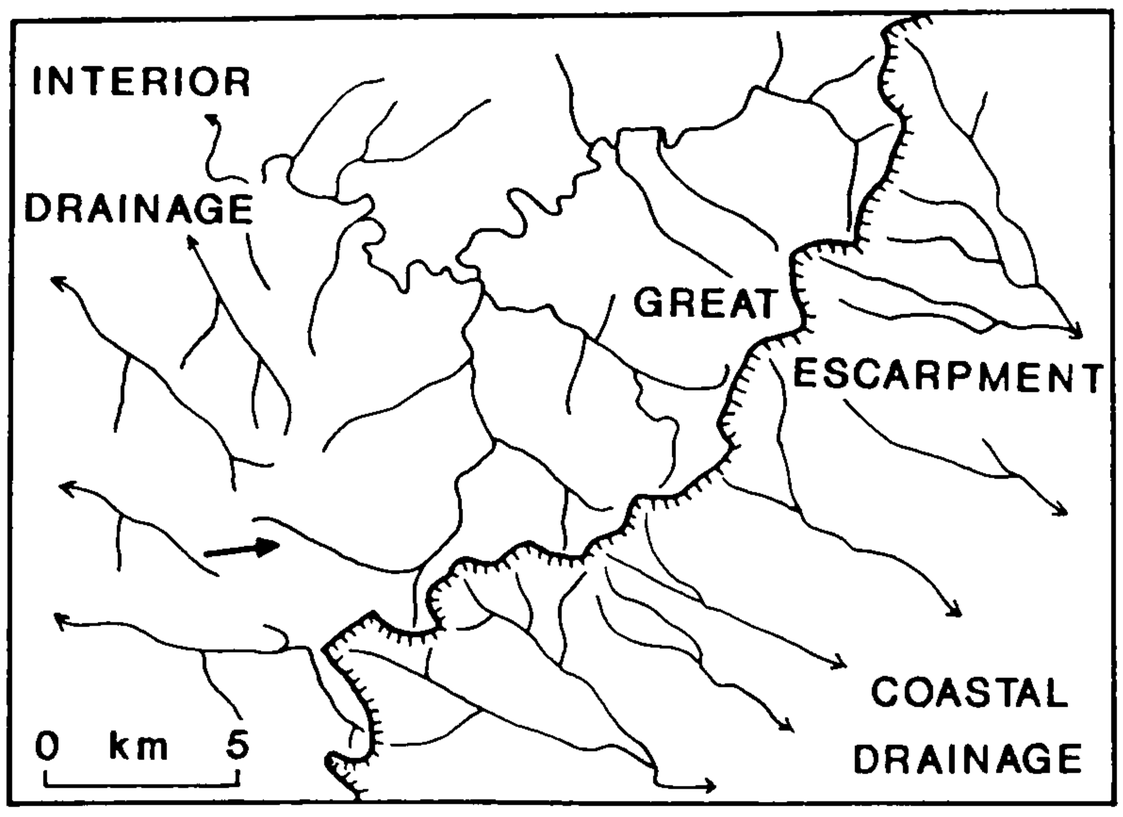

Fig. 4.2. Location of the drainage divide, which coincides with the Great Escarpment, separating Atlantic and Indian Ocean draining catchment areas, from the summit of Thabana Ntlenyana (3482 m), Lesotho. The map shows the main morphological features depicted in the photo overleaf and its orientation. Data from 1:250000 map of South Africa.

Fig. 4.2. Continued from previous page.

Fig. 4.3. The Great Escarpment, delineated by basalt lava flows of the Lebombo Group, from Sani Pass (2874 m), Lesotho. The road traversing the lower half of the photo gives a scale.

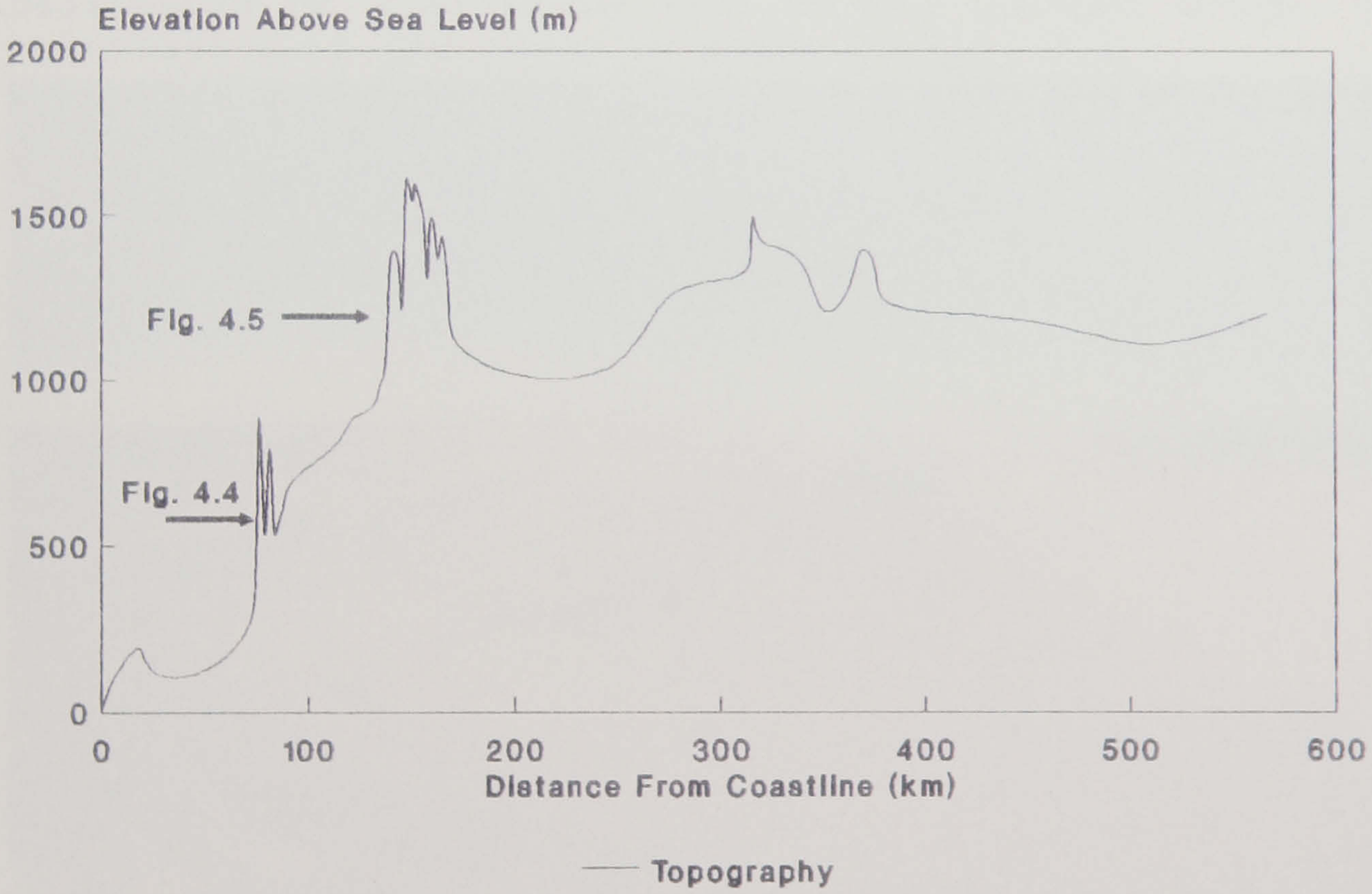

Fig. 4.4. The lower escarpment on the HAN profile, location on Fig. 4.1, delineated by the Table Mountain (sandstone) Group of the Cape Supergroup. The accompanying topographic profile indicates the orientation of the photograph, with respect to the points of a compass, and its location on the profile. This system provides a scale for reference and has been used throughout this chapter. The orientation of the photo in Fig. 4.5 is also shown.

Fig. 4.5. The upper escarpment on the HAN profile delineated by a dolerite sill of the Lebombo Group. The orientation of the photo is shown in Fig. 4.4.

Fig. 4.6. The Great Escarpment on the TIR profile delineated by thin caprocks of the Nama System overlying the Namaqualand Granite-Gneiss Complex. The location and orientation of the photograph are shown overleaf.

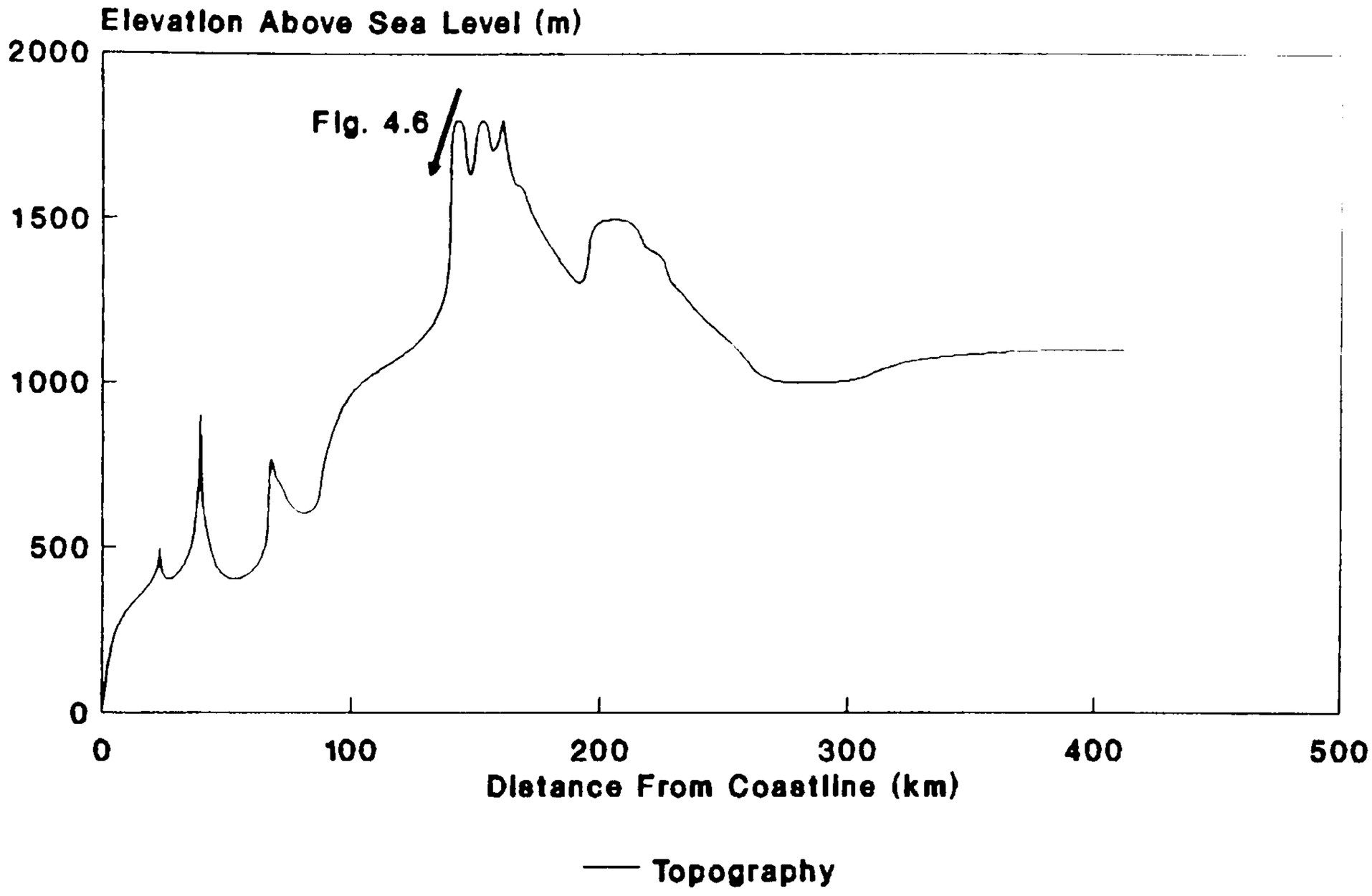

Fig. 4.6. Continued from the previous page.

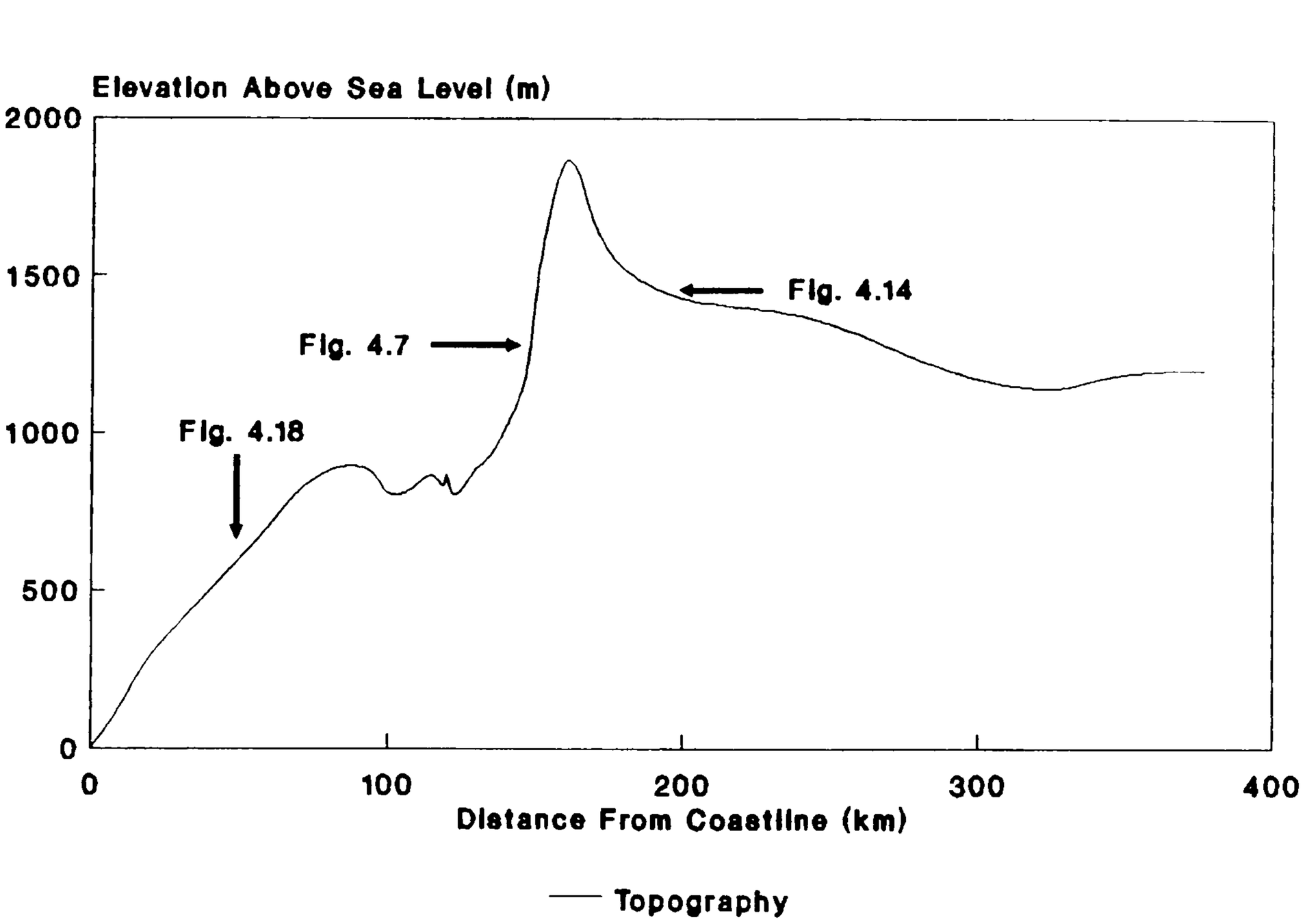

Fig. 4.7. Location and orientation of the photograph shown overleaf plus Figs. 14 and 18.

Fig. 4.7. Continued. Uniform stream spacing incising the Great Escarpment, delineated by Nama System caprocks, on the TIR profile. The location and orientation of the photograph are shown on the previous page.

Fig. 4.8. Irregular incision of the Great Escarpment, delineated by basalt lava flows of the Lebombo Group, in the Drakensberg, Natal, South Africa. On the right is Cathedral Peak (3004 m) and the obvious horizontal line of vegetation in the lower half of the photo is at ≈1900 m.

Fig. 4.9. The Great Escarpment on the ROO profile delineated by structural planes in the porphyritic granite of the Spektakel Suite.

Fig. 4.10. The Great Escarpment on the BRA profile delineated by the seawards face of the Brandberg inselberg, which is composed of granite.

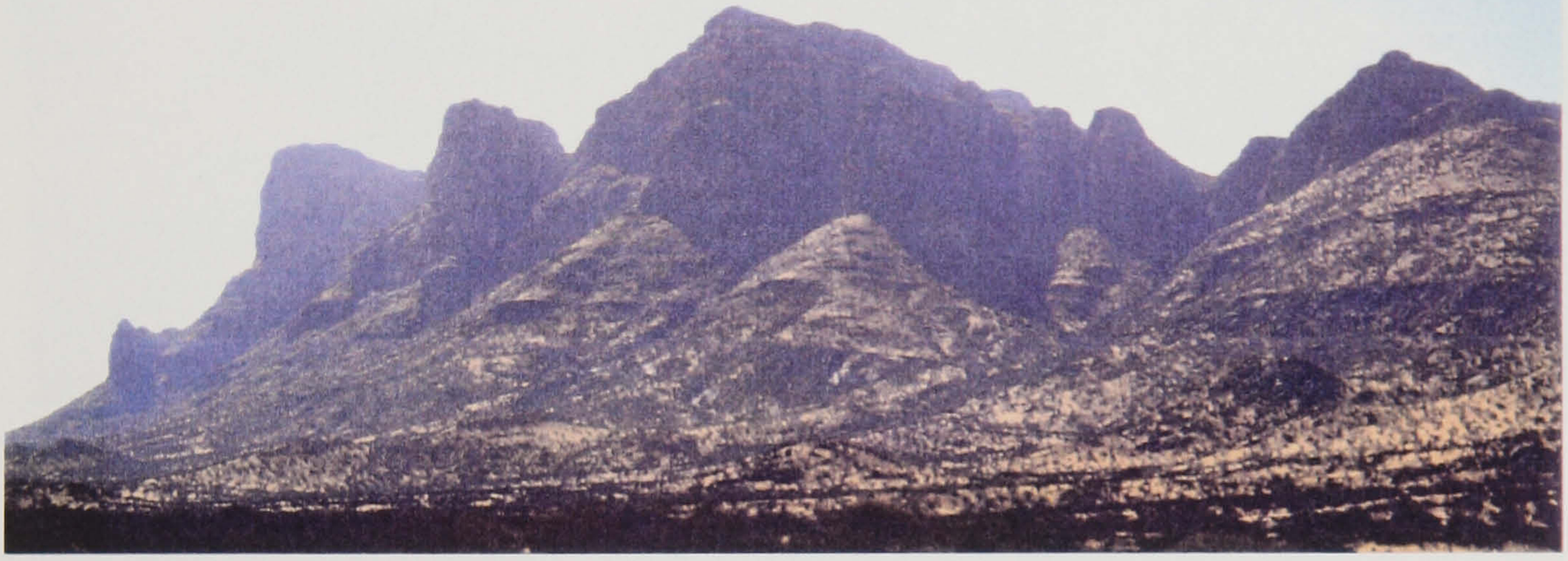

Fig. 4.11. The Great Escarpment on the ERO profile delineated by basalt lava flows of the Stormberg Series.

Fig. 4.12. Low local relief of the continental interior catchment. The orientation of the photo is shown in Fig. 4.9.

Fig. 4.13. The Etosha Pan on the GRO profile. Note the ungulate footprints in the foreground.

Fig. 4.14. Fluvial incision, through the caprocks of the Nama System on the TSA profile, at the headwaters of the Fish River. The orientation of the photo is shown in Fig. 4.7.

Fig. 4.15. Fluvial incision in the confluent zone of the Fish River, Fish River Canyon, Namibia. At this point the Canyon is ≈500 m deep and ≈10 km wide.

Fig. 4.16. The Augrabies Gorge on the Orange River, South Africa. At this point the gorge is ≈200 m deep.

Fig. 4.17. Fluvial incision of the coastal catchment area on the GAM profile. The local relief is relatively high with respect to the continental interior catchment shown in Fig. 4.12.

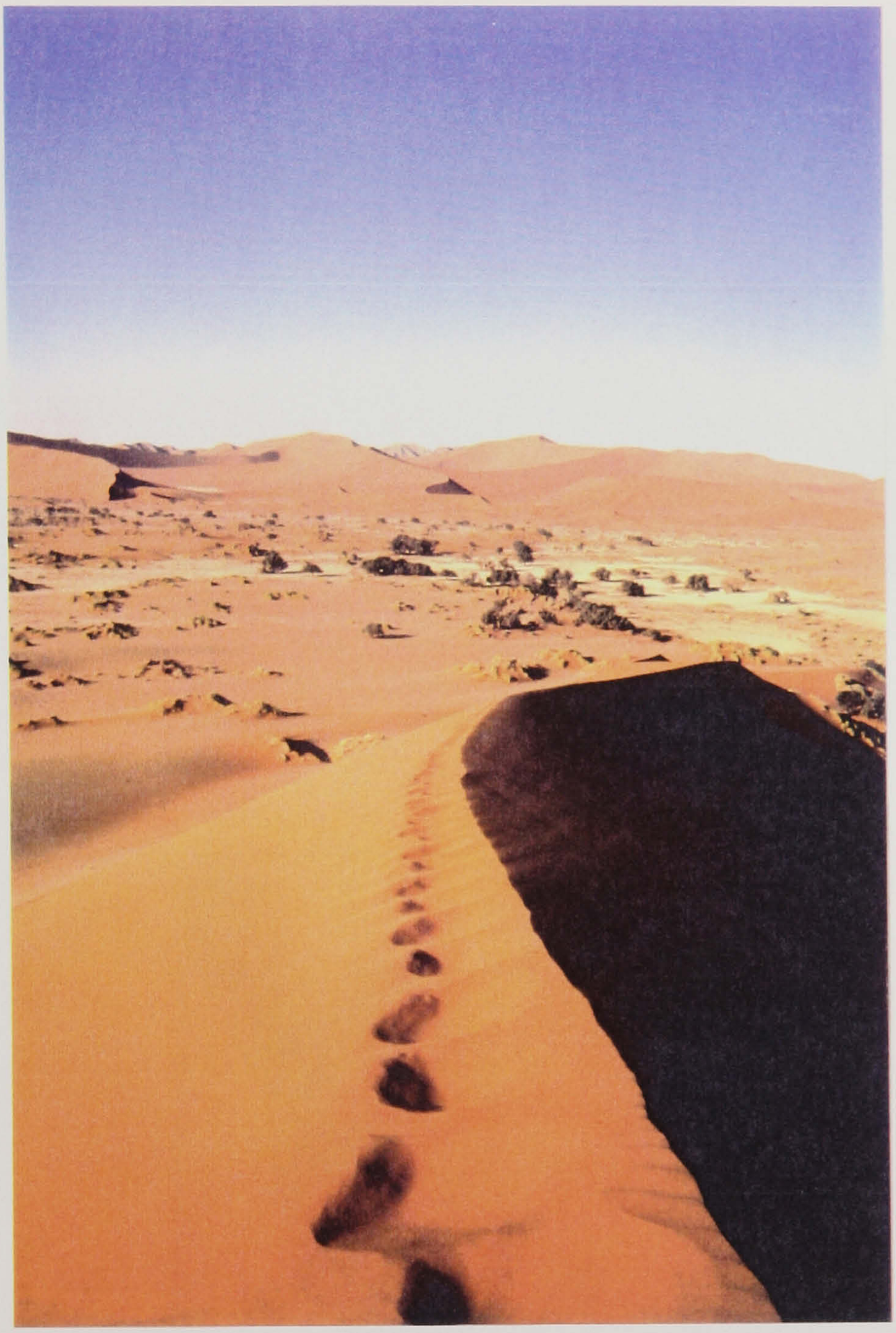

Fig. 4.18. The Namib Sand Sea , Sossusvlei, Namibia. Note the vehicles by the trees, middle right, for scale. The orientation of the photo is shown in Fig. 4.7.

Fig. 4.19. Structurally controlled drainage due to a pre-existing fault on the ROO profile. Note the different colour of the bedrock either side of the valley floor due to bedrock displacement. The orientation of the photo is shown in Fig. 4.9.

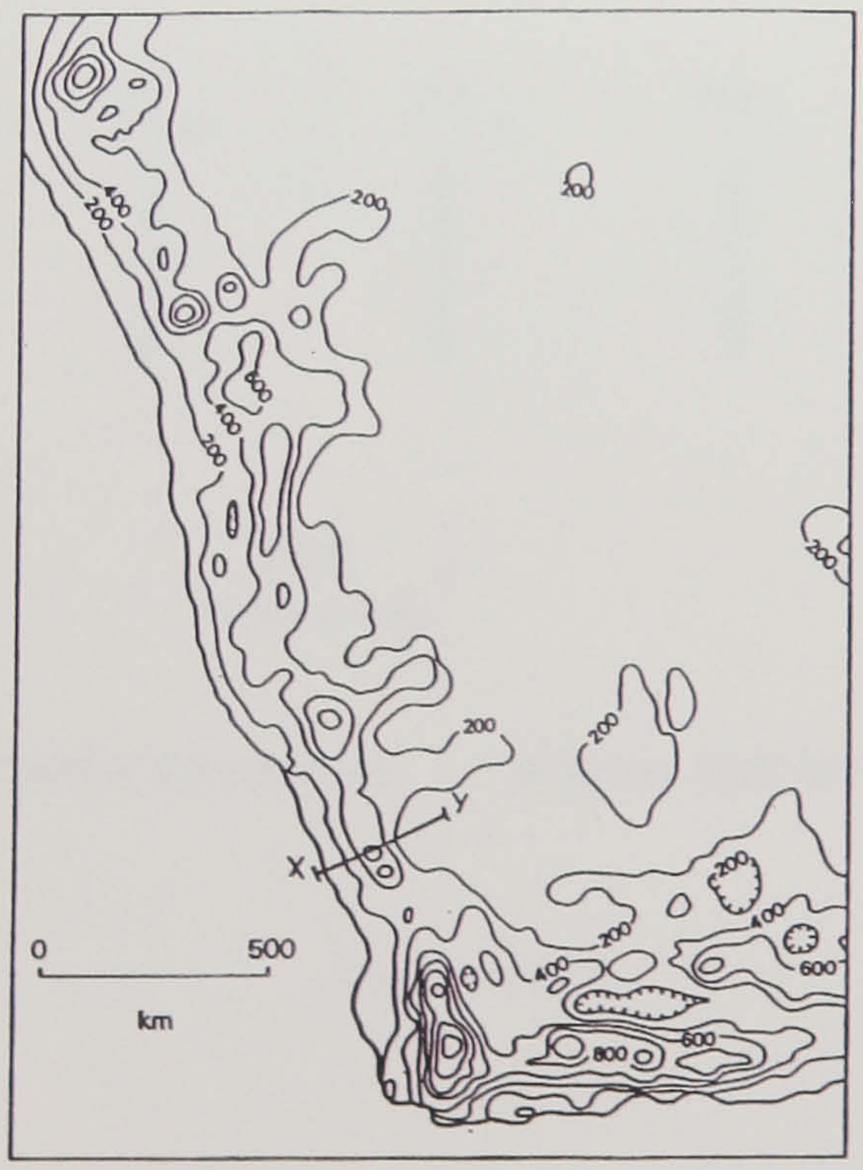

Fig. 4.20. Local topographic relief (m) of south-western Africa. Data derived from the 10-minute digital data set from the National Geophysical Data Center, Boulder, Colorado.

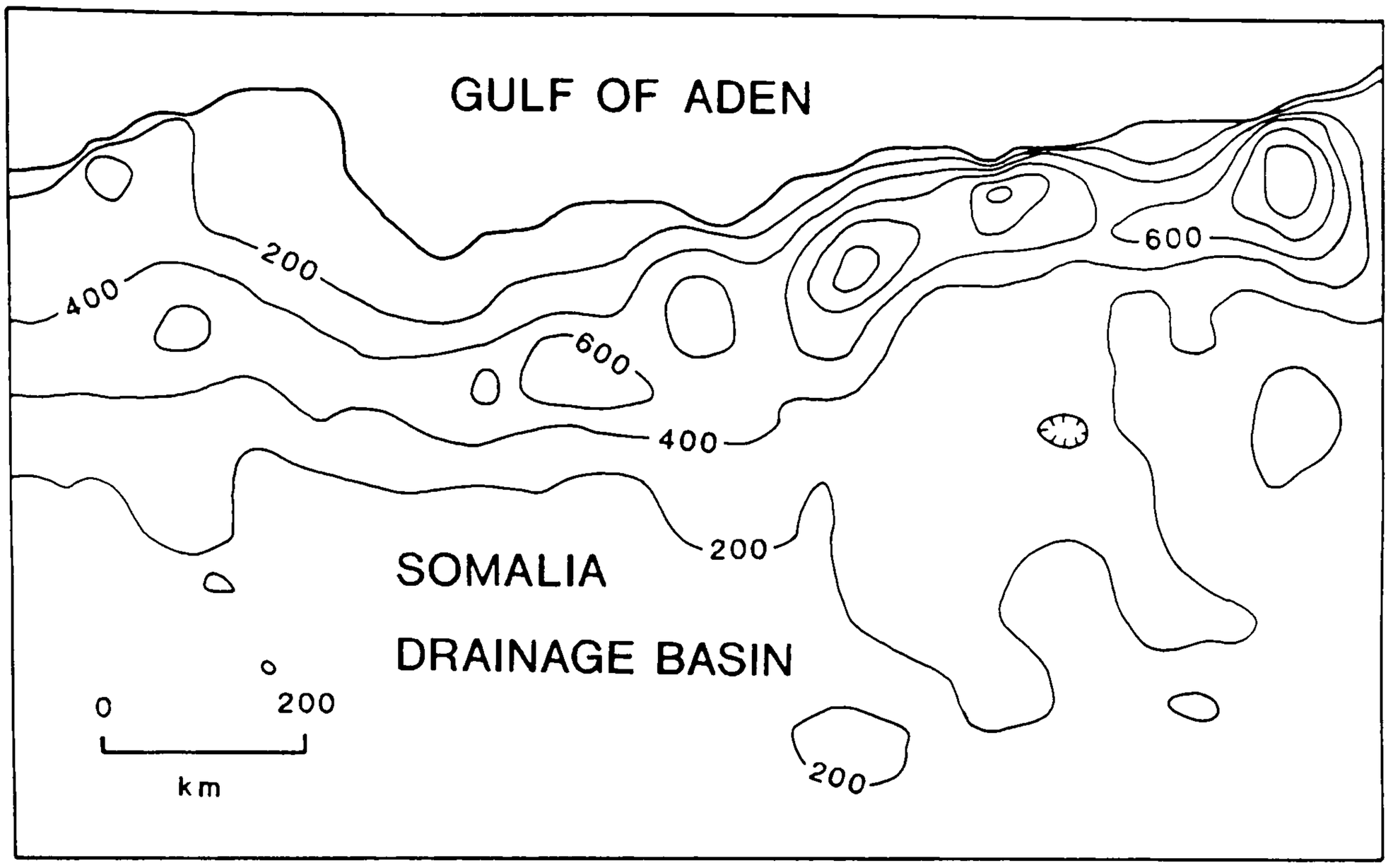

Fig. 4.21. Local topographic relief (m) of the Somalia drainage basin south of the Gulf of Aden. The rift was initiated ≈40 Ma BP (Bohannon et. al., 1989). Data source as in Fig. 4.20.

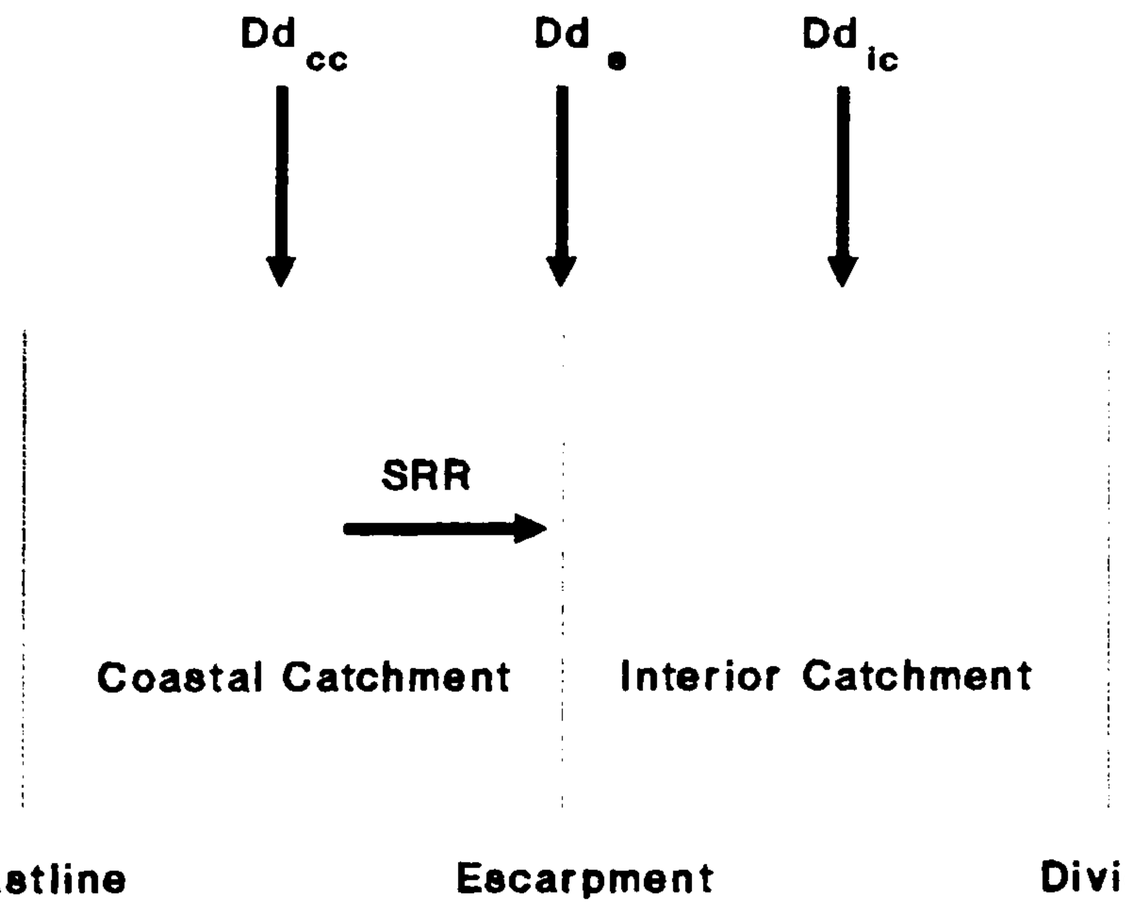

Fig. 4.22. Conceptual denudational model for high-elevation passive margins. Abbreviations: Dd_{cc}-coastal catchment denudation rate; Dd_{e}-escarpment denudation rate; Dd_{ic}-interior catchment denudation rate; SRR-escarpment retreat rate.

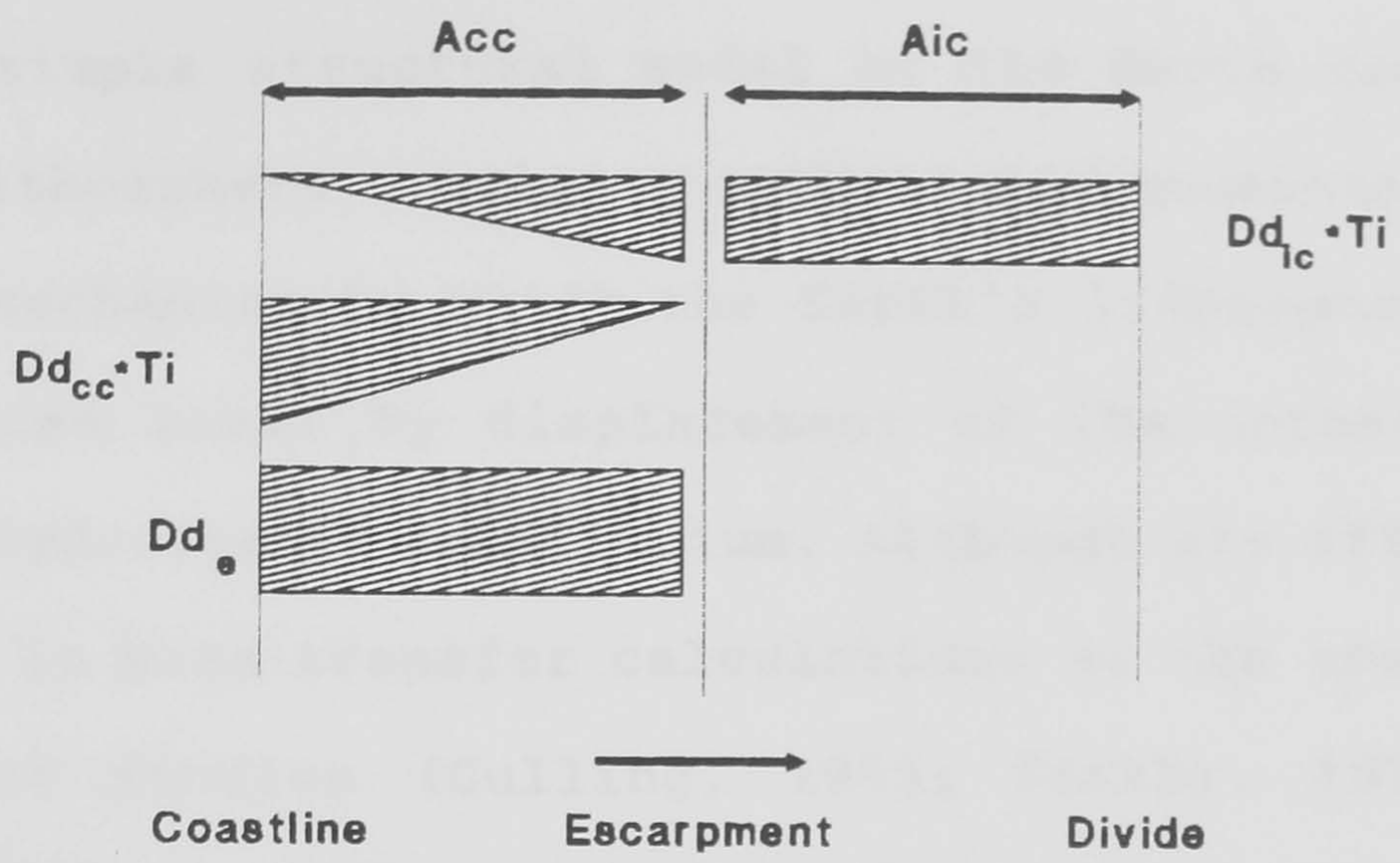

Fig. 4.23. Quantitative denudational model calibration. Abbreviations: T_i-Run time of model; A_{cc}-coastal catchment area; A_{ic}-interior catchment area. Other parameters as in Fig. 4.22.

5 ISOSTASY OF PASSIVE MARGINS

5.1 Introduction

A simple structural model of the Earth consists of a solid lithosphere overlying a fluid asthenosphere. Isostasy is the mechanism by which the Earth's lithosphere responds to applied loads by displacement of the asthenosphere to attain hydrostatic equilibrium. Although its effects can be ignored in mass transfer calculations at the scale of small catchment studies (Culling, 1965; Kirkby, 1971; Ahnert, 1973; Kirkby, 1986; Anderson and Humphrey, 1989), at the macroscale of regional denudation, isostatic restoring forces are an integral part of the mass transfer system. It has, for example, long been acknowledged that the isostatic response to denudational unloading significantly increases the time required to reduce the mean elevation of a landscape by a specific amount (Gilluly, 1955; Schumm, 1963, 1977; Holmes, 1965; Ahnert, 1970). Moreover, the spatial and temporal characteristics of isostatically induced landsurface deformation in response to ice sheet unloading and lake desiccation have provided important data for the estimation of sub-lithospheric mantle properties (Peltier and Andrews, 1976; Mörner, 1980; Bills and May, 1987). Other aspects of the nature of isostasy, principally the regional compensation of loads by flexure, have been determined from lithospheric load studies (Walcott, 1970a; Watts et al., 1975; McKenzie and Bowin, 1976; Watts, 1978; Forsyth, 1985).

5.2 Historical Application of Isostasy to Models of Landscape Evolution

The geomorphological literature reveals a fundamental misunderstanding of the way in which the lithosphere responds to applied loads at the spatial and temporal scales relevant to landscape evolution. In particular, the notion that isostatic uplift in response to continuous denudation over cyclic time scales (10^6 a) is episodic in nature has become firmly established in the literature.

The significance for models of landscape evolution of supposedly discontinuous isostatic adjustment to denudational unloading was first systematically considered in the co-published papers by King (1955) and Pugh (1955), in the context of escarpment retreat from passive margins. King (1955) argued that the retreat of escarpments from the coastlines of Africa initiated by the break up of Gondwana would have resulted in unloading of the crust along the coastal hinterlands coupled with crustal loading by sediment deposition offshore. The isostatic response should thus hinge about this coastal zone with uplift inland and subsidence offshore. Noting that the marginal upwarp which characterises much of the coastal hinterland is around 400 km wide, and that the continental shelf is about 80 km in width, King (1955) pointed out that the total span of the zone affected by isostatic adjustment is approximately the same as the estimate of 480 km by Gunn (1949) "for the length of the circumferential arc that cannot be rigidly supported by the Earth's crust for more than a limited

period". From this King concluded that isostatic recovery only commences once a threshold distance of escarpment retreat has occurred and that, consequently, a sequence of erosion cycles could be generated by this episodic isostatic response. Pugh (1955) similarly interpreted Gunn's summary of isostasy to mean that isostatic recovery was delayed until a critical width of denudation had occurred. Both authors correlated the hypothetical elevations of erosion surfaces subject to episodic isostatic uplift with the actual altitude of erosion surfaces in Africa assumed to be associated with distinct denudational cycles.

Subsequently, Carson and Kirkby (1972) reiterated this interpretation of isostatic adjustment to escarpment retreat and, following Pugh (1955), asserted that whereas the isostatic response to vertical lowering of a landscape (as in Davisian peneplanation) will be almost immediate, there is a threshold of lateral denudation (associated with scarp retreat) before isostatic adjustment occurs. In a detailed assessment of landscape development in southern Africa supporting episodic post-Gondwana surface uplift parallel to the continental margin, Partridge and Maud (1987) have concluded that "any workable model [of surface uplift] must involve an episodic, isostatic response both to the recession of the Great Escarpment on the one hand and to concomitant sedimentation of the continental shelf on the other". Furthermore, they suggest that their hypothesised Late Pliocene surface uplift of up to 900 m

may be attributable in part to a delayed isostatic response to the load imbalance between onshore denudation and offshore sedimentation created during the 'African' cycle of erosion which was terminated at the end of the Early Miocene.

The notion of episodic isostatic uplift in response to long-term denudational unloading has now become widely accepted by the geomorphological community, as is illustrated by its inclusion in widely used text books (Chorley et al., 1984; Selby, 1985). The idea, however, is based on a fundamental misunderstanding of the principles of isostasy as outlined by Gunn (1943, 1949) and elaborated by later workers.

5.3 Models of Isostasy Applicable to Landscape Evolution

The seminal review of Gunn (1949) was focused specifically on a model of isostasy involving a strong elastic lithosphere supported by weak underlying asthenosphere. Referred to as the theory of 'isobaric equilibrium' by Gunn, this model, which has subsequently become known as flexural isostasy, considers local 'Airy' isostasy as a special case where the lithosphere has no lateral strength when subject to a load. This was developed to help explain gravity anomalies.

More recent work has led to the development of two distinct flexural models describing deformation of the lithosphere during loading (denudation representing a negative load). The elastic plate model, as outlined by

Gunn (1949), assumes that the lithosphere can be represented by an elastic lithospheric plate overlying an inviscid asthenosphere, where the isostatic response to a single loading event is instantaneous and therefore does not exhibit time-dependent behaviour. By contrast, in the Maxwell viscoelastic model the lithosphere behaves elastically at short time scales but deforms as a viscous fluid over long periods of time (Walcott, 1970b). As demonstrated by the response of the lithosphere to the unloading of ice sheets and evaporation of lakes, time-dependent behaviour is only relevant at time scales of the order of 10^4 -10^5 a (Mörner, 1980). Consequently, for changes in load, such as that associated with long-term denudation, which occur over much longer time spans in excess of 10^4 a, the elastic model of flexural isostasy is adequate for predicting the response of the lithosphere to loading events (Karner et al., 1983).

The elastic plate model represents the response to an applied load in terms of the elastic bending resistance of the lithosphere and the buoyancy forces acting upon it. This can be expressed by the equation;

$$\frac{d^2}{dx^2}\left[\frac{D d^2 W}{dx^2}\right] + (\rho_a - \rho_1) g W = l(x) \qquad (5.1)$$

where W is vertical flexure, D is flexural rigidity, ρ_a is mantle density, ρ_1 is flexure infill density, g is

acceleration due to gravity and $l(x)$ is the load as a function of horizontal distance x (Nadai, 1963). Thus, on application of a load, flexural deformation extends beyond the load boundaries due to the elastic bending resistance of the lithosphere and the load is said to be regionally compensated (Fig. 5.1a). The spatial distribution of the flexural response is dependent on the flexural rigidity (D) of the elastic plate where;

$$D = \frac{ET_e^3}{12(1-\nu^2)} \qquad (5.2)$$

and E is Young's modulus, T_e is the effective elastic thickness of the lithosphere and ν is Poisson's ratio. For a higher flexural rigidity the vertical displacement below an applied load is less, but the deformation occurs over a larger area. The Airy model is thus simply a special case of the elastic plate model where the flexural rigidity of the lithosphere is assumed to be zero, and the applied load is totally compensated locally due to the displacement of the immediately underlying asthenosphere (Fig. 5.1b).

The degree of load compensation (C) is defined as the ratio of the deflection of the lithosphere to its maximum, or hydrostatic, deflection (Turcotte and Schubert, 1982). It relates the flexural deformation of the lithosphere to the applied periodic load of wavelength μ, and is given by the following equation.

$$C = \frac{\rho_m - \rho_l}{\rho_m - \rho_l + (D \div g)(2\pi \div \mu)^4} \qquad (5.3)$$

When C = 1.0 the load is compensated locally according to the Airy isostatic model (Fig. 5.1b). When C = 0.0 the isostatic system behaves rigidly and a load is supported by the lateral strength of the lithosphere (Fig. 5.1c). Between these two extremes loads are compensated both by elastic bending resistances and by buoyancy forces.

Using the elastic plate model parameters of Gunn (1949) [$E=1.2\times10^{11}$ Nm^{-2}, $T_e=50$ km, $v=0.25$, $\rho_m=3100$ kgm^{-3}, $\rho_l=0$ kgm^{-3} and $g=9.8$ ms^{-2}] yields the compensation function shown in Figure 5.2. This illustrates that for a T_e value of 50 km, an applied periodic load is 50% compensated (C=0.5) when $\mu\approx480$ km. Periodic loads of greater wavelength are only partially supported by the rigidity of the lithosphere, whereas shorter wavelength loads are substantially supported. There is consequently a continuous spatial variation in the degree of load compensation dependent on the wavelength of the applied load. Hence there is not, as suggested by King (1955) and Pugh (1955), a lateral threshold of unloading before isostatic readjustment is initiated.

Varying the elastic thickness of the lithosphere changes the form of the compensation function, and thus the isostatic response to a loading event (Fig. 5.2). For a T_e

of 20 km an applied periodic load is 50 per cent compensated (C=0.5) when μ≈250 km. For a similarly compensated load with a T_e of 60 km then μ≈575 km. Recently, the wide variation in the effective elastic thickness of continental lithosphere has become appreciated. T_e values in Africa, for instance, range from an estimated 5-10 km for the rifted lithosphere below the Cape Basin in south-western Africa (Karner and Watts, 1982) to 64-90 km in the cratonic interior (Ebinger et al., 1989). Similarly, in North America the effective elastic thickness of the lithosphere varies from a minimum of ≈4 km in the Basin and Range Province to ≈128 km in the cratonic core of the continent (Bechtel et al., 1990).

Isostatic compensation is only episodic on the time scale of small, individual crustal displacements along faults in response to progressive loading. It exhibits lags in response to applied loads only on the time scale of sub-lithospheric mantle flow, that is over periods of the order of 10^4 -10^8 a. Over the time scale of landscape evolution isostatic compensation occurs continuously, but in a manner dependent on the relationship between flexural rigidity (characterized by effective elastic thickness) and the wavelength of applied loads.

5.4 Isostatic Properties of Passive Margins

Since rifted passive margins represent the trailing edges of continents (Bond and Kominz, 1988), they consist of three components when break up occurs and new oceanic

lithosphere is produced at mid-oceanic ridges (Fig. 5.3): (1) Oceanic lithosphere; (2) rifted continental lithosphere; and (3) unrifted continental lithosphere. The flexural properties of oceanic and continental lithosphere have previously been investigated by studying the response of the lithosphere to surface loads such as seamounts, oceanic islands, sediments, extension on major faults and the relationship between gravity and surface/subsurface topography (Watts et al., 1982). The results of such studies are briefly discussed below.

5.4.1 Oceanic Lithosphere

Watts (1978) considered the deformational response of oceanic lithosphere in response to surface loads of different ages. He found that this isostatic system could be represented by an elastic plate model where the rigidity of the plate increases with age. Characterising the rigidity in terms of the effective elastic thickness (T_e) of an elastic plate, he concluded that this corresponded approximately to the 450 'C isotherm of a cooling plate model (Fig. 5.4). This gave a T_e of 0 km at the time of formation to a T_e of ≈30 km for 100 Ma old oceanic lithosphere.

5.4.2 Rifted Continental Lithosphere.

Gravity studies suggest that the flexural rigidity of rifted continental lithosphere increases with age after rifting (Karner and Watts, 1982). On the basis of load

deformation data (Watts et al., 1982; Watts, 1982) it has been concluded that the rigidity of rifted continental lithosphere increases with age in a similar fashion to oceanic lithosphere, after asthenospheric upwelling during crustal thinning/rifting (McKenzie, 1978). The implication is that an Airy isostatic model is applicable early in the history of the margin, when the rifted continental lithosphere is weak due to the thermal perturbation, but its flexural strength increases with age. This view has been challenged on the basis of rheological considerations by White and McKenzie (1988) who argue that, "only the top few kilometres of the continental lithosphere can maintain elastic stresses over significant periods of time". Numerical models which consider the fault geometry and sedimentation within rift basins (Kusznir et al., 1987; Kusznir and Egan 1989; Marsden et al., 1990; Kusznir et al., 1990) indicate that the flexural rigidity of the lithosphere is an important variable in determining basin geometry. Numerical modelling of the northern North Sea basin (Marsden et al., 1990) indicates that a T_e of $\leq$ 6 km is required to model the evolution of the rift. Other studies indicate that the T_e of the lithosphere remains $\leq$ 5 km during the post-rift phase (Nunn and Sleep, 1984; Barton and Wood, 1984). A possible explanation is that rifted continental lithosphere remains flexurally weak due to faulting (Beaumont et al., 1982). Such values of T_e cited above are much less then the thickness of the brittle upper crust. It has been suggested that flexural bending

stresses, due to crustal extension on planar faults, are large enough to cause brittle failure in the upper crust, and so decrease the T_e of continental lithosphere after rifting (Kusznir et al., 1990; Fig. 5.5).

The spatial/temporal deformational response of rifted continental lithosphere is incompletely understood at present. However, it would appear that flexure is an important consideration in rifted basin evolution, and that in general the rigidity of rifted continental lithosphere is probably less than that of oceanic lithosphere with the same thermal age.

5.4.3 Unrifted Continental Lithosphere

The study of the relationship between topography and gravity has been extensively used to determine the flexural rigidity of continental lithosphere (Forsyth, 1985). Different approaches have been used but they generally indicate that the flexural rigidity of unrifted continental lithosphere is higher than that of rifted continental lithosphere. Cratonic areas of Africa have a T_e of ≈64-90 km (Ebinger et al.,1989), those of Australia a T_e of up to ≈130 km (Zuber et al., 1989), while the Canadian Shield has a T_e of up to ≈123 km (Bechtel et al., 1990). Such areas are relatively stable regions, with tectonic activity concentrated around the periphery of the cratons.

5.5 Discussion of Isostatic Models Previously Applied to Landscape Evolution

From Fig. 5.3 the subaerial domain of passive margins, with which this study is concerned, are generally located on unrifted continental lithosphere. Flexural isostasy is therefore expected to be an important consideration in modelling the isostatic effect of denudational unloading.

Several studies of the isostatic response to denudation on passive margins use 'local' Airy isostasy, for example on eastern Australia (Wellman, 1987). Wellman's rationale is that the physical properties of the lithosphere are poorly known, but simple gravity models indicate that the T_e of eastern Australia is ≈17 km (Zuber et al., 1989). This degree of flexural rigidity will have a significant effect on the relationship between denudation and isostasy.

Lambeck and Stephenson (1986) used a Maxwell viscoelastic model in their analysis of the landscape evolution of the eastern Australia highlands. However, as previously explained, the relaxation time constant of the viscoelastic plate is so small that at the macroscale of regional denudation, over time scales of 10^6 -10^7 a, the elastic plate model gives an adequate solution. This simplified approach will be used in this study.

5.6 Solution of the Elastic Thin Plate Equation

The basic approach follows that outlined by Nunn and Aires (1988). The fourth order differential equation

governing deformation of a loaded elastic plate of finite rigidity is given by equation 5.1. Given discretely sampled data at fixed horizontal intervals (h), equation 5.1 can be approximated by finite difference methods using a central difference scheme;

$$\frac{dW}{dx} = \frac{W_{i+1} - W_{i-1}}{2h} \qquad (5.4)$$

$$\frac{d^2W}{dx^2} = \frac{W_{i+1} - 2W_i + W_{i-1}}{h^2} \qquad (5.5)$$

$$\frac{d^4W}{dx^4} = \frac{W_{i+2} - 4W_{i+1} + 6W_i - 4W_{i-1} + W_{i-2}}{h^4} \qquad (5.6)$$

where W and D are discretely sampled at point x_i. Substituting equation 5.5 into equation 5.1 and rearranging gives the following.

$$\begin{aligned}[D_{i+1}W_{i+2} - 2(D_{i+1}+D_i)W_{i+1} \\ + (D_{i+1} + 4D_i + D_{i-1} + (p_i - p_1)gh^4)W_i \\ -2(D_i + D_{i-1})W_{i-1} + D_{i-1}W_{i-2}] = h^4 l_i\end{aligned} \qquad (5.7)$$

Given that the function W_i has n=0, N discretely sampled points there are N+1 simultaneous equations of the form given in equation 5.7. These can be displayed as a five

banded diagonal matrix;

$$
\begin{aligned}
a_{11}x_1 + a_{12}x_2 + \ldots\ldots\ldots\ldots + a_{1n}x_n &= b_1 \\
a_{21}x_1 + a_{22}x_2 + \ldots\ldots\ldots\ldots + a_{2n}x_n &= b_2 \\
\vdots \qquad\qquad \vdots & \qquad\qquad \vdots \\
a_{n1}x_1 + a_{n2}x_2 + \ldots\ldots\ldots\ldots + a_{nn}x_n &= b_n
\end{aligned}
$$

which can be written as;

$$A.x = b \qquad (5.8)$$

where A is the matrix of coefficients and b is a column vector.

$$
A = \begin{bmatrix}
a_{11} & a_{12} & \ldots\ldots\ldots & a_{1n} \\
a_{21} & a_{22} & \ldots\ldots\ldots & a_{2n} \\
\vdots & \vdots & & \vdots \\
a_{n1} & a_{n2} & \ldots\ldots\ldots & a_{nn}
\end{bmatrix}
\qquad
b = \begin{bmatrix}
b_1 \\ b_2 \\ \vdots \\ b_n
\end{bmatrix}
$$

The boundary conditions of the model are as follows.

$$
\begin{aligned}
x = 0 \qquad & W = 0 \qquad & W_0 &= 0 \\
x = 0 \qquad & W' = 0 \qquad & W_{-1} &= W_1 \\
x = \infty \qquad & W = 0 \qquad & W_n &= 0 \\
x = \infty \qquad & W' = 0 \qquad & W_{n+1} &= W_{n-1}
\end{aligned}
$$

The matrix can be solved by Gaussian elimination with back substitution. However, this method is very inefficient

in terms of the internal computer memory required to store the matrix which has dimensions $(N+1)^2$. In fact only the diagonal, plus the two super and sub diagonals, are non-zero. The matrix can therefore be stored more efficiently in banded format. The memory saved is considerable. For a function described by 100 nodes the banded form of the matrix occupies only 5 % of the memory required for the full matrix, and for 1000 nodes it is 0.5 %. However, further savings can be made by exploiting the fact that the matrix is symmetrical about the principal diagonal and so can be represented by a half-banded diagonal matrix. For 100 nodes the half-banded form of the matrix occupies 3 % of the memory required for the full matrix and for 1000 nodes it is 0.3 %. This half-banded matrix was solved using Choleski's decomposition method.

Using this scheme the rigidity across a modelled profile can be varied as a function of horizontal displacement. This can be used to investigate different scenarios for the flexural coupling of rifted and unrifted continental lithosphere across passive margins. From the discussion in section 5.4 it is expected that the flexural rigidity of rifted continental lithosphere is less than that of unrifted continental lithosphere. This isostatic model is formulated in chapter 6.

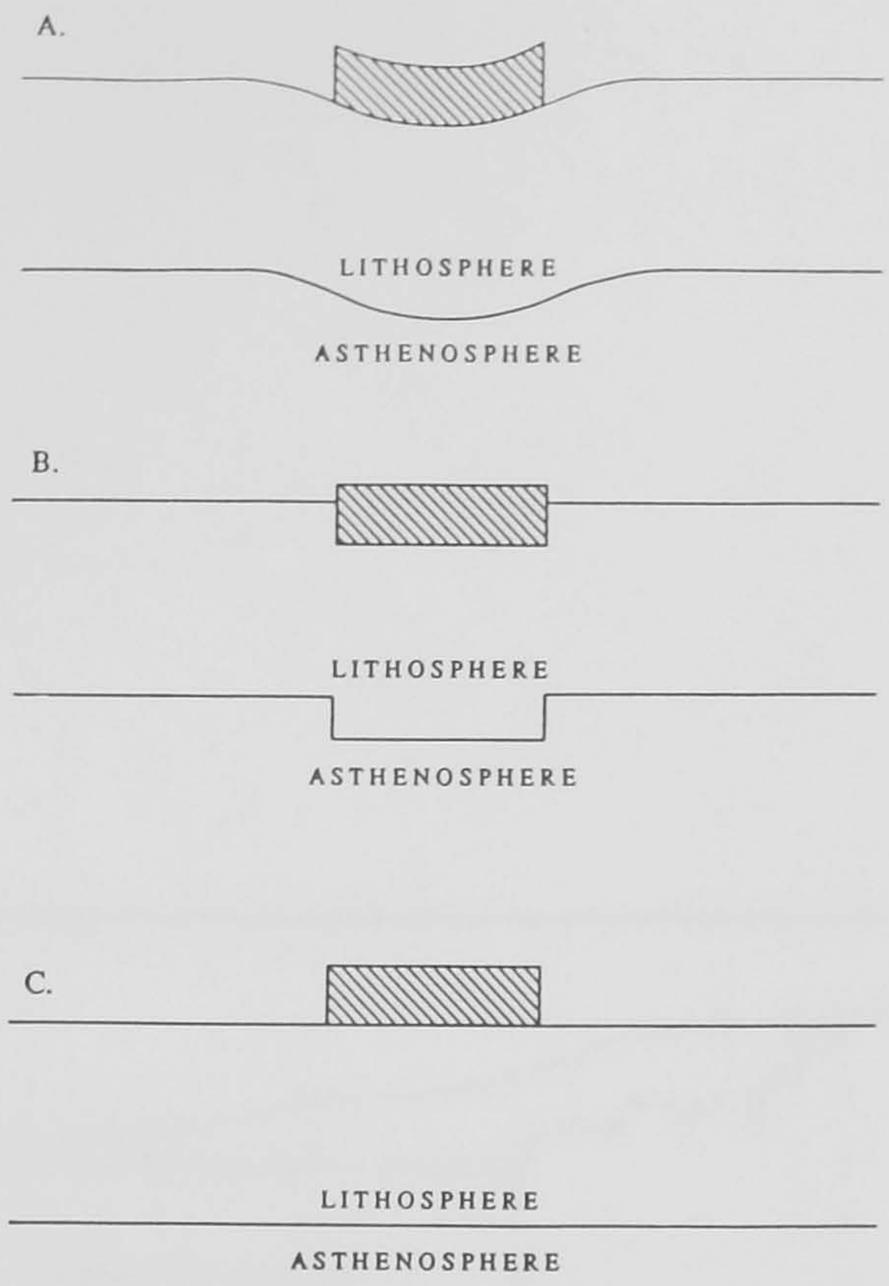

Fig. 5.1. Schematic representations of the response to an applied load of an elastic lithosphere with finite rigidity (a), no lateral rigidity (b), and infinite rigidity (c). Note that denudation is represented by a negative load.

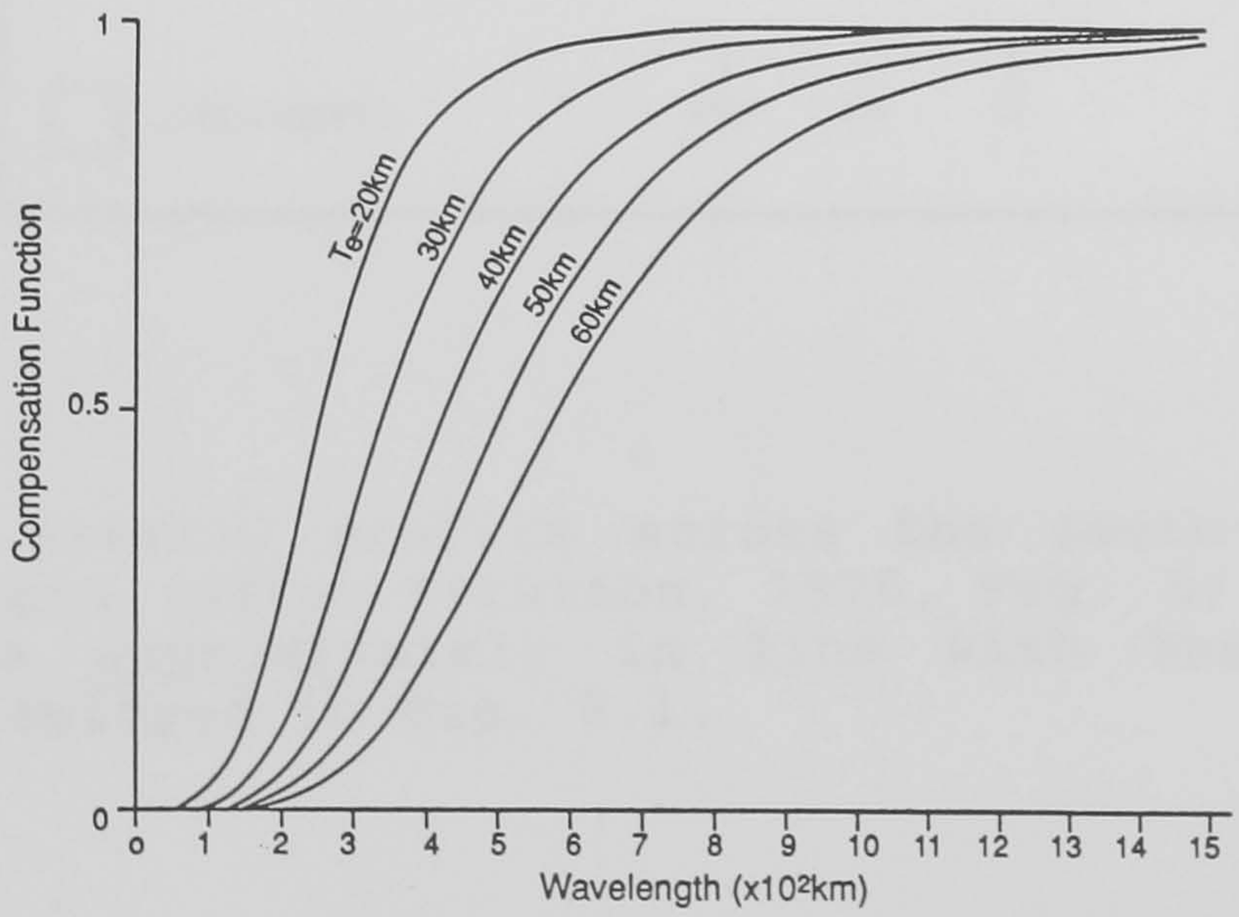

Fig. 5.2. Compensation functions of an elastic lithosphere for a range of effective elastic thicknesses (T_e) and variable wavelength loading. Model parameters are given in the text. The curve for T_e=50 km illustrates the model presented by Gunn (1949).

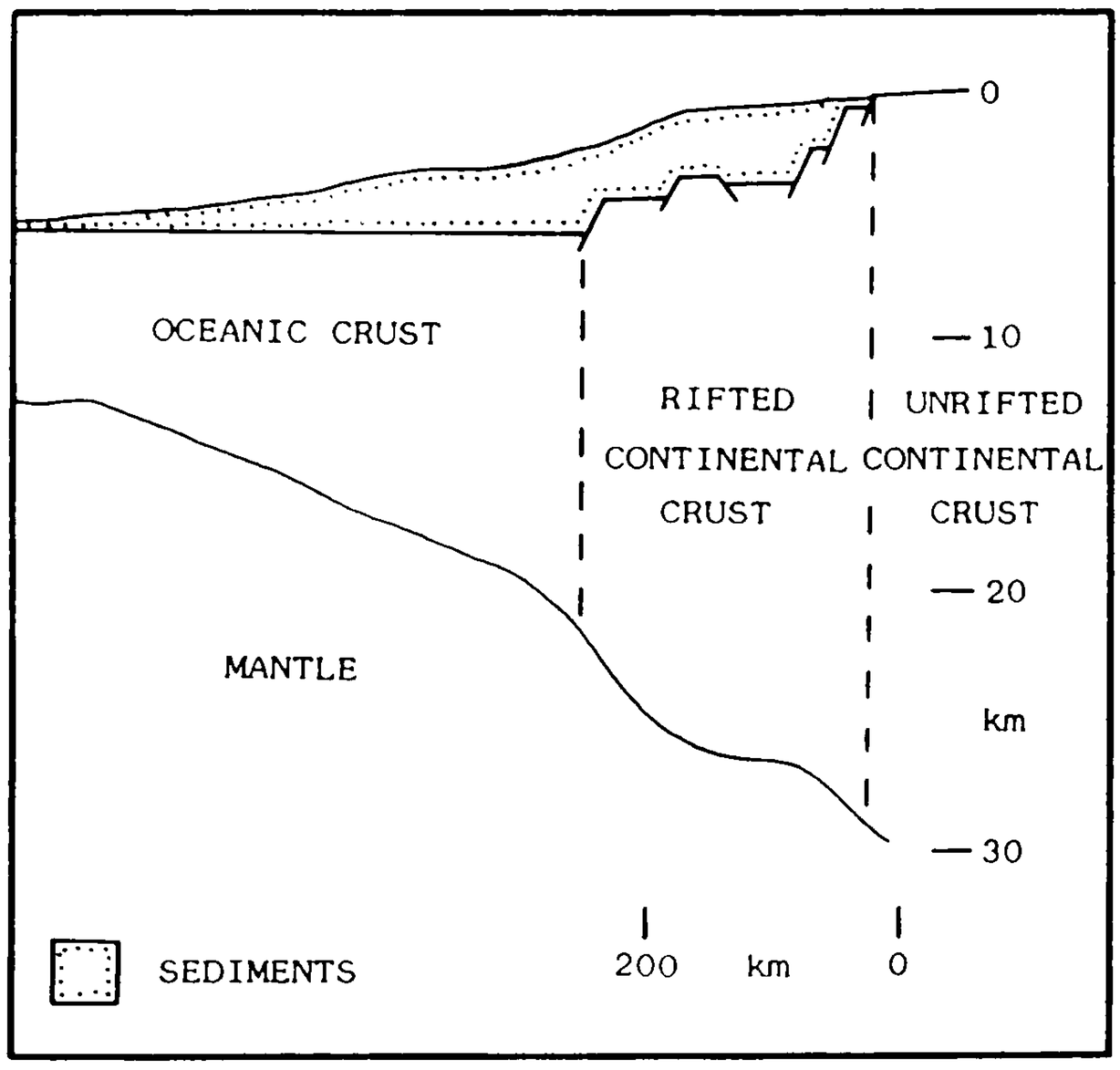

Fig. 5.3. Crustal profile across the south-west African rifted margin (after Scrutton, 1976, Fig. 5). The crustal profile is approximately in line with the topographic profile displayed in Fig. 6.1.

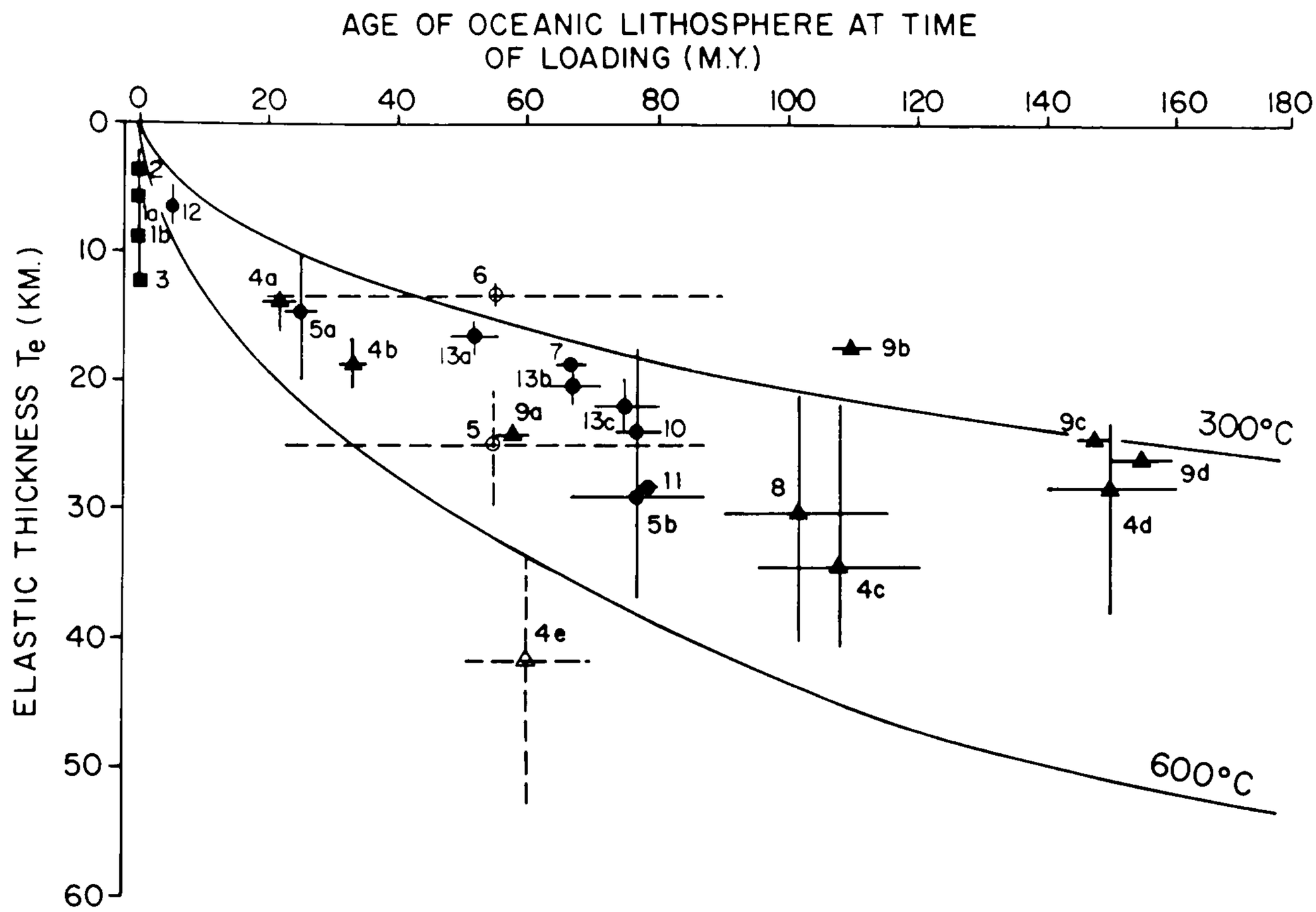

Fig. 5.4. Plot of elastic thickness, T_e, against age of the oceanic lithosphere at the time of loading (after Watts et al., 1980). The estimates of T_e are based on studies of oceanic crustal topography (solid squares), seamounts and oceanic islands (solid circles) and deep sea trench-outer rise systems (solid triangles). The solid curved lines are the 300°C and 600°C oceanic isotherms based on the cooling plate model.

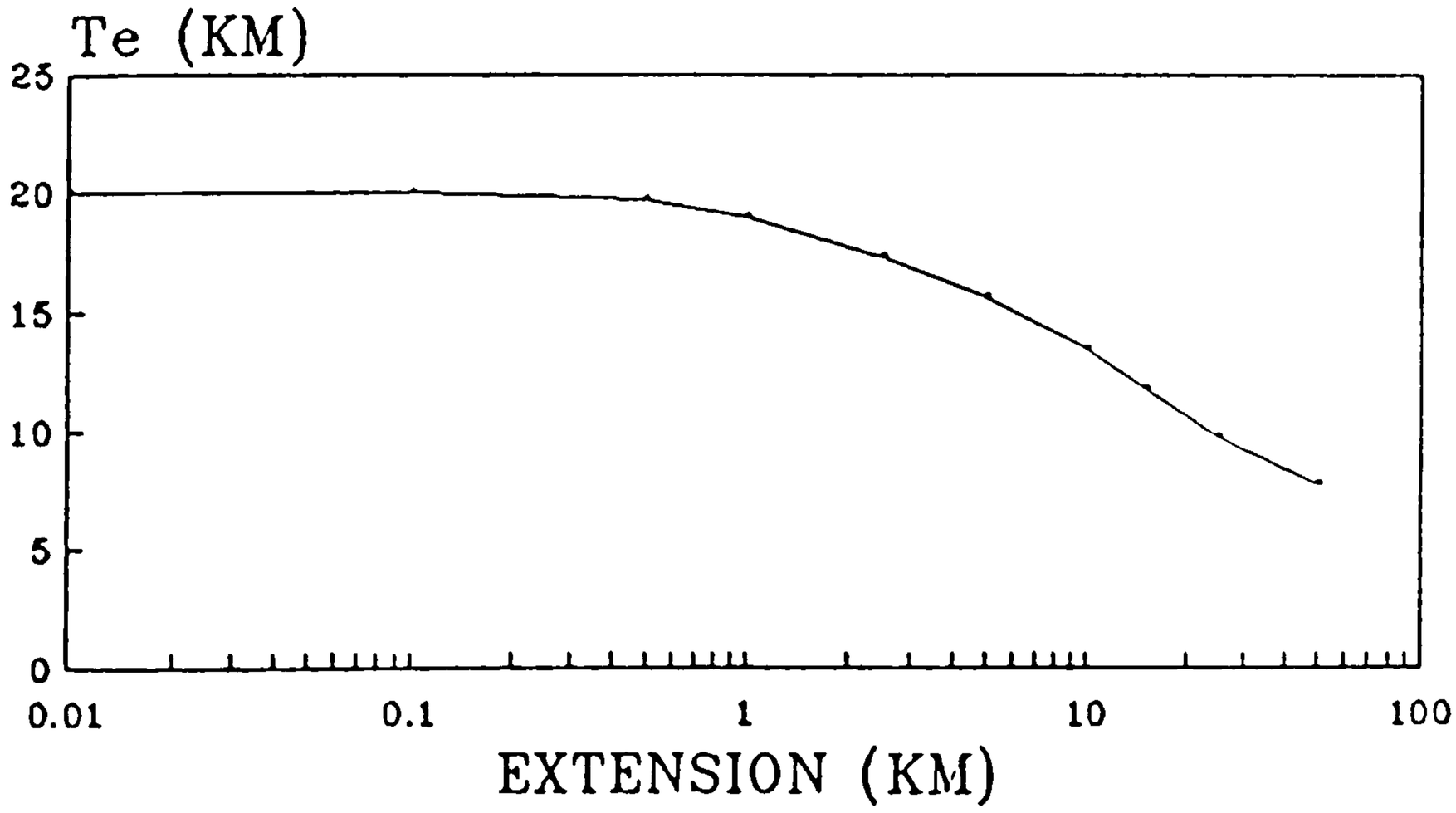

Fig. 5.5. The decrease in T_e with increase in fault extension, predicted by the flexural cantilever model, due to brittle failure generated by flexural bending stresses (after Kusznir et al., 1990).

6 QUANTITATIVE MORPHOTECTONIC MODEL OF PASSIVE MARGIN EVOLUTION

6.1 Introduction

The major factors thought to control the post-rift geomorphological evolution of passive margins have been outlined as the conceptual morphotectonic model in chapter 3. It is postulated that these consist of denudation and offshore sedimentation, coupled with isostasy. This chapter links these components together and formulates a numerical model. This is in order to assess the importance of each effect in influencing the landscape evolution of passive margins. The quantitative morphotectonic model will then be applied to a single topographic profile across the south-west African rifted margin (Fig. 6.1) and the parameters will be changed systematically in order to explore the properties of the model.

6.2 Morphotectonic Model Formulation

The morphotectonic model consists of two parts: (1) Load component; and (2) isostatic component.

6.2.1 Load Component

During the post-rift evolution of passive margins material is denuded from the continental landsurface and deposited offshore in sedimentary basins. Therefore, the mass transfer system, which loads the lithosphere causing an isostatic response, consists of two parts: (1) Onshore

denudation; and (2) offshore sedimentation.

6.2.1.1 Onshore Denudation

A denudational model, applicable to high-elevation passive margins, has been formulated in chapter 4. It consists of a coastal catchment, of relatively high local relief and high denudation rates, separated from the continental interior catchment, of lower local relief and low denudation rates, by an erosional escarpment. This feature, which forms a distinct topographic discontinuity (Fig. 6.2), is assumed to have retreated from the rift hinge to its present position with a constant horizontal velocity (Fig. 6.1). The present position of the escarpment is defined, for modelling purposes, as the base of the erosional escarpment where there is a break in slope and the gradient increases (Fig. 6.3). For the profile in Fig. 6.1 the escarpment retreat rate has been calculated as 630 mMa^{-1}, given that rifting in the Cape Basin began ≈150 Ma BP (Gerrard and Smith, 1980). The vertical denudation rate of the escarpment (Dd_t) is given, in this case, as the current vertical height of the escarpment. Hence, for the topographic profile in Fig. 6.2 Dd_t is ≈900 m. This is assumed to have remained constant throughout the evolution of the rifted margin, in the absence of data indicating otherwise, and will maintain an erosional escarpment 900 m high.

The present drainage basin outlines for southern Africa are shown in Fig. 6.4. Calibration of the

denudational model from equations 4.1 and 4.2 requires the average local relief values for the coastal and interior (Orange) catchment areas (MLR_{cc} and MLR_{ic}), which are 456 m and 191 m respectively for the topographic profile in Fig. 6.1. These values were determined from the 10-minute digital topographic data set of the National Geophysical Data Center, Boulder, Colorado. This data set was also used to calculate the present coastal and interior catchment areas (A_{cc} and A_{ic}) as 685908 km^2 and 914328 km^2 respectively. Given the linear relationship between mean local relief and denudation (Ahnert, 1970), the difference in average local relief values suggest that the present mean denudation rate of the coastal catchment is ≈2.4 times that of the interior catchment.

The volume of material that has been denuded from the present Atlantic draining catchments, since rifting began in the South Atlantic, has been estimated as ≈2.773035x10^6 km^3 (Rust and Summerfield, 1990). Given that the total area of the Atlantic draining catchments (A_{cc} + A_{ic}) is ≈1.6x10^6 km^2 then the average post-rift denudation over the whole of this area has been ≈1.733 km. Employing equations 4.1 and 4.2 the average post-rift coastal catchment denudation rate (Dd_{cc}) and that of the interior catchment (Dd_{ic}) have been calculated respectively as 16.5 and 6.9 mMa^{-1}, for the topographic profile in Fig. 6.1.

6.2.1.2 Offshore Sedimentation

During the syn-rift phase of passive margin evolution

sediments accumulate in restricted fault-bounded sedimentary basins. Subsequently, sedimentation transgresses the syn-rift basins to cover a far greater extent during the post-rift phase (Fig. 1.2). Sedimentation loads the lithosphere and generates subsidence in rifted margin basins. The offshore sediment stratigraphic profile, corresponding to the topographic profile in Fig. 6.1, is shown in Fig. 6.5. This has been used to determine the sediment load for each stratigraphic horizon.

Denuded continental material accumulating in offshore sedimentary basins will compact during burial. Hence, sediments have a non-uniform density with depth. Porosity measures the degree of sediment compaction, and can be defined as the ratio of the pore volume to the total sediment volume. The analysis of Sclater and Christie (1980) assumed that sediment porosity (Φ) experiences a simple exponential decrease with increasing burial depth (Z).

$$\Phi = \Phi_0 e^{-cz} \qquad (6.1)$$

In this equation Φ_0 is surface sediment porosity and C is an exponential constant. In the absence of detailed sedimentological data for the offshore Cape Basin these parameters have been assigned values of 56 % and 3.9×10^{-4} m^{-1} for Φ_0 and C respectively. These correspond to the shaley sand lithology of Sclater and Christie (1980). The shaley sand parameters Φ_0 and C lie between the extremes of the

sand and chalk parameters. A sediment column of constant lithology, with a total volume V_{tv}, is composed of the sediment matrix (V_{ss}) and pore fluid (V_{pf}) volumes (Fig. 6.6).

$$V_{ss} = V_{tv} - V_{pf} \qquad (6.2)$$

If the cross-sectional area of the sediment column is assumed to be unity, then the effective thickness of the sediment column occupied by pore fluid (Z_{pf}) is given by the following integral;

$$Z_{pf} = \int_{Zt}^{Zb} \Phi dZ \qquad (6.3)$$

where Zt is the burial depth to the top of the sedimentary unit and Zb is the burial depth to the bottom of the sedimentary unit. When evaluated, equation 6.3 is given by the following.

$$Z_{pf} = (\Phi_0 \div C)\,[e^{-CZt} - e^{-CZb}] \qquad (6.4)$$

Substituting equation 6.4 into equation 6.2 then;

$$Z_{ss} = (Zb - Zt) - (\,[\Phi_0 \div C]\,\{e^{-CZt} - e^{-CZb}\}\,) \qquad (6.5)$$

assuming no deformation of the sediment matrix.

At each node sampled across the offshore stratigraphic profile (Fig. 6.5), the total mass of material in each horizon has been calculated by combining the sediment matrix and pore fluid masses. The effective thickness of sediment matrix and pore fluid for each horizon in Fig. 6.5 are shown in Fig. 6.7 and Fig. 6.8 respectively. The total mass in each horizon was calculated assuming that the density of pore fluid is 1000 kgm^{-3} and sediment matrix is 2800 kgm^{-3}.

In order to simulate the progressive sediment loading of the lithosphere in the morphotectonic model, the calculated load for each horizon was applied at the chrono-stratigraphic midpoint of that horizon. Thus, from Fig. 6.5 sediment loads were computed for four horizons and applied at 142, 124, 89 and 33 Ma BP during the model run.

6.2.2 Isostatic Component

When the lithosphere is loaded then isostatic compensation occurs, by displacement of the fluid asthenosphere, to maintain the system in equilibrium. This has previously been described in chapter 5. In this study the isostatic response of the lithosphere is modelled as an elastic plate. Two variants will be considered here: (1) Constant rigidity; and (2) laterally variable rigidity.

6.2.2.1 Constant Rigidity

This is the simplest form of the elastic plate model, where the total profile length of the model is assigned the

same flexural rigidity, characterized by the effective elastic thickness (T_e). It has been noted in section 5.4 that the subaerial portion of the south-west African rifted margin is located on unrifted lithosphere, whereas the offshore rifted basins are formed on rifted continental lithosphere, which probably has a lower flexural rigidity due to attenuation and faulting of the continental lithosphere during rifting. It is postulated that this may be important in assessing the isostatic response to loading and so laterally variable rigidity is considered in the next section.

6.2.2.2 Laterally Variable Rigidity

The isostatic component is assumed to consist of two terranes of contrasting flexural rigidity, which coincide with the spatial location of rifted and unrifted continental lithosphere. The unrifted region is assumed to exhibit a higher flexural rigidity then the rifted region, as indicated by gravity and load compensation data (sections 5.4.2 and 5.4.3) and it is assumed that the T_e of each region does not vary spatially or temporally. The T_e of the rifted continental lithosphere is termed T_{e1} and that of the unrifted lithosphere T_{e1}.

6.3 Model Run Procedure

6.3.1 Best Modelled Fit Criteria

The numerical morphotectonic model presented in this chapter is thought to quantify the key mechanisms that

control the morphological evolution of high-elevation passive margins. Because there are several unknown, but constrained, model parameters (section 6.3.2) there has to be a criterion which defines the best modelled fit. The observed topographic signal is highly irregular (Fig. 6.2), which is probably due to non-uniform fluvial incision by drainage networks (Fig. 1.13). The best modelled fit is defined as that totally enclosing the observed topography as closely as possible without actually crossing it. This criteria is relaxed occasionally in the coastal region because it is thought that the model imperfectly describes the interface between subaerial denudation and offshore sedimentation. Therefore, the largest potential error in the model is thought to be found in this area.

6.3.2 Unknown Model Parameters

There are two unknown model parameters in the modelling approach adopted: (1) Initial topography; and (2) flexural rigidity. These are constrained but are varied in order to give the best modelled fit.

6.3.2.1 Initial Topography

The precise pre-rifting topographic distribution of southern Africa is unknown because of post-rift denudation. The mean elevation of the present-day Atlantic draining catchments is ≈930 m, which has been derived from the 10-minute digital topographic data set from the National Geophysical Data Center, Boulder, Colorado. The depth of

post-rift denudation is ≈1800 m (Rust and Summerfield, 1990; section 6.2.1.1). Therefore, the mean syn-rift elevation of the region defining the Atlantic draining catchments can be approximated by reloading the estimate of denuded material from these catchments (d) onto the present landsurface and allowing for adjustment by Airy isostasy. The syn-rift elevation will have been higher than the current elevation by e, which can be calculated from the following equation.

$$e = d(p_m - p_c) \div p_m \qquad (6.6)$$

Employing a crustal density (p_c) of 2800 kgm^{-3} and a mantle density (p_m) of 3300 kgm^{-3} the mean pre-rifting elevation of the Atlantic draining catchments is estimated to have been ≈1200 m, which has been used as an initial reference elevation during the following analysis. The initial elevation was varied, either up or down, to give the best modelled fit for a particular topographic profile.

In this simple model, surface uplift associated with the thermo-mechanical evolution of the margin is ignored because it would be substantially compensated by sediment loading offshore (Weissel and Karner, 1989). In addition any such surface uplift is confined to the area immediately adjacent to the rift hinge and does not extend more then ≈50 km onshore (sections 3.3.1 and 3.3.2). Thus, the largest potential error in the model will be in the coastal region. In order specifically to assess the development of

the marginal upwarp, the initial topography was assumed to be a block terminating at the rift hinge.

6.3.2.2 Flexural Rigidity

The calibration of this component of the model depends upon the variant under consideration (sections 6.2.2.1-6.2.2.2), but can be constrained for each model run. The minimum end-member is represented by the highly faulted lithosphere below the Cape Basin, whose temporally averaged T_e has been estimated as 5-10 km (Karner and Watts, 1982). The maximum end-member is represented by the cratonic interior of the continent, which has a T_e estimated as 64-90 km (Ebinger et al., 1989). The topographic profile considered here (Fig. 6.1) occupies an intermediate location between these two regions and the best modelled fit will, therefore, be obtained with a function of T_e between these two end-members.

6.4 Modelled Topographic Profile

The quantitative morphotectonic model formulated in section 6.2, within which onshore denudation and offshore sedimentation are coupled to flexural isostasy, has been applied to a topographic profile across the south-west African rifted margin (Fig. 6.2). The load component of the model has been calibrated in section 6.2.1.

6.4.1 Constant Rigidity

The constant rigidity isostatic component (section

6.2.2.1) is employed in this section. By an iterative process the initial topographic elevation of 1225 m has been determined for the profile and variations in this parameter are not considered further. This is because such variations only change the modelled elevation, on each node across the profile, by a constant amount. Fig. 6.9 shows topographic profiles calculated using different values of T_e. This indicates that the best modelled fit across the profile is obtained with a T_e of ≈16.5 km. Fig. 6.10 indicates how the marginal upwarp develops as the escarpment retreats from the rift hinge. This suggests that the marginal drainage divide may not have coincided with the Great Escarpment during the early history of the margin, but could have been located landward of this feature. In Fig. 6.11 the model run shown in Fig. 6.9, using a T_e of 16.5 km and including offshore sedimentation, is compared to a model run employing the same T_e but excluding offshore sedimentation. The difference between the two solutions is minimal indicating that offshore sedimentation has little effect upon the morphological evolution of the profile.

6.4.2 Laterally Variable Rigidity

In this section the two terrane isostatic component outlined in section 6.2.2.2 has been employed. This takes account of the observation that the T_e of rifted continental lithosphere is less then that of unrifted continental lithosphere (sections 5.4.2 and 5.4.3). The load component

has been explained in section 6.2.1 and the initial model elevation (H_i) of 1225 m, used in the previous section, has also been employed here. Fig. 6.12 shows topographic profiles calculated using a constant T_e for the unrifted lithosphere (T_{eu}). This has been taken to be 16.5 km, as in the best modelled fit in section 6.4.1 above, and various values of T_e for the rifted lithosphere (T_{er}) have been used [2, 6 and 10 km]. Fig. 6.12 indicates that changing T_{er} has little effect upon the geomorphological evolution of the profile, but does determine the coastline location. When the same isostatic model parameters are employed (T_{eu}=16.5 km; T_{er}=2, 6 and 10 km) but offshore sedimentation is excluded (Fig. 6.13) then the coastline is located slightly further offshore than the corresponding model run including offshore sedimentation. However, the amplitude of the marginal topographic upwarp is unaffected.

6.5 Brittle Failure of the Lithosphere

The onshore denudation/offshore sedimentation couple on passive margins suggests that the flexural rotation of the lithosphere will be at a maximum around the subaerial/subaqueous interface, since these forces are acting in opposing directions. It may, therefore, be expected that any brittle failure associated with this couple will also be located in the region of the rift hinge. This section develops a theory of brittle failure for the lithosphere. This has been used to assess the importance of this effect in modifying the flexural

properties of the isostatic system.

For the following analysis the morphotectonic model employs the laterally variable rigidity version of the isostatic component (section 6.2.2.2). The load component model parameters used for the modelled run are explained in section 6.2.1. The best modelled fit has been achieved with a T_{e1} of 5 km and a T_{e2} of 16.5 km (section 6.4).

Onshore denudation and adjacent offshore sedimentation create a rotational couple which deforms the elastic lithosphere and generates flexural bending stresses (σ_{xx}) within the lithosphere. For a perfectly elastic plate the distribution of σ_{xx} is described by the equation;

$$\sigma_{xx} = -(Ey \div [1-\nu^2]) \frac{d^2W}{dx^2} \qquad (6.7)$$

(Turcotte and Schubert, 1982, p112-115) where E is Young's Modulus, ν is Poisson's Ratio, W is vertical flexure, x is the horizontal dimension and y is the distance from the midpoint of the elastic plate (upwards is positive). This shows that the maximum bending stress occurs at the top and bottom of the plate, when $y=\pm T_e \div 2$, but is of the opposite sign, and is zero at the midpoint of the plate which is termed the neutral fibre (Fig. 6.14).

The bending moment (M) is defined as the integral of the torque exerted about the midpoint of the plate (Turcotte and Schubert, 1982) and is given by;

$$M = \int_{-T_e \div 2}^{T_e \div 2} \sigma_{11} y dy \qquad (6.8)$$

which equals;

$$M = -D \frac{d^2 W}{dx^2} \qquad (6.9)$$

The brittle seismogenic layer is the region of the lithosphere able to sustain deviatoric stress over geological timescales (10^6 a), and is approximately 15-20 km thick (Kusznir et al., 1990). The T_e of the lithosphere is defined as the thickness of an unbroken lithospheric plate that would have the same effective flexural rigidity as the lithosphere (Kusznir et al., 1990). Therefore, from the following equation;

$$D = (ET_e^3) \div 12(1-\nu^2) \qquad (6.10)$$

where $E=1x10^{11}$ Nm^{-2} and $\nu=0.25$, the effective rigidity of rifted continental lithosphere (D_1) is $1.1x10^{21}$ Nm (T_{e1}=5 km), and the effective rigidity of the unrifted lithosphere (D_2) is $4.0x10^{22}$ Nm (T_{e2}=16.5 km) for the best modelled fit.

The bending stresses are distributed over the thickness of the seismogenic layer, which in this model is

assumed to be 16.5 km across the width of the whole profile. Thus, although the effective elastic thickness of the rifted lithosphere (T_{e1}) is 5 km in the best modelled fit, the bending stresses are distributed over a thickness of 16.5 km.

The maximum bending stress at the top of the lithosphere, due to the accumulative flexural deformation at the end of the model run, has been calculated from equation 6.9 and is shown in Fig. 6.15. This indicates that the region of maximum bending stress is located in the coastal region ≈40 km inland of the rift hinge. At this point the top of the plate is in tension and exhibits a bending stress of ≈5.5 kbars. This compares to bending stresses of up to 5 kbars generated below large deltas and up to 10 kbars due to the flexing of oceanic lithosphere at subduction zones (Bott and Kusznir, 1984). By comparison the deviatoric stresses induced by the addition or removal of overburden tend to be up to 2 kbars (Haxby and Turcotte, 1976).

Experimental rock mechanic data (Byerlee, 1978) indicate that the maximum shear stress in the continental crust increases with depth (confining pressure) and defines the brittle failure envelope (Fig. 6.16). The calculated theoretical bending stresses in Fig. 6.15 will exceed the brittle strength of the lithosphere in the upper crust (Fig. 6.16) and this will, therefore, decrease the bending moment (M), which in turn will tend to reduce the effective rigidity of the lithosphere. If it is assumed that the

brittle strength of the lithosphere is defined by dry sample data (Fig. 6.16) then the modified bending moment (M') due to failure in the upper crust can be calculated from equation 6.8. Assuming that the partially failed lithosphere still behaves approximately as a perfectly elastic plate, but with a lower T_e, then equation 6.9 still applies and the bending moment ratio between the modified plate, due to brittle failure, and a perfectly elastic plate is given by;

$$M' \div M = D' \div D \qquad (6.11)$$

where D' is the modified effective flexural rigidity of the lithosphere, due to brittle failure, and from equation 6.10;

$$M' \div M = T_e'^3 \div T_e^3 \qquad (6.12)$$

where T_e' is the modified effective elastic thickness of the lithosphere due to brittle failure. If the rigidity of the lithosphere is characterised by the effective elastic thickness then;

$$T_e' = ([M'/M]T_e^3)^{1/3} \qquad (6.13)$$

where T_e is T_{e1} or T_{e2} depending upon spatial location on the profile. For the model run in Fig. 6.15 the bending moment ratio has been calculated together with T_e' (Fig. 6.17).

This indicates that the maximum amount of brittle failure, at the top of the plate, has occurred in areas of horizontal tension associated with isostatic uplift due to denudational unloading, from ≈30 km offshore of the rift hinge to 150 km onshore. This spatial distribution of brittle failure, probably manifesting itself as seismic activity, has not been observed over the recent past ≈350 a in southern Africa (Fernandez and Guzman, 1979). The present day seismicity (Fig. 6.18) has been proposed as due to the southwards propagation of the east African rift system, or due to epeirogenic causes involving a postulated sub-lithospheric hot spot below the Drakensberg mountains (Hartnady, 1989).

In this analysis brittle failure, due to the accumulative effect of denudation and sedimentation, has only been considered as a single event at the end of a model to demonstrate the principle. In actual fact brittle failure, manifesting itself as seismic activity, will have probably occurred throughout the development of the margin. It will have most likely been greatest when sedimentation and denudation rates were at a maximum early in the history of the margin (Rust and Summerfield, 1990; Brown et al., 1990). This may account for the absence of seismic activity due to this mechanism at the present day. Such brittle failure is probably dissipated by fault reactivation, and may thus aid continental extension during the rifting process.

Brittle failure of the lithosphere due to post-rift

loading events, measured in terms of the decrease in T_e, is slight (Fig. 6.17) and does not appear to have affected the isostatic response of the south-west African rifted margin. Such failure would have been superimposed on other rift related stress that has probably caused more fracturing of the lithosphere (Fig. 5.5).

6.6 Morphotectonic Model Properties

The quantitative morphotectonic model presented in section 6.2 links denudation and sedimentation on high-elevation rifted margins, such as south-western Africa, with isostasy. This formulation has enabled the importance of each component, thought to affect the morphological evolution of the morphotectonic system under consideration, to be assessed. The model runs of section 6.4 indicate that the sediment loading evolution of the margin has not significantly affected the morphological evolution of the modelled profile across south-western Africa (Fig. 6.11). Since the distance between the rift hinge and the present coastline on this profile is at a minimum (Fig. 6.1), it can be assumed that the morphological evolution of the entire south-west African rifted margin has been largely unaffected by offshore sedimentation. This is because the sedimentary depocentres are located further offshore, and are thinner, on other transects across the margin. Therefore, the isostatic response to offshore sedimentation onshore will be less significant than on the profile modelled in section 6.4. As a consequence, it is assumed

that the most important factor controlling the morphological evolution of high-elevation passive margins, with similar characteristics to south-western Africa, is the link between onshore denudation and isostasy. This appears to be decoupled from the offshore rift evolution.

The role of isostasy is critical in assessing the role of denudation in influencing the post-rift morphological evolution of south-western Africa. However, the results from section 6.4.2 indicate that the laterally variable rigidity isostatic component is not required to model the profile in Fig. 6.2, and the constant rigidity isostatic component gives an adequate solution. This is presumably because the sediment load is not large enough, given the assumed values of T_e, to generate significant surface uplift inland of the rift hinge.

The subsequent analysis in this thesis only considers a simplified morphotectonic model, which links denudation and isostasy. The constant rigidity isostatic component (section 6.2.2.1) has been employed. This will be applied to the topographic profile in Fig. 6.2 in order to explore the properties of the system.

6.6.1 Best Modelled Fit

The best modelled fit using the simplified morphotectonic model is shown in Fig. 6.19. This has an initial topographic elevation (Hi) of 1225 m and a T_e of 16.5 km, which is consistent with the range of 5-90 km indicated in section 6.3.2.2. In the region of the

escarpment, the model generates a maximum of ≈600 m of surface uplift with respect to the slowly eroding continental interior and closely replicates the characteristic curved profile of the marginal upwarp. Given the spatial variation in total denudation for the best modelled fit (Fig. 6.20), which has also been recorded on other rifted margins such as eastern Australia (Speight, 1987) and eastern Brazil (K. Gallagher, pers. comm.), and assuming that compensation to denudational unloading occurs flexurally, then the creation of a marginal upwarp is inevitable. The mismatch between the modelled and observed topographic profiles is probably due to enhanced rates of denudation in the zone of the marginal upwarp associated with drainage incision (Fig. 1.13), which have not been incorporated into this version of the model. The evolution of the marginal upwarp, as the escarpment retreats, is shown in Fig. 6.21. This indicates that the maximum elevation of the escarpment is only reached ≈100 Ma after rifting. Fig. 6.22 shows the evolution of the flexural deformation, due to denudational unloading, and indicates that the marginal upwarp migrates away from the rifted region during the ageing of the margin.

The generation of marginal upwarps as a result of differential denudational unloading not only explains their presence along mature rifted margins but also has important geomorphological and sedimentological implications. The presence of marginal upwarps up to 100 Ma or more after rifting may account for the deflection of drainage systems

away from many mature rifted margins (Summerfield, 1981, 1985; Cox, 1989). The persistence of such a barrier to sediment transport across high-elevation rifted margins suggests that patterns of offshore deposition are likely to be controlled by a dual drainage system. This comprises numerous small aggressively eroding coastal catchments and widely spaced outlets of large basins draining continental interiors well into the mature rifted margin stage. It has recently been suggested that the nature of sediment sources is an important factor in controlling the distribution of sedimentary facies within rifted margin basins (Reading and Orton, 1991). Thus, the focusing of incoming detritus into sedimentary basins will probably determine the sequence of facies in conjunction with sediment calibre and local tectonic conditions. Where drainage systems breach a marginal upwarp, the isostatically generated uplift will tend to maintain a significant change in channel gradient, such as the Augrabies Falls on the Orange River.

6.6.2 Flexural Rigidity Variations

In this section the denudational parameters for the best modelled fit in Fig. 6.19 (Dd_t, Dd_{cc}, Dd_{ic} and SRR) have been kept constant, as calibrated previously (section 6.2.1.1), and the flexural rigidity is varied. Fig 6.23 shows computed topographic profiles for T_e values of 8.25, 16.5 and 33 km. Varying the T_e changes the distribution of the upwarped region, but the zone of maximum surface uplift remains in approximately the same position in the coastal

catchment area.

For a comprehensive analysis the extreme end members of flexural rigidity will now be considered. These consist of the Airy case, which corresponds to a flexural rigidity of zero (Fig. 6.24), and the infinite rigidity case (Fig. 6.25). Neither of the modelled profiles gives a good fit with the observed topography. In the Airy case the coastal region, in particular, is anomalously high due to isostatic rebound. In the infinite rigidity case, the average elevation of the computed profile is anomalously low, because no isostatic rebound has occurred, with the calculated coastline location far too inland of the rift hinge. In both cases no surface uplift has occurred and so they are unable to create a marginal upwarp. The inclusion of flexural isostasy in the model is, therefore, a necessary component in order to form marginal topographic upwarps by the isostatic response to denudation.

6.6.3 Denudation Rate Variations

In this section the best modelled fit parameters of T_e, H_l, SRR and Dd_t are retained from section 6.6.1. The coastal and interior catchment denudation rates (Dd_{cc} and Dd_{ic}) have been changed to show the effect of varying the denudation rate contrast between these two terrains. This is because the denudational model calibration assumes that the present day local relief differential has been maintained at a constant value throughout the evolution of the margin. However, in reality it was probably greater during the

early evolution of the margin, when fluvial systems were incising the rift-flanks, due to lower base-levels established during rifting.

Fig. 6.26 shows the scenario when Dd_{cc} equals Dd_{ic}, which are calibrated from equation 4.1 as 9 mMa^{-1}. In this case a marginal upwarp is still created, although of a smaller amplitude than in Fig. 6.19 (the best modelled fit), but the average coastal elevation is too high. Fig 6.27 is a model run where Dd_{cc} equals Dd_{ic} which equals zero, so that the denudational model is characterised only by the escarpment retreat parameters Dd_e and SRR. The modelled escarpment fits as well as in Fig. 6.19, and predicts the same amount of surface uplift at that point, but the modelled coastal and interior catchment average elevations are both too high. In Fig. 6.28, Dd_{ic} is the same as in Fig. 6.19 (6.9 mMa^{-1}) but in the coastal catchment area the landscape is graded to sea level, so that the coastline coincides with the escarpment. Because of the increased denudation in the coastal region, the model generates ≈1000 m of surface uplift around the escarpment, with respect to the slowly eroding continental interior. This is less than twice the amount of surface uplift produced by the best modelled fit (Fig. 6.19) and indicates that even though the average coastal denudation rate is much greater than 16.5 mMa^{-1}, the amount of surface uplift produced in the region of the escarpment is relatively insensitive to changes in Dd_{cc}.

The three model scenarios considered above (Figs.

6.26, 6.27 and 6.28) suggest that the amplitude of the marginal upwarp is principally controlled by Dd_t, with Dd_{cc} and Dd_{ic} being second order effects in this respect. However, Dd_{cc} and Dd_{ic} are the controlling factors in shoreline location and coastal and interior catchment elevation.

The average denudation rate of mid-latitude drainage basins has been empirically shown to be a linear function of mean local relief (Ahnert, 1970), and this relationship was used to calibrate the parameters Dd_{cc} and Dd_{ic}. However, an alternative empirical analysis correlates average denudation rate with mean drainage basin elevation (Pinet and Souriau, 1988). This relationship has been used, given that the mean drainage basin elevation of the coastal and interior catchments are 545 m and 1255 m respectively and in conjunction with equation 4.1, to calibrate Dd_{cc} and Dd_{ic} as 4.4 and 10.2 mMa^{-1} respectively. Thus, the coastal catchment has a lower mean denudation rate than the interior catchment. Fig. 6.29 shows the modelled fit with these new values of Dd_{cc} and Dd_{ic}. Although a marginal upwarp is still created it has a lower amplitude than Fig. 6.19 (the best modelled fit) and the average coastal elevation is too high. Using the calibration of Pinet and Souriau (1988), this will always be the case. The Ahnert (1970) calibration gives a better modelled fit (Fig. 6.19) and conceptually makes more sense. It is thought that higher denudation rates in the coastal region, with comparison to the interior catchment, more accurately characterises the

denudational system on high-elevation rifted margins. This is due to the creation of new, lower, base levels during rifting which promote steep slopes in the coastal region and enhance denudation rates. On the contrary the continental interior, remote from the site of rifting, will be unaffected.

Slope angle is a primary determinant of denudation rates and a recent analysis concerning southern Africa (Summmerfield, 1991b) shows that only 0.5% of the variance in mean sine slope can be accounted for by regional (modal) elevation within a drainage basin. Therefore, regional elevation cannot be employed to predict denudation rates on this passive margin. However, a close relationship exists between mean sine slope and local relief, given a product moment correlation coefficient of 0.87 (Summerfield, 1991b). This indicates that local relief models provide a better basis for modelling denudation rates on the passive margins of southern Africa.

6.6.4 Forward Modelling into the Future

Using the best modelled fit parameters (Fig. 6.19) the numerical simulation has been run for an additional 150 Ma into the future (Fig. 6.30). This suggests that the maximum elevation of the top of the escarpment has probably been reached at the present day and thereafter declines slowly from ≈1600 m to ≈1400 m. This creates a second, minor, drainage divide in the coastal catchment area approximately midway between the modelled escarpment location and

coastline. This morphology has not been observed on high-elevation rifted margins of different ages, which perhaps indicates that a quasi-equilibrium landform is produced and the creation of a second, minor, drainage divide does not in fact occur.

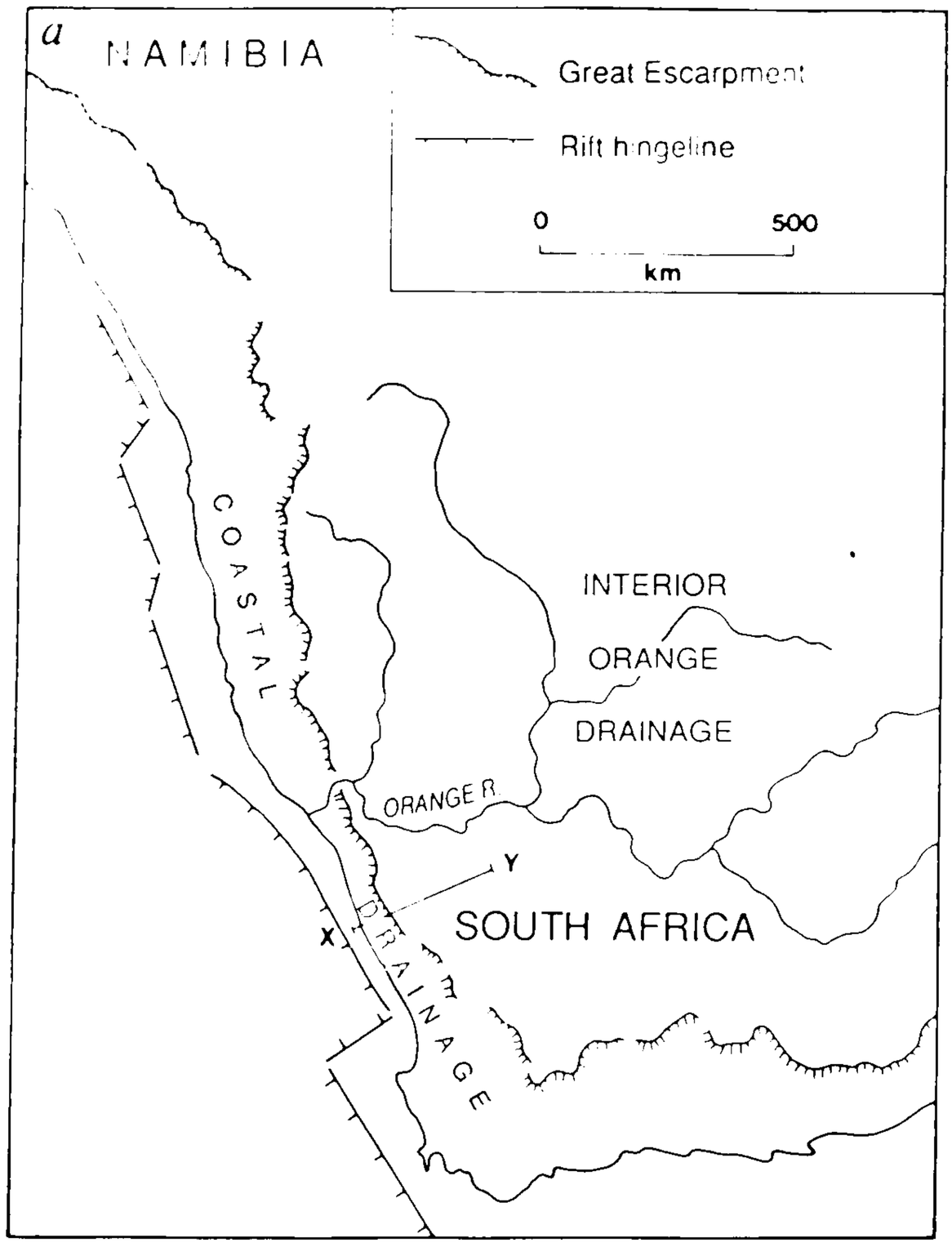

Fig. 6.1. Major morphological features along the south-west African rifted margin. The topographic profile in Fig. 6.2 is shown by X-Y.

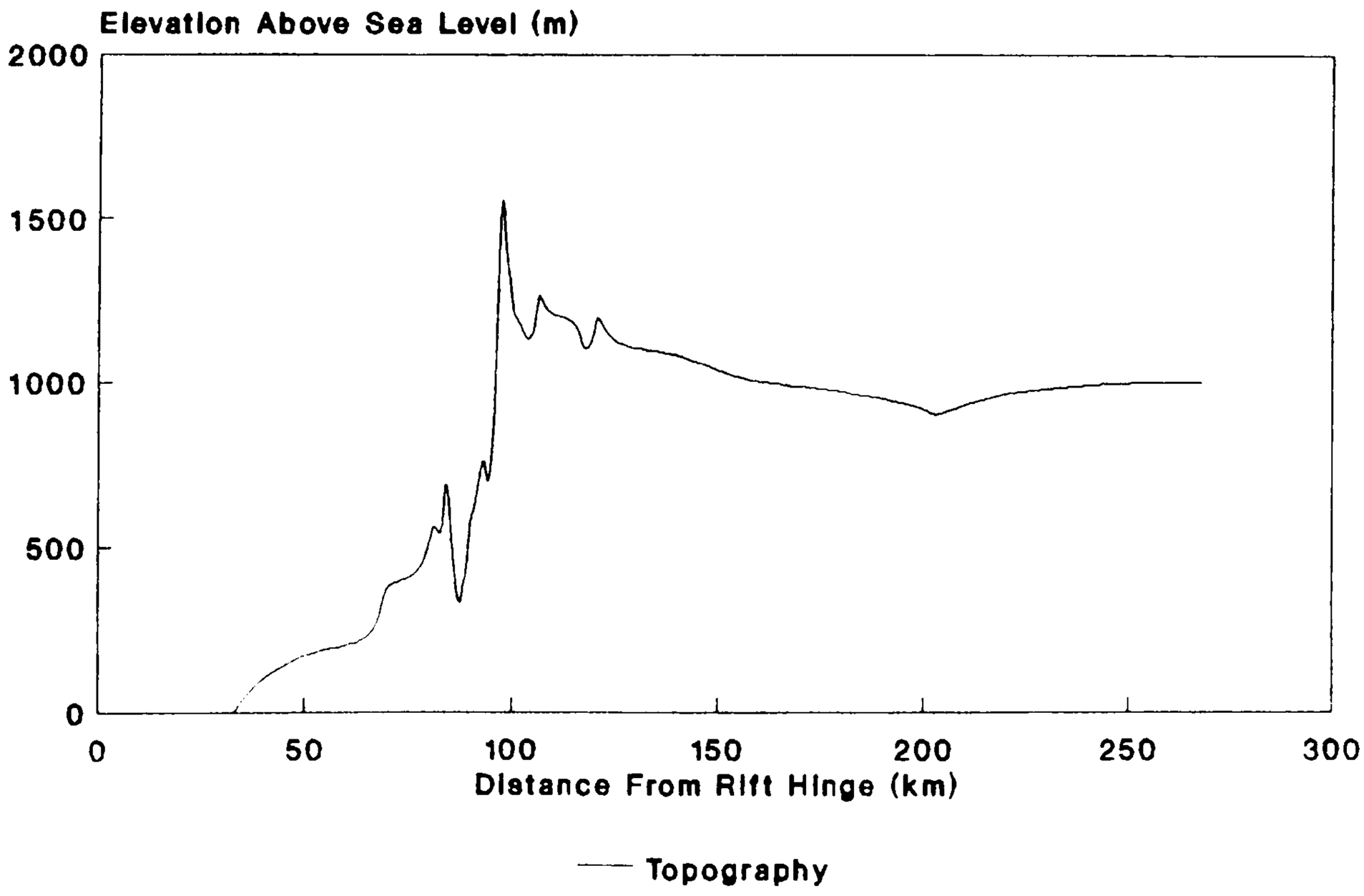

Fig. 6.2. Topographic profile across the south-west African rifted margin. The profile location is shown in Fig. 6.1.

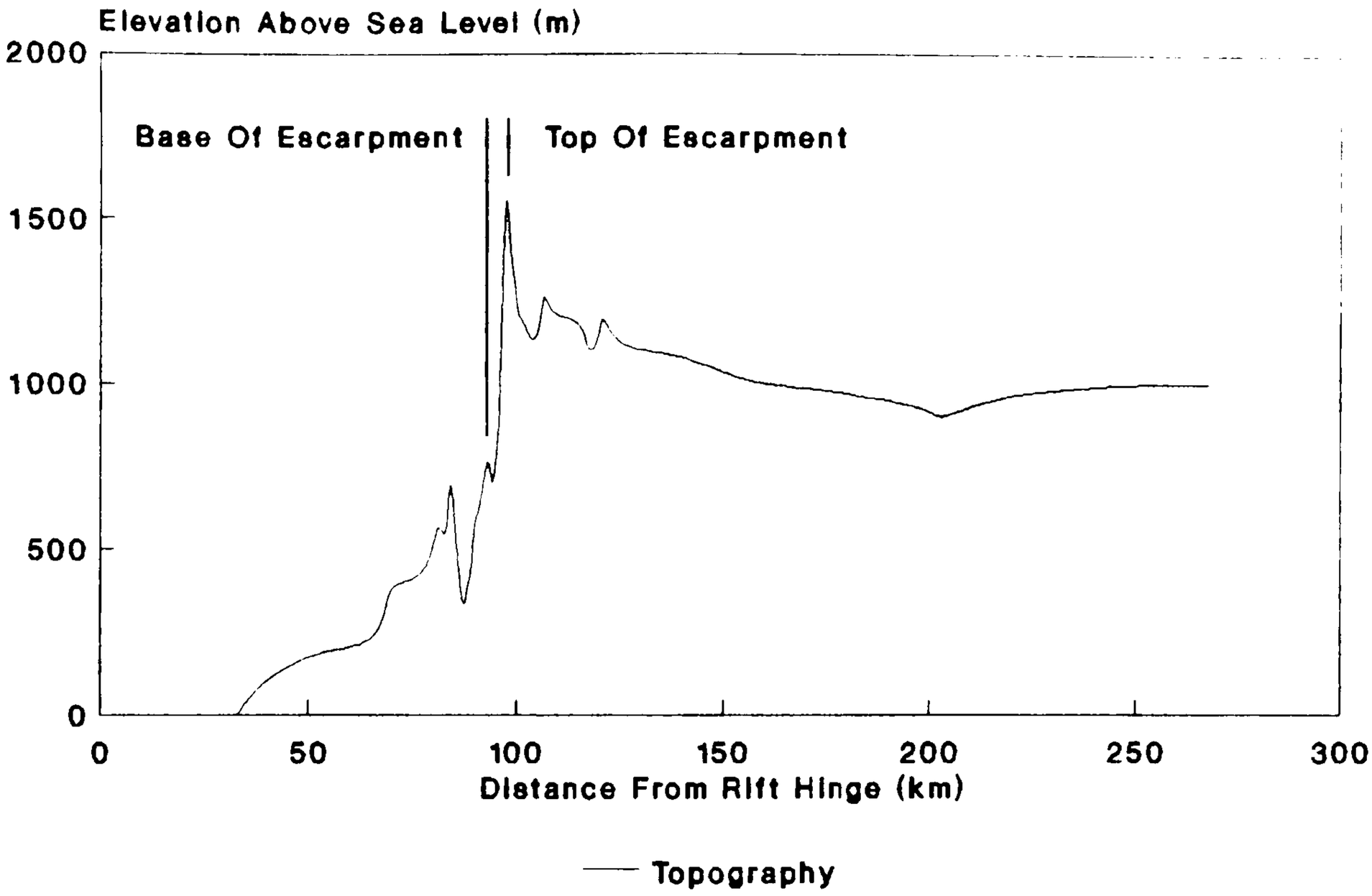

Fig. 6.3. The location of the top and base of the Great Escarpment.

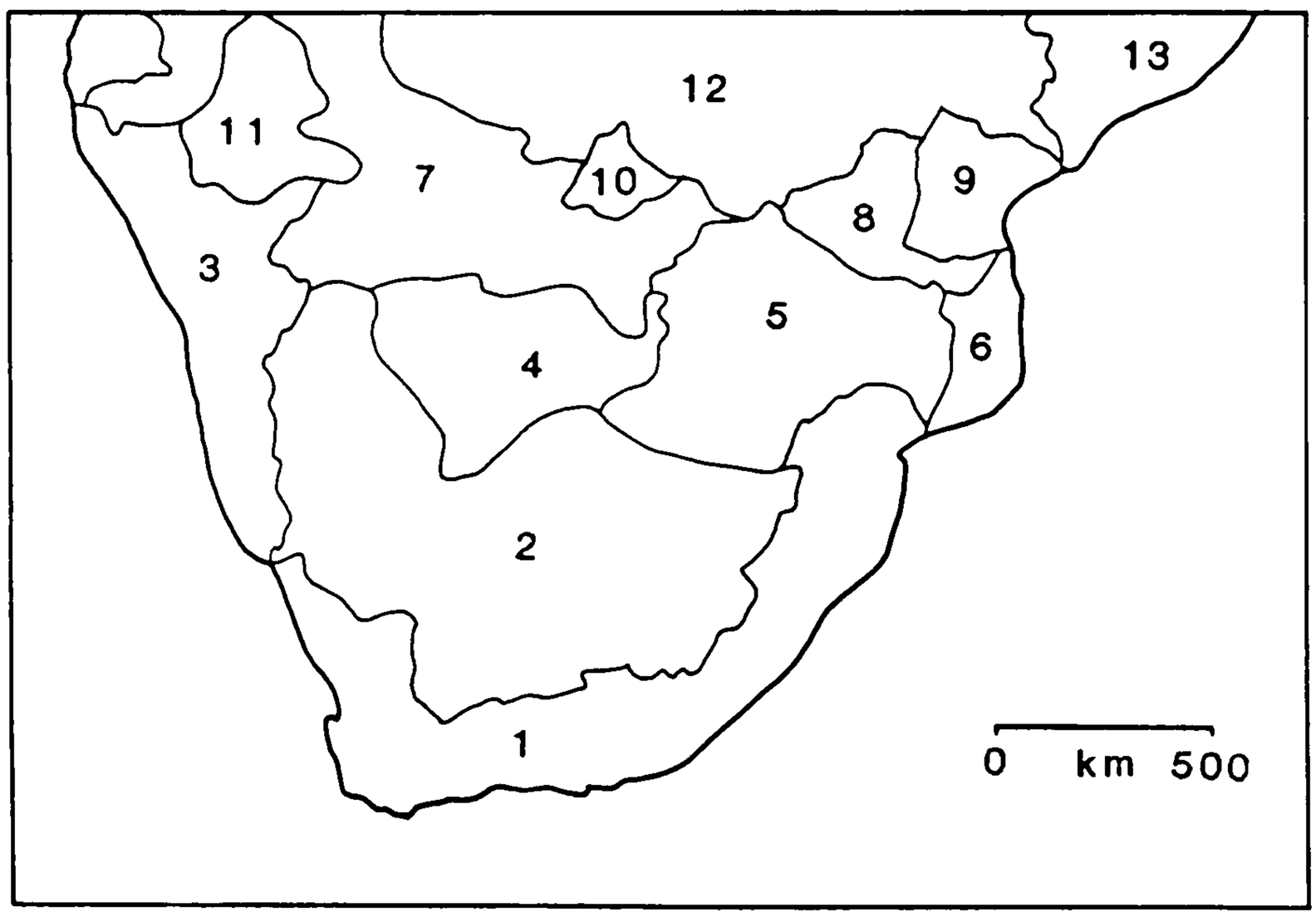

Fig. 6.4. Drainage basin outlines in southern Africa: (1) Southern coastal; (2) Orange; (3) Namib; (4) Kalahari; (5) Limpopo; (6) Inhambane; (7) Okavango; (8) Save; (9) Sofala; (10) Chobe; (11) Etosha; (12) Zambezi; and (13) Nampula.

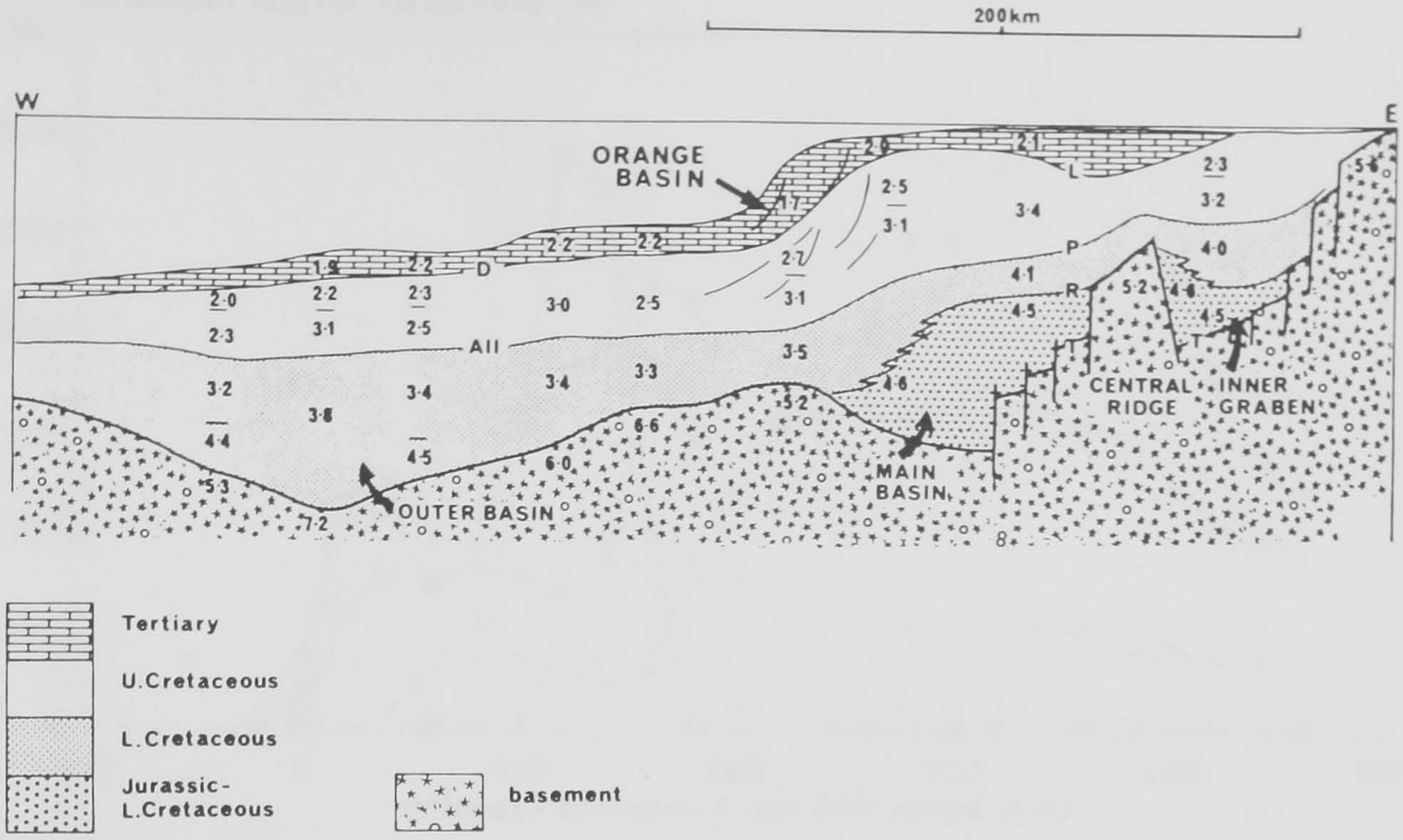

Fig. 6.5. Stratigraphic profile across the Cape Sedimentary Basin (after Dingle et al., 1983, Fig. 120c).
The numbers are P-wave interval velocities (kmsec^{-1}) and A11, D, T, R, P and L are regional seismic reflectors. The profile is approximately in line with the topographic profile in Fig. 6.1.

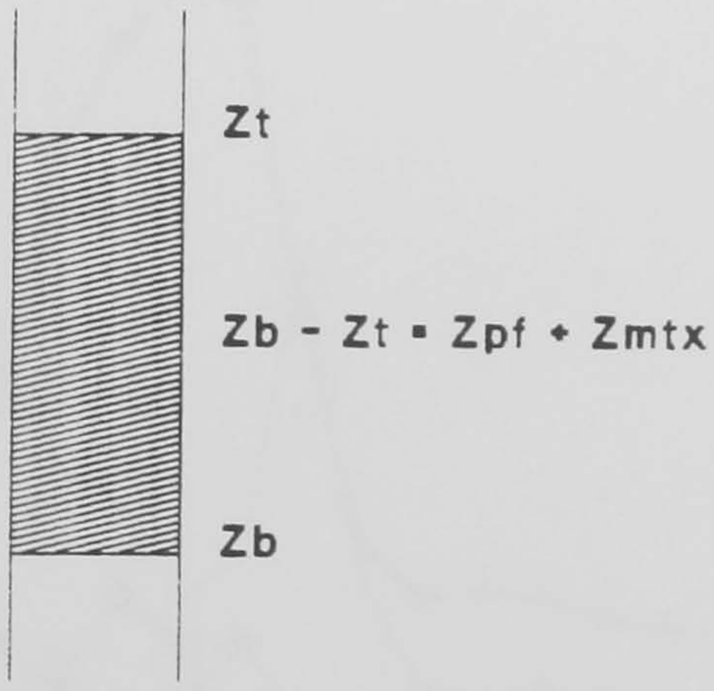

Fig. 6.6. Schematic diagram of a sediment column of constant lithology: Zt is the depth to the top of the sediment column; Zb is the depth to the base of the sediment column; Z_{pf} is the thickness of the sediment column occupied by pore fluid; and Z_{mtx} is the thickness of the sediment column occupied by sediment matrix.

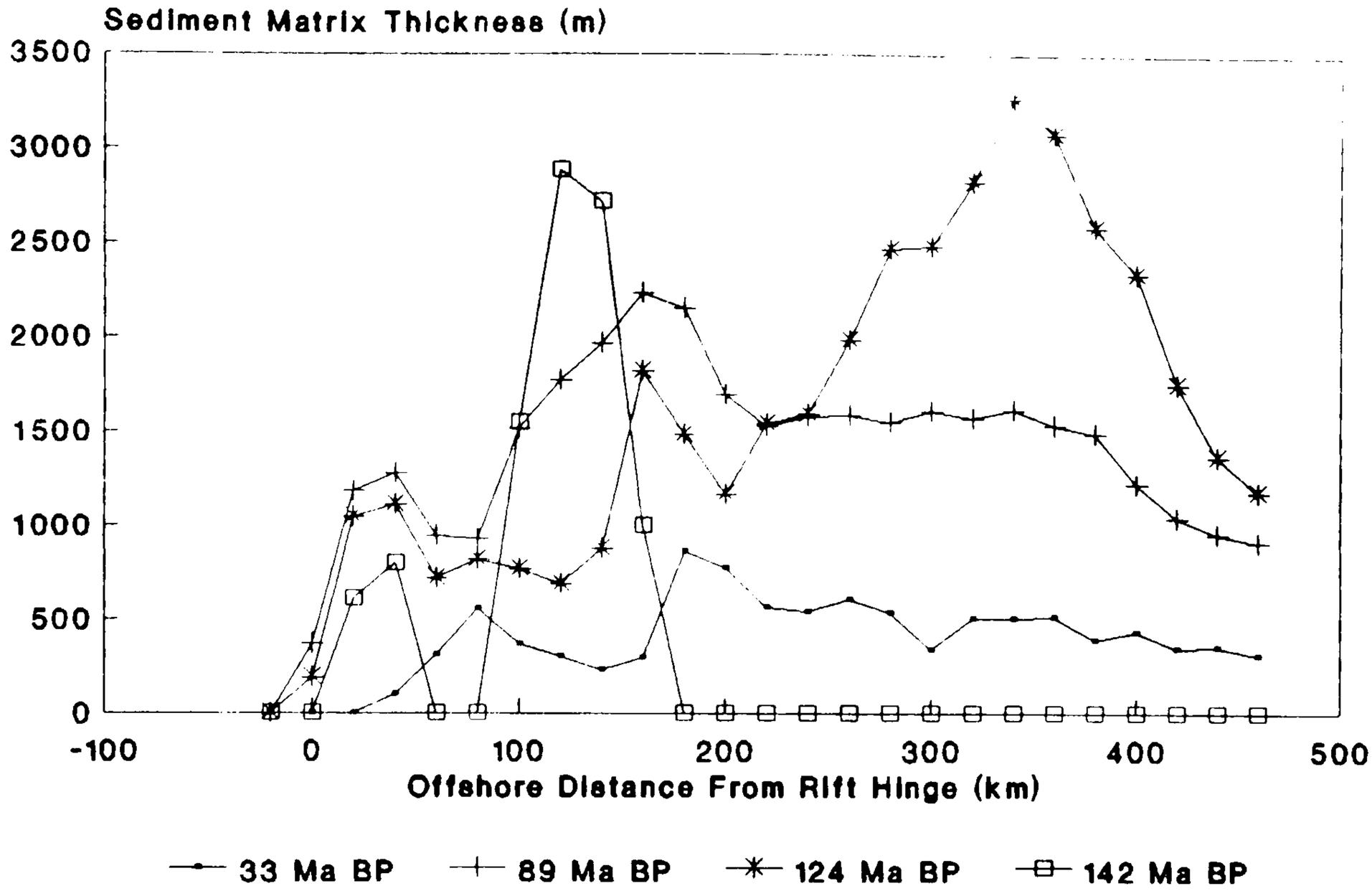

Fig. 6.7. Sediment matrix thickness within each horizon of the stratigraphic profile in Fig. 6.5. Each horizon is referred to by its approximate chrono-stratigraphic midpoint. Therefore, 142 Ma BP represents the Jurassic-Lower Cretaceous, 124 Ma BP represents the Lower Cretaceous, 89 Ma BP represents the Upper Cretaceous and 33 Ma BP represents the Tertiary.

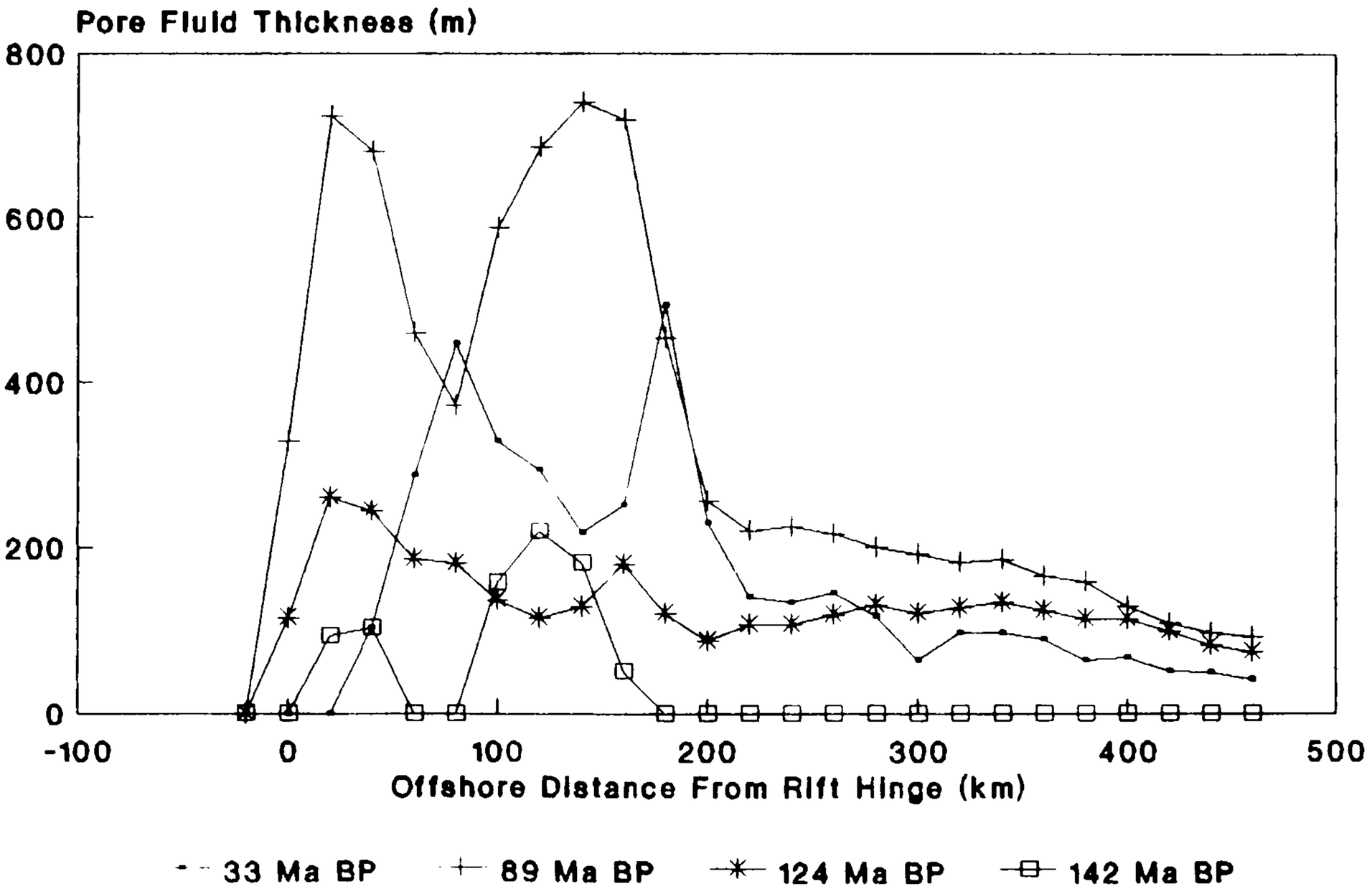

Fig 6.8. Pore fluid thickness within each horizon of the stratigraphic profile in Fig. 6.5. Nomenclature as in Fig. 6.7.

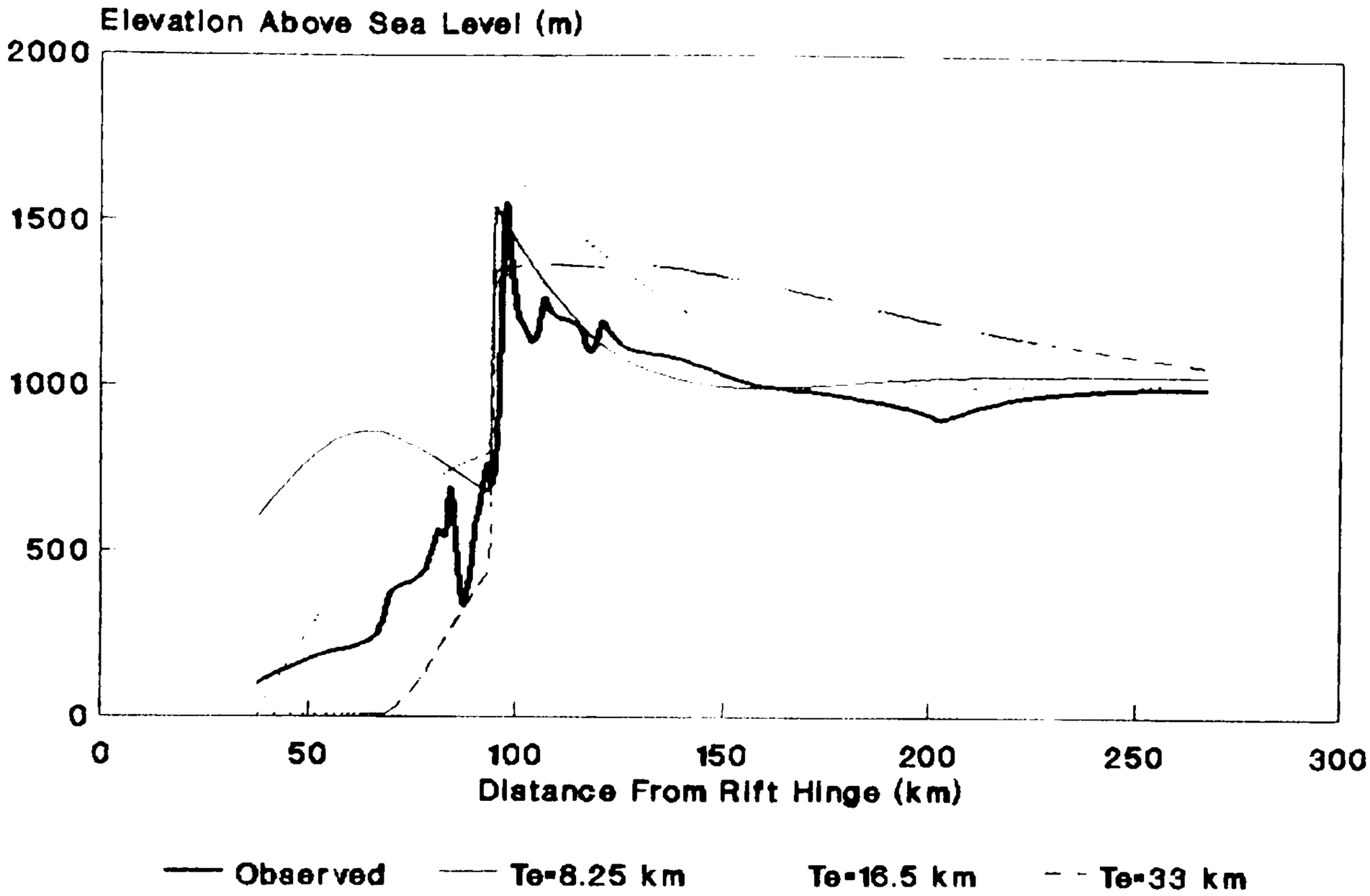

Fig. 6.9. Calculated topographic profiles for various T_e values, displayed with observed topography. The load component is comprised of onshore denudation, calibrated in section 6.2.1.1 (Dd_e=900 mMa^{-1}, Dd_{cc}=16.5 mMa^{-1}, Dd_{ic}=6.9 mMa^{-1} and SRR=630 mMa^{-1}) and offshore sedimentation calibrated in section 6.2.1.2. The isostatic component is modelled as a constant rigidity elastic plate (section 6.2.2.1). Flexural model parameters are E=1x10^{11} Nm^{-2}, ν=0.25, g=9.81 ms^{-2}, ρ_s=3300 kgm^{-3} and ρ_i=0 kgm^{-3}.

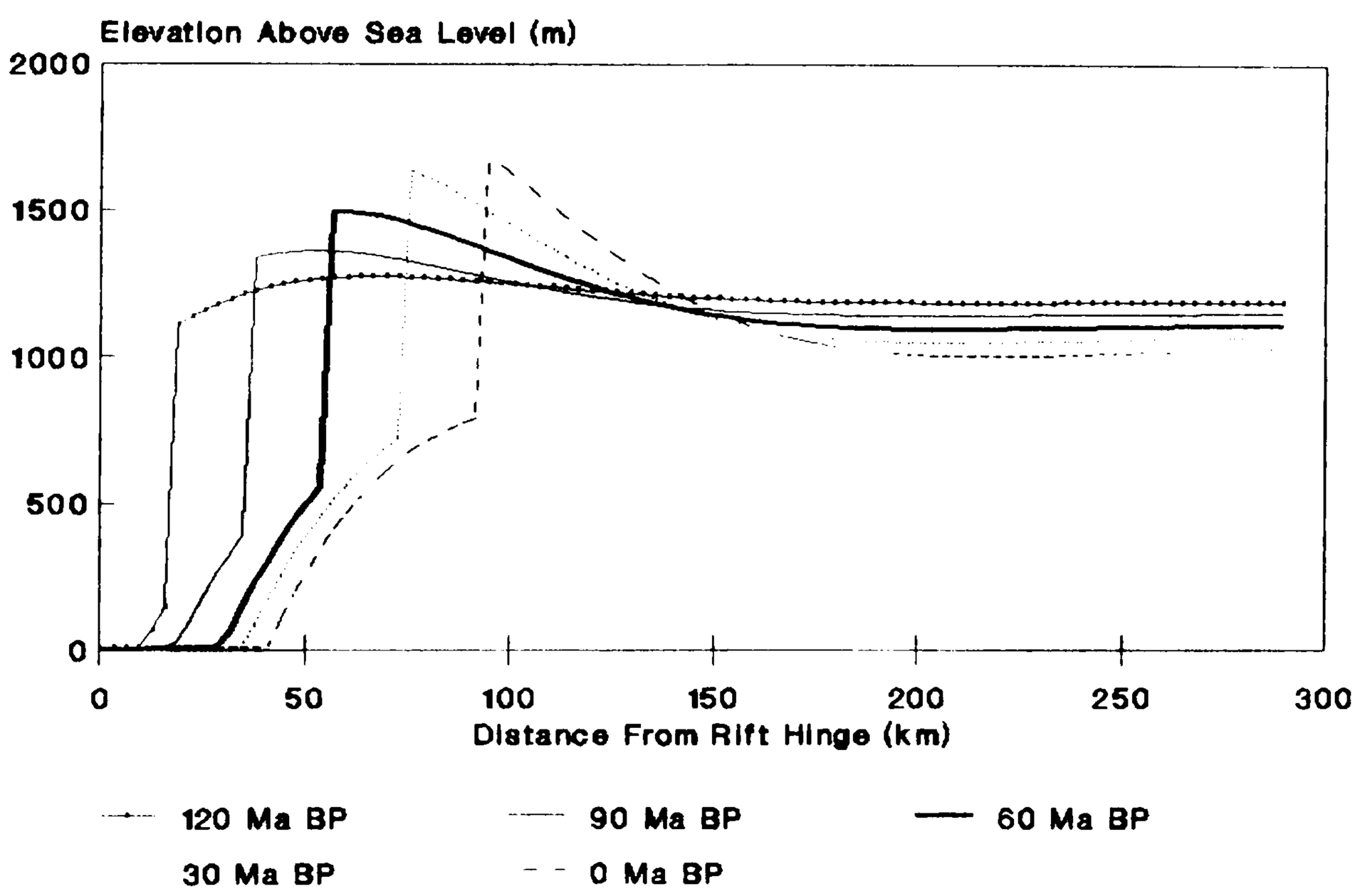

Fig. 6.10. Evolution of the calculated topographic profile in Fig. 6.9 for T_e=16.5 km. Other model parameters as in Fig. 6.9.

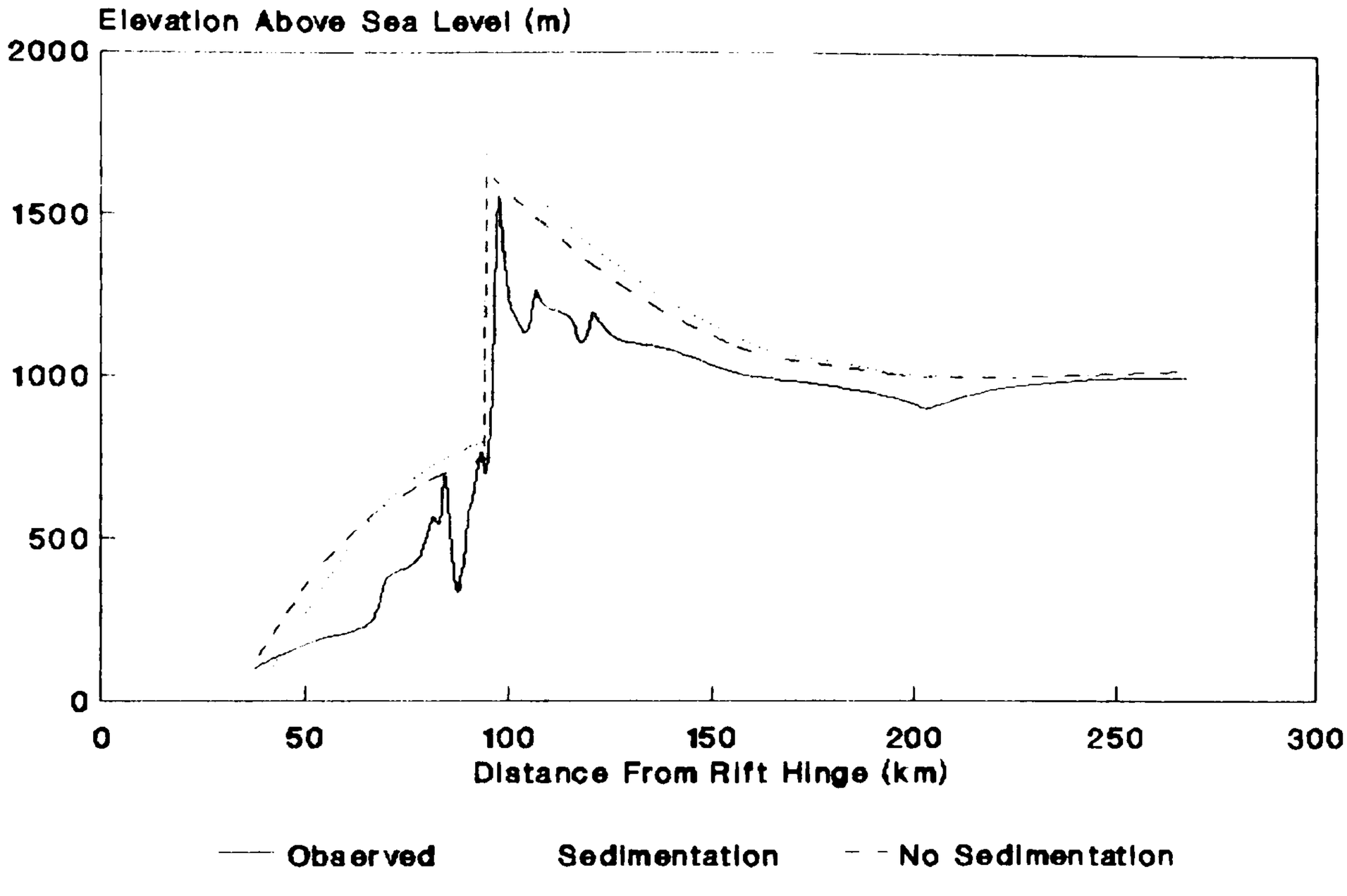

Fig. 6.11. Calculated topographic profiles for T_e=16.5 km with and without offshore sedimentation, displayed with observed topography. Other model parameters as in Fig. 6.9.

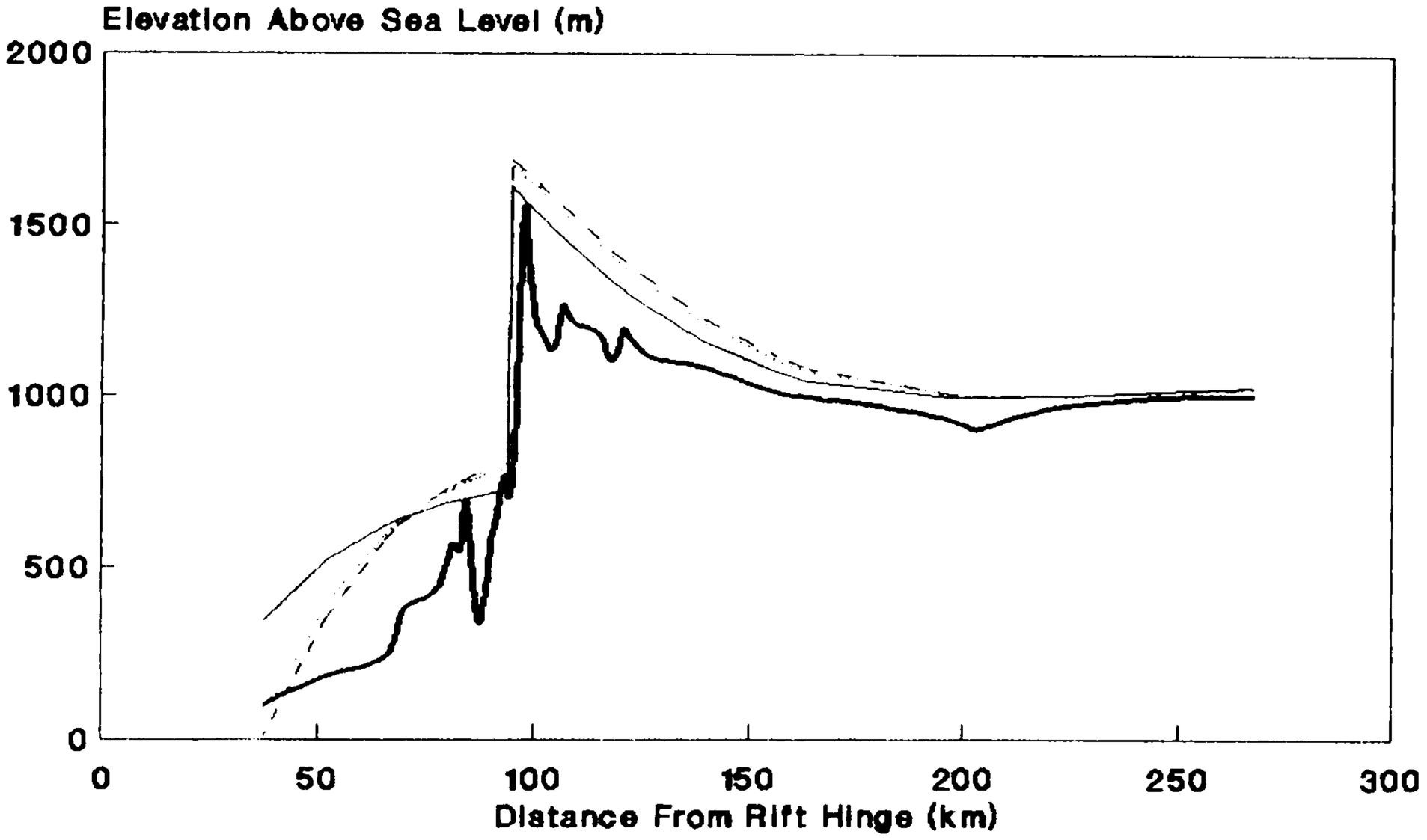

Fig. 6.12. Calculated topographic profiles employing the two terrane flexural model (section 6.2.2.2) for various T_{e1} values with T_{e2} constant at 16.5 km. The load component is comprised of onshore denudation, calibrated in section 6.2.1.1 (Dd_e=900 mMa^{-1}, Dd_{sc}=16.5 mMa^{-1}, Dd_{ic}=6.9 mMa^{-1} and SRR=630 mMa^{-1}) and offshore sedimentation calibrated in section 6.2.1.2. The flexural model parameters are E=1x10^{11} Nm^{-2}, ν=0.25, g=9.81 ms^{-2}, ρ_m=3300 kgm^{-3} and ρ_s=0 kgm^{-3}.

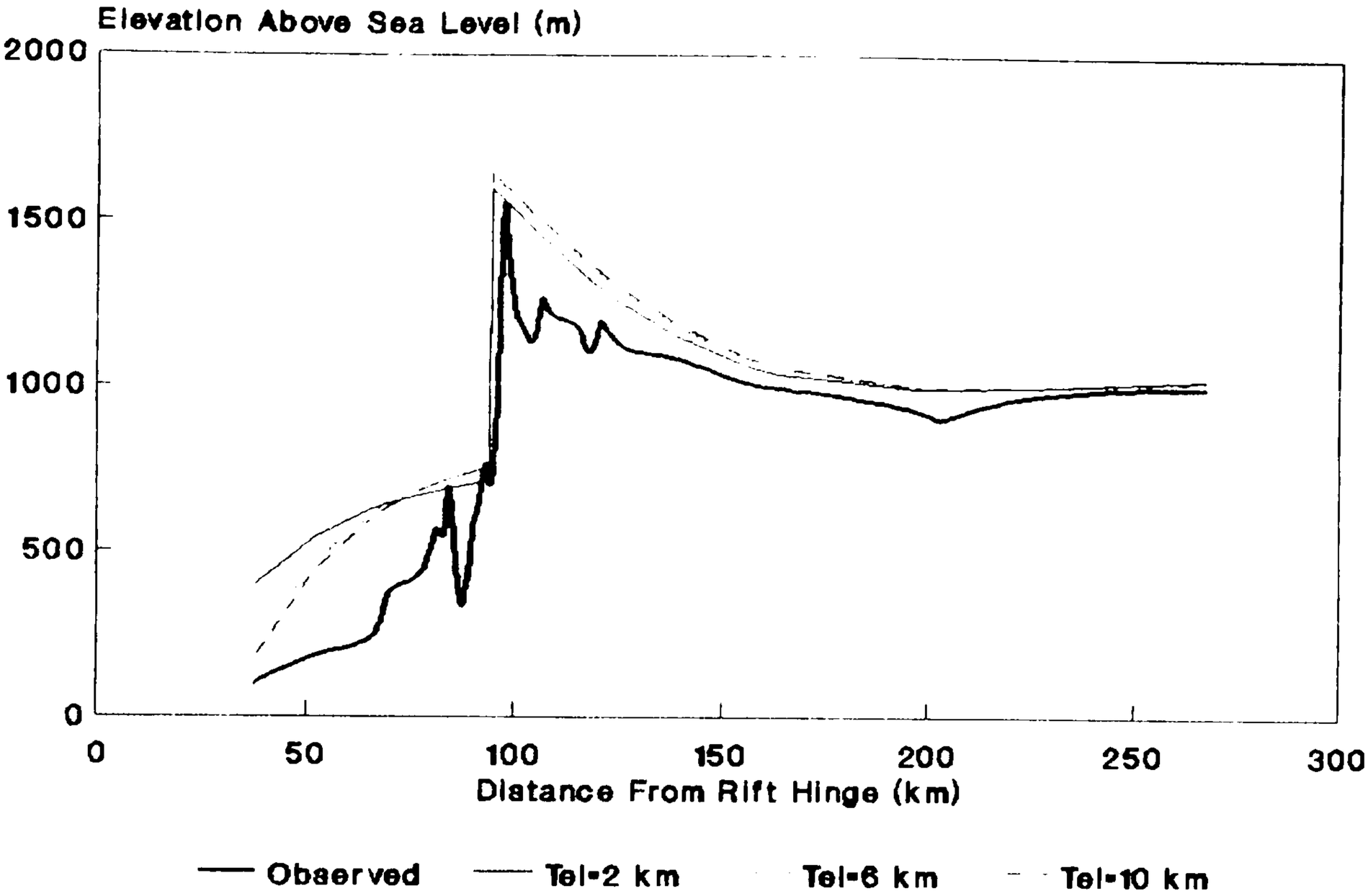

Fig. 6.13. Calculated topographic profiles for various T_{el} values with T_{el} constant at 16.5 km. In contrast to Fig. 6.12 offshore sedimentation is excluded from the load component. Other model parameters as in Fig. 6.12.

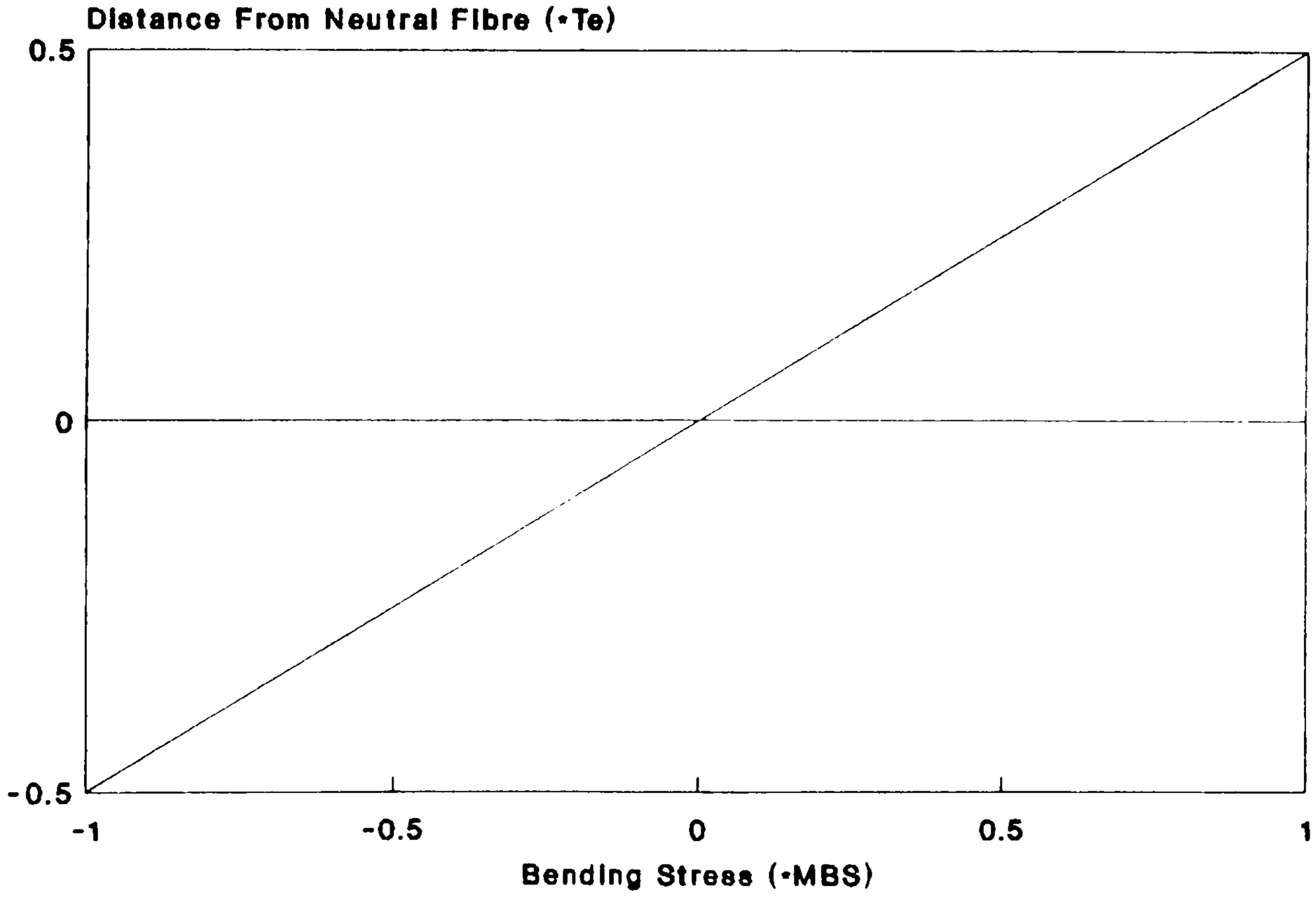

Fig. 6.14. Elastic bending stresses versus depth for a perfectly elastic plate. T_e is the effective elastic thickness of the plate and MBS is the maximum bending stress (+ is compression and - is tension).

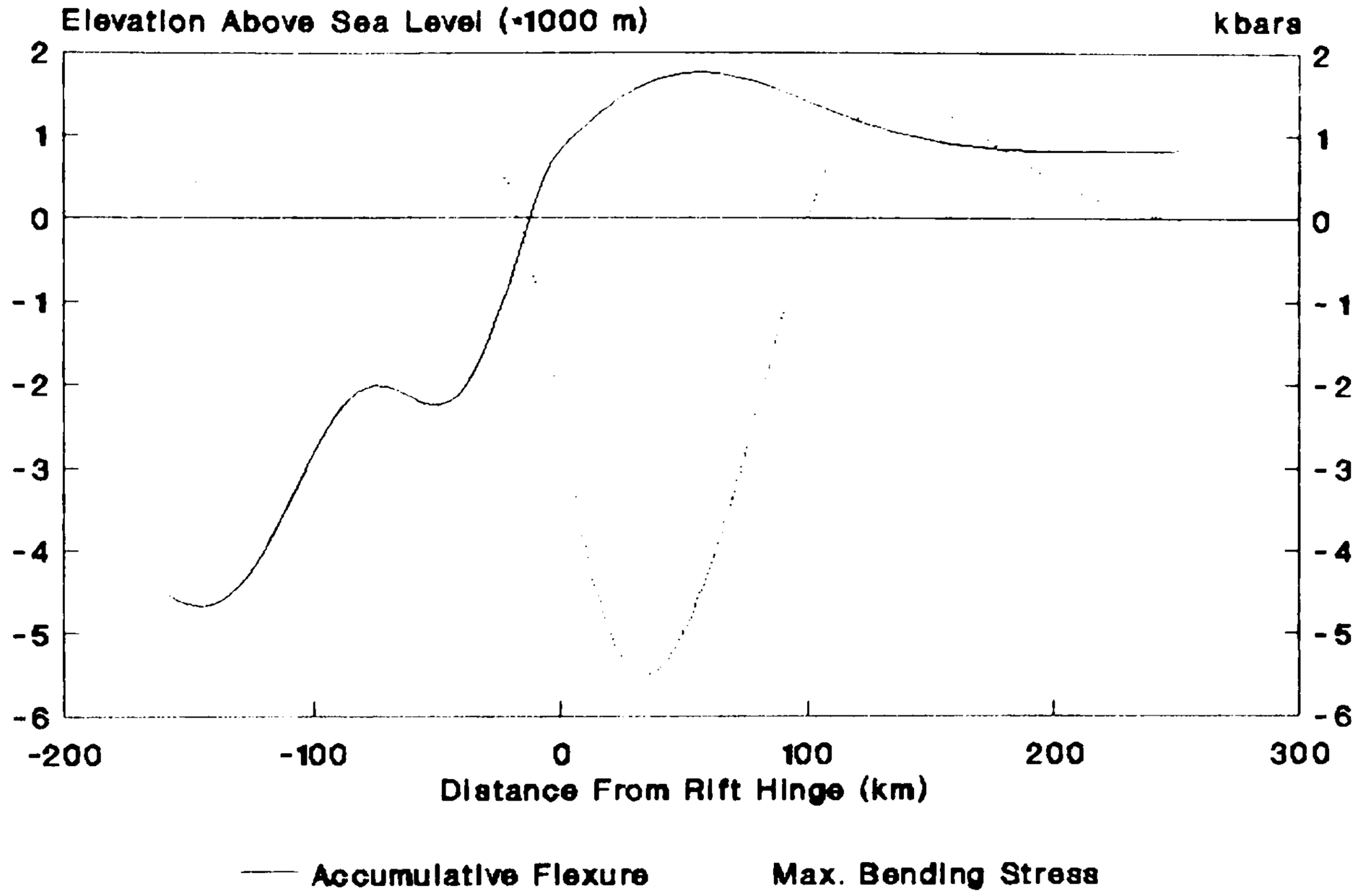

Fig. 6.15. Total flexure and maximum bending stress (at the top of the elastic plate) for the modelled profile in Fig. 6.12 with T_{el}=5 km and other model parameters as in Fig. 6.12.

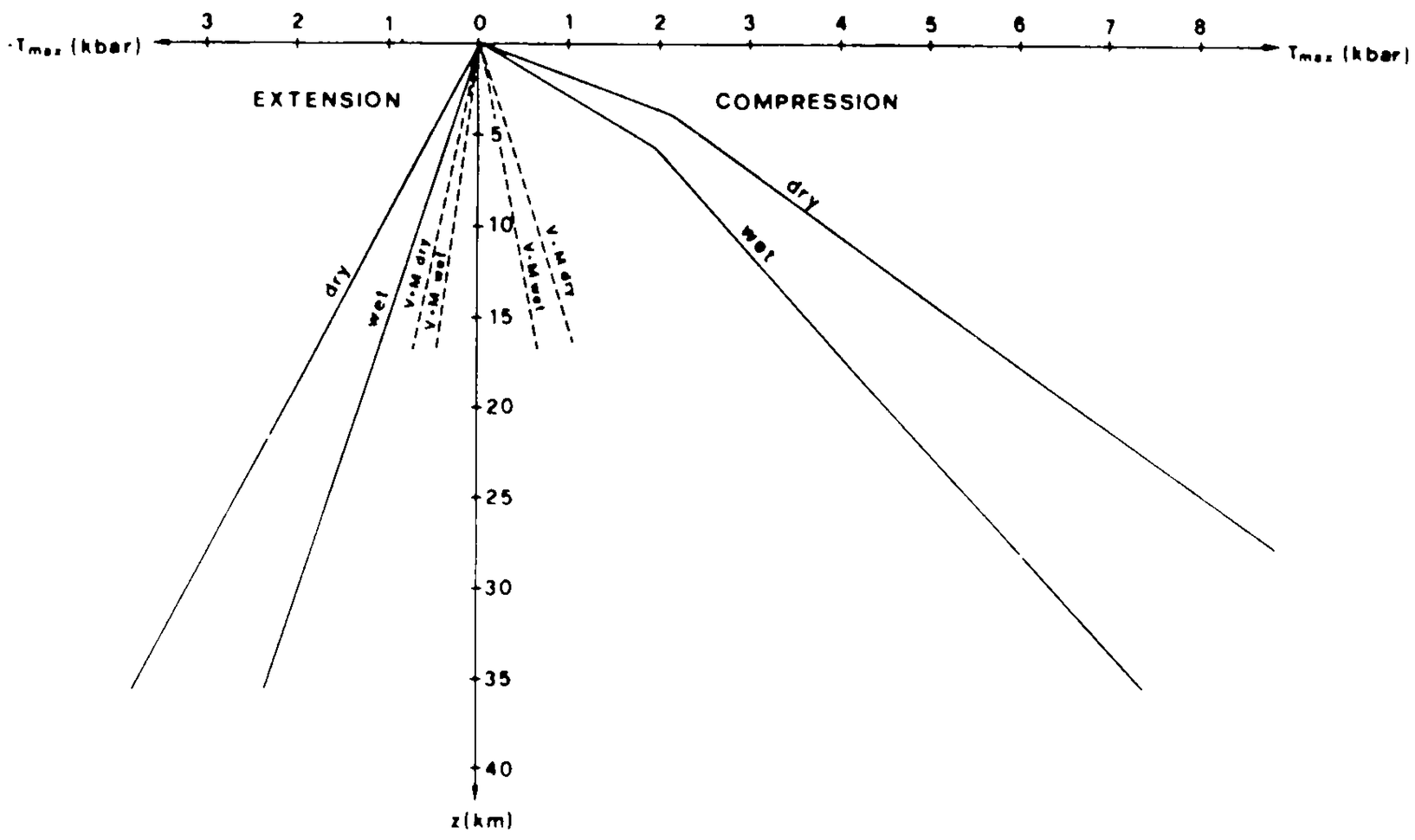

Fig. 6.16. Maximum shear stresses [τ_{MAX}] (brittle failure envelope) with depth below the surface of the Earth (after Meissner and Strehlau, 1982, Fig. 1). Dry: measurements performed on a great number of dry samples, no pore pressure; wet: pore pressure, assumed to be hydrostatic; V+M: measurement on vermiculite and montmorillonite.

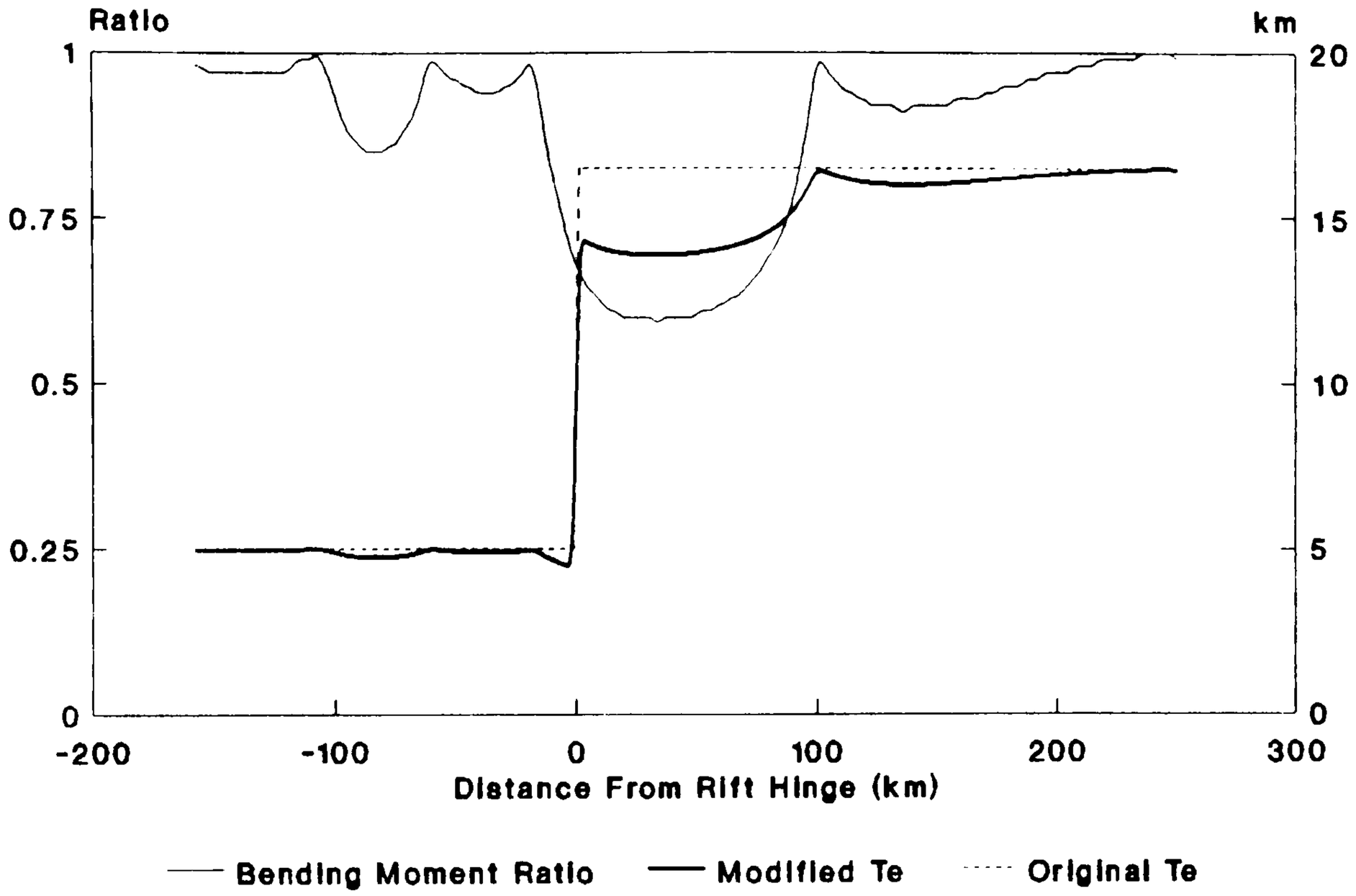

Fig. 6.17. Bending moment ratio and modified T_e, due to brittle failure in the upper crust, for the modelled profile in Fig. 6.15.

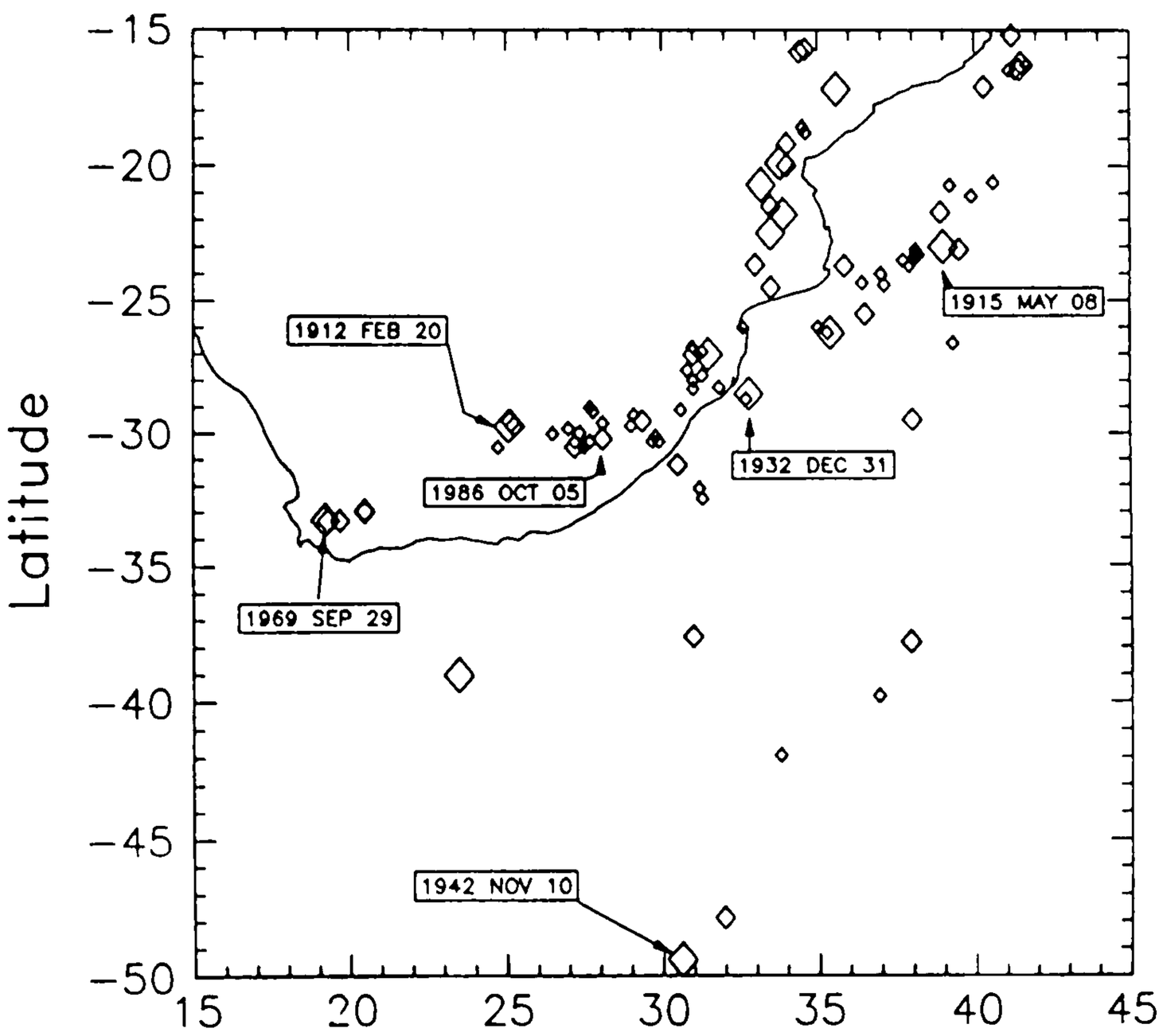

Fig. 6.18. Present day southern Africa seismicity (after Hartnady, 1989). Large open diamond symbols represent events with magnitude ≥6 (Richter magnitude scale), intermediate symbols with magnitude ≥5 and small symbols with magnitude ≥4.

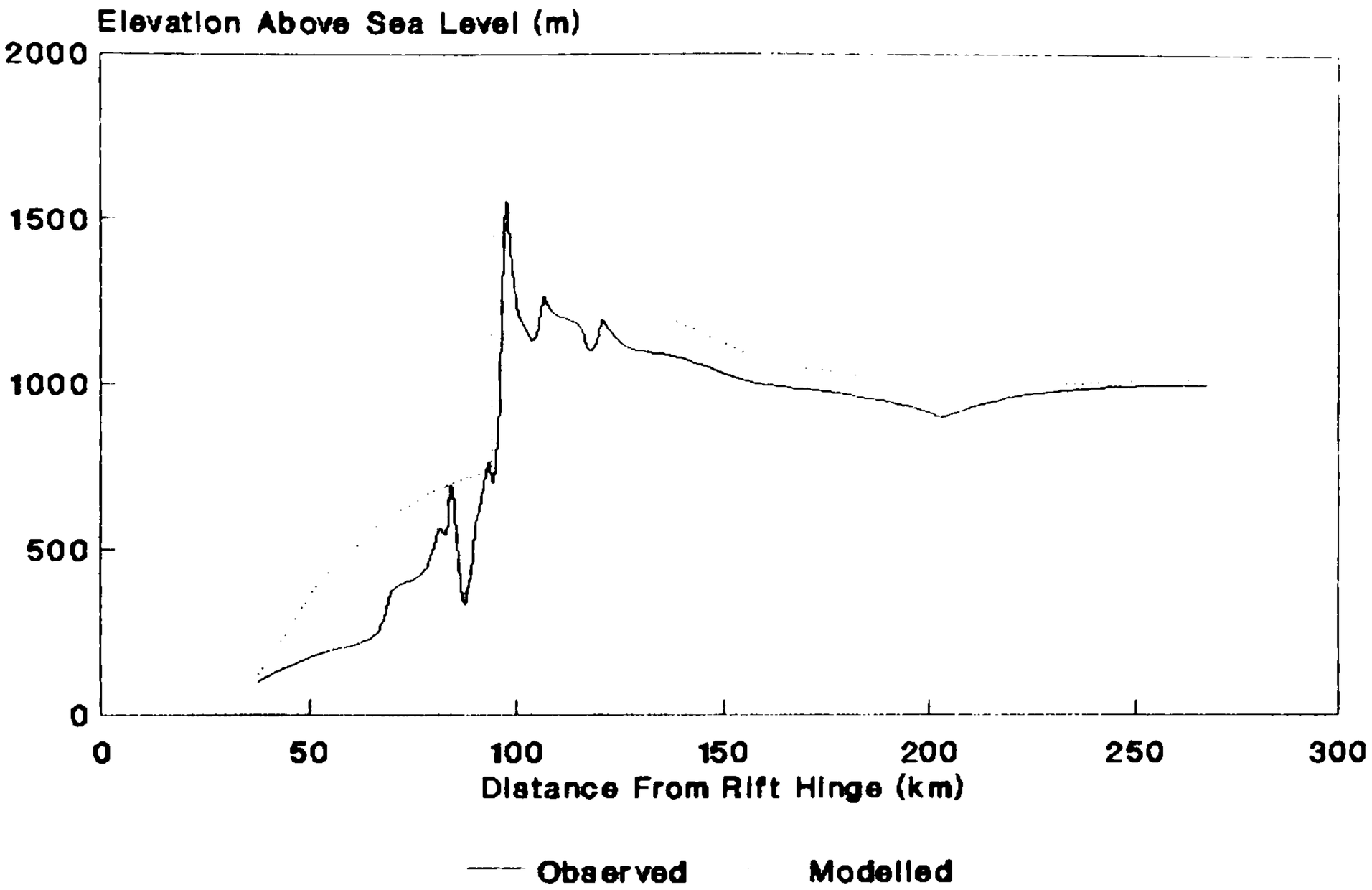

Fig. 6.19. Best modelled fit with T_e=16.5 km displayed with observed topography. The load component comprises onshore denudation, calibrated in section 6.2.1.1 (Dd_e=900 mMa^{-1}, Dd_{cc}=16.5 mMa^{-1}, Dd_{ic}=6.9 mMa^{-1} and SRR=630 mMa^{-1}) but excludes offshore sedimentation. The isostatic component is modelled as a constant rigidity elastic plate (section 6.2.2.1). Flexural model parameters are E=1x10^{11} Nm^{-2}, ν=0.25, g=9.81 ms^{-2}, ρ_m=3300 kgm^{-3} and ρ_i=0 kgm^{-3}.

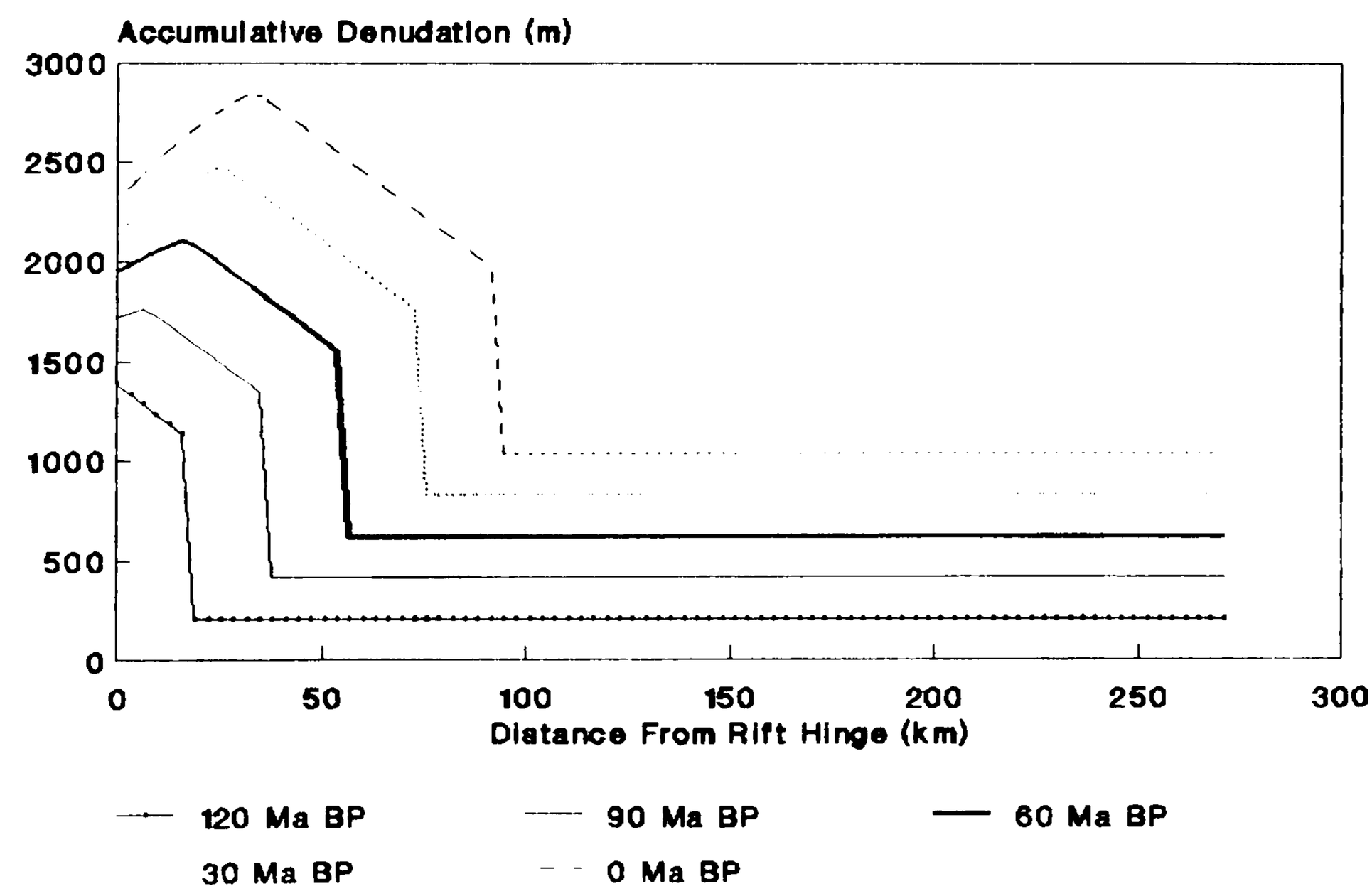

Fig. 6.20. Evolution of the accumulative denudation for the modelled profile in Fig. 6.19.

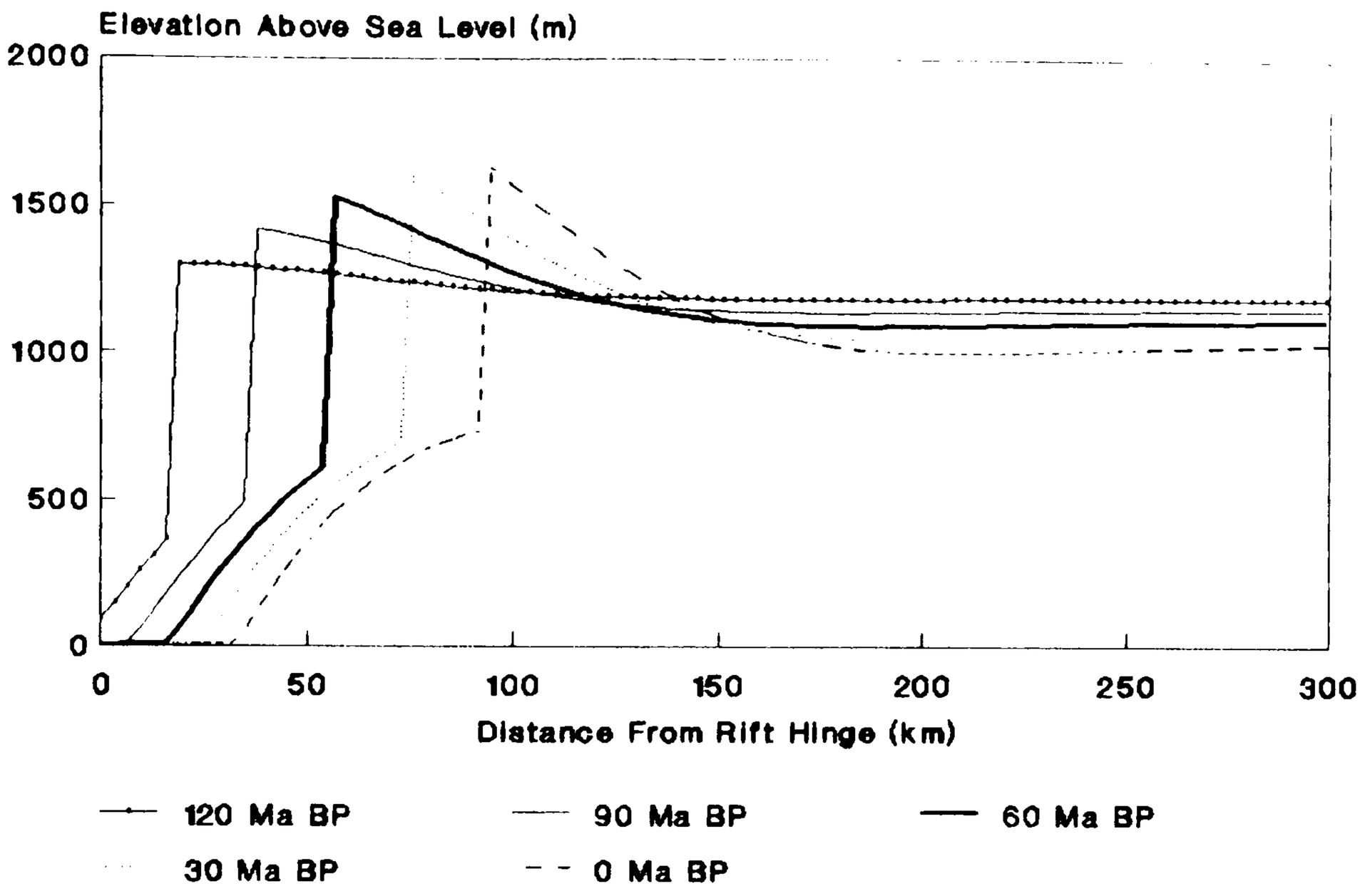

Fig. 6.21. Evolution of the calculated topographic profile in Fig. 6.19.

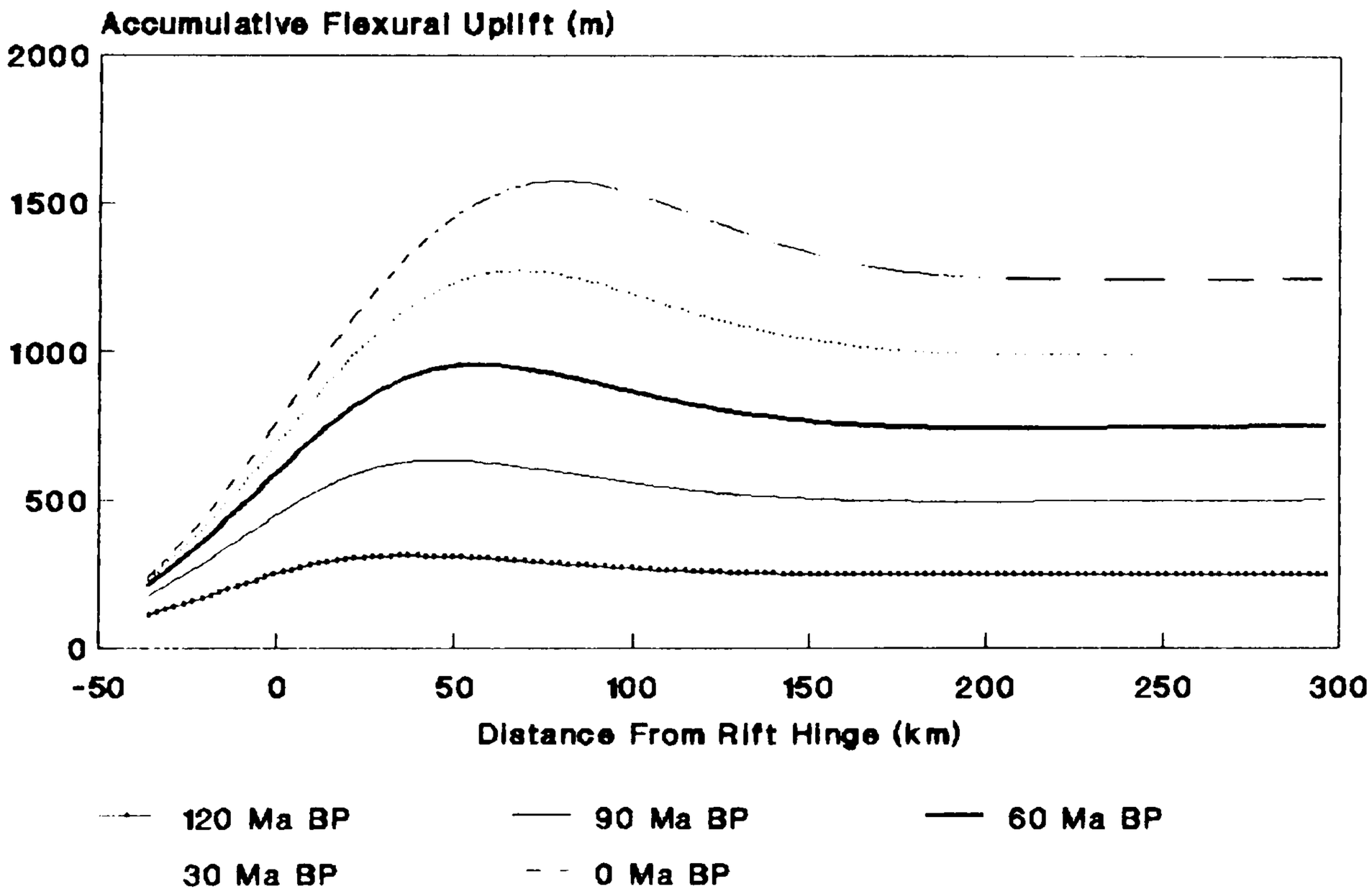

Fig. 6.22. Evolution of the accumulative flexural uplift for the modelled profile in Fig. 6.19.

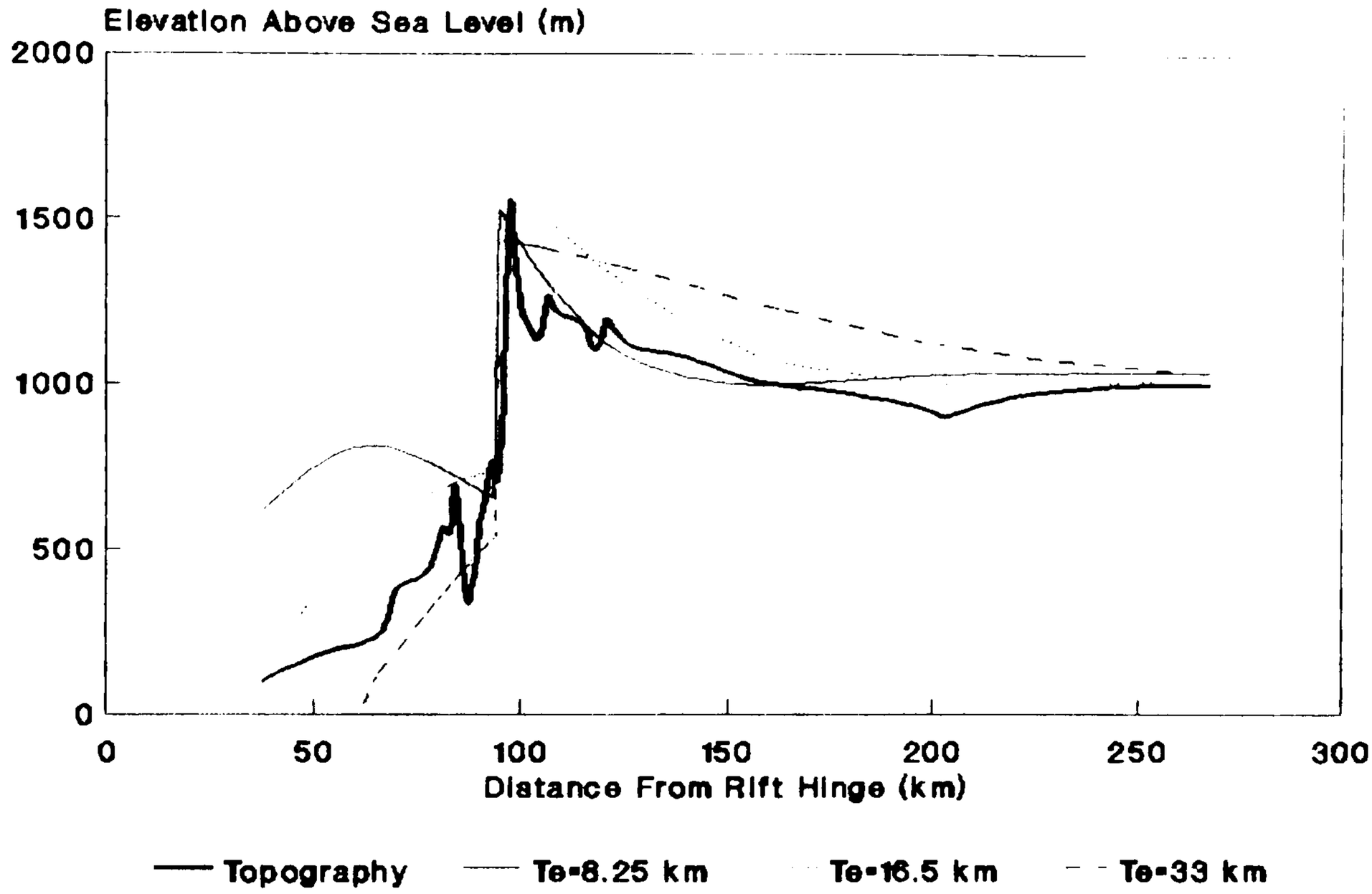

Fig. 6.23. Calculated topographic profiles with various T_e values, displayed with observed topography. Other model parameters as in Fig. 6.19.

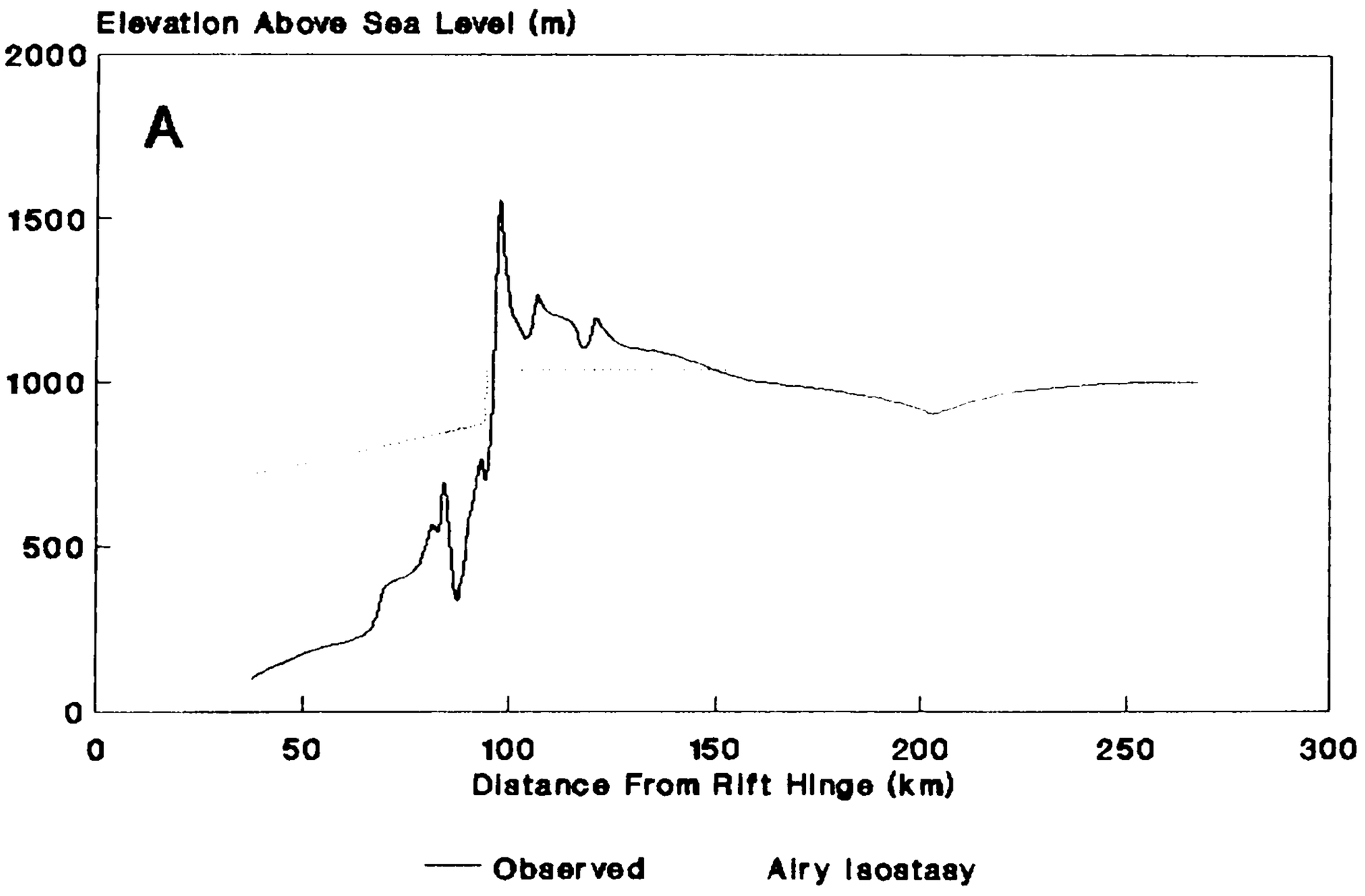

Fig. 6.24. (a) Modelled profile when T_e=0 km (Airy isostasy) displayed with observed topography and (b) evolution of the calculated profile. Other model parameters as in Fig. 6.19.

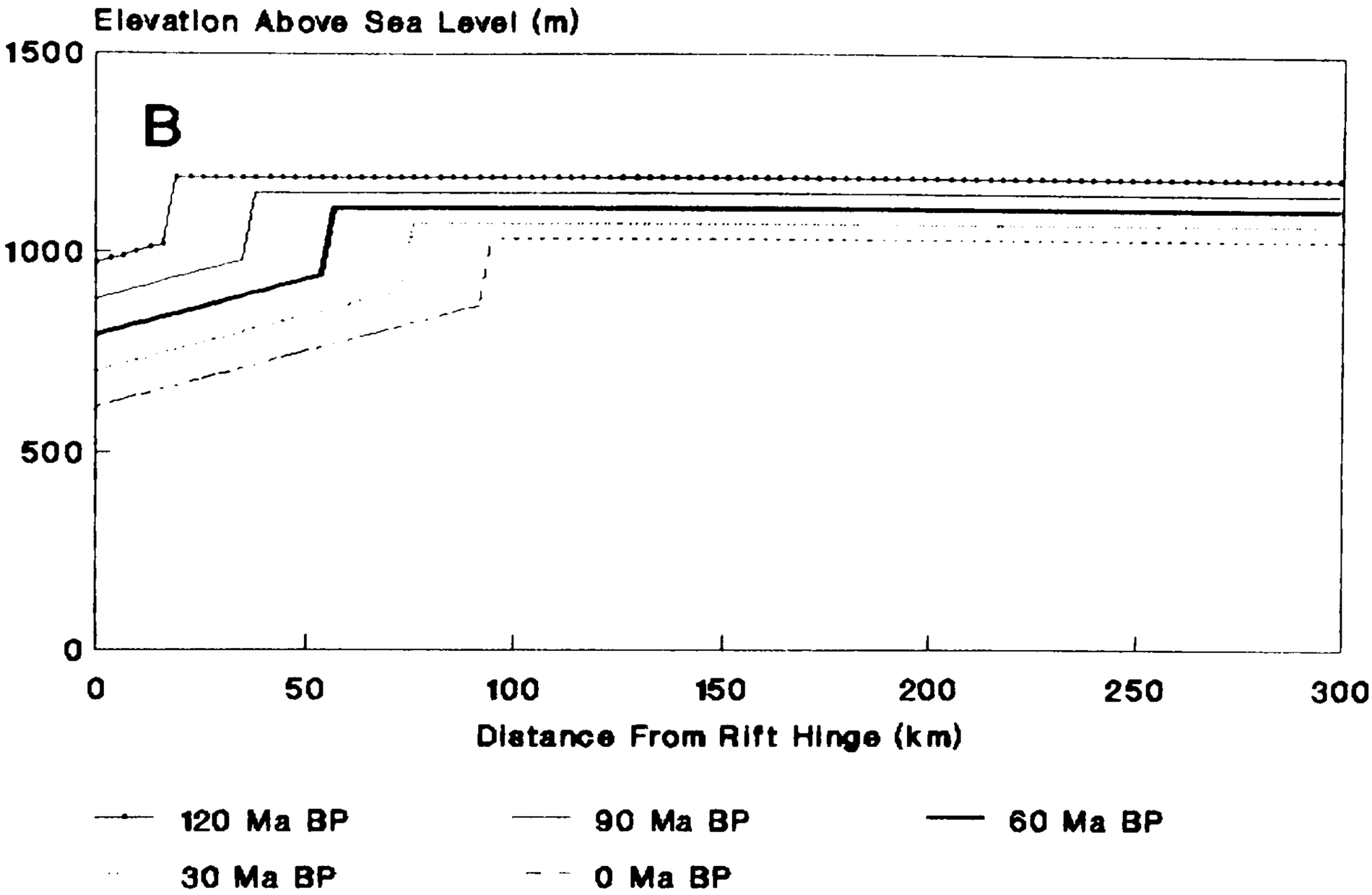

Fig. 6.24. Continued from previous page.

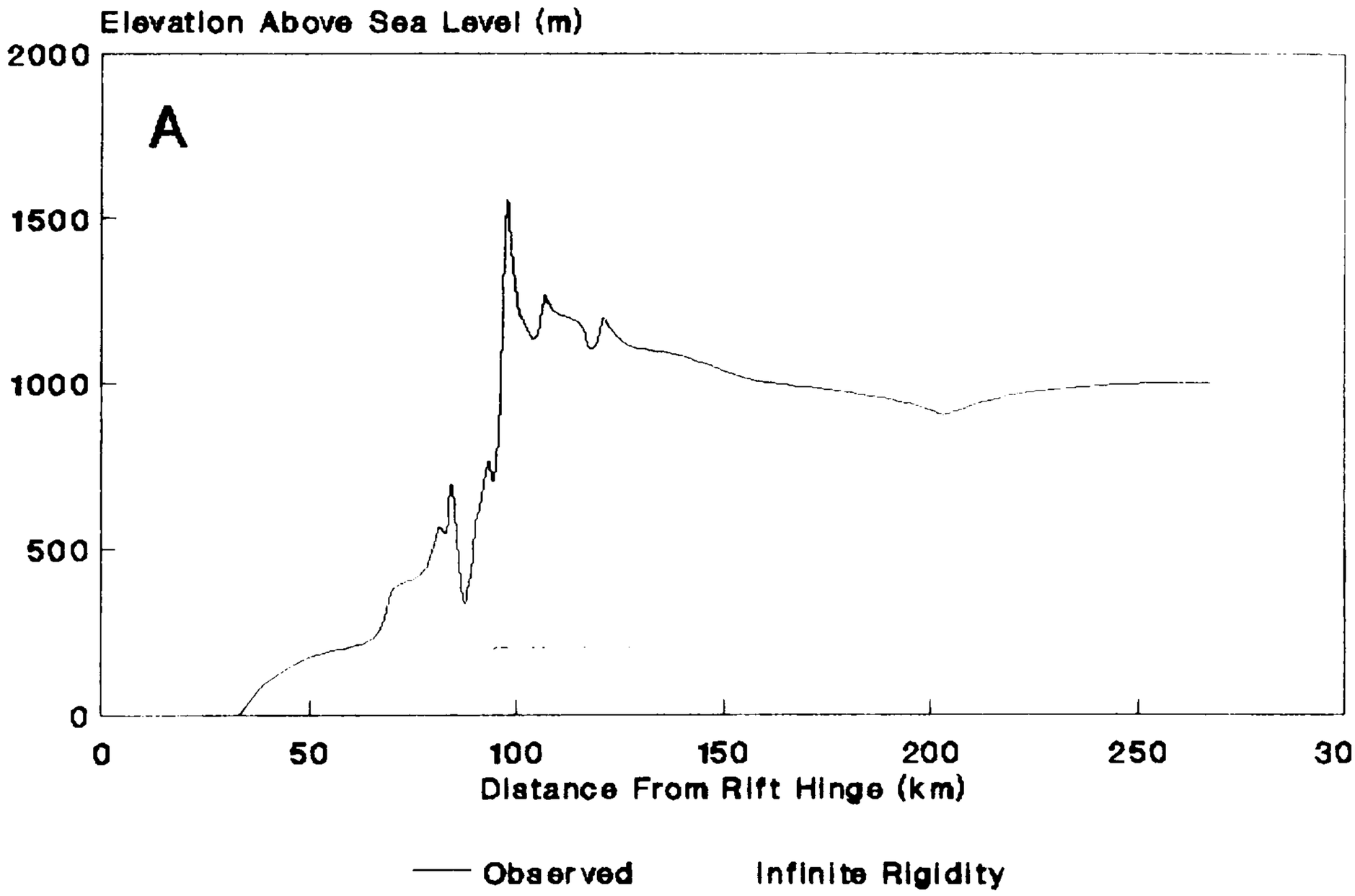

Fig. 6.25. (a) Modelled profile when $T_e=\infty$ km (infinite rigidity) displayed with observed topography and (b) evolution of the calculated profile. Other model parameters as in Fig. 6.19.

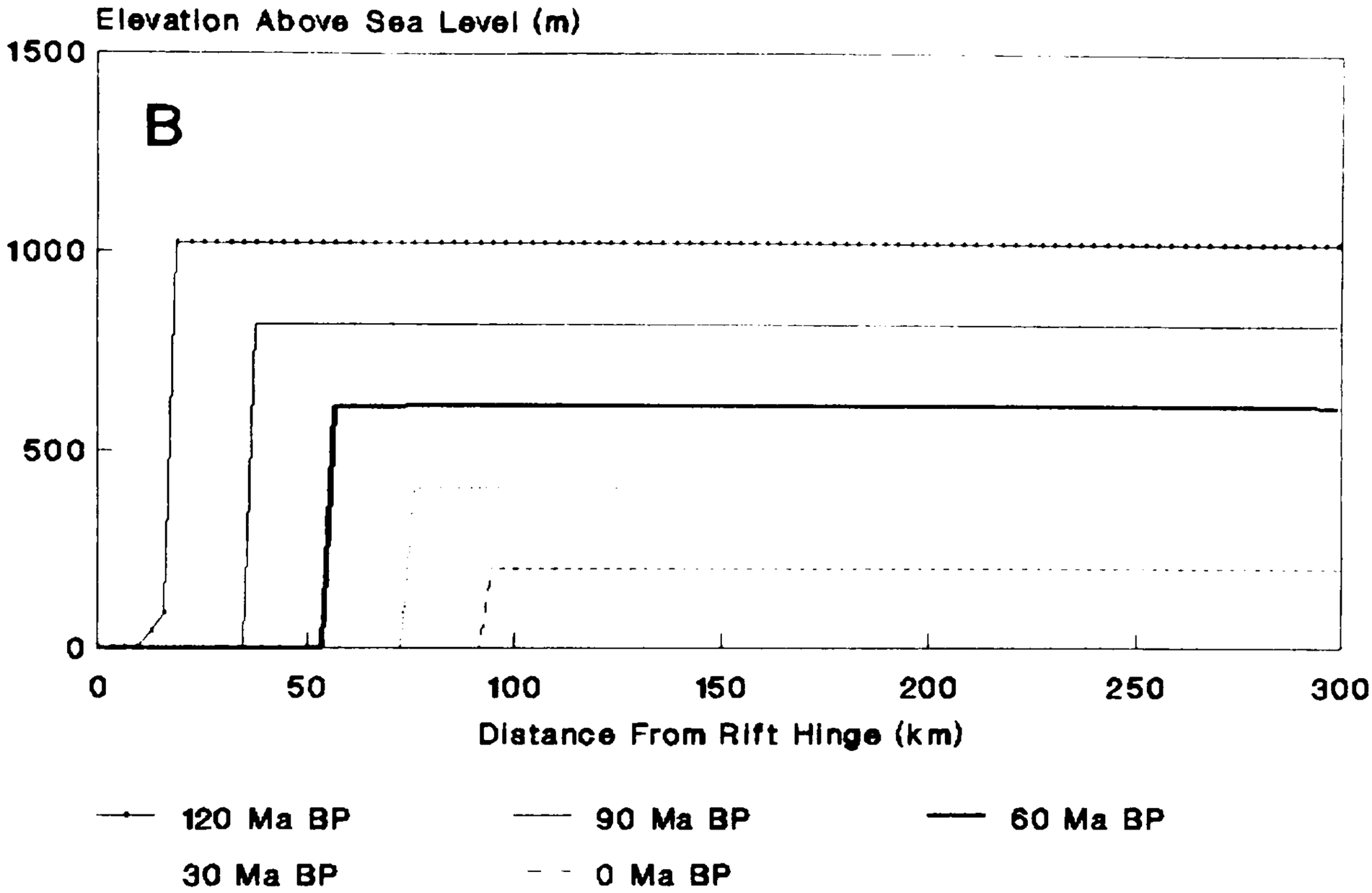

Fig. 6.25. Continued from previous page.

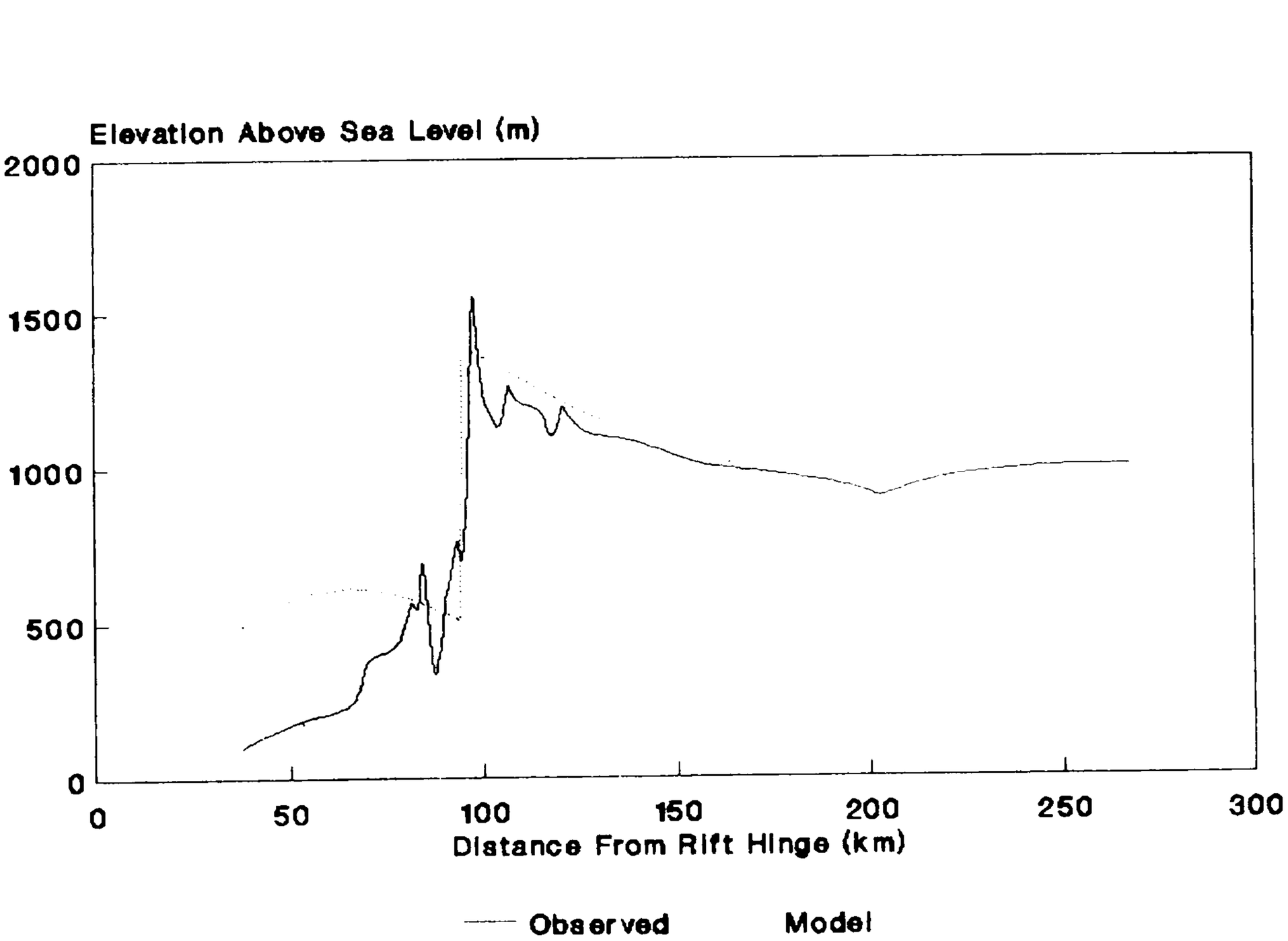

Fig. 6.26. Modelled profile when $Dd_{cc}=Dd_{ic}=9$ mMa^{-1} displayed with observed topography. Other model parameters as in Fig. 6.19.

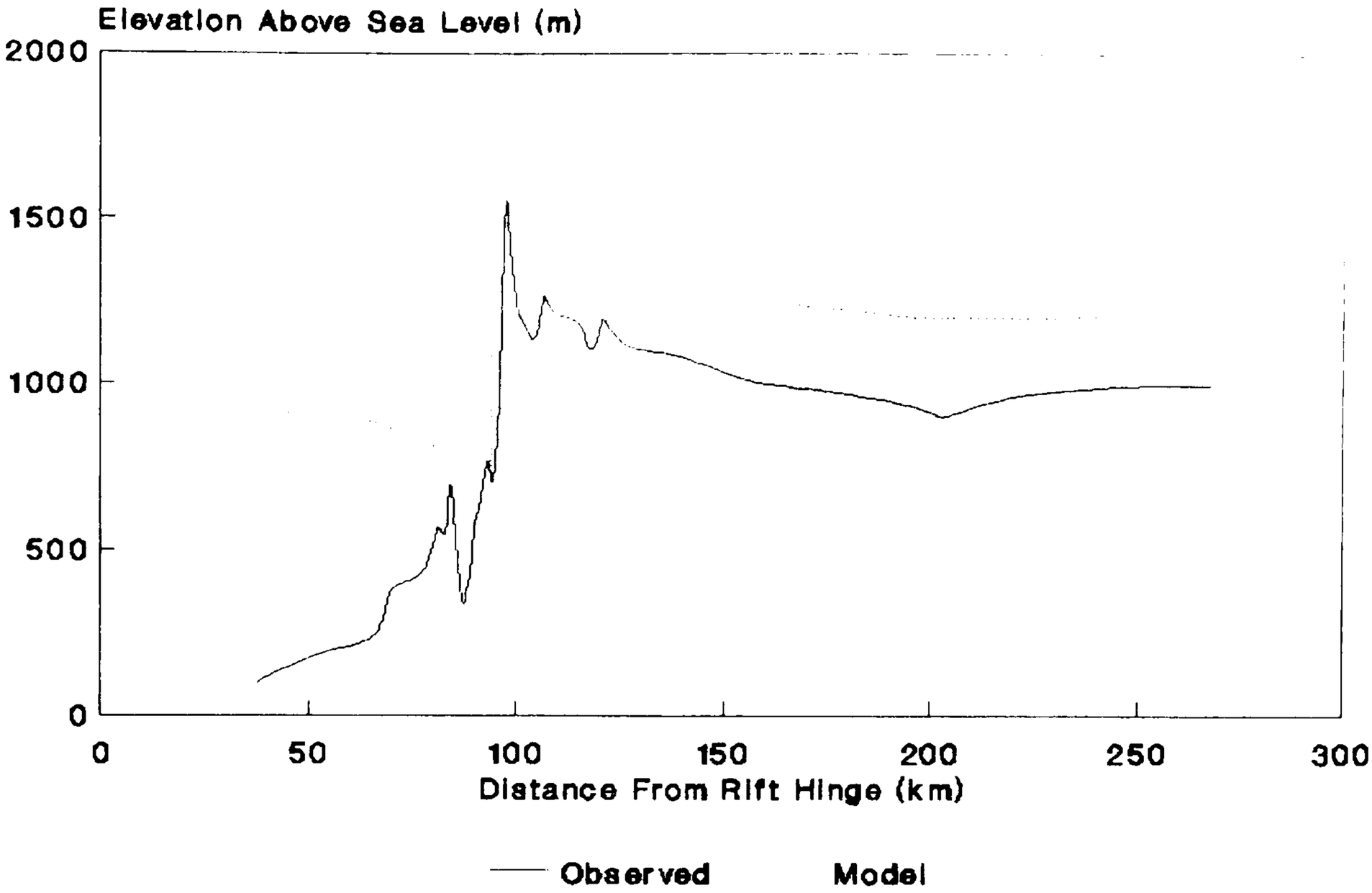

Fig. 6.27. Modelled profile when $Dd_{cc}=Dd_{ic}=0$ mMa^{-1}, so the denudational component of the model is only characterised by Dd_e displayed with observed topography. Other model parameters as in Fig. 6.19.

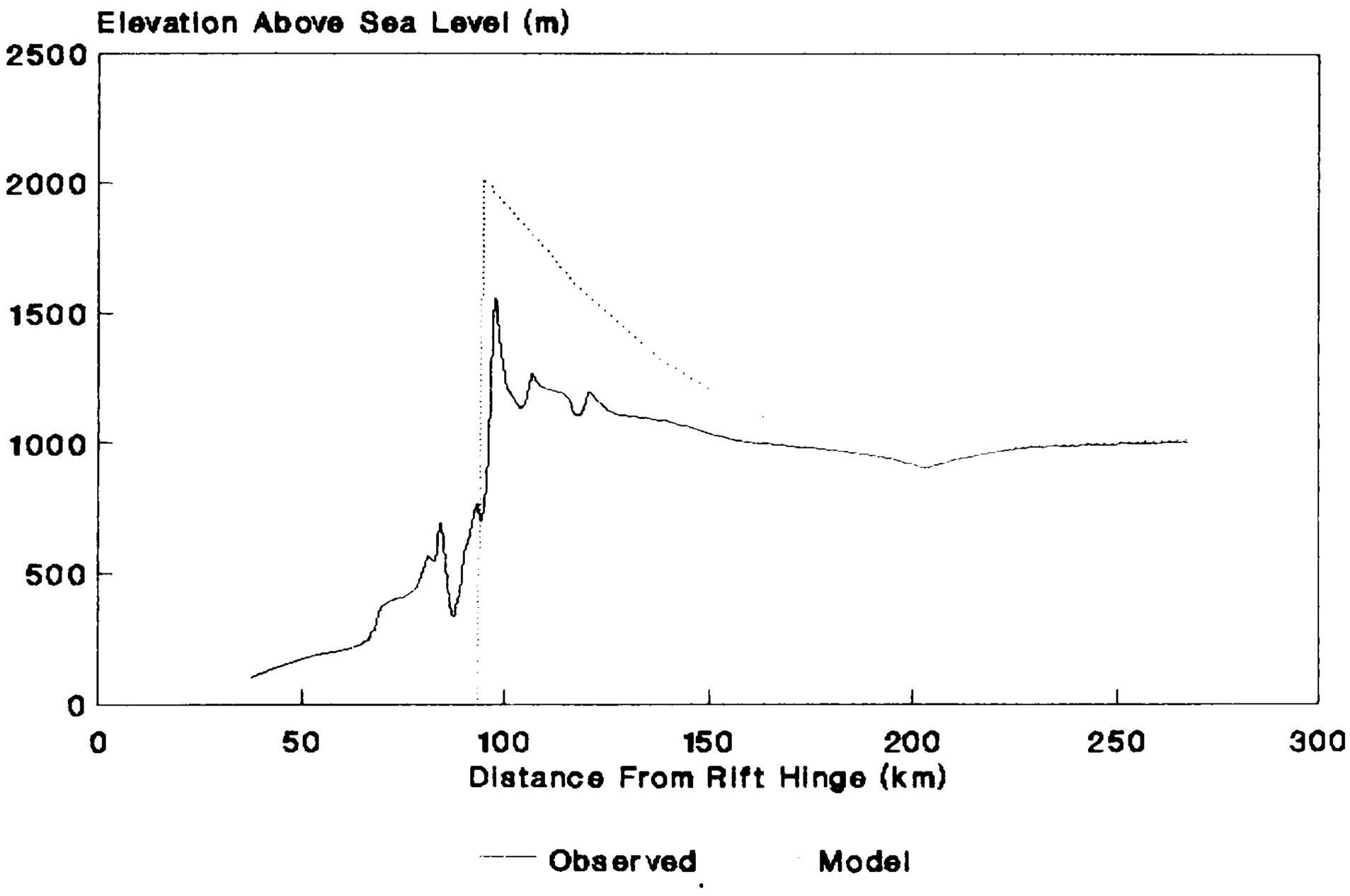

Fig. 6.28. Modelled profile when $Dd_{cc}>>Dd_{ic}=6.9$ mMa^{-1}, so that the coastal region is graded to sea level, displayed with observed topography. Other model parameters as in Fig. 6.19.

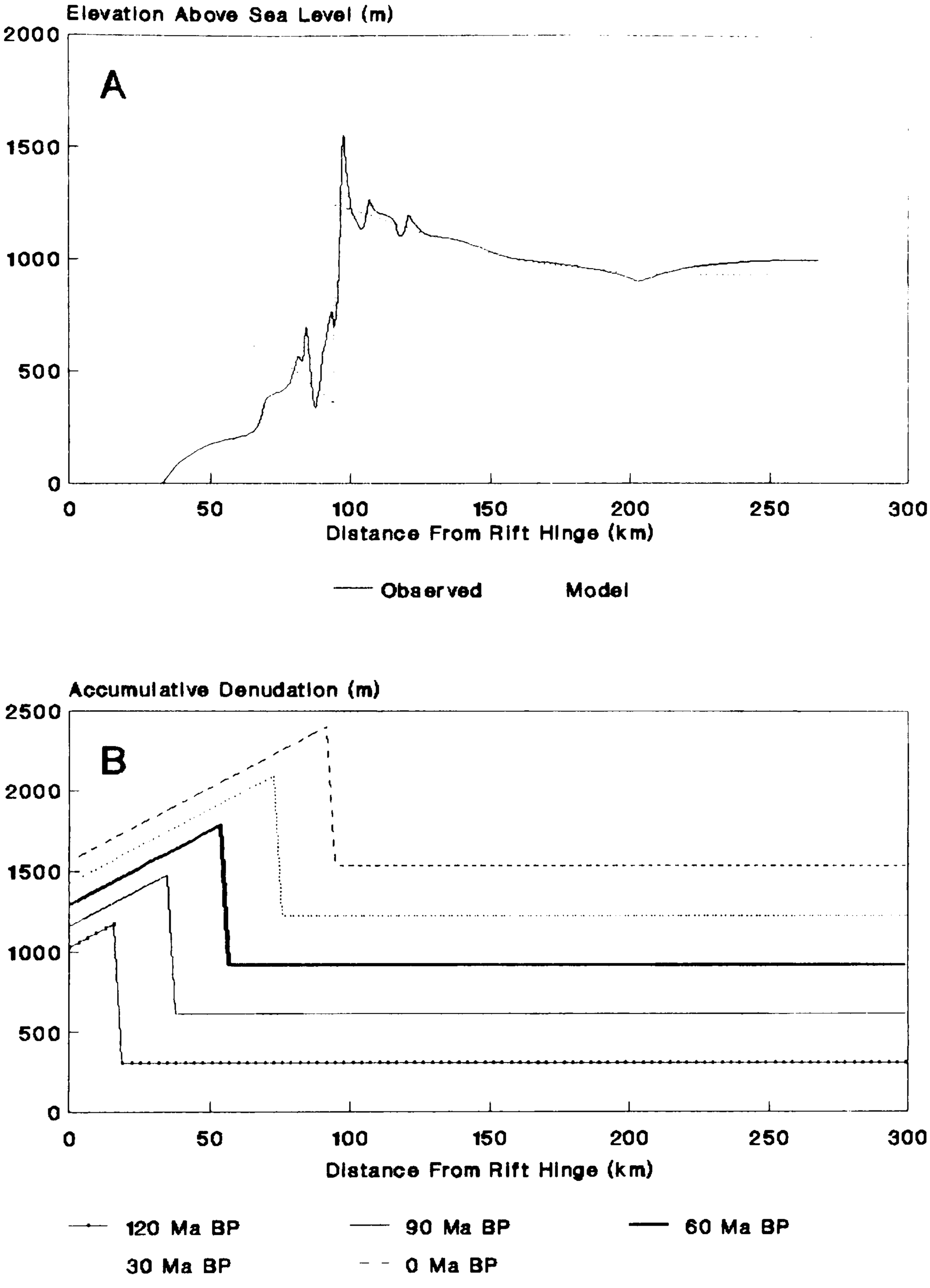

Fig. 6.29. Modelled profile using the denudational model calibration of Pinot and Sourieu (1988), which correlates average drainage basin denudation with average regional elevation. The denudation component parameters are Dd_e=900 mMa^{-1}, Dd_{cc}=4.4 mMa^{-1} Dd_{ic}=10.2 mMa^{-1} and SRR=630 mMa^{-1}. Isostatic component parameters as in Fig. 6.19. (a) Modelled profile displayed with observed topography. (b) Evolution of the accumulative denudation profile.

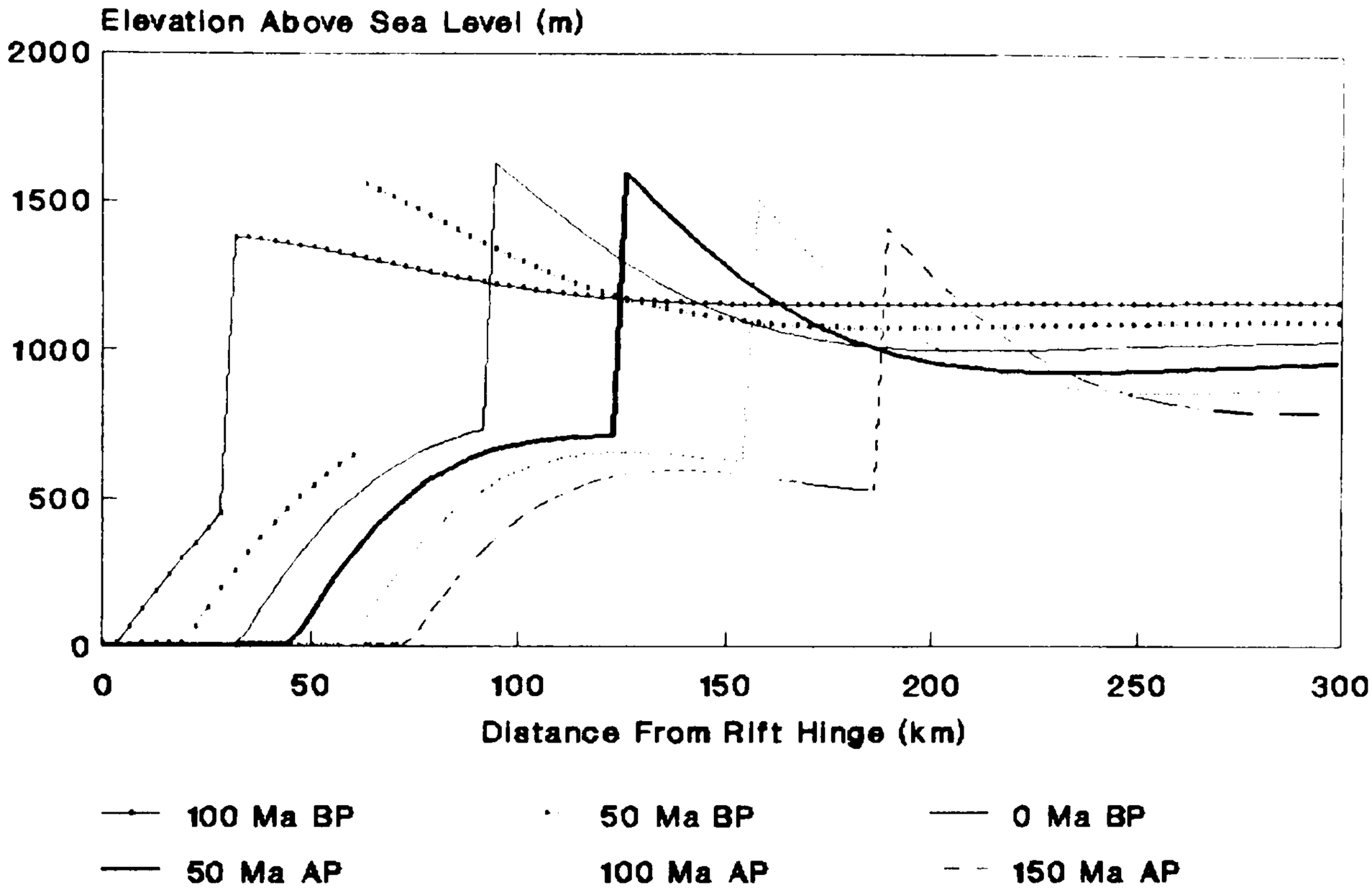

Fig. 6.30. Extrapolation of the modelled profile in Fig. 6.19 one hundred and fifty million years into the future. Abbreviations: AP-after present.

7 MODEL APPLICATION TO SOUTH-WESTERN AFRICA

7.1 Introduction

It was demonstrated in the previous chapter that offshore sedimentation has probably had little effect on the post-rift morphological evolution of south-western Africa. Therefore, in this chapter, which considers ten topographic profiles across the south-west African rifted margin (Fig. 7.1), the simplified morphotectonic model will be employed. This only considers the link between denudation and isostasy. It will be used to help construct the drainage evolution of the margin and suggest mechanisms that control the origin of topography on this passive margin. The results will also be discussed in light of their implications for geodynamic and landscape evolution theories.

7.2 Modelled Topographic Profiles

7.2.1 Denudation Model Calibration

The procedure outlined in section 6.2.1.1 has been used to calibrate the denudation parameters of the model (Dd_{cc}, Dd_{ic}, Dd_t and SRR). For the profiles HAN, ROO and COR which traverse the Southern coastal catchment, the local relief ratio between coastal and interior (Orange) catchment areas indicate that from equation 4.2;

$$Dd_{cc} = 2.38743Dd_{ic} \qquad (7.1)$$

where Dd_{cc} is the coastal catchment denudation rate and Dd_{ic} is the interior catchment denudation rate. Equation 7.1 has previously been used to calibrate the denudational parameters of the model for the ROO profile in chapter 6. The other profiles traverse the Namib coastal catchment which has an average local relief of 345 m, and the continental interior catchments of the Okavango or the Etosha (Fig. 6.4), with an average local relief of 59 m and 71 m respectively. These values have been determined from the 10-minute topographic data set of the National Geophysical Data Center, Boulder, Colorado. The average of the two values (65 m) has been used in equation 4.2 for the calibration of Dd_{cc} and Dd_{ic} and is thought to be representative of the interior catchment in this region. This is because the local relief of the periphery of the Orange catchment (mean local relief of 191 m) is lower than in the confluent zone. The relief ratio employed in the model is not critical as shown in section 6.6.3, and so the average local relief of the combined Okavango and Etosha catchments is thought to be adequate. Therefore, for profiles that traverse the Namib coastal catchment, equation 4.2 is expressed by the following.

$$Dd_{cc} = 5.3077Dd_{ic} \qquad (7.2)$$

For those profiles in the north of the study area which do not traverse the Orange drainage basin, its catchment area (A_{ic}) has still been employed in equation 4.1 for the

calibration of Dd_{cc} and Dd_{ic}. This is because denudation rates on these profiles are likely to have been similar to those to the south, and also the detailed drainage history of the periphery of the Atlantic draining catchments is uncertain. The vertical escarpment denudation rate (Dd_e) is given as the present height of the escarpment, except where the modelled fit criteria in the coastal and interior catchment regions cannot be obtained using this approach. In these cases an increased Dd_e is generally used in order to give the best modelled fit which, therefore, assumes that relatively recent denudational modification has decreased the observed height of the escarpment. The average rate of escarpment retreat, for each profile, has been calculated given the location of the rift hinge and the present position of the Great Escarpment (Fig. 7.1), and assuming that rifting in the Cape Basin began ≈150 Ma BP (Gerrard and Smith, 1980). The calibrated denudation parameters for each profile are displayed in Fig. 7.2.

7.2.2 Best Modelled Fits

An iterative model run approach, changing the effective elastic thickness (T_e) and the initial topographic elevation (H_i) parameters of the model, has been used to determine the best modelled fit as explained in section 6.3.2. Each modelled topographic profile traverses the margin from the present coastline to the point in the continental interior where the pre-Cenozoic strata are covered by the Kalahari Beds. The parameters for the best

modelled fits are shown in Fig. 7.2, and the fits themselves in Figs. 7.3-7.12. Each figure contains four parts: (a) Best topographic fit of the model compared with observed topography; (b) computed topographic sequence; (c) evolutionary accumulative denudation sequence; (d) denudation residual between observed and modelled topography at the end of the model run invoking isostatic rebound. Stream magnitude data is also displayed (see next section).

If the correspondence between observed and modelled topography is considered, there is a wide difference in how accurately the model coincides with reality. This can be broadly considered in three areas, namely coastal, escarpment and continental interior regions. Profiles such as ROO (modelled previously in chapter 6) and TSA generally show a good correspondence between modelled and observed topography in all three regions. For the other profiles the coastal catchment is most reliably modelled on profiles GRO, BRA, ERO and COR, while the continental interior shows the largest deviation on profiles GRO, BRA, ERO, TIR, NAM and HAN. In general the escarpment fit is good, which is to be expected since the present escarpment height is normally one of the model input parameters, with the exception of profiles GRO, NAM, COR and HAN.

7.2.3 Drainage Incision

The simple denudational model presented in this thesis does not consider variations in denudation rates due to

non-uniform drainage incision. Intuitively, areas of large catchments in the lower reaches of drainage systems, such as the Orange and Fish Rivers, will exhibit increased denudation rates. This is due to the increased stream discharge through these areas, in comparison to the peripheral margins of the drainage basin. Some regions are also preferentially incised due to the presence of highly erodible lithology or structural weaknesses, such as areas of faulted bedrock (Fig. 4.19).

The approach adopted in this study to consider variations in drainage incision is to determine the denudation residual between observed and modelled topography at the end of a model run and postulate that this is due to recent drainage incision (part d in Figs. 7.3-7.12). This 'additional denudation' has been calculated iteratively invoking isostatic rebound between each step, until the model solution coincides with the observed topography to within ±50 m, the resolution of the original topographic data set. This denudation residual is then compared to the present stream magnitude profile which has been determined from 1:500000 topographic maps. The stream magnitude at any point on a topographic profile is a surrogate for relative discharge and is characterised by the total number of first magnitude streams draining through that point. This has been used to indicate approximate stream discharge at a point on a profile. This assumes that runoff is constant over the whole catchment area and the catchment area of each first magnitude stream

is approximately the same.

It should be noted that only the present day drainage network can be considered, so spatial variations in the drainage network are assumed to have been negligible. Because of the increasing aridity of south-western Africa during the Tertiary, the drainage is ephemeral in nature and may not accurately represent the network prior to this time. In particular the rates of fluvial incision will almost certainly have been reduced in response to the changing climate.

The denudation residual is quantitively compared to the stream magnitude for the profiles ROO (Fig. 7.13) and GAM (Fig. 7.14). The data contained in these figures are representative of all the profiles and indicate that there is no simple linear relationship between the two variables. This is probably a result of; (1) non-uniform drainage incision due to variable bedrock geology and structure; (2) fluvial incision being controlled by a function of channel gradient and stream magnitude; and (3) incorrect assumptions concerning the initial topographic distribution of the model, which affect the denudation residual computed by the model.

However, on many profiles there is a qualitative relationship between the denudation residual and stream magnitude. For example on profiles BRA, ERO and HAN there are areas where large differences in elevation between modelled and observed topography exist, which coincide with regions of high stream magnitude. This suggests that these

regions have been subjected to increased, temporally averaged, denudation rates which are higher than originally proposed by the conceptual denudational model. This qualitative relationship is further shown in Fig. 7.15, which is a section along the Fish River, a feature approximately parallel and landward of the Great Escarpment in Namibia (Fig. 7.1). This shows that the denudation residual increases downstream with increasing stream magnitude. This would be expected if drainage basins develop by headwaters retreat of fluvial systems.

The Orange River, which breaches the marginal upwarp and drains the continental interior of southern Africa, crosses the profile COR (Fig. 7.10) ≈80 km inland of the coast. At this point the denudation residual has been calculated as ≈2500m (Fig. 7.10d), in addition to the model predicted denudation of ≈1000m (Fig. 7.10b). This suggests a minimal, temporally averaged, incision rate of ≈23 mMa^{-1} for the Orange River, assuming it has occurred over 150 Ma and the Orange River has always drained to the Cape Basin. If the marginal upwarp was not breached until ≈50 million years after rifting, which Rust and Summerfield (1990) have suggested, then the average incision rate increases to ≈35 mMa^{-1}. This suggested rate of fluvial incision would have probably been in response to surface uplift generated by the isostatic rebound to denudation.

On many profiles the worst area of the modelled fit is at the continental interior end of the profile, for example GRO, BRA, GAM, TIR, NAM and HAN. In such areas the stream

magnitude is generally minimal and so drainage incision may not be the reason for the mismatch, if the present day network is representative of the past. Other possibilities that exist to explain this mismatch include the depression of the landsurface due to sedimentation in the terrestrial Kalahari basin. However, modelling of this phenomenon indicates that this mechanism can only account for a few tens of metres of flexural deformation (Fig. 7.16). The most likely explanation of the topographic mismatch between the observed and modelled topography is an initial landsurface that is not horizontal, as assumed in this analysis, but is at a lower elevation in the continental interior.

7.3 Initial Modelled Topography

7.3.1 Syn-Rift Reconstruction

It has previously been discussed in section 6.3.2.1 that the initial topographic elevation (H_i) is an unknown, but constrained, parameter of the model. The postulated value for each profile is given in Fig 7.2. From these values the initial topography of the model has been constructed along a section which approximately coincides with the current coastline (Fig. 7.17). This represents a topographic profile through the Gondwana super-continent at the time of rifting (syn-rift) in the South Atlantic (Fig. 7.18). This irregular surface can be considered to consist of three components.

First, there is a domal feature which approximately

coincides with the postulated mantle plume location of White and McKenzie (1989), and has an amplitude of ≈1600 m from the edge to the centre. Since this plume has been assigned an age of formation coincident with drifting in the South Atlantic (≈120 Ma BP), the associated dynamic thermal uplift would have decayed by now, which indicates that this, presumably permanent, domal feature may be due to magmatic underplating, as suggested by Cox (1989). Given that the density of underplated igneous material is ≈2800 kgm^{-3} (Nisbet, 1982) and invoking Airy isostatic compensation (equation 6.6), due to the extensive regional extent of the effect, the approximate amount of magmatic underplating can be estimated. This assumes that the top surface of the dome was at sea level prior to underplating. If the density of the asthenosphere is ≈3300 kgm^{-3} then this gives an underplating thickness of ≈10.5 km at the centre of the dome, which has a radius of ≈1500 km, declining to 0 km at the edge. Such values of melt thickness can feasibly be generated by a mantle plume sited beneath a region of lithospheric extension (McKenzie and Bickle, 1988; White and McKenzie, 1989). Dated shoreline deposits in the Ecca and Beaufort Groups of the Karoo system in the southern sector of the dome indicate that this area was at sea level during the Permian ≈280 Ma BP. The absence of more recent shoreline deposits means that changes in topographic elevation have to be inferred indirectly. Assuming that surface uplift in this region has been purely due to magmatic crustal underplating, then this indicates

that surface uplift has occurred between the Permian and the commencement of continental drift in the South Atlantic.

Secondly, just to the south of the postulated plume centre is a residual topographic high (Fig. 7.18). This residual topographic high is a feature that predates rifting in the South Atlantic and represents part of the pre-rift Gondwana landsurface. By reference to the tectono-sedimentary terranes of southern Africa (Fig. 7.19), this elevated region was located between two Karoo age sedimentary basins. The Etjo Basin to the north consists of aeolian deposits, while the Botswana Basin to the south was filled with fluvial detritus from a northerly source (Dingle et al., 1983). This corroborates the palaeo-topographic reconstruction suggested here.

Thirdly, the most southerly point on the reconstructed profile is highly elevated, with respect to adjacent points, and is located in the Cape Fold Belt. This feature was a compressional orogen which has undergone vertical crustal thickening in response to horizontal crustal shortening (section 2.2.2.3). With reference to contemporary orogens, such as the European Alps and the Himalayas, the tectonic and isostatic response to this compensation is surface uplift. This view is consistent with palaeodrainage data concerning the evolution of the Karoo system which indicate that an elevated region lay to the south of the main Karoo basin in the position of the Cape Fold Belt. It has been postulated that the Cape Fold

Belt was originally up to ≈4.2 km high (Theron, 1962). This indicates that denudation has significantly reduced the amplitude of the Cape Mountains. Material denuded during this episode was probably deposited in the adjacent Karoo sedimentary basin before the break up of Gondwana.

7.3.2 Gondwana Super-continent Drainage

The previous analysis indicates that the initial syn-rift drainage of the study area, around 150 Ma BP, was probably essentially radial in nature directed away from the dome centre. Plume related volcanics span 190-120 Ma BP (section 2.2.3.2) and so the associated spatial/temporal variations in surface uplift due to magmatic underplating cannot be precisely defined. The assumption in the morphotectonic model is that surface uplift was essentially completed by 150 Ma BP. Provided that there was a significant regional elevation by this time, then the model results are not adversely affected since the relative difference between regional elevation and base level is not a controlling variable of the denudational model.

Disrupting this postulated simple drainage pattern were at least two areas of anomalously high terrain. One was located to the south of the postulated dome centre and the other to the south of the mantle plume periphery in the Cape Fold Belt. From geological evidence (section 7.3.1) these features pre-date rifting in the South Atlantic. Both probably had a controlling influence on sedimentation in the Karoo Basin.

7.3.3 Implications for Post-Rift Topographic Modelled Fits

It has already been noted that the largest denudation residual calculated for the modelled profiles is often found towards the continental interior. If the topography of this region of Gondwana was influenced by mantle plume activity, then it has been suggested that this topography was probably domal in shape, centred where the Walvis Ridge meets the present coastline. This is as opposed to horizontal as originally assumed in the model. Therefore, this domal initial topographic condition, derived from Fig. 7.18, has been imposed upon each best modelled fit for profiles GRO (Fig. 7.20), BRA (Fig. 7.21), ERO (Fig. 7.22) and GAM (Fig. 7.23). These profiles will be most affected by the postulated region of crustal underplating since they are all located near to the centre of the dome.

On each profile (Figs. 7.20-7.23) the calculated and observed topography have a better correspondence in the continental interior catchment area, although the total difference between the calculated and observed topography cannot be accounted for. The remaining difference is most likely due to a combination of an irregular initial landsurface, which was depressed in this region, and uncertainty concerning the denudational chronology of the region.

7.4 Spatial Variations in Flexural Rigidity

Sections 5.4.1-3 discussed the nature of isostasy, with reference to passive margins. Numerical modelling of

the long-term thermo-mechanical properties of continental lithosphere indicates that flexural rigidity increases with age following a major thermal event (Karner et al., 1983; Kusznir and Karner, 1985). This idea will be tested using data from south-western Africa.

For the ten profiles in Fig. 7.3-7.12, a best modelled fit has been determined. One of the unknown model parameters in this approach is the effective elastic thickness (T_e) which characterises the continental lithosphere rigidity. This value of T_e represents the spatially and temporally averaged flexural rigidity of the margin since rifting. The approximate age of the continental basement for southern Africa is shown in Fig. 2.2, although in most cases the location of tectonic boundaries are uncertain and many profiles traverse more than one structural terrane with contrasting ages. When this occurs, the age of the region through which the greater part of the profile traverses has been taken as the age of the basement. From Fig. 2.2 the basement of Middle Proterozoic, Late Proterozoic and Pan African ages are ≈1300, ≈800 and ≈400 Ma BP respectively, which represent the chrono-stratigraphic mid-point of these horizons. Following Karner et al. (1983) the age of the plate is shown against rigidity (Fig. 7.24). This indicates that there is no strong relationship, from the data presented here, between flexural rigidity and basement age.

However, the geothermal gradient of the lithosphere is crucial in determining the strength of the lithosphere, due

to the temperature-dependent rheology of the crust and mantle (Kusznir and Karner, 1985). Increasing the geothermal gradient decreases the rigidity of the lithosphere and vice-versa. Therefore, the postulated mantle plume of White and McKenzie (1989), which used to underlay part of the study area ≈120 Ma BP, may have influenced the recent geothermal history of the lithosphere in this region. In Fig 7.25 the location of each profile and its associated T_e determination, with respect to the centre of the mantle plume, is shown. This indicates a roughly linear trend from lower values of T_e (≈20 km) at the centre of the mantle plume to higher values (≈45 km) at the plume edge. This trend suggests that the geothermal gradient, which will probably be higher at the centre of a mantle plume than at its edge, may have effectively lowered the thermal age of the continental lithosphere towards the centre of the mantle plume, and hence the rigidity of the lithosphere. It would, therefore, appear that a thermal event, represented by the mantle plume of White and McKenzie (1989), has determined the recent (<≈ 120 Ma BP) flexural rigidity of the continental lithosphere of this region.

7.5 Great Escarpment Location on Passive Margins

In the quantitative morphotectonic model presented in chapter 6 the Great Escarpment of south-western Africa was assumed to have been initiated at the rift hinge, in response to rifting, and have retreated to its present

position with a constant horizontal velocity. From Fig. 7.2 the variation in scarp retreat rates (SRR) are between 630 mMa^{-1} for the ROO profile and 1479 mMa^{-1} for the TSA profile. These temporally averaged rates for the south-west African rifted margin compare to contemporary scarp retreat rates of 500-6700 mMa^{-1} for the Colorado plateau (Schmidt, 1989). The study of Schmidt (1989) has shown that the rates of scarp retreat are controlled by the thickness and denudational resistance of caprocks. This suggests that large variations in SRR occur in response to localised geological/structural conditions. Thus, in reality large variations in SRR will probably have occurred during the evolution of the south-west African rifted margin due to non-uniform bedrock geology..

The distance of escarpment retreat, with respect to the rift hinge, for passive margins of different ages has been deduced (Fig. 7.26). Scarp retreat rates have been calculated from this data and although each margin shows a wide variation in these values, younger margins tend to display higher rates. For example the Red Sea region, with an age of formation of ≈30 Ma BP, exhibits an average escarpment retreat rate of up to 2767 mMa^{-1}, approximately twice the temporally averaged rate in south-western Africa. This indicates that escarpment retreat rates are probably greater during the early history of passive margin evolution in response to the creation of new geomorphic base levels during rifting. This would cause rapid fluvial incision and escarpment retreat, which would decrease as

the evolving fluvial systems tended towards a graded quasi-equilibrium.

With reference to Fig. 7.2, there appears to be a strong relationship between escarpment retreat rate (or escarpment position with respect to the rift hinge) and the effective rigidity of the lithosphere, characterised by the effective elastic thickness (T_e). This is shown in Fig. 7.27. In this analysis T_e is a model unknown and is varied in order to give the best modelled fit. Varying the T_e of a model run tends to have the most effect in the coastal catchment region, the amplitude of the marginal topographic upwarp being barely affected (section 6.6.2). Increasing T_e causes the modelled coastline to be located landwards of its observed position. Decreasing T_e tends to promote additional surface uplift in the coastal catchment region and the generation of a second, minor, drainage divide. By allowing the model to run 'into the future' (temporal as opposed to spatial changes) the width of the coastal catchment is increased. In addition, a second, minor, drainage divide is also generated (section 6.6.4). None of the topographic profiles across the south-west African rifted margin (Figs. 7.3-7.12) display this morphology, with a second drainage divide. This suggests that flexural rigidity influences the morphological evolution of passive margins, perhaps as the graded response of denudational processes to flexural isostatic uplift.

7.6 Instantaneous Down-wearing Denudational Model

It has been noted in section 4.3 that the conceptual denudational model, describing escarpment retreat on high-elevation passive margins, may not be applicable to regions where the bedrock geology is not dominated by horizontal stratification with frequent caprocks in the sequence. In these areas sub-vertical structural discontinuities, such as the edges of igneous intrusions, often control the landscape evolution of inselbergs, or erosional remnants. In these cases landscape evolution may be dominated by vertical down-wearing, as in Davisian peneplanation, in contrast to the escarpment retreat, or pediplanation, model of landscape evolution.

At the present day, denudation process rates in south-western Africa are low in response to the prevailing arid climate (Ward et al., 1983). In this section it is assumed that an alternative landscape evolution model, which envisages instantaneous down-wearing of the landscape, applies to the post-rift landscape evolution of south-western Africa (Fig. 7.28). This may have been in response to fluvial incision and is calculated as an iterative solution invoking isostatic uplift between each model step, until the resolution between modelled and observed topography is ±50 m, the resolution of the original data set. As in section 7.2.3 the final solution of the modelled topography is the observed topography, and so there is no residual to explain. For three profiles (BRA, ERO and ROO), where extensive caprock controlled escarpments are absent,

the accumulative denudation profile for the escarpment retreat model including fluvial incision (model 1), is displayed with reference to the accumulative denudation profile which has been calculated using the 'instantaneous' landscape lowering model (model 2) [profiles BRA (Fig. 7.29), ERO (Fig. 7.30) and ROO (Fig. 7.31)]. Both models use the same T_e for each profile, as given in Fig. 7.2. These indicate that, in order to replicate the observed topography exactly, model 2 requires a greater amount of accumulative denudation than model 1 in the coastal catchment region, although the difference is not great. The mismatch between the two curves is due to the mechanics of how flexural isostasy compensates different spatial and temporal variations in denudation rates. In both models the maximum amount of denudation is located in the coastal catchment region. Model 1 assumes that a linear escarpment retreat is followed by instantaneous vertical drainage incision, whereas model 2 assumes instantaneous vertical denudation at the beginning of the model run and then quiescence to the present day.

The comparison between the two denudational models in Figs. 7.29, 7.30 and 7.31 generally indicate that for an assumed initial topography and known final topography, different temporal denudation sequences at a point on a profile do not greatly affect the accumulative denudation at that point, given the same isostatic model parameters. It would, therefore, be useful if an independent quantitative technique could be employed to constrain

temporal variations in denudation rates, and resolve the basic ambiguity between the two conceptual models of landscape development. Apatite fission track analysis (AFTA) has the potential to document variations in denudation rates (Green et. al., 1989). For the south-west African margin AFTA data indicate that there was an accelerated phase of denudation during the early stages of the margin development (Brown et al., 1990). This generally agrees with offshore sediment volume data concerning the Cape Basin which indicate declining denudation rates from rifting to the present (Rust and Summerfield, 1990).

7.7 Denudation Rates - Contemporary and Long-Term Estimates

In this section contemporary and long-term estimates of denudation rates will be compared for the Orange River (interior catchment) and Cape coastal (coastal catchment) regions of southern Africa. Denudation rates for Namibia will not be considered due to the paucity of data for this region.

The denudation rate of the Upper Orange River Basin for the period 1929-1969, calculated from mean sediment yield data, (Rooseboom and Harms, 1979) is $\approx$55 mmka^{-1} (mMa^{-1}). Using the regression analysis of Ahnert (1970), which correlates the denudation rate of large mid-latitude drainage basins with mean catchment local relief Summerfield (1991b) has determined that contemporary denudation rates are $>$ 80 mMa^{-1} over much of the coastal region and $<$ 20 mMa^{-1} across most of the elevated interior

region.

Long-term denudation rates derived from offshore sediment volume data (Rust and Summerfield, 1990) indicate that the average denudation rates for all of the Atlantic draining catchments, comprising coastal and continental interior regions, has declined from 41-82 mMa^{-1} during the period ≈152-113 Ma BP to 7-9 mMa^{-1} during ≈37-0 Ma BP, and the average depth of post-rift denudation is ≈1800 m. It should be noted that the uncertainty in these estimates is high, due to the absence of data concerning the detailed drainage evolution of the margin. The estimate of the average depth of post-rift denudation has been used to calibrate the conceptual denudation model for high-elevation passive margins presented in chapter 4. This gives average denudation rates for the margin evolution (≈150-0 Ma) of ≈16.5 mMa^{-1} and ≈6.9 mMa^{-1} respectively for the coastal and interior Orange river catchments and 900 mMa^{-1} for the Great Escarpment (Gilchrist and Summerfield, 1990).

The comparison of long-term and contemporary denudation rates between the coastal and interior catchments indicate that contemporary rates are approximately four times that of the long-term estimates. Correlating the accumulative rate of Al_2O_3 in deep sea sediments with continental denudation rates, Donelly (1982) suggests that there has been a vast increase in worldwide denudation rates during the past 15 Ma which may have been in response to climatic deterioration. This proposal may

account for the discrepancy between contemporary and long-term estimates of denudation rates for southern Africa, although the increase in non-biogenic sediment may also have been aeolian in origin, which would be compatible with increasing late Cenozoic aridity. Other possibilities include anthropogenic factors, such as intensive farming techniques, which have increased historical denudation rates in response to changes in land management and farming techniques. In a comparison of sedimentation rates in the Natal Valley, south-western Indian Ocean, with modern sediment yields in rivers of south-eastern Africa, Martin (1987) has found that modern rates of sediment supply are ≈12-22 times that of the geological average. He attributes this increase in modern sediment yields as due to the influence of man.

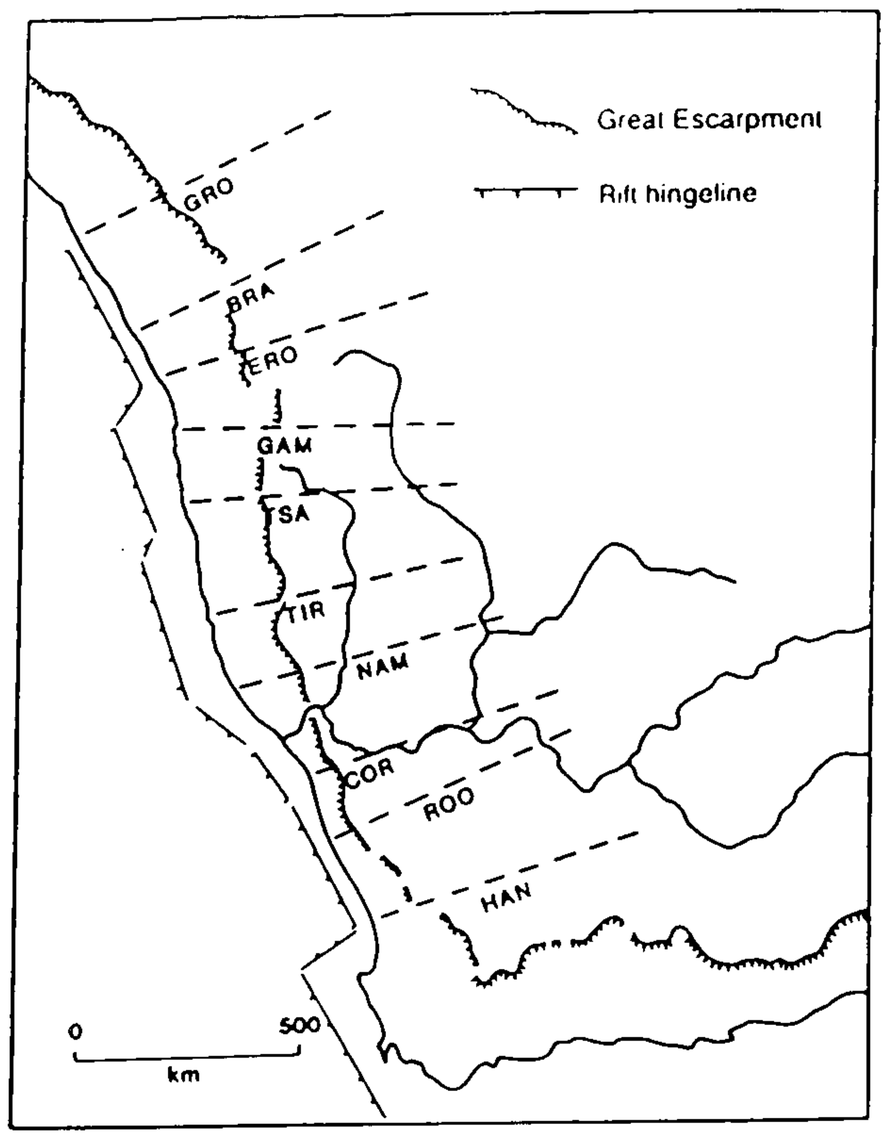

Fig. 7.1. Location map of the ten topographic profiles modelled in chapter 7. The designation for each profile is derived from the first three letters of the marginal upwarp mountains which the profile traverses: GRO-Grootberg; BRA-Brandberg; ERO-Erongoberge; GAM-Gamsberg; TSA-Tsarisberge; TIR-Tirasberge; NAM-Namisberg; COR-Cornellberg; ROO-Rooiberg; and HAN-Hantamsberg.

Profile	Dd_e (mMa^{-1})	Dd_{cc} (mMa^{-1})	Dd_{ic} (mMa^{-1})	SRR (mMa^{-1})	T_e (km)	H_i (m)	DRC (km)
GRO	1200	22.4	4.2	807	20.0	1575	20.5
BRA	1800	17.7	3.3	705	20.0	1700	33.7
ERO	1500	20.1	3.8	1106	35.0	1850	39.9
GAM	1000	24.0	4.5	1330	32.5	1700	28.0
TSA	1000	24.0	4.5	1479	40.0	1450	82.8
TIR	1000	24.0	4.5	1280	30.0	1550	57.0
NAM	1150	22.8	4.3	1361	45.0	1350	98.2
COR	1200	15.8	6.0	749	22.5	1100	64.4
ROO	900	16.5	6.9	630	16.5	1225	33.0
HAN	1200	15.8	6.0	1142	42.0	1700	36.8

Fig. 7.2. Table of the model parameters for the best fit between calculated and observed topography for the ten profiles shown on Fig. 7.1. Abbreviations: Dd_e-escarpment denudation rate; Dd_{cc}-coastal catchment denudation rate; Dd_{ic}-continental interior catchment denudation rate; SRR-escarpment retreat rate; T_e-effective elastic thickness of the lithosphere; H_i-initial elevation of the topographic profile; and DRC-distance from the rift hinge to the present coastline.

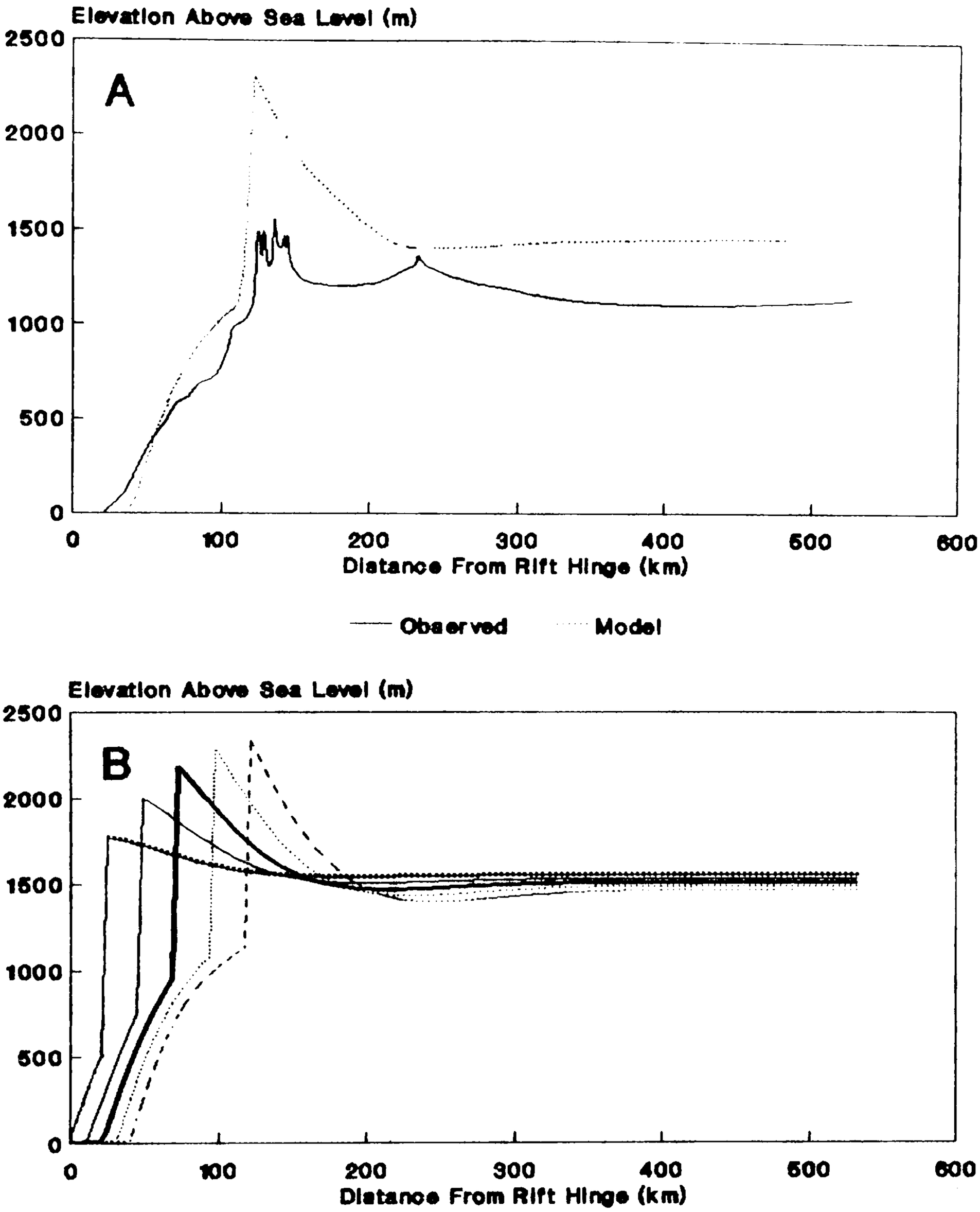

Fig. 7.3. Best modelled fit for profile GRO: (a) Calculated topographic profile displayed with observed topography; (b) evolution of the modelled topographic profile; (c) evolution of the modelled accumulative denudation; and (d) residual denudation between the modelled and observed topography at the end of the model run so that the two profiles coincide. This has been added to the accumulative denudation at the end of the model run to give the total denudation. The stream magnitude across the profile is displayed for comparison and has been derived from 1:500000 maps of South Africa and Namibia. Continued overleaf.

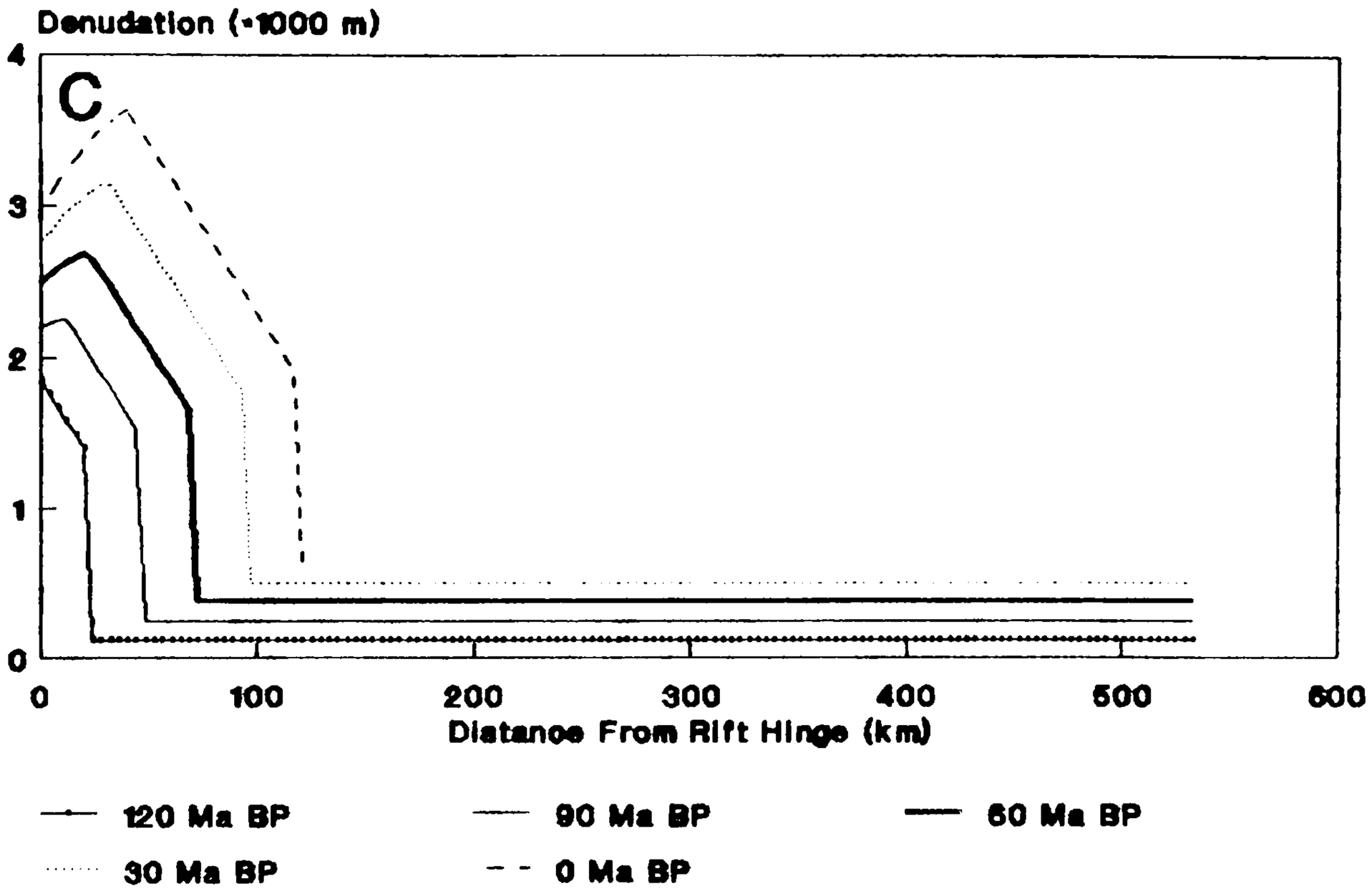

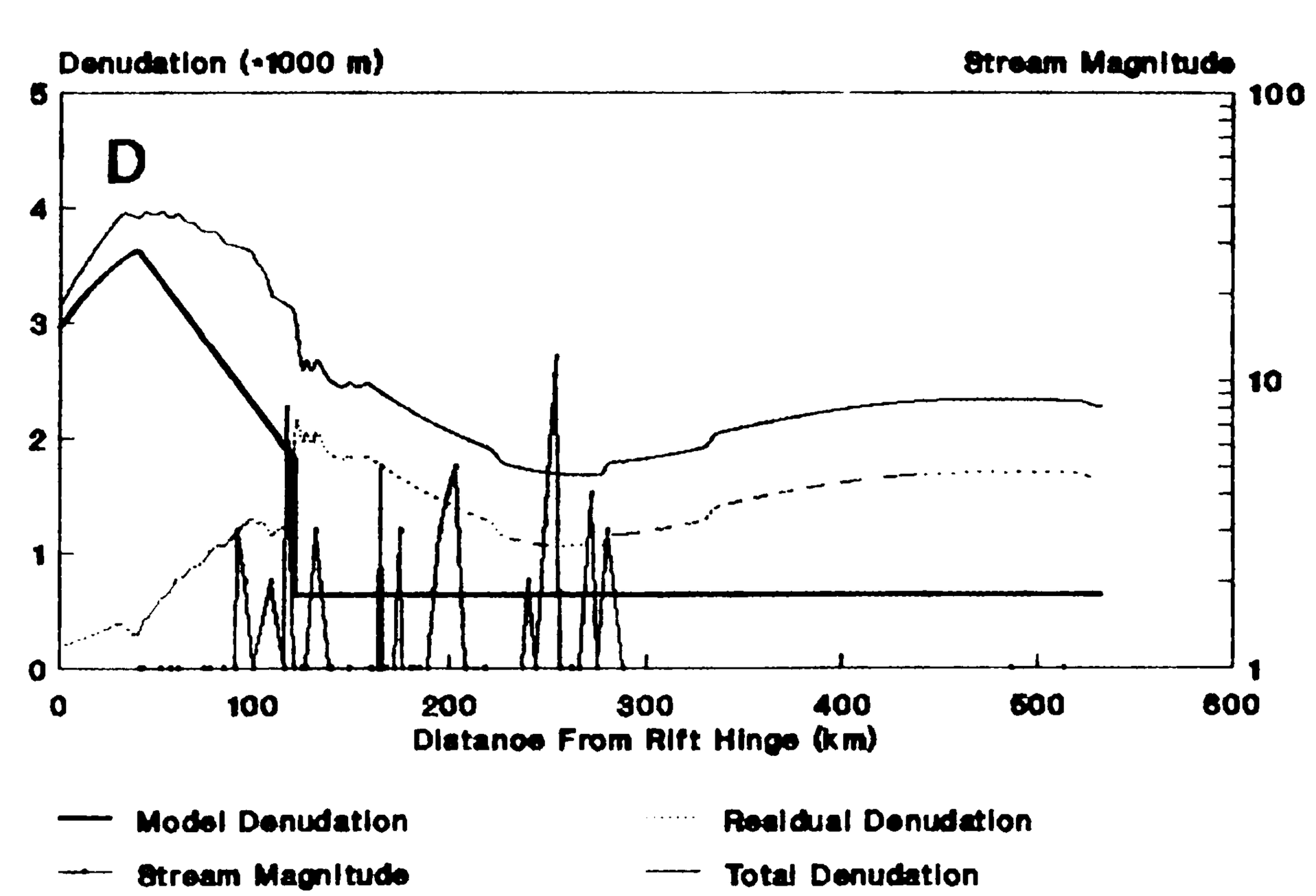

Fig. 7.3. Continued from the previous page. The best modelled fit parameters are displayed in Fig. 7.2. Other flexural model parameters are $E=1\times10^{11}$ Nm^{-2}, $v=0.25$, $g=9.81$ ms^{-2}, $\rho_m=3300$ kgm^{-3} and $\rho_f=0$ kgm^{-3}.

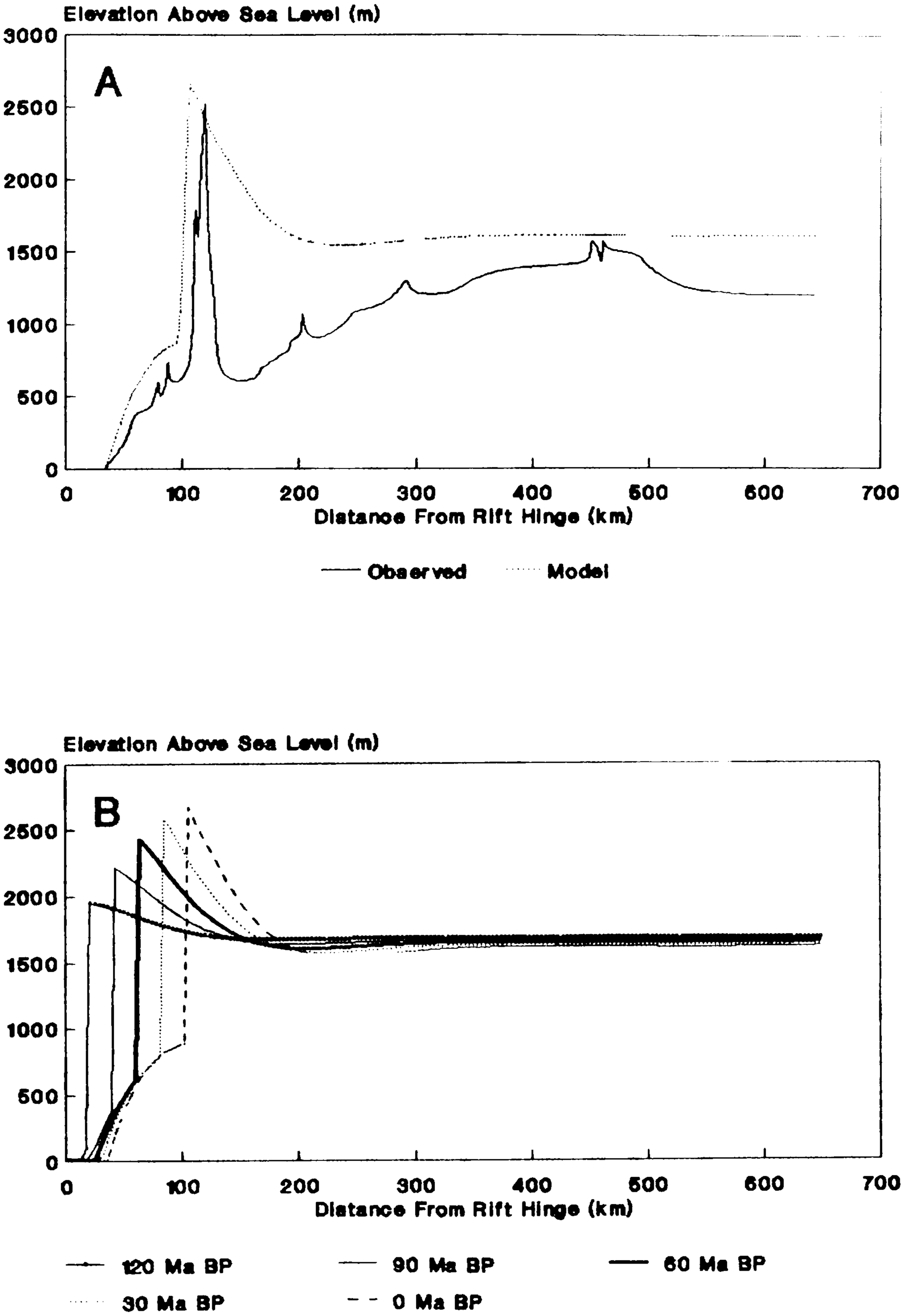

Fig. 7.4. Best modelled fit for profile BRA. Refer to Fig. 7.3 for layout and model details.

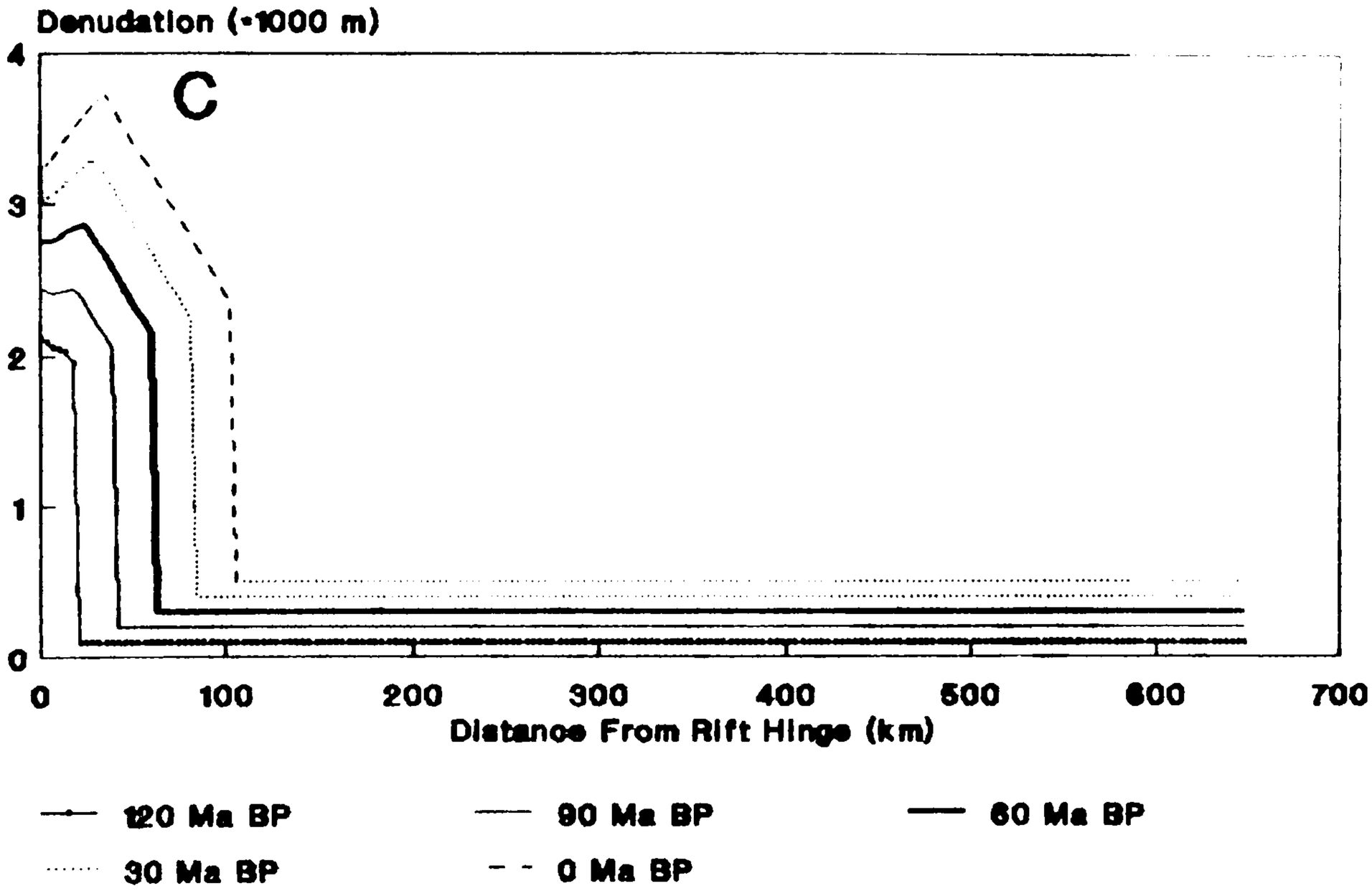

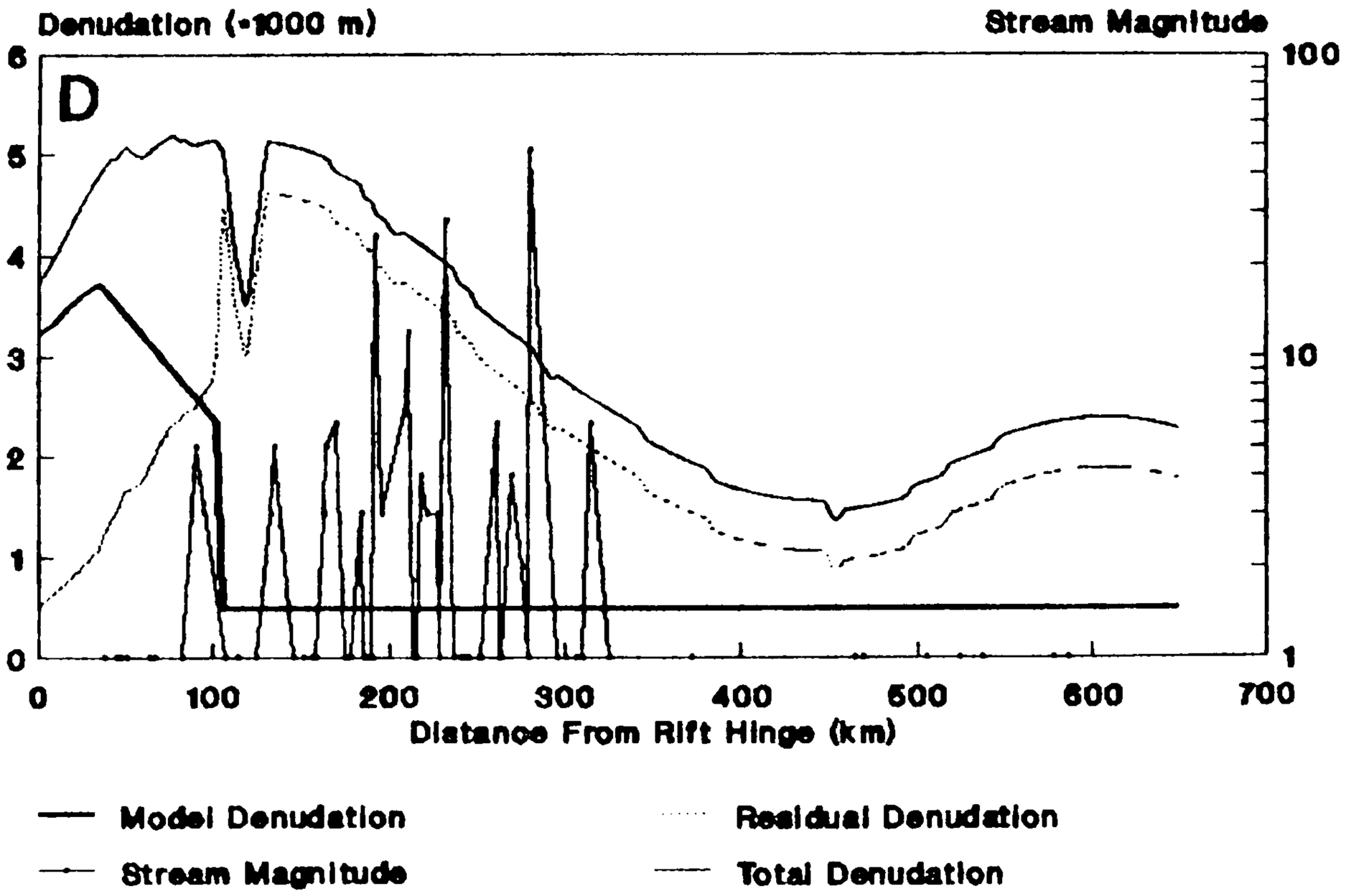

Fig. 7.4. Continued from previous page.

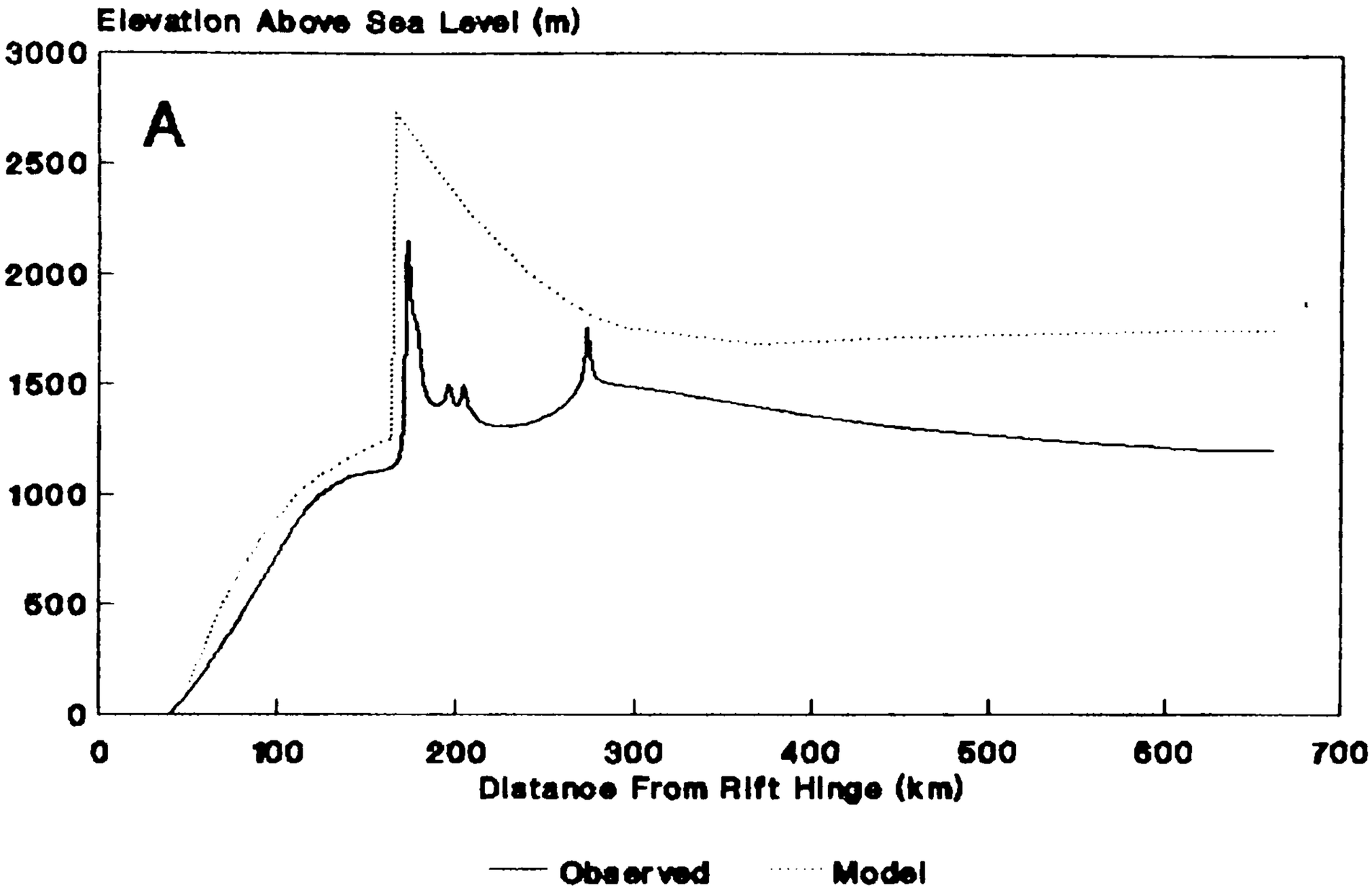

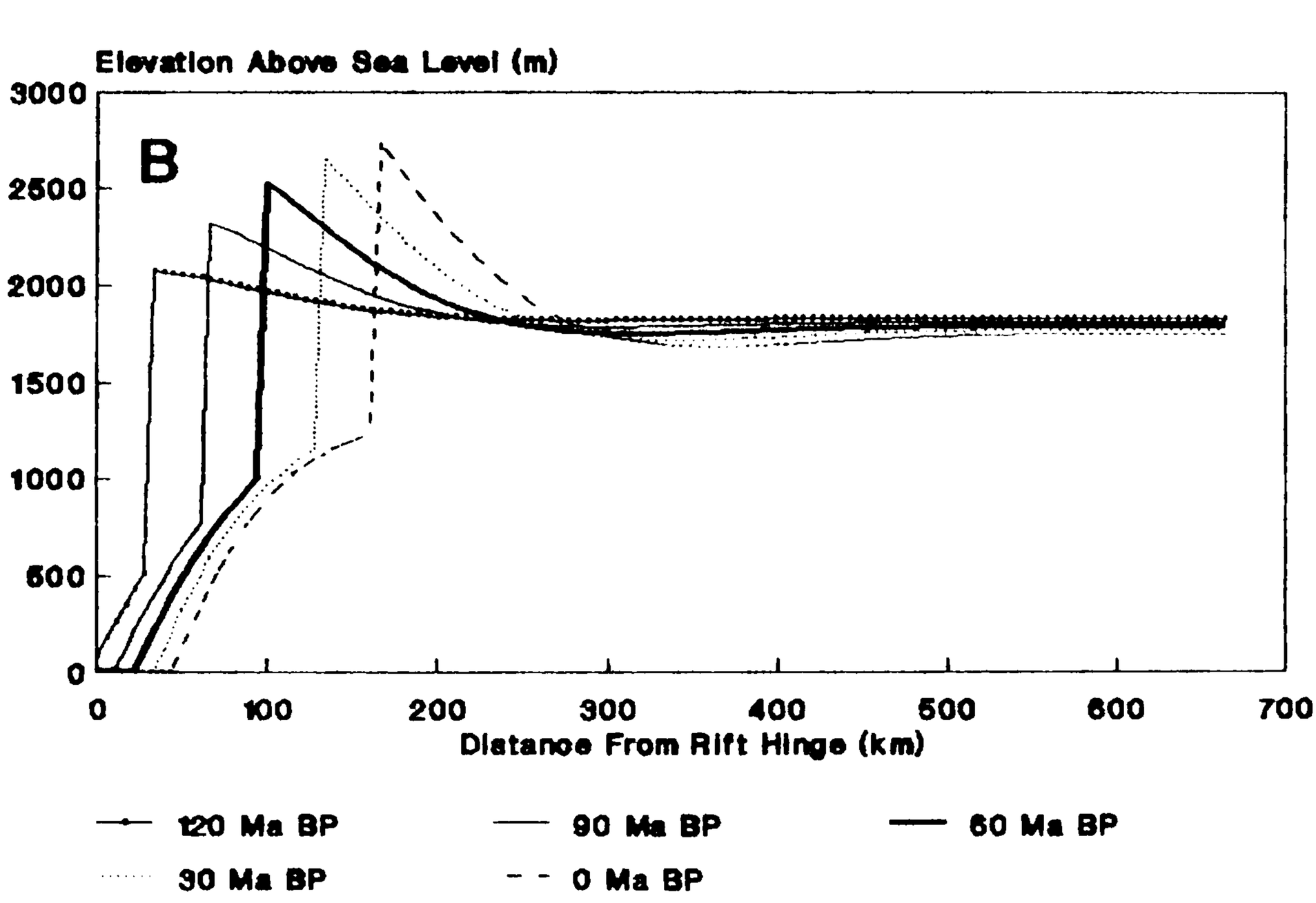

Fig. 7.5. Best modelled fit for profile ERO. Refer to Fig. 7.3 for layout and model details.

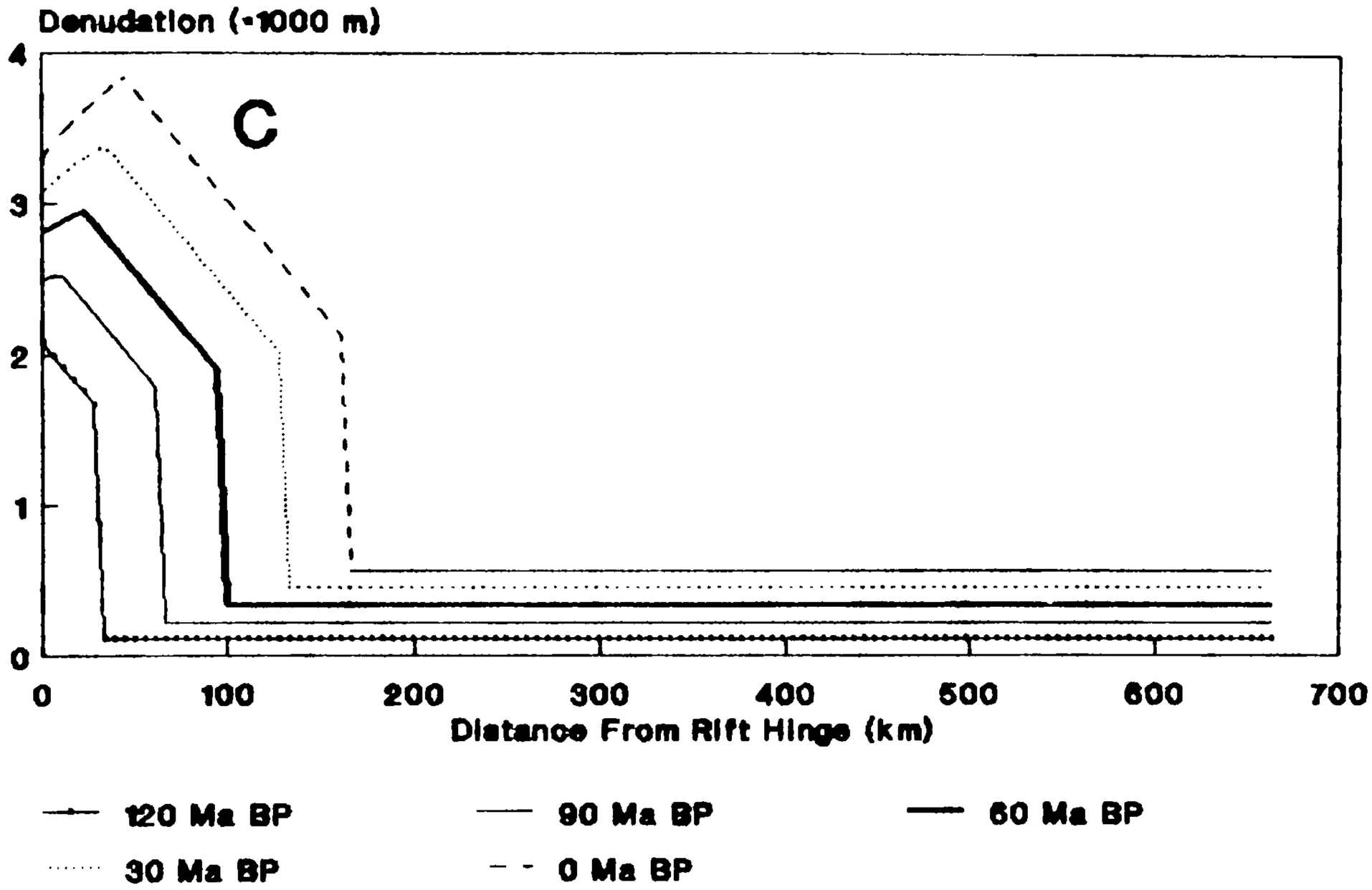

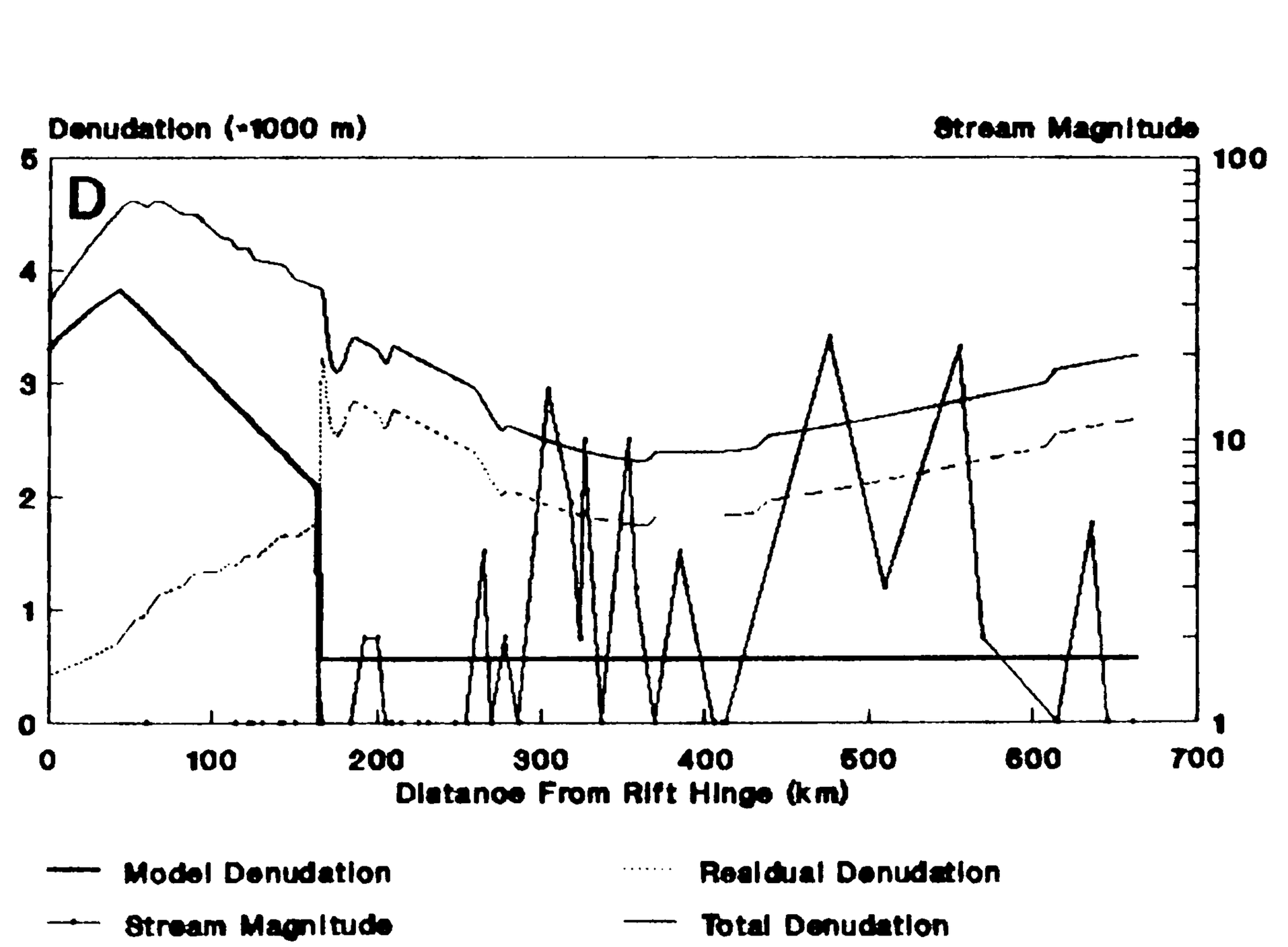

Fog. 7.5. Continued from previous page.

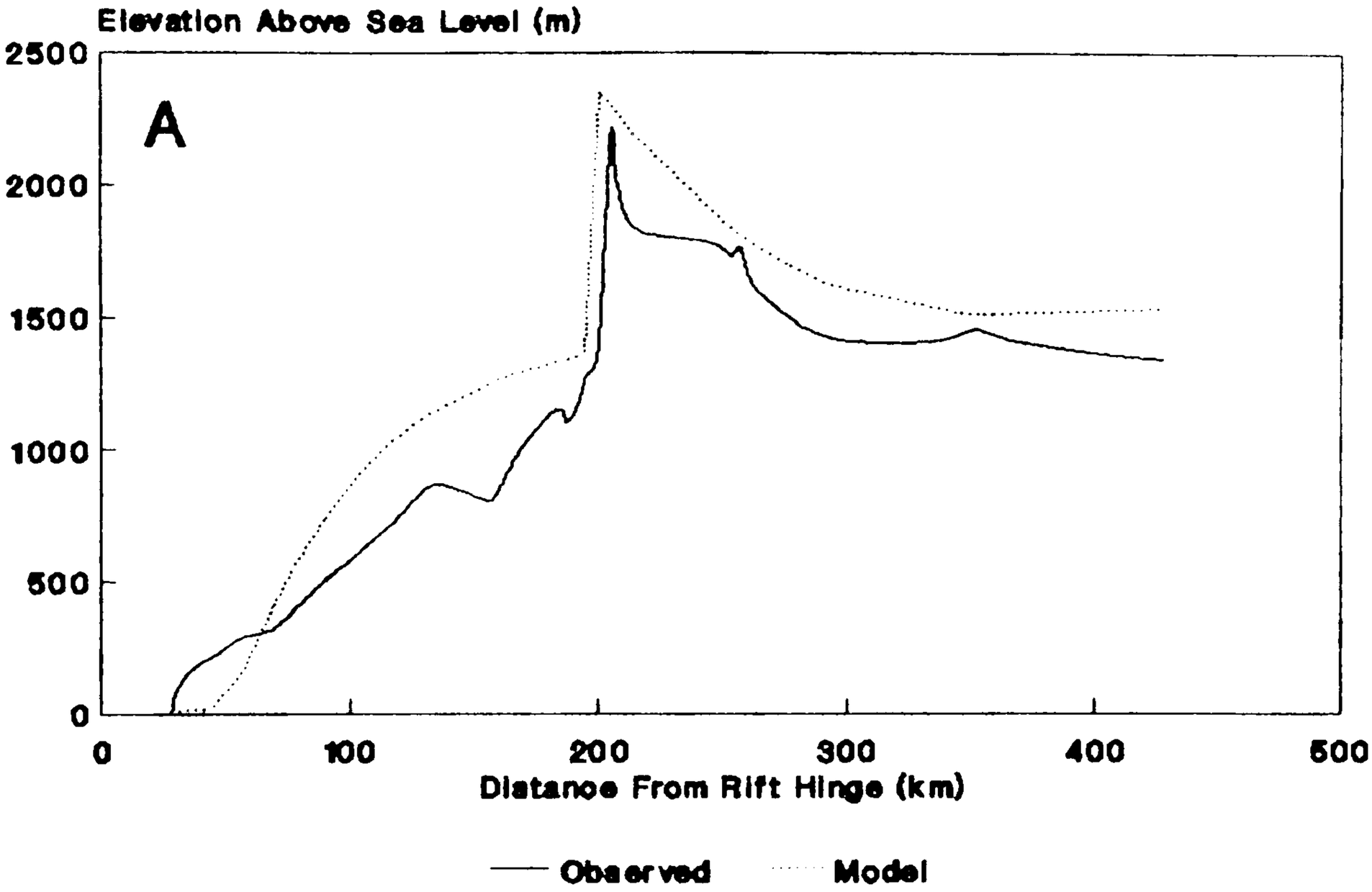

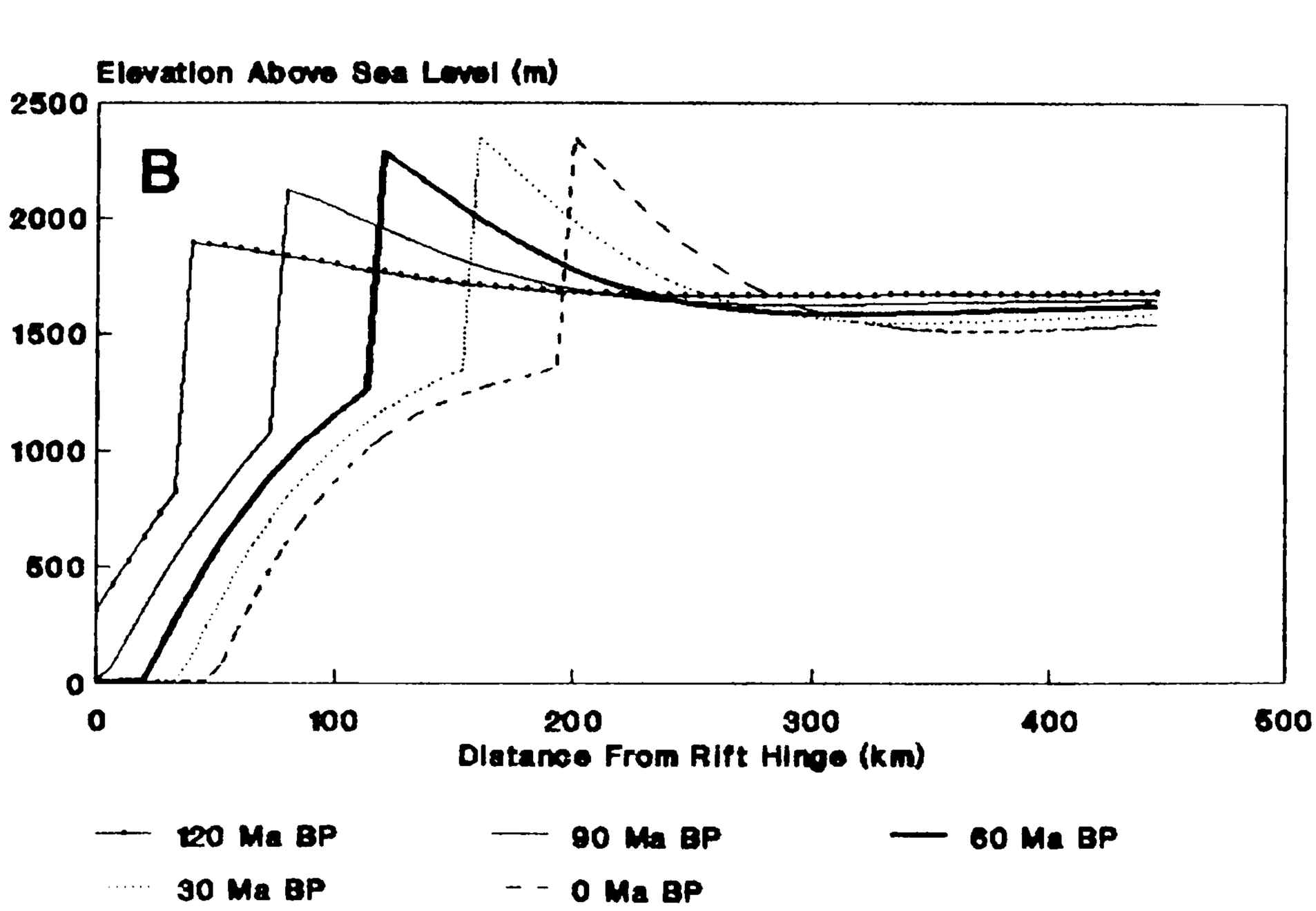

Fig. 7.6. Best modelled fit for profile GAM. Refer to Fig. 7.3 for layout and model details.

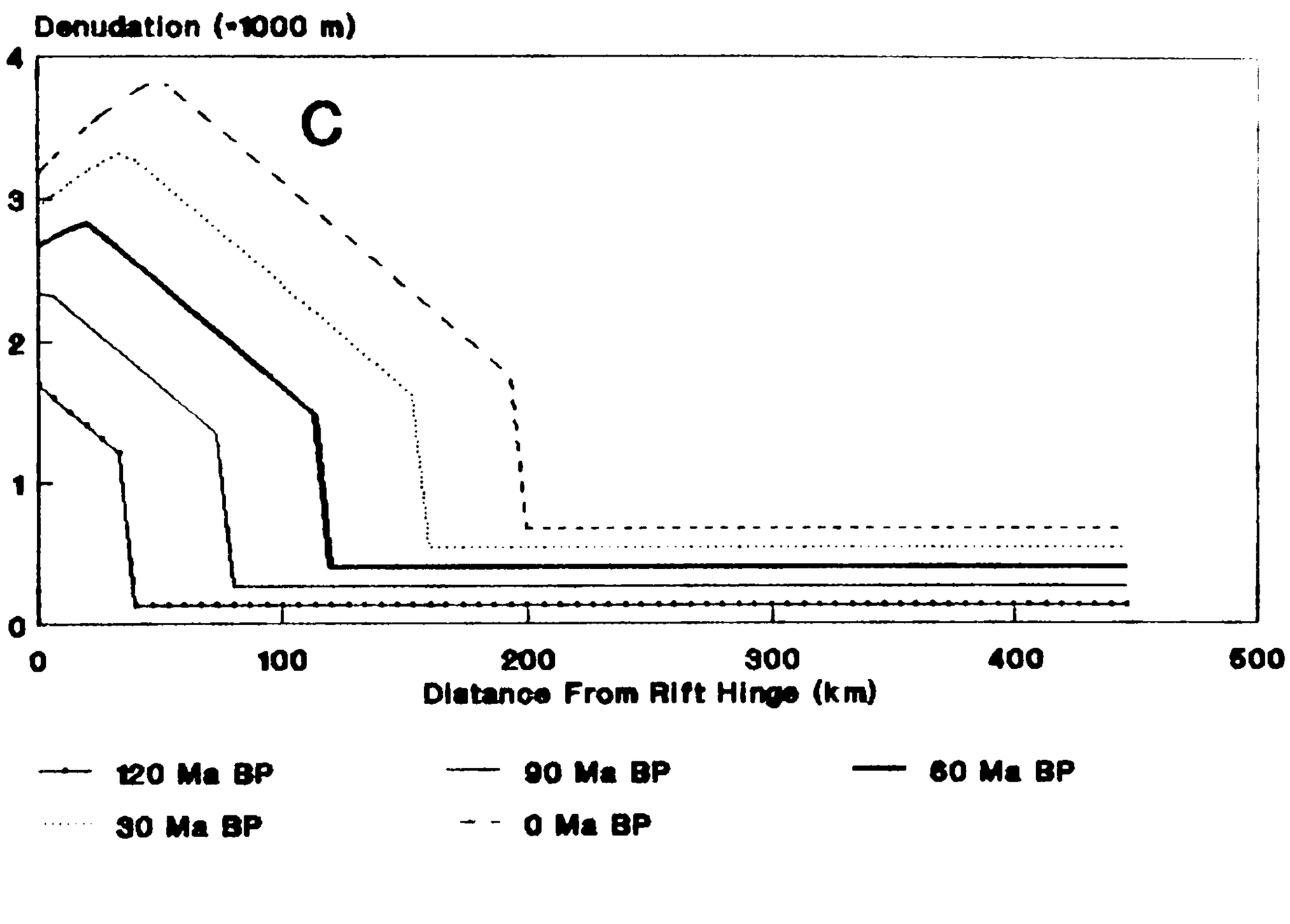

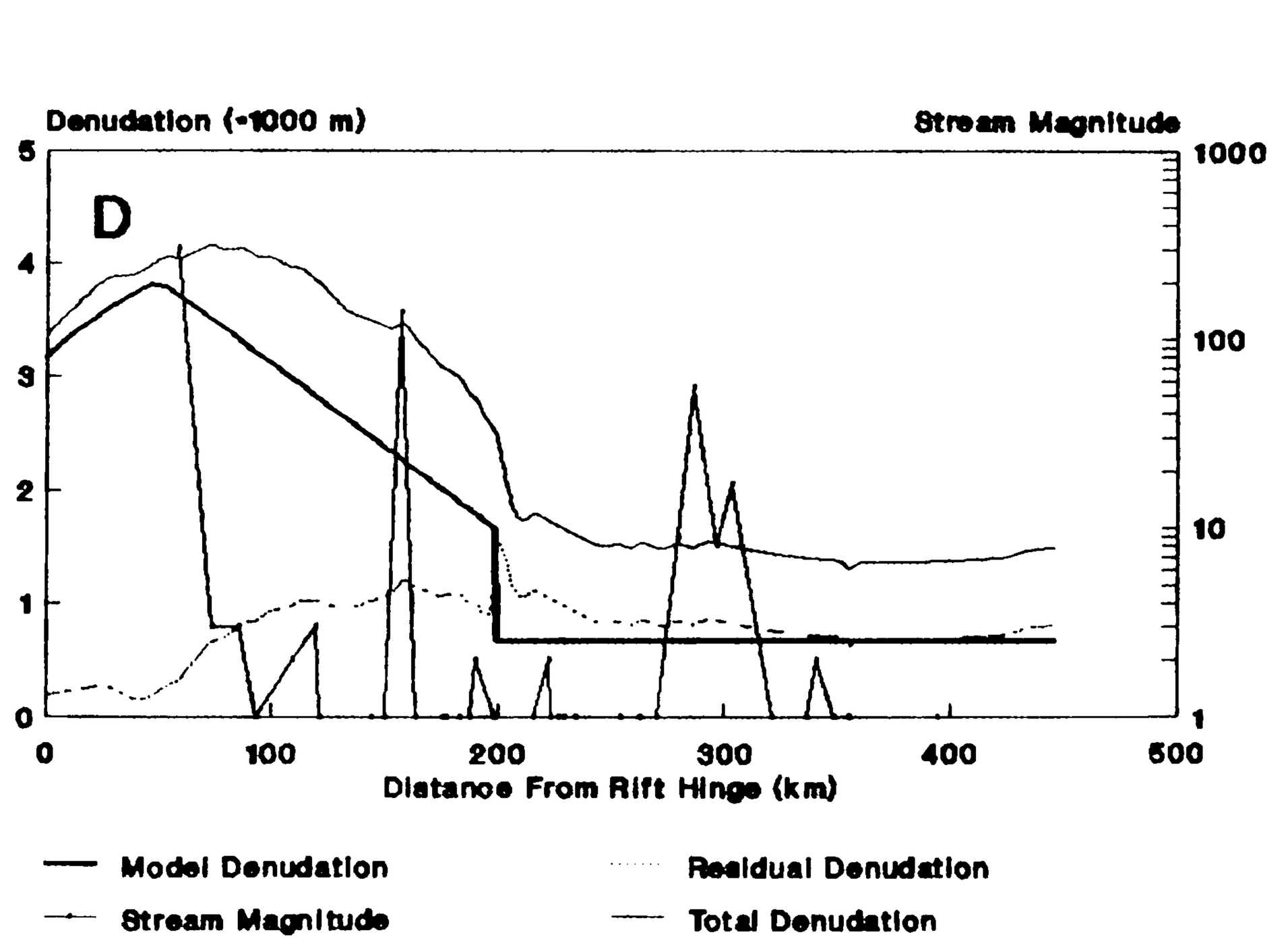

Fig. 7.6. Continued from previous page.

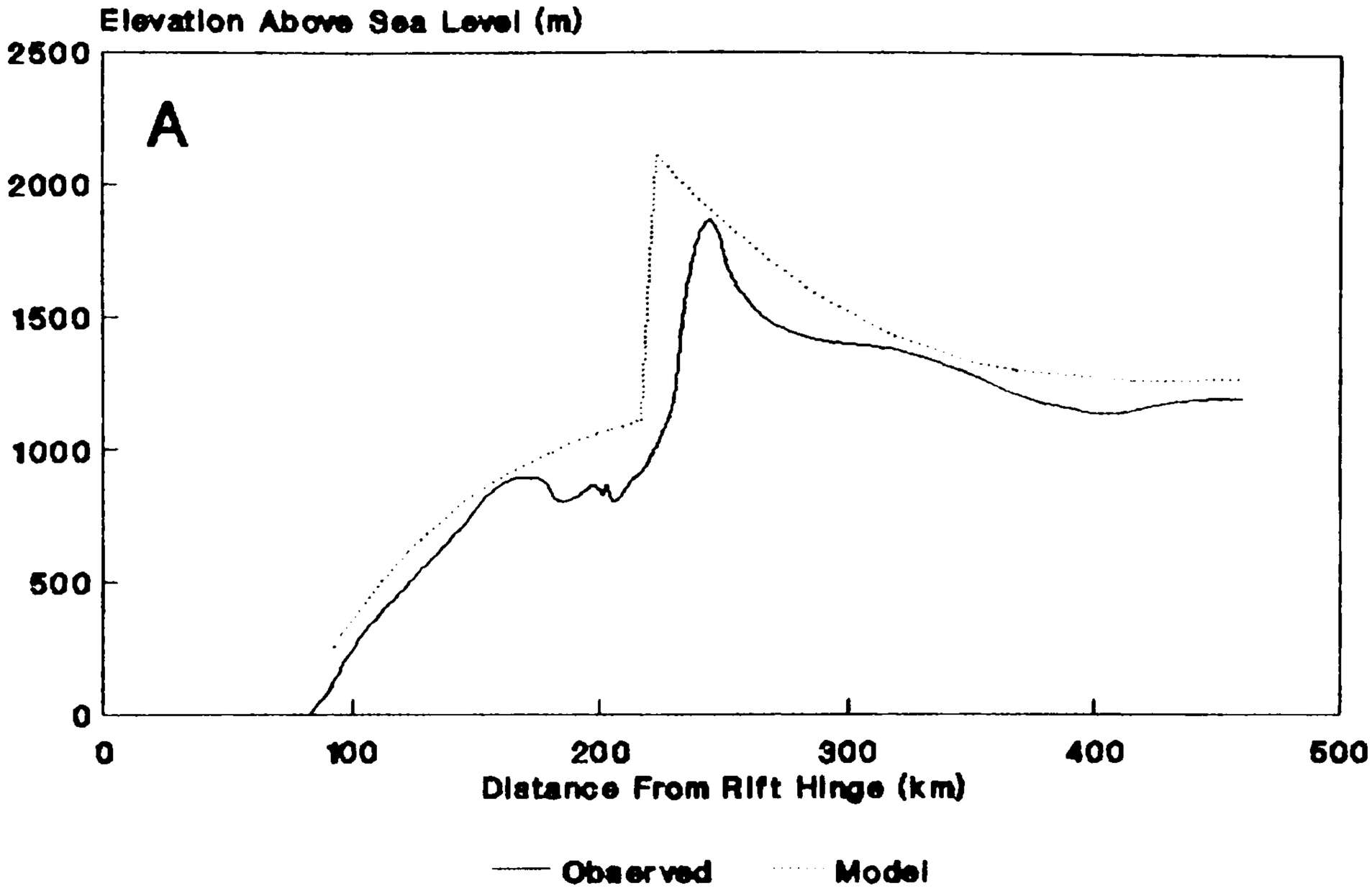

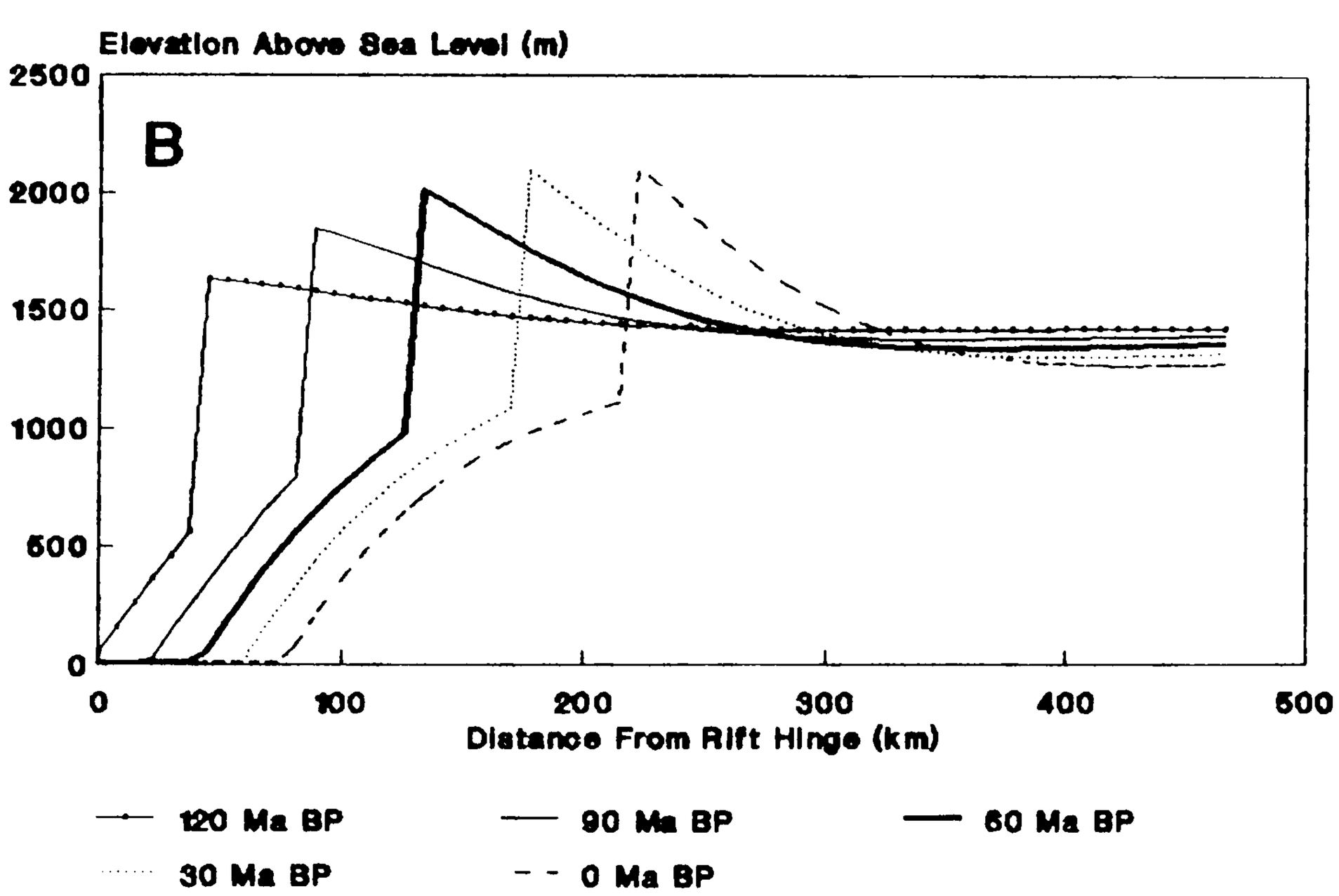

Fig. 7.7. Best modelled fit for profile TSA. Refer to Fig. 7.3 for layout and model details.

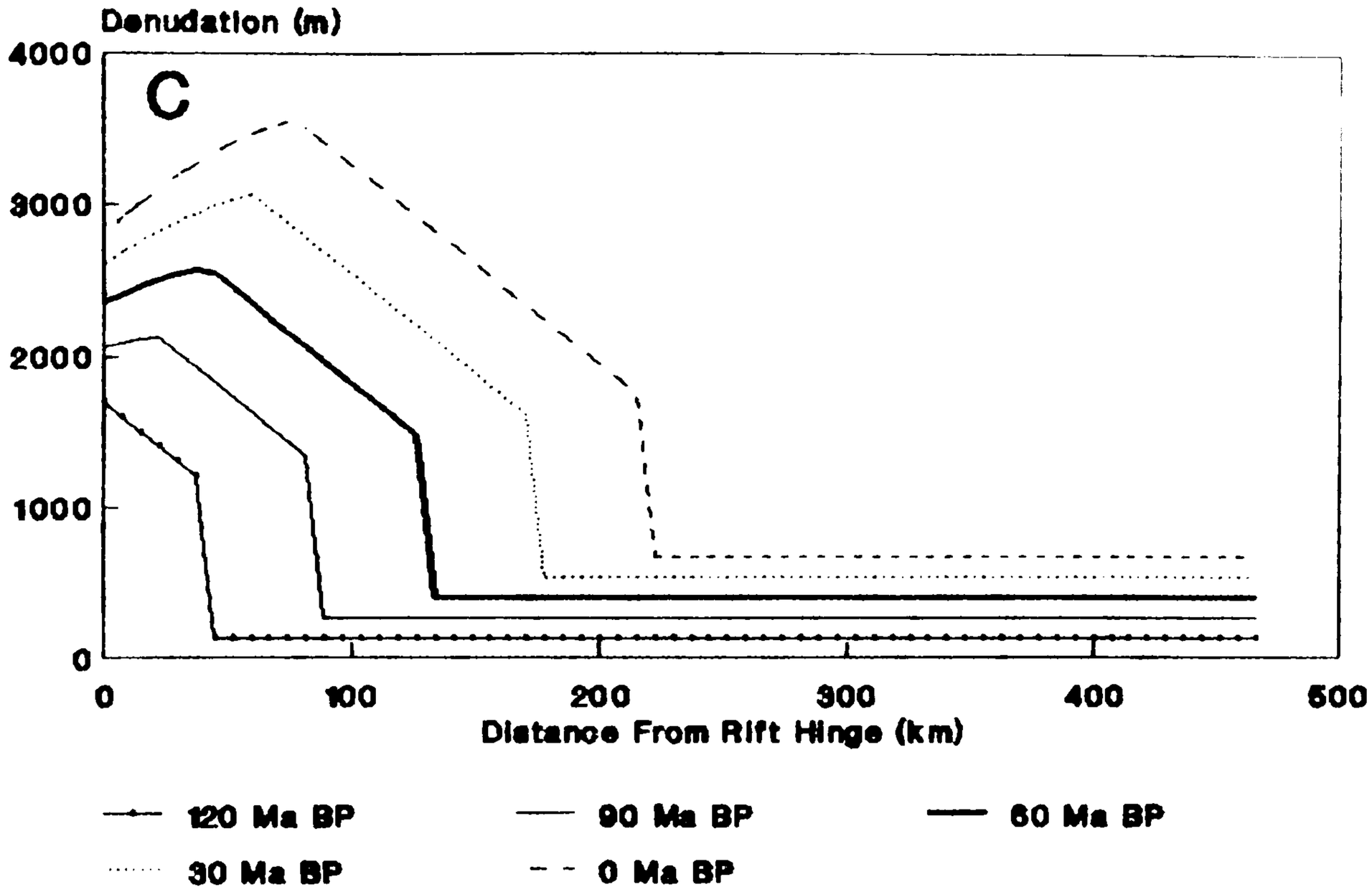

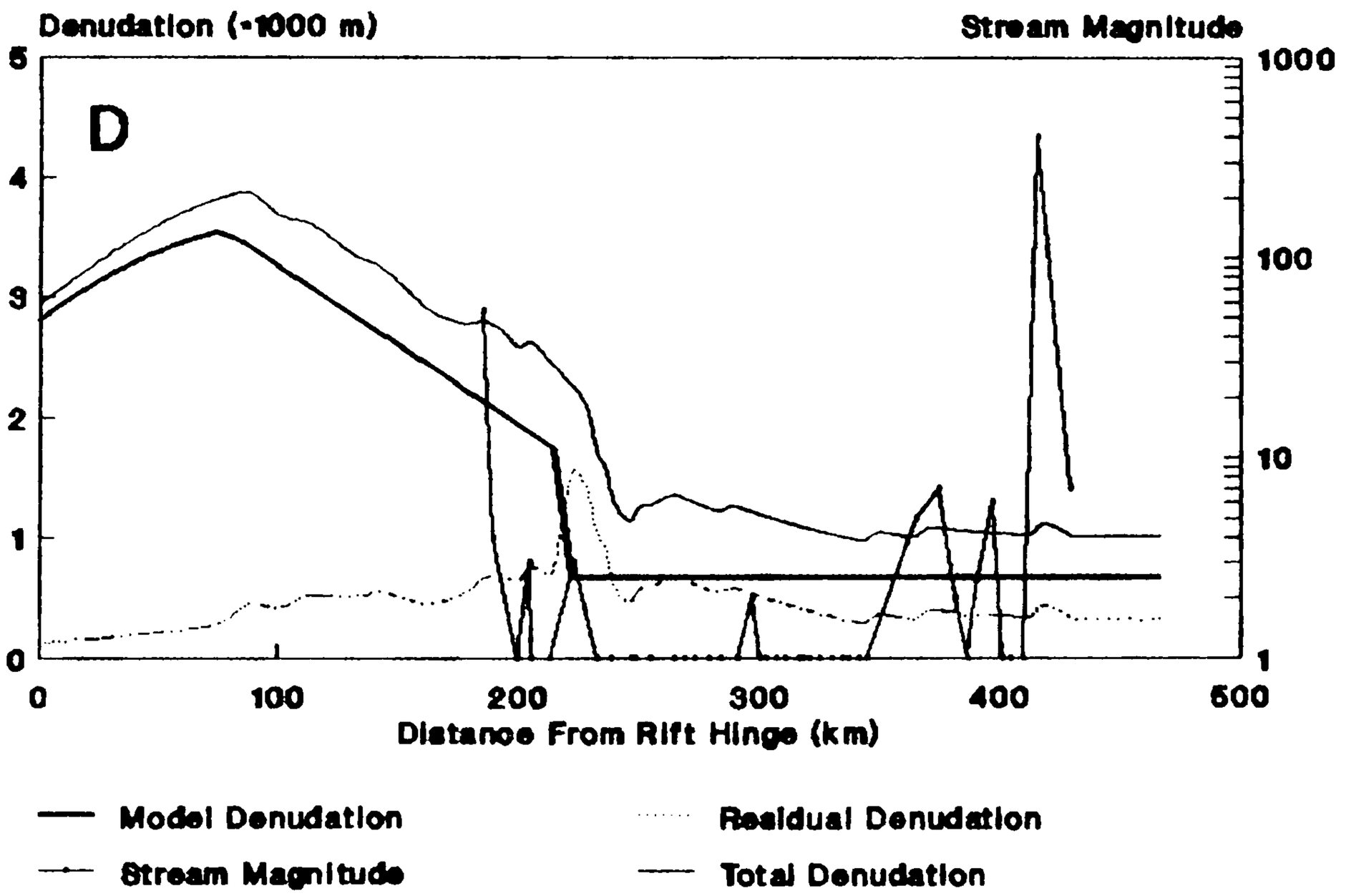

Fig. 7.7. Continued from previous page.

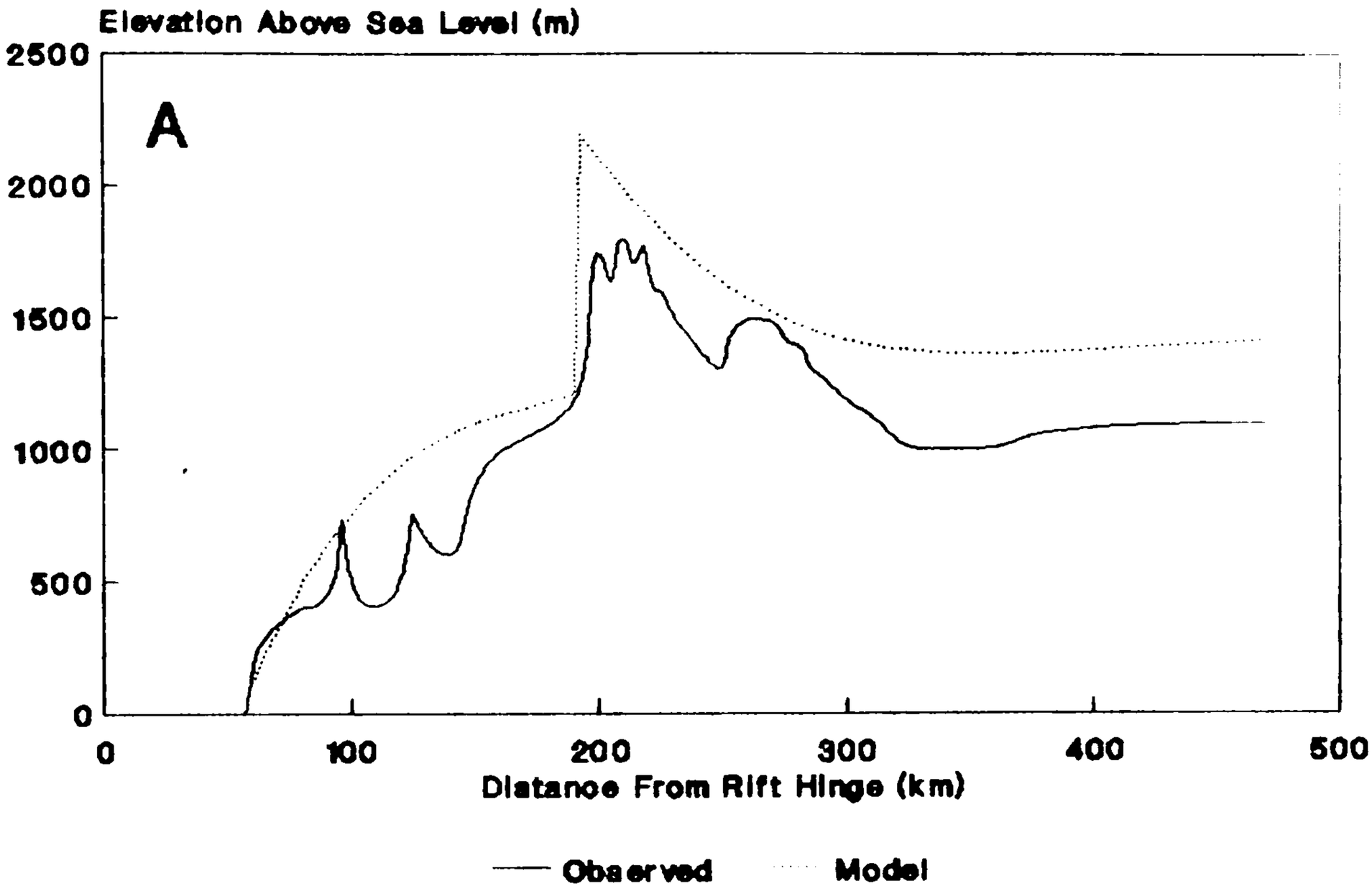

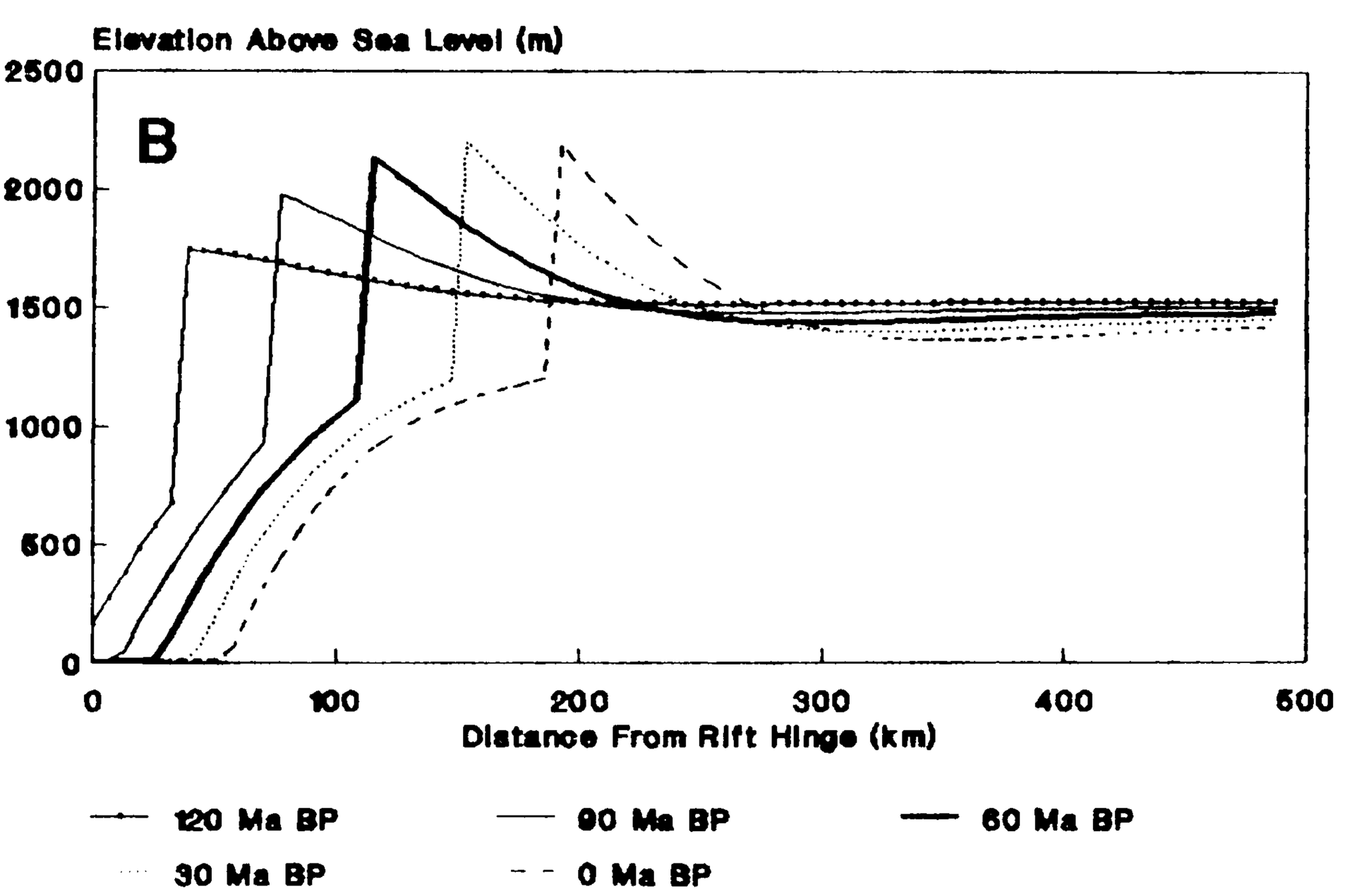

Fig. 7.8. Best modelled fit for profile TIR. Refer to Fig. 7.3 for layout and model details.

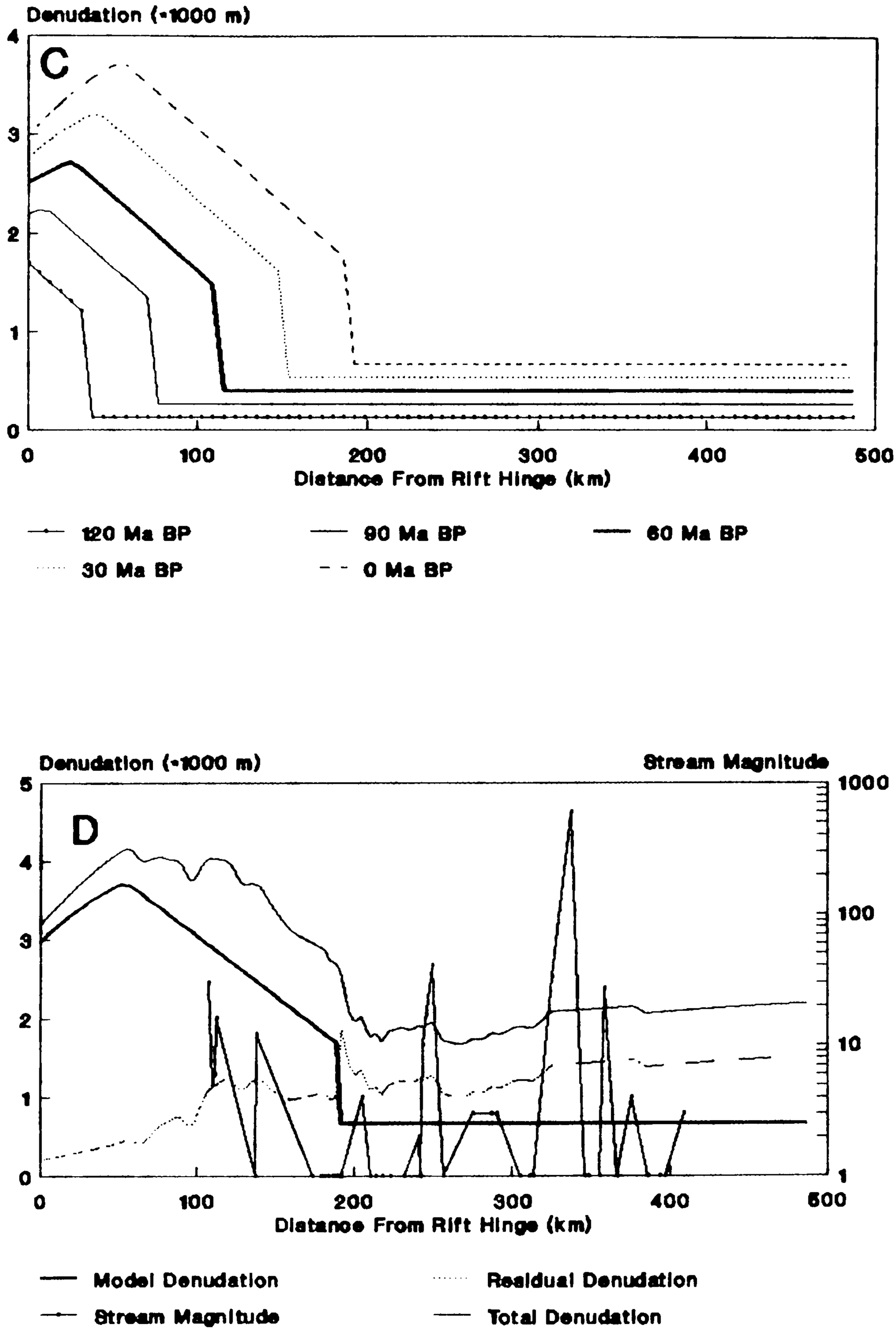

Fig. 7.8. Continued from previous page.

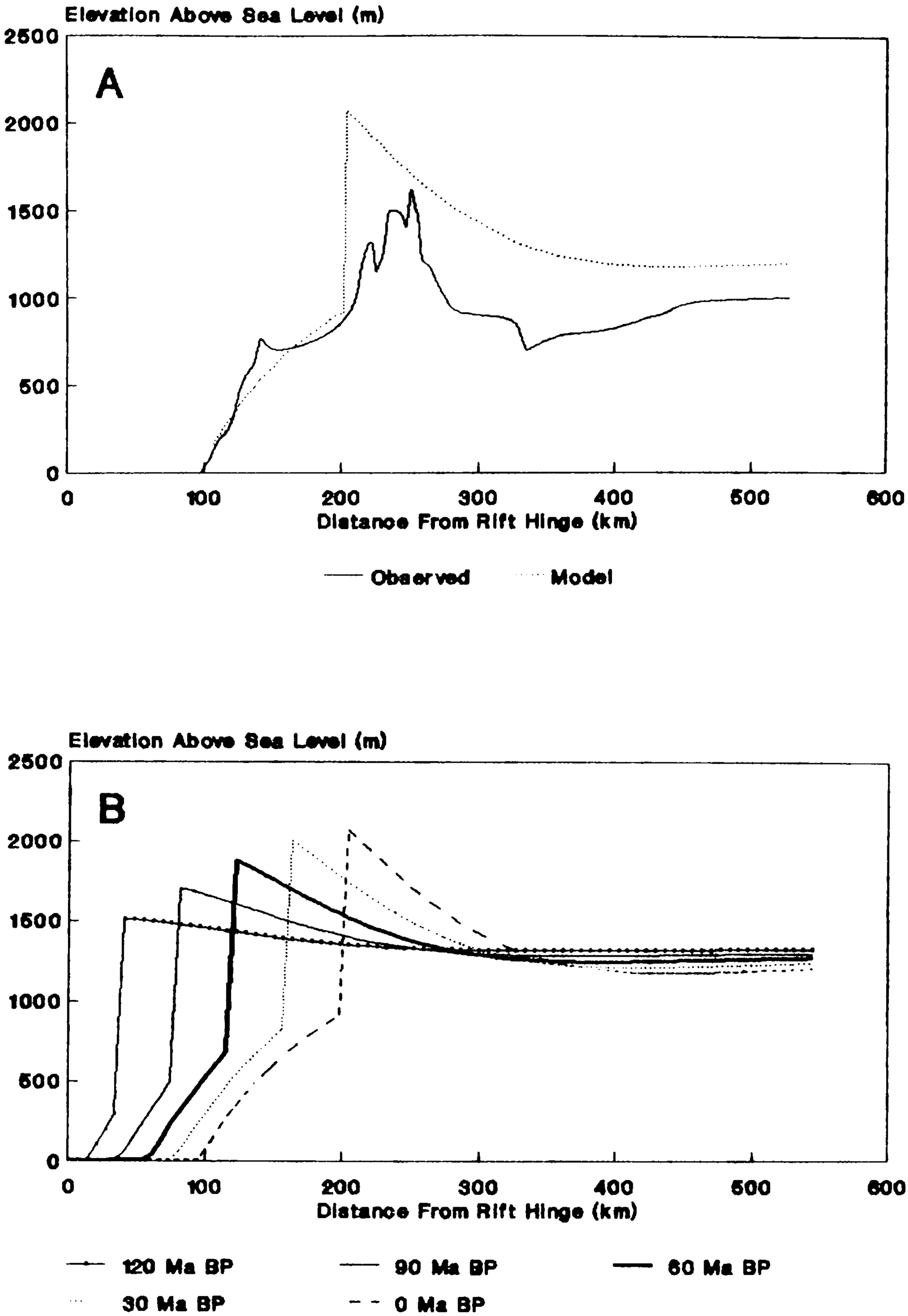

Fig. 7.9. Best modelled fit for profile NAM. Refer to Fig. 7.3 for layout and model details.

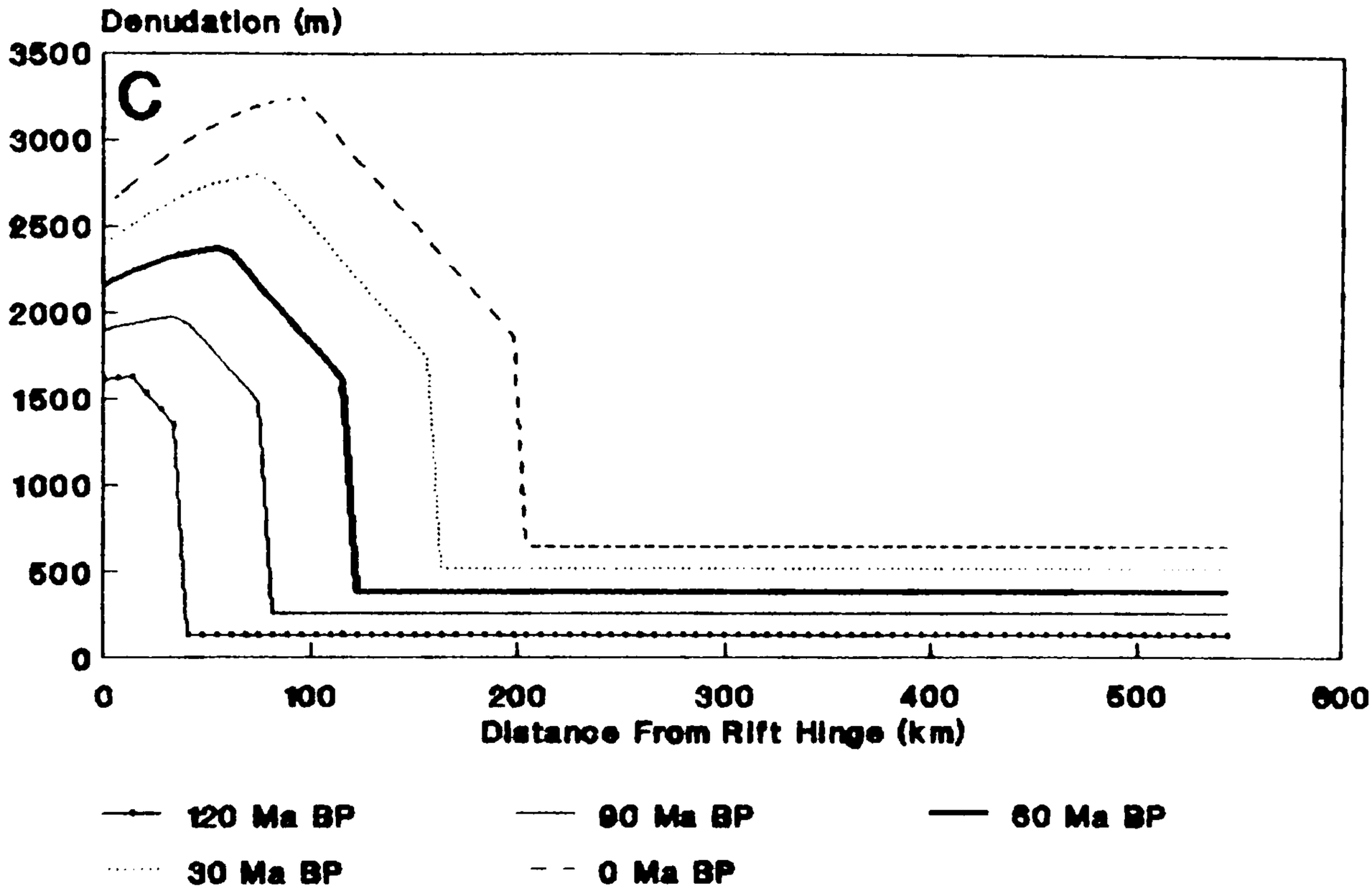

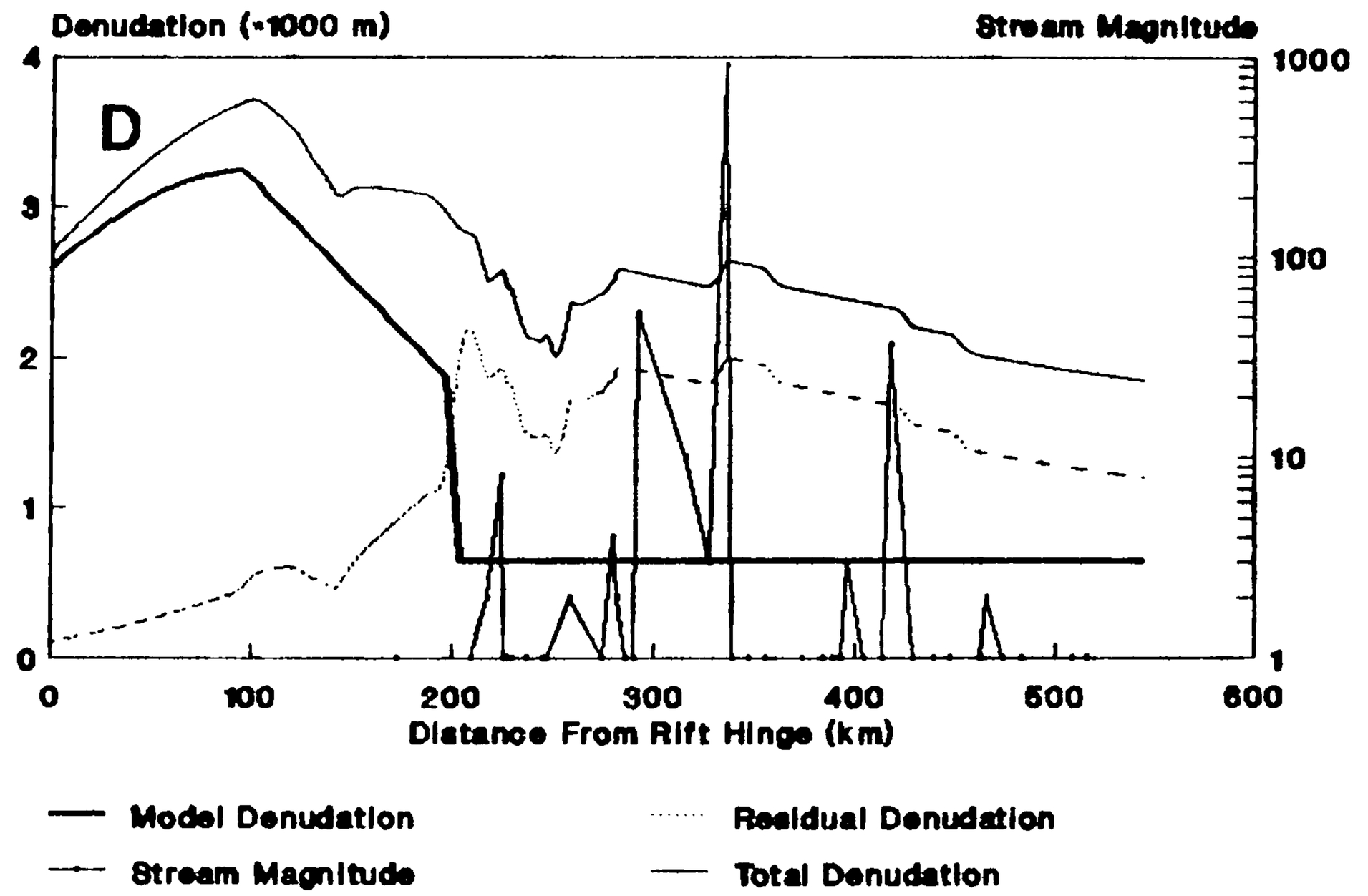

Fig. 7.9. Continued from the previous page.

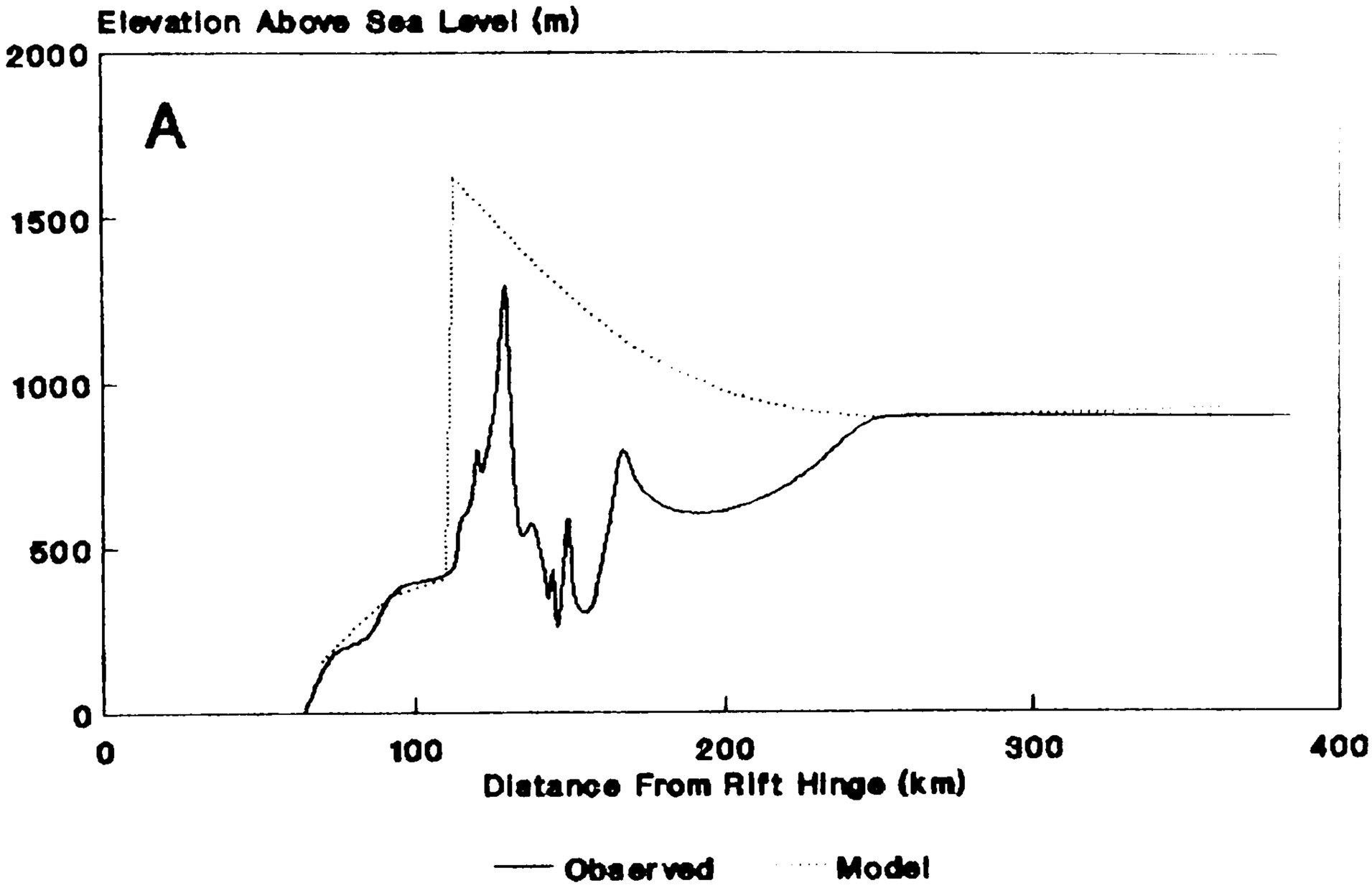

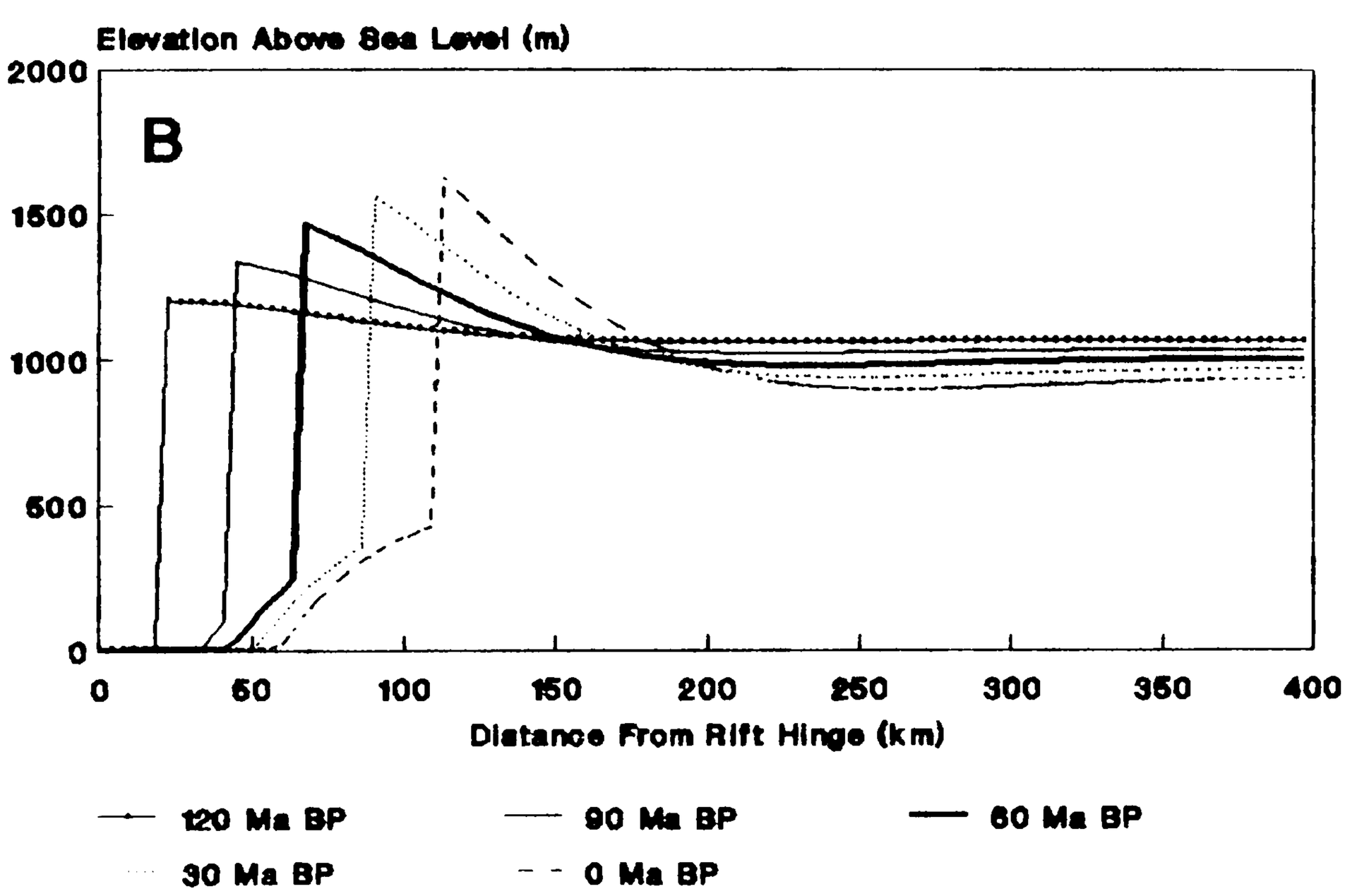

Fig. 7.10. Best modelled fit for profile COR. Refer to Fig. 7.3 for layout and model details.

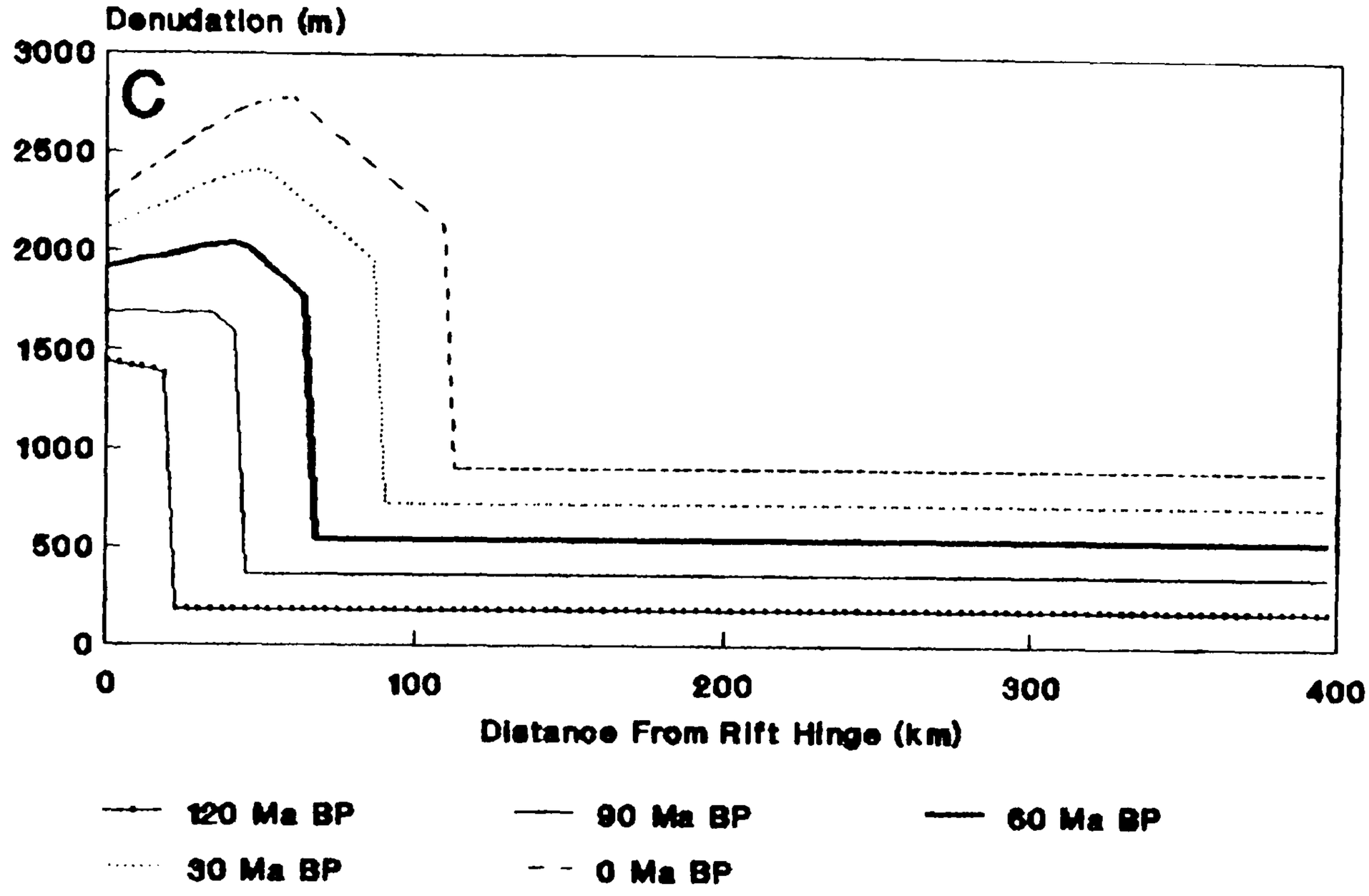

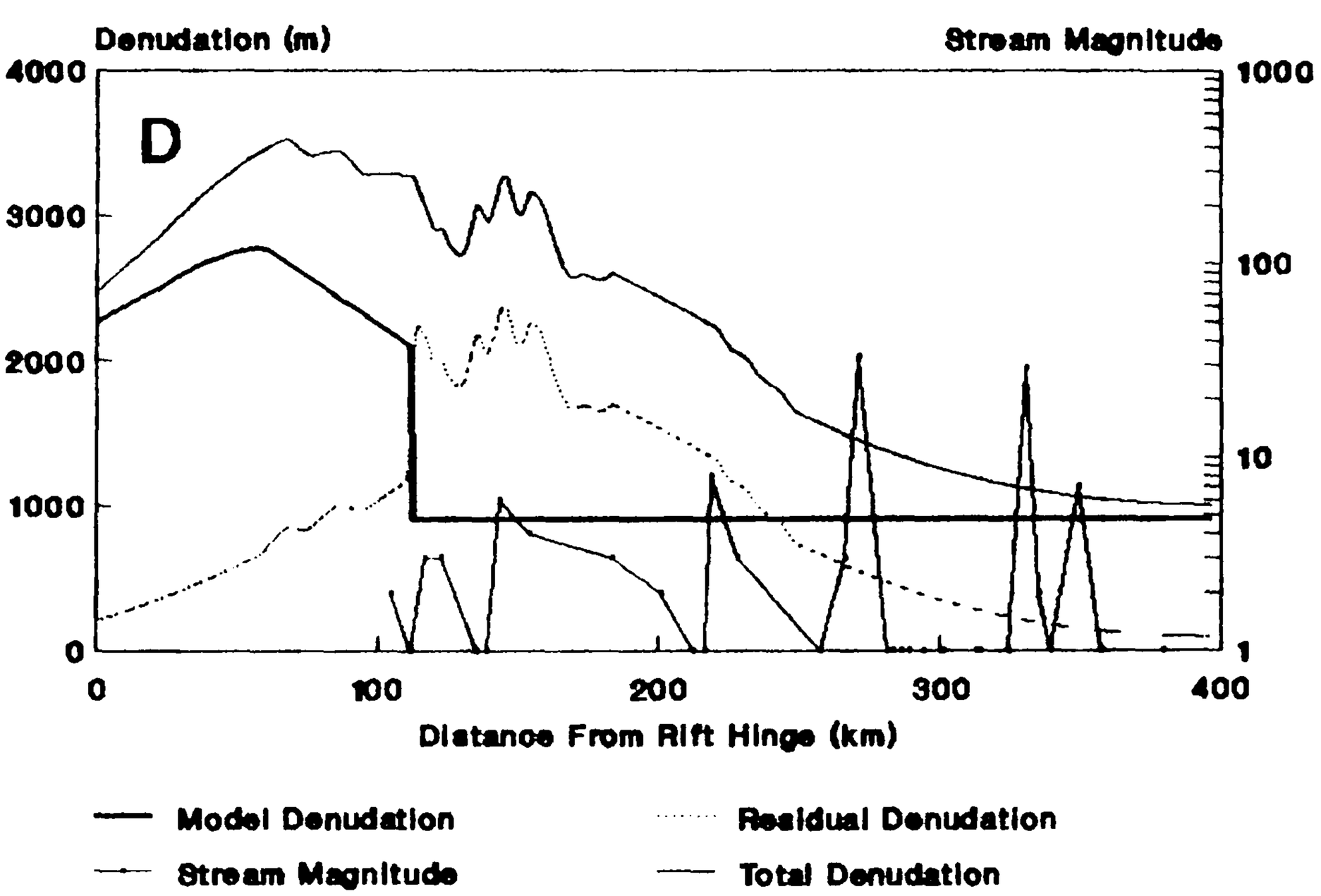

Fig. 7.10. Continued from the previous page.

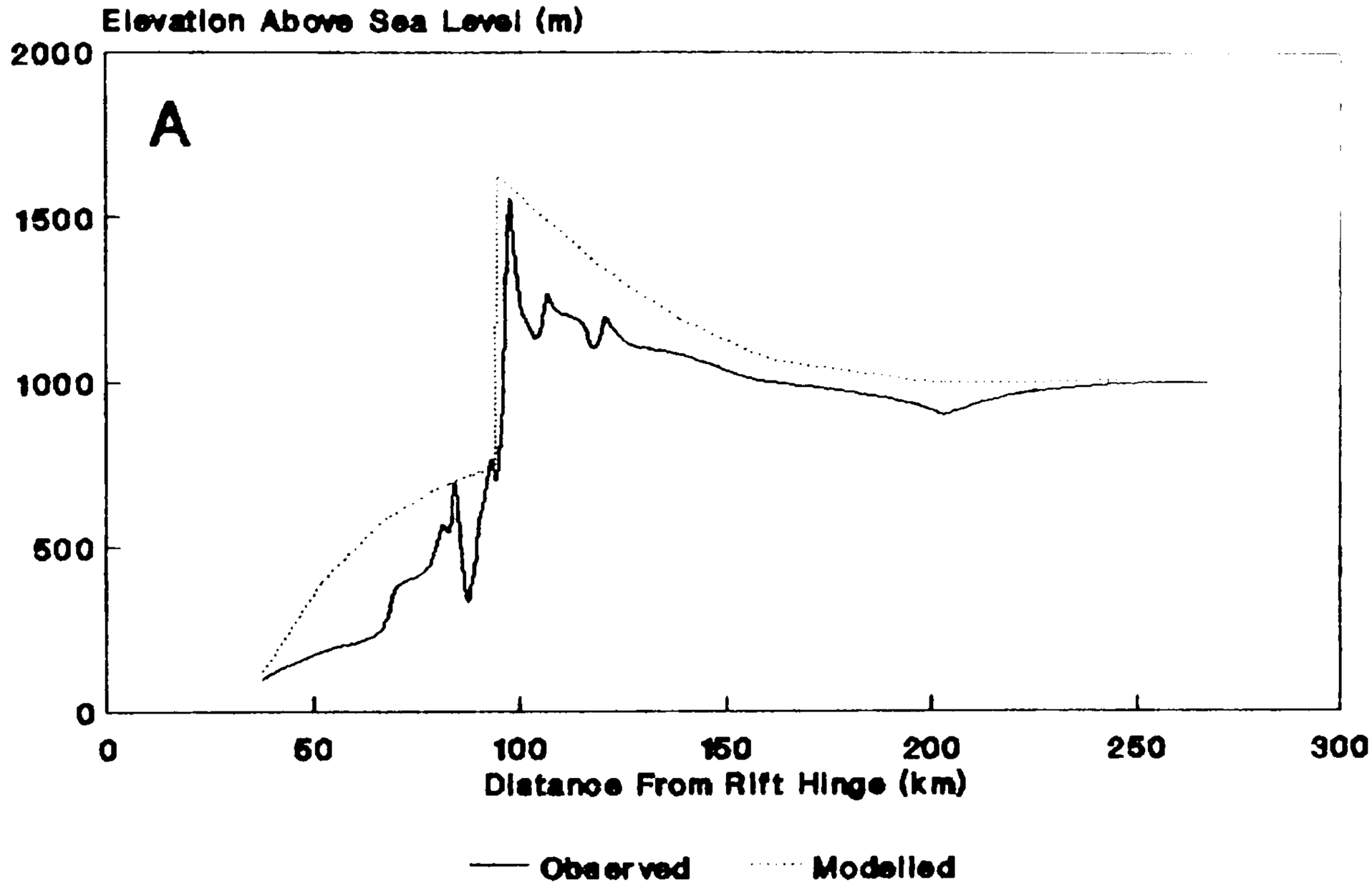

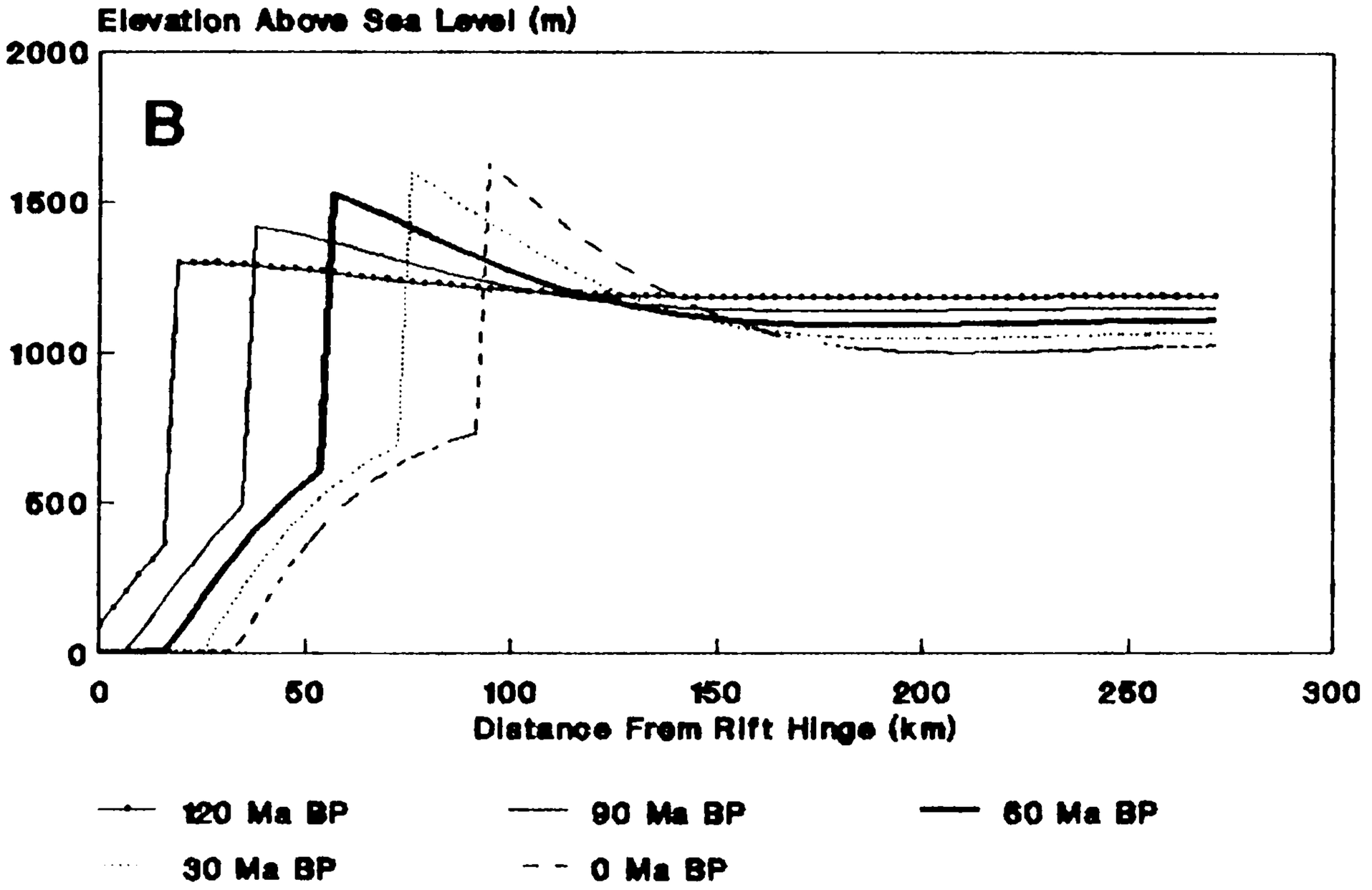

Fig. 7.11. Best modelled fit for profile ROO. Refer to Fig. 7.3 for layout and model details.

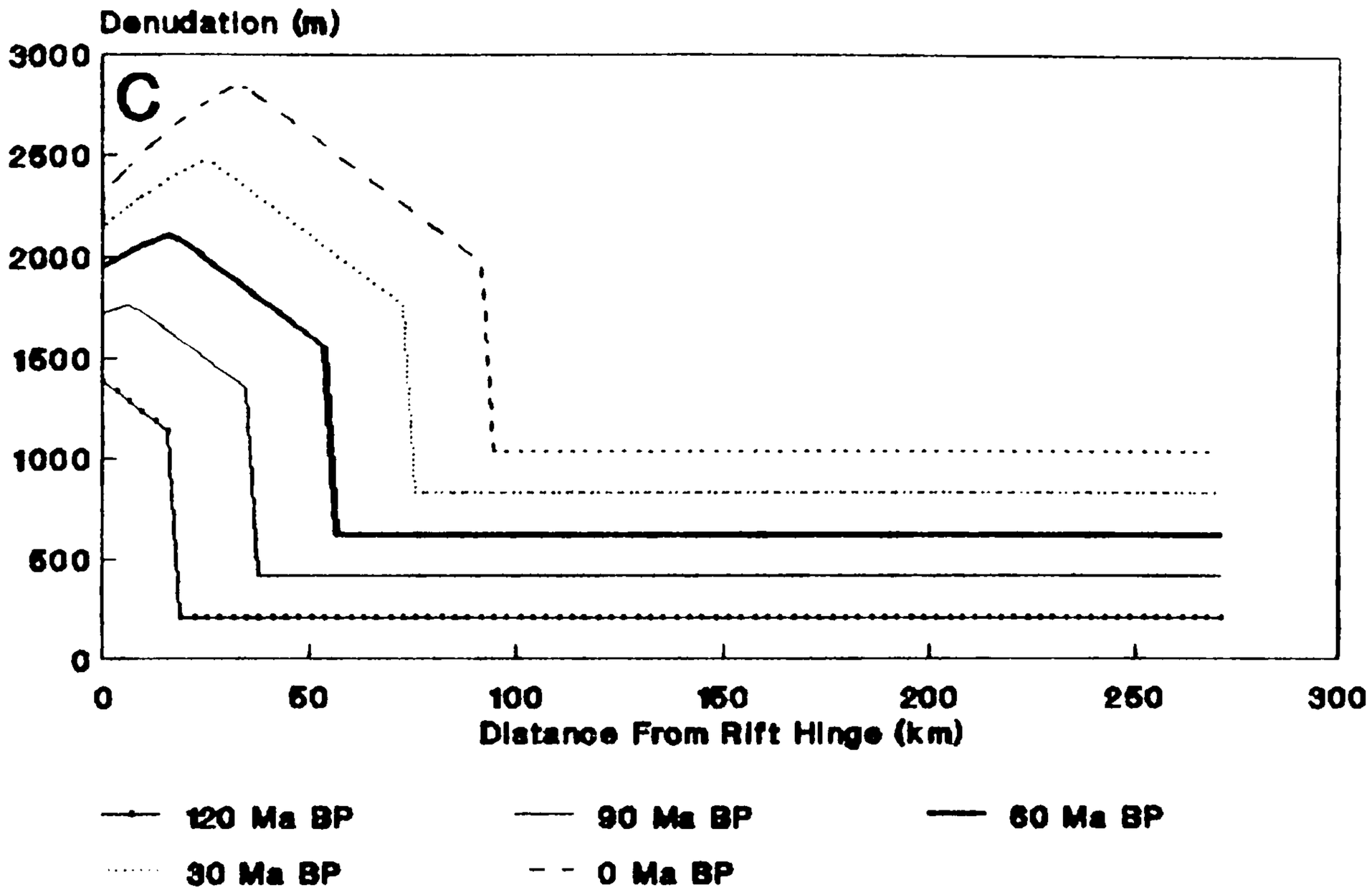

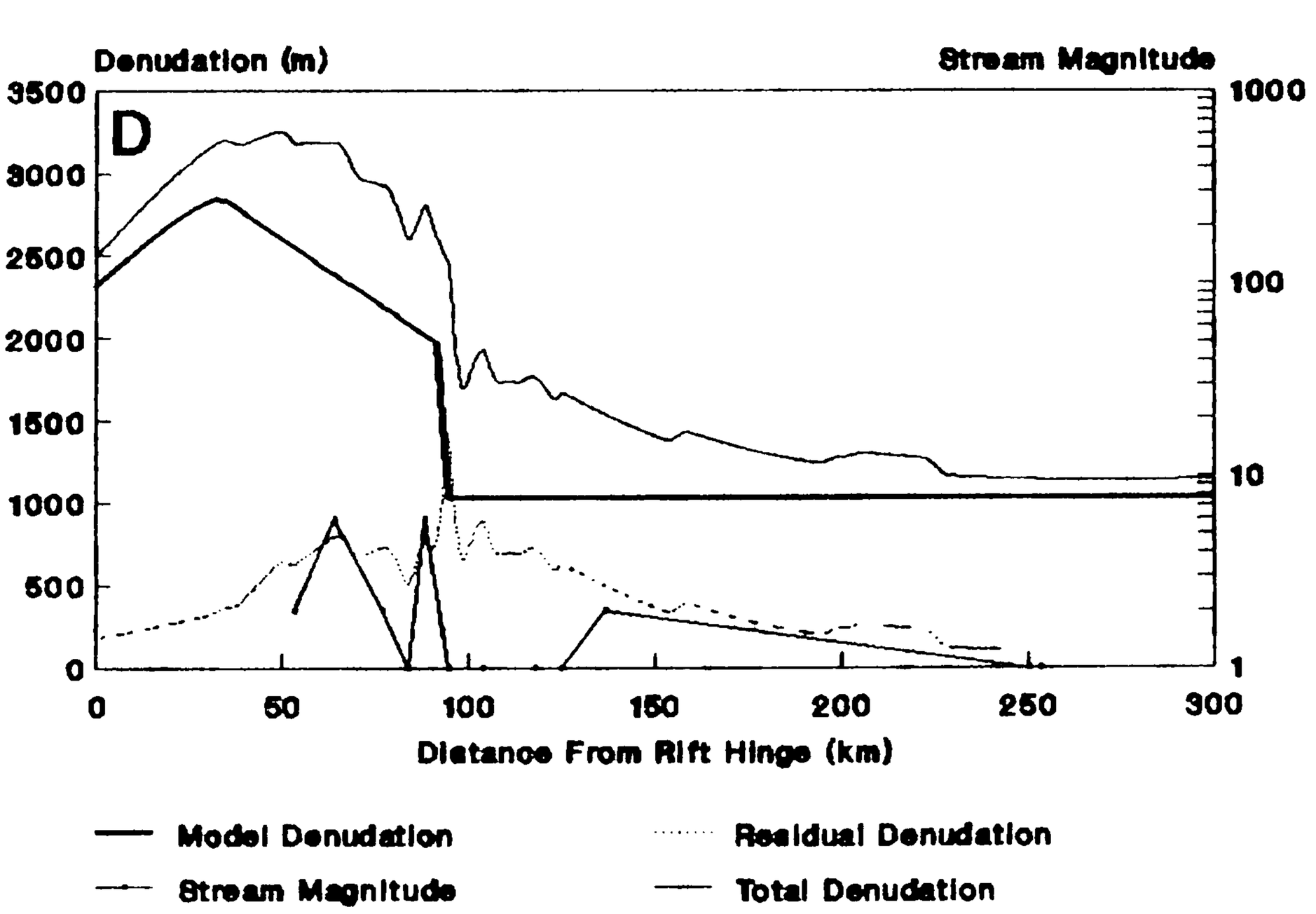

Fig. 7.11. Continued from the previous page.

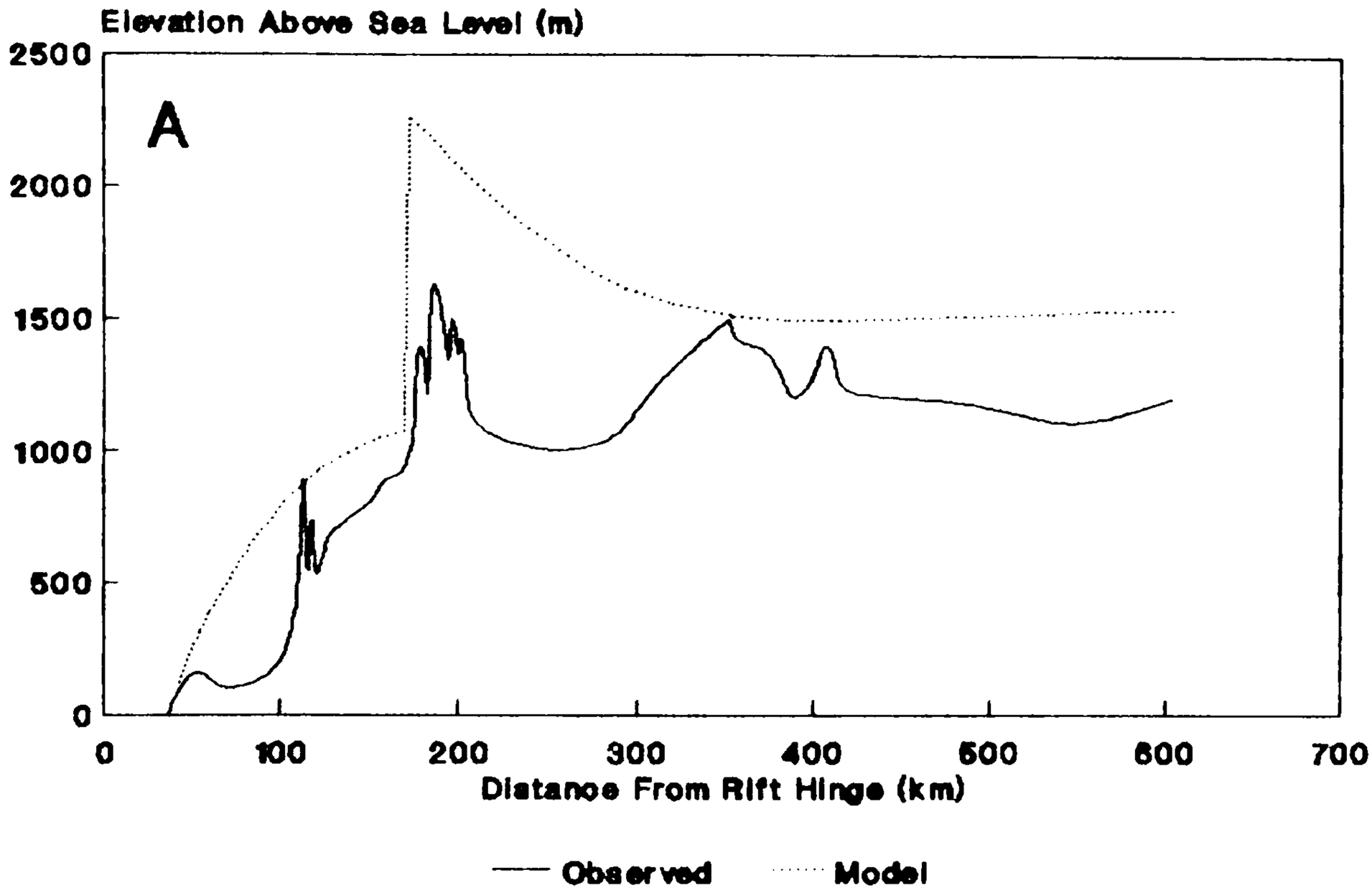

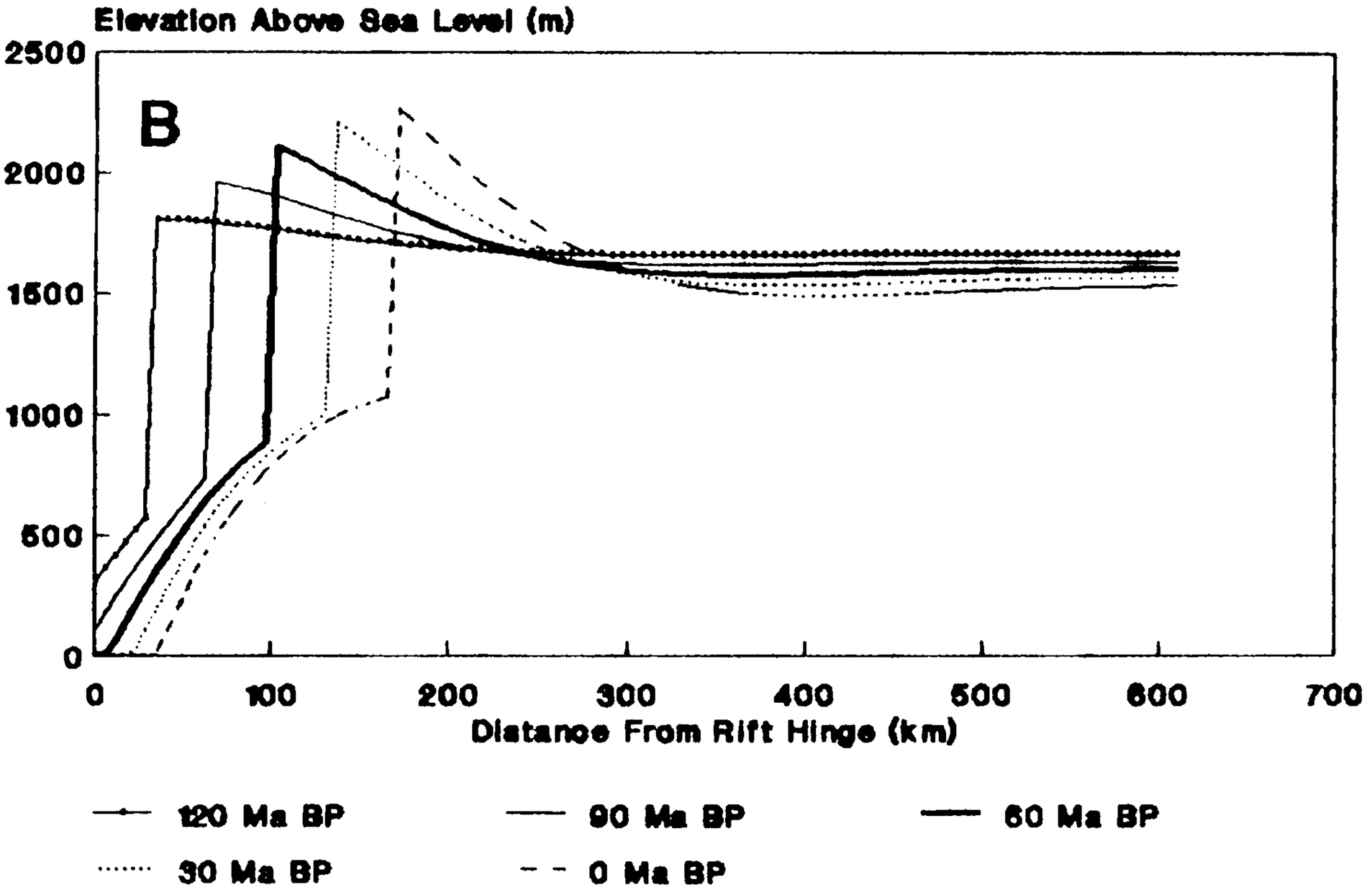

Fig. 7.12. Best modelled fit for profile HAN. Refer to Fig. 7.3 for layout and model details.

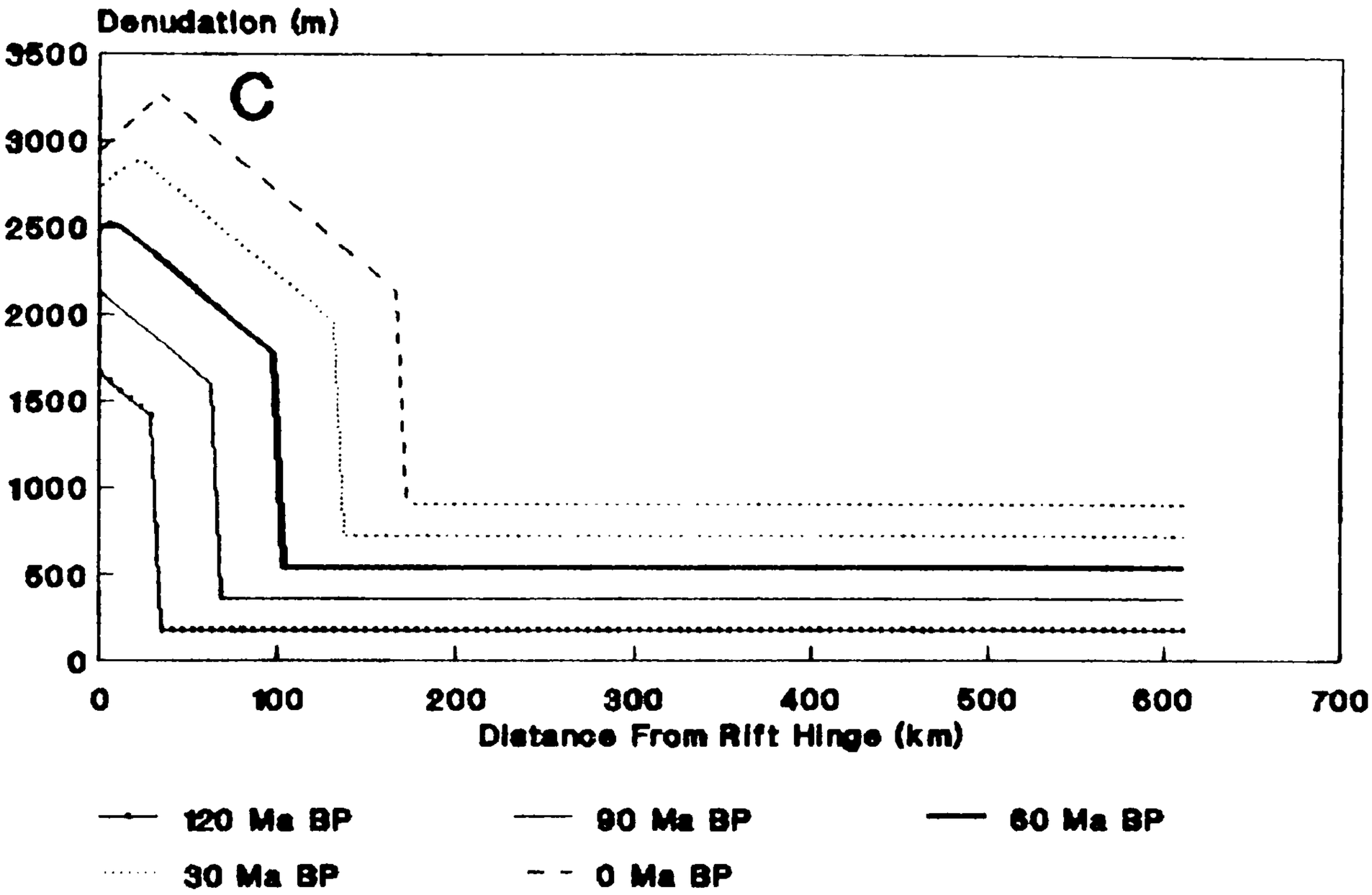

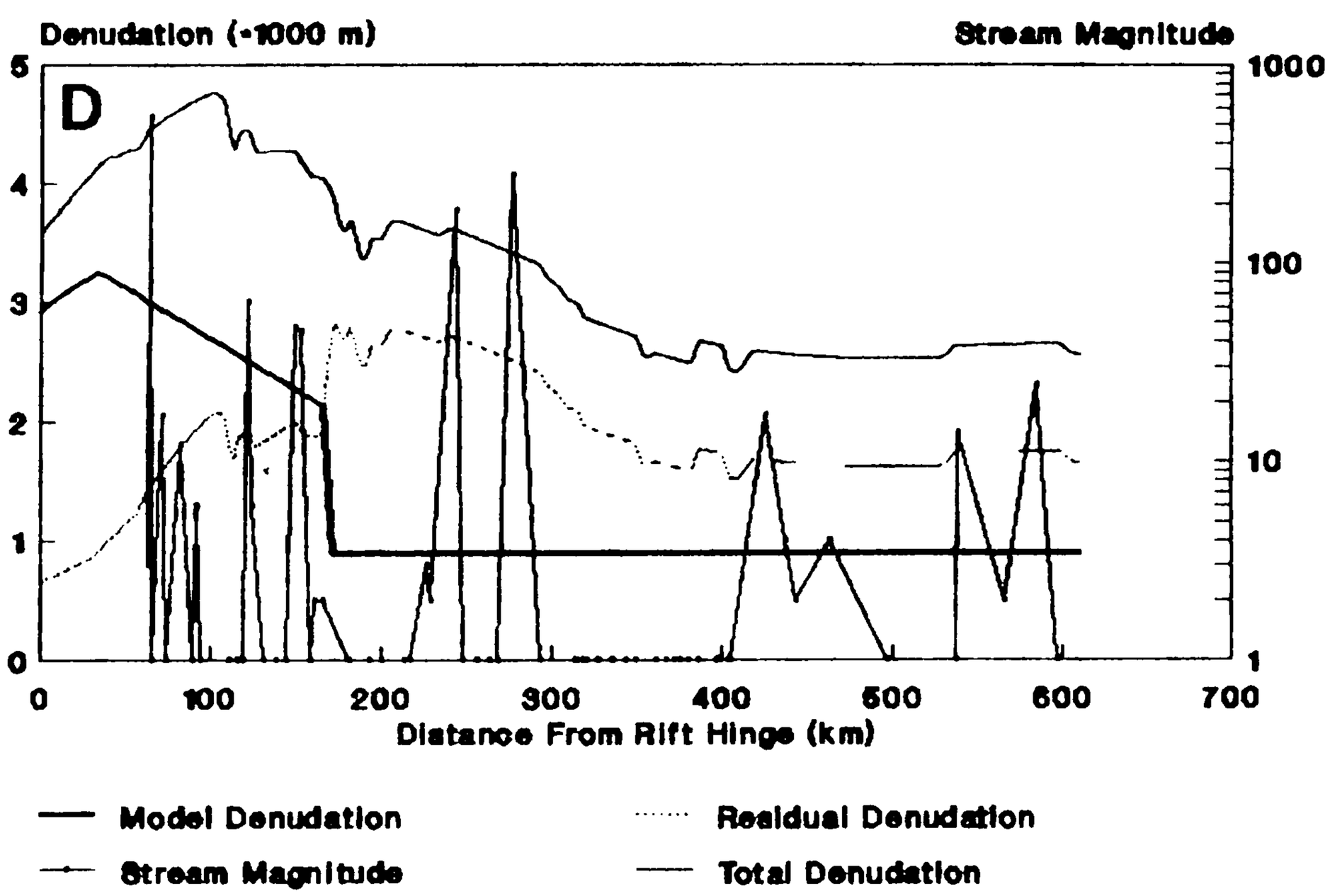

Fig. 7.12. Continued from the previous page.

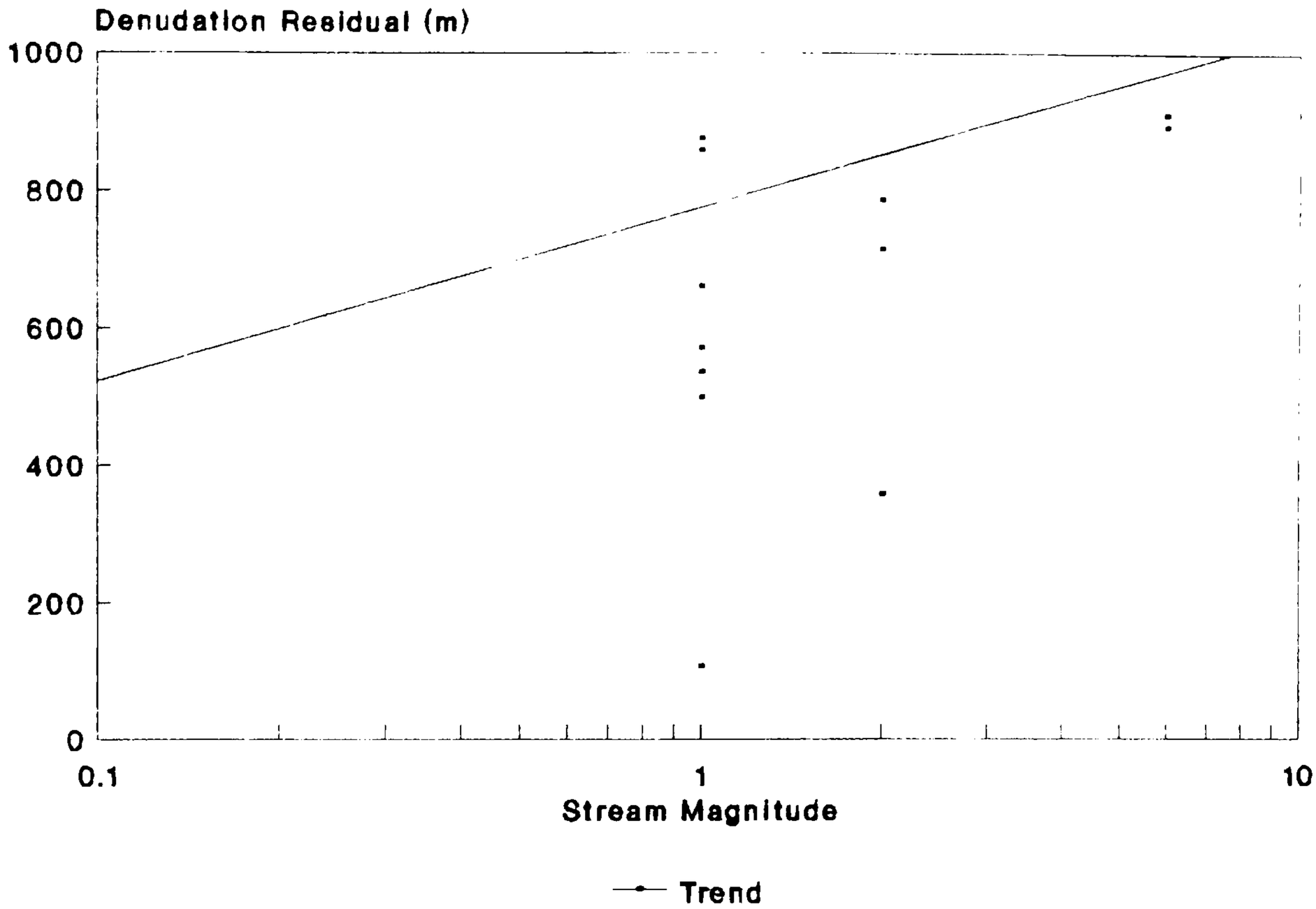

Fig. 7.13. Stream magnitude versus denudation residual, derived from Fig. 7.11d, for profile ROO.

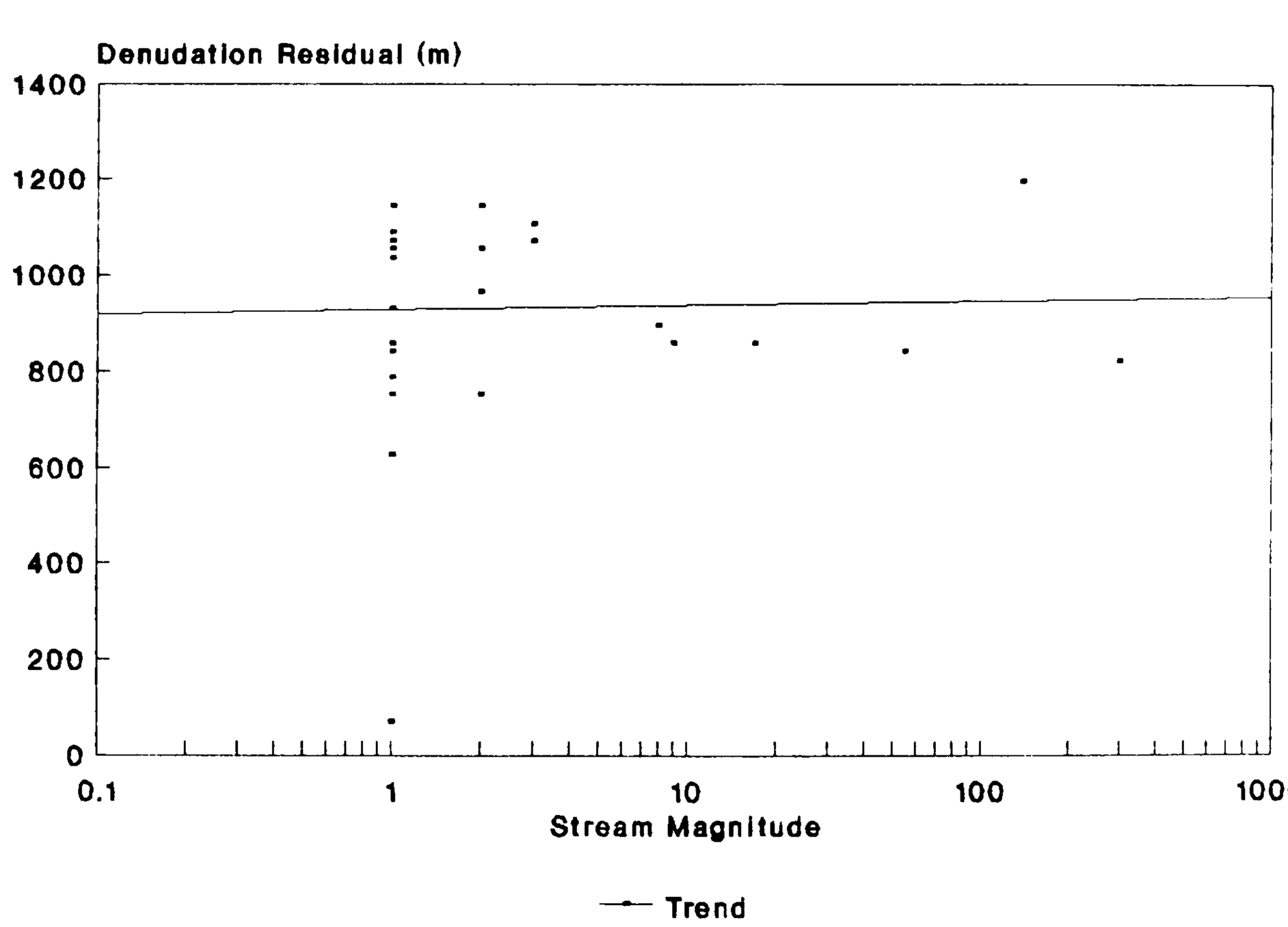

Fig. 7.14. Stream magnitude versus denudation residual, derived from Fig. 7.6d, for profile GAM.

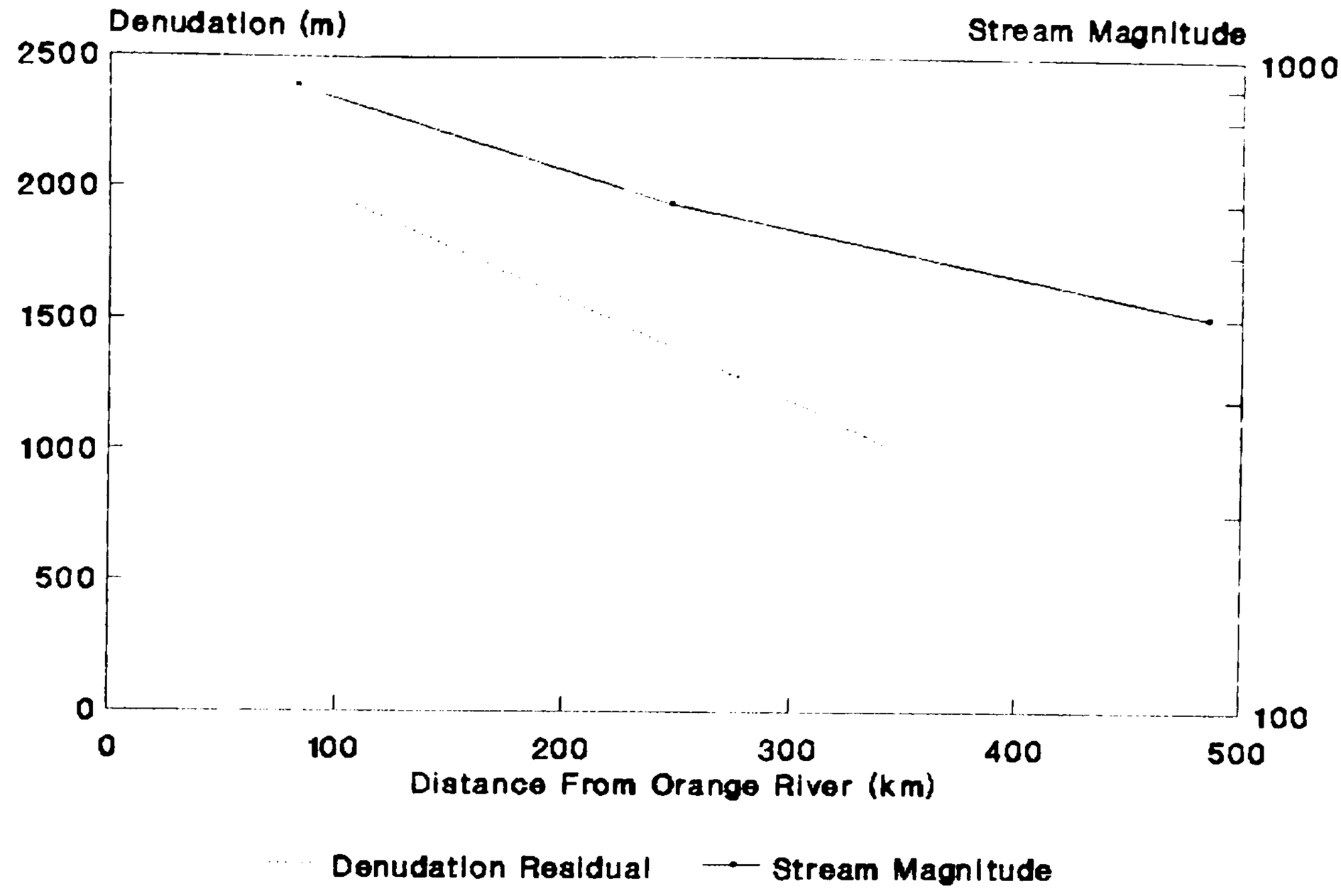

Fig. 7.15. Stream magnitude versus denudation residual, derived from Figs. 7.7d, 7.8d and 7.9d for a profile along the Fish River, Namibia (Fig. 7.1).

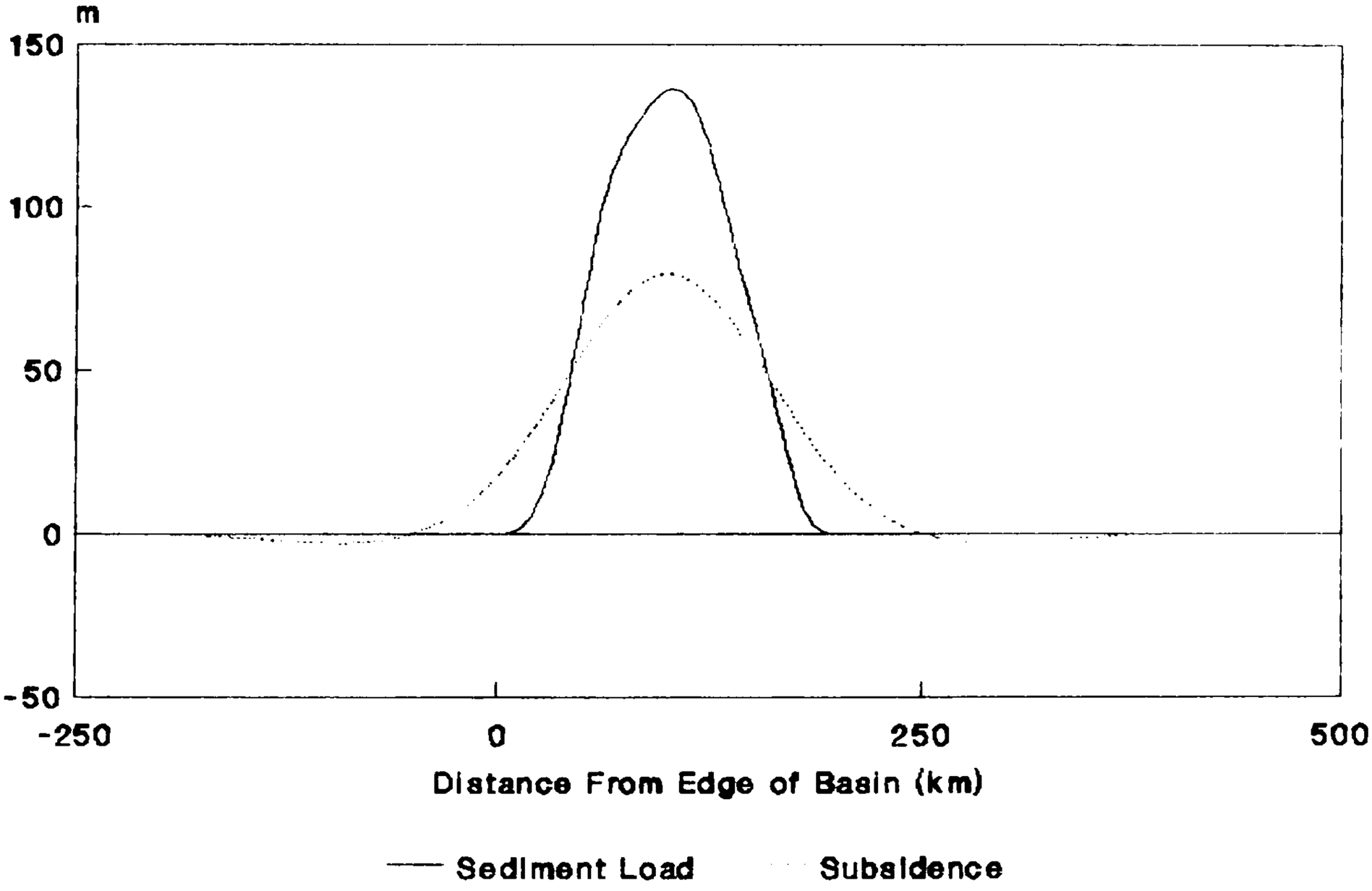

Fig. 7.16. Sedimentary load due to the Kalahari Beds of the Etosha basin (derived from Thomas and Shaw, 1987) and predicted flexurally compensated subsidence. The profile is continuous with the GRO topographic profile. The load component takes account of depth dependent porosity (section 6.2.1.2) and the isostatic component assumes a T_e of 20 km (employed for the best modelled fit of the GRO profile). Other flexural model parameters as in Fig. 7.3.

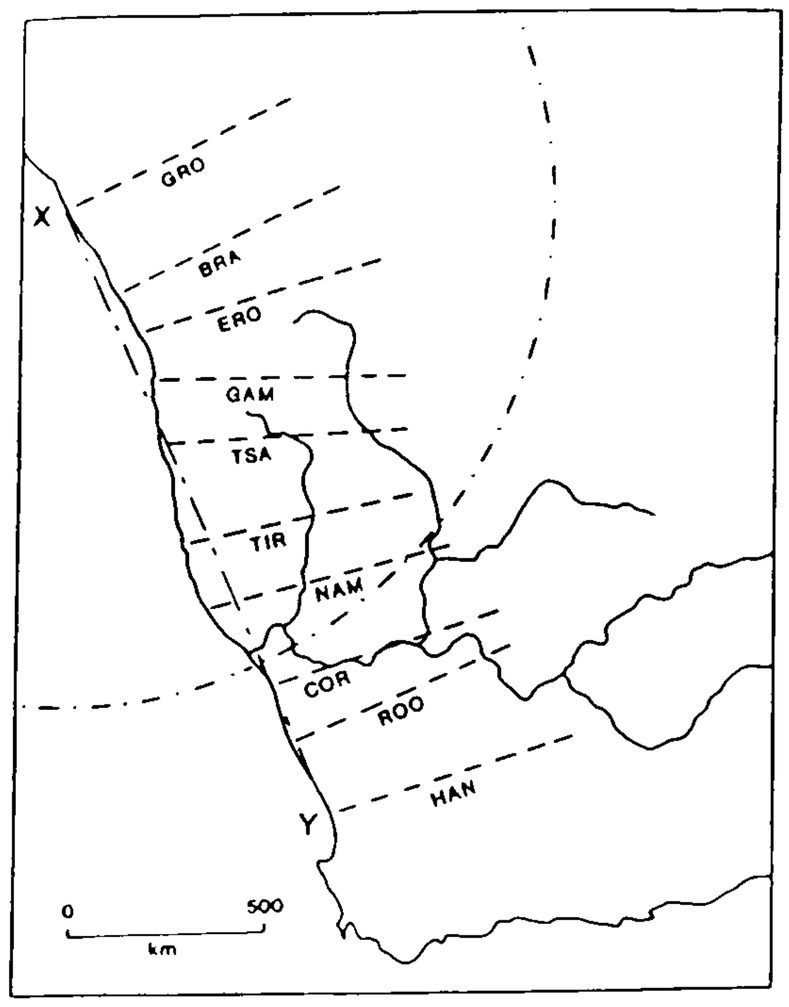

Fig. 7.17. Profile location of the initial topographic configuration of the model, shown by X-Y. The postulated mantle plume location of White and McKenzie (1989) is shown as a semi-circular dot-dashed line.

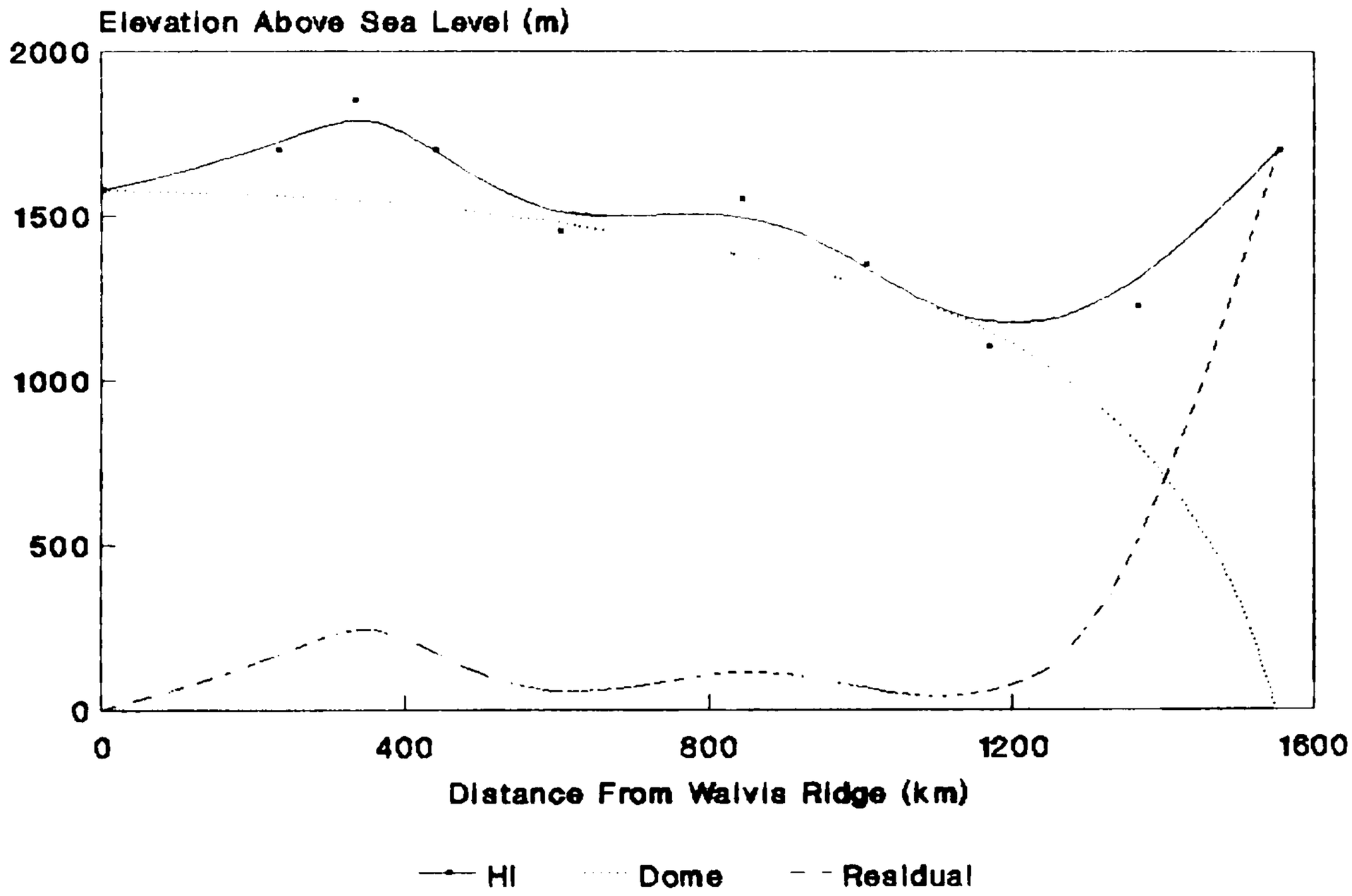

Fig. 7.18. Initial topographic configuration of the model. This consists of a domal feature, which coincides with the postulated mantle plume location of White and McKenzie (1989), and a topographic residual. The centre of the postulated mantle plume, at the time of break up in the south Atlantic, is thought to have coincided with the point where the Walvis Ridge meets the African continental lithosphere.

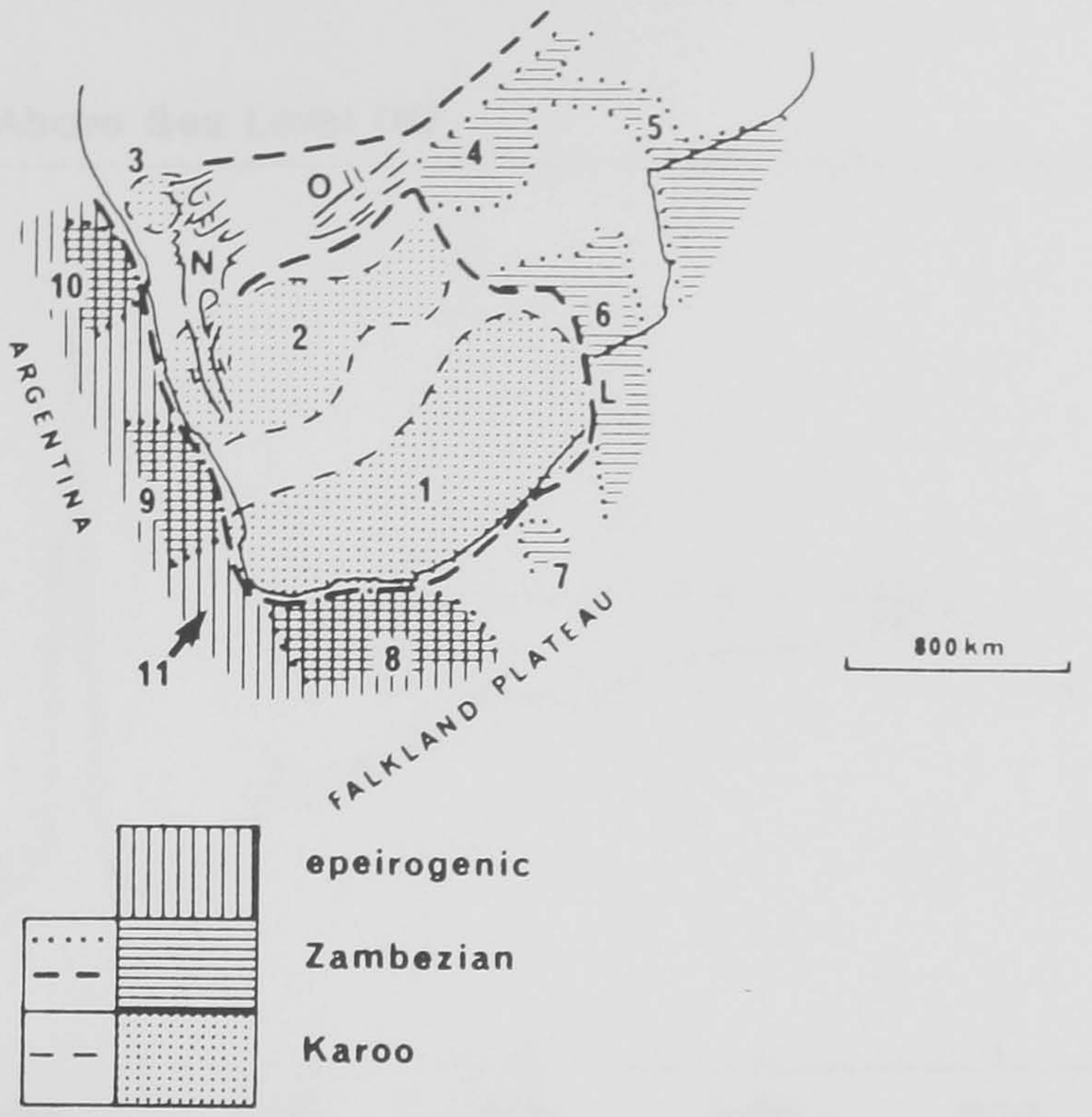

Fig. 7.19. Tectono-sedimentary terranes of southern Africa (after Dingle et al., 1983, Fig. 3). Karoo- broad downwarping on cratonic blocks with no significant faulting (Permo-Triassic). Zambezian- syn-rift style (Triassic-Lower Cretaceous). Epeirogenic- post-rift regional subsidence, mainly along continental edges, no significant faulting (Upper Cretaceous-Present). Abbreviations: (1) Main Karoo Basin; (2) Botswana Basin; (3) Etjo Basin; (4) mid-Zambezi Basin; (5) Zambezi Graben; (6) N.Transvaal, S.Mozambique and N.Natal Valley; (7) St.Johns Basin; (8) Outeniqua Basin; (9) Orange Basin; (10) Walvis Basin; (11) outer continental margin; (O) Okavango Graben; (N) W.Namibia Karoo; and (L) Lebombo line.

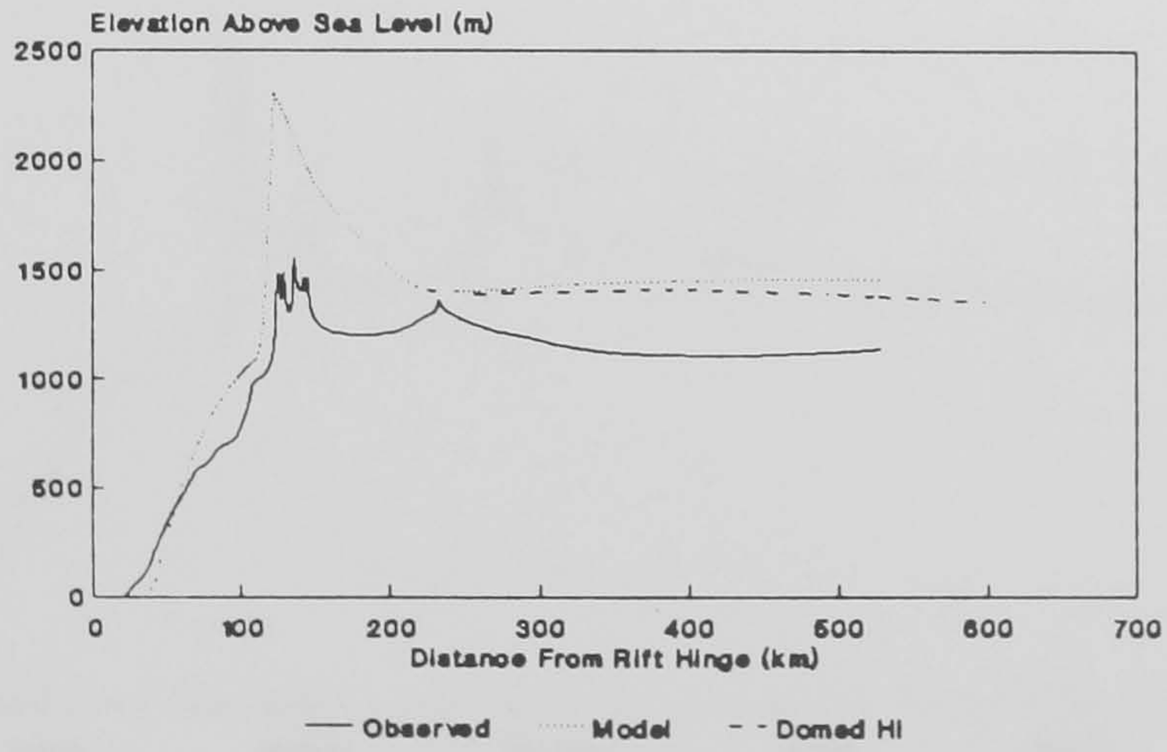

Fig. 7.20. Calculated topography for profile GRO from Fig. 7.3a, which assumes a constant initial elevation for the modelled landsurface, displayed with the calculated topographic profile assuming a domal initial topography, as indicated by Fig. 7.18. Other model parameters as in Fig. 7.2.

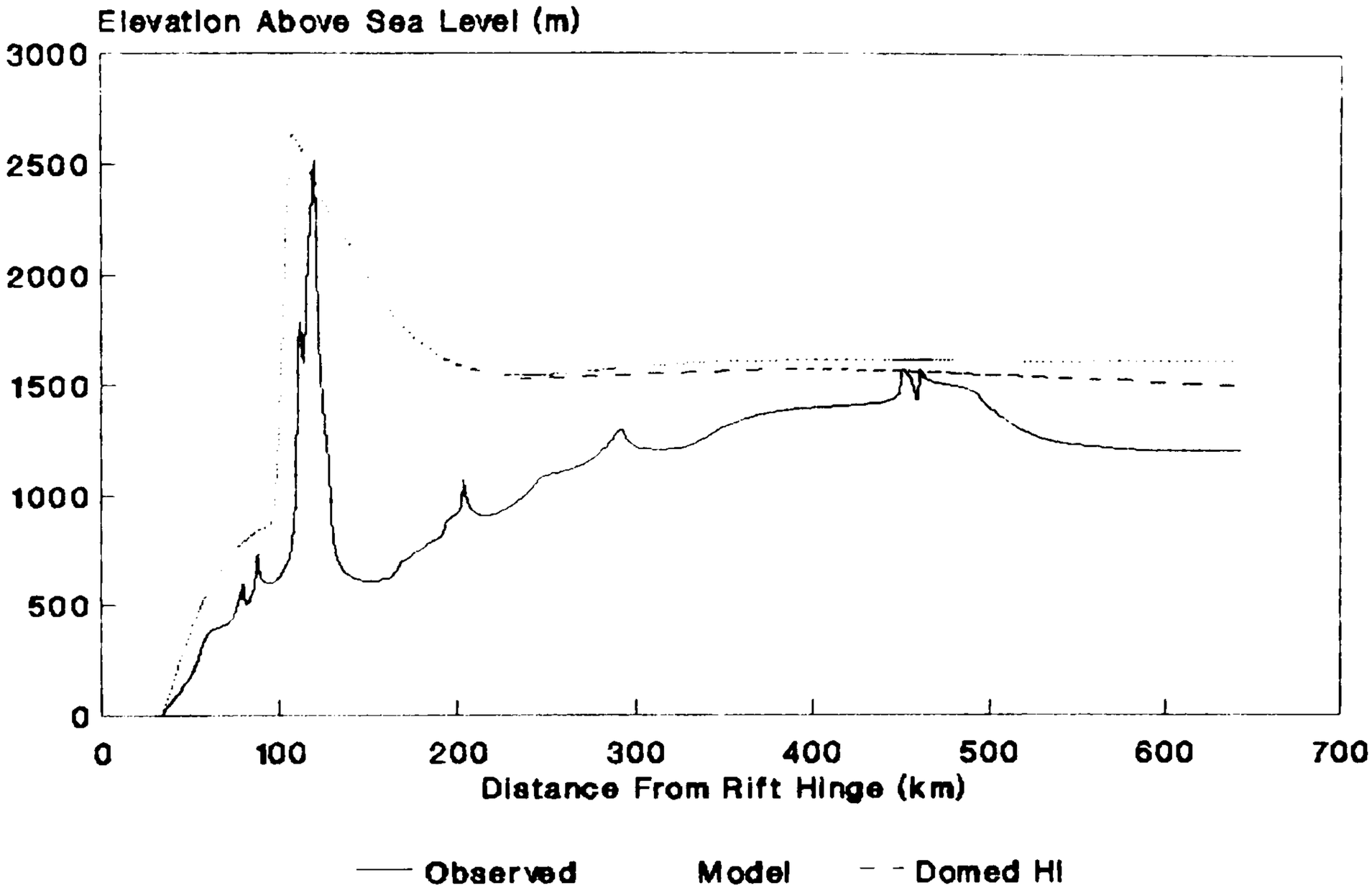

Fig. 7.21. Revised modelled fit for profile BRA. See Fig. 7.20 for details.

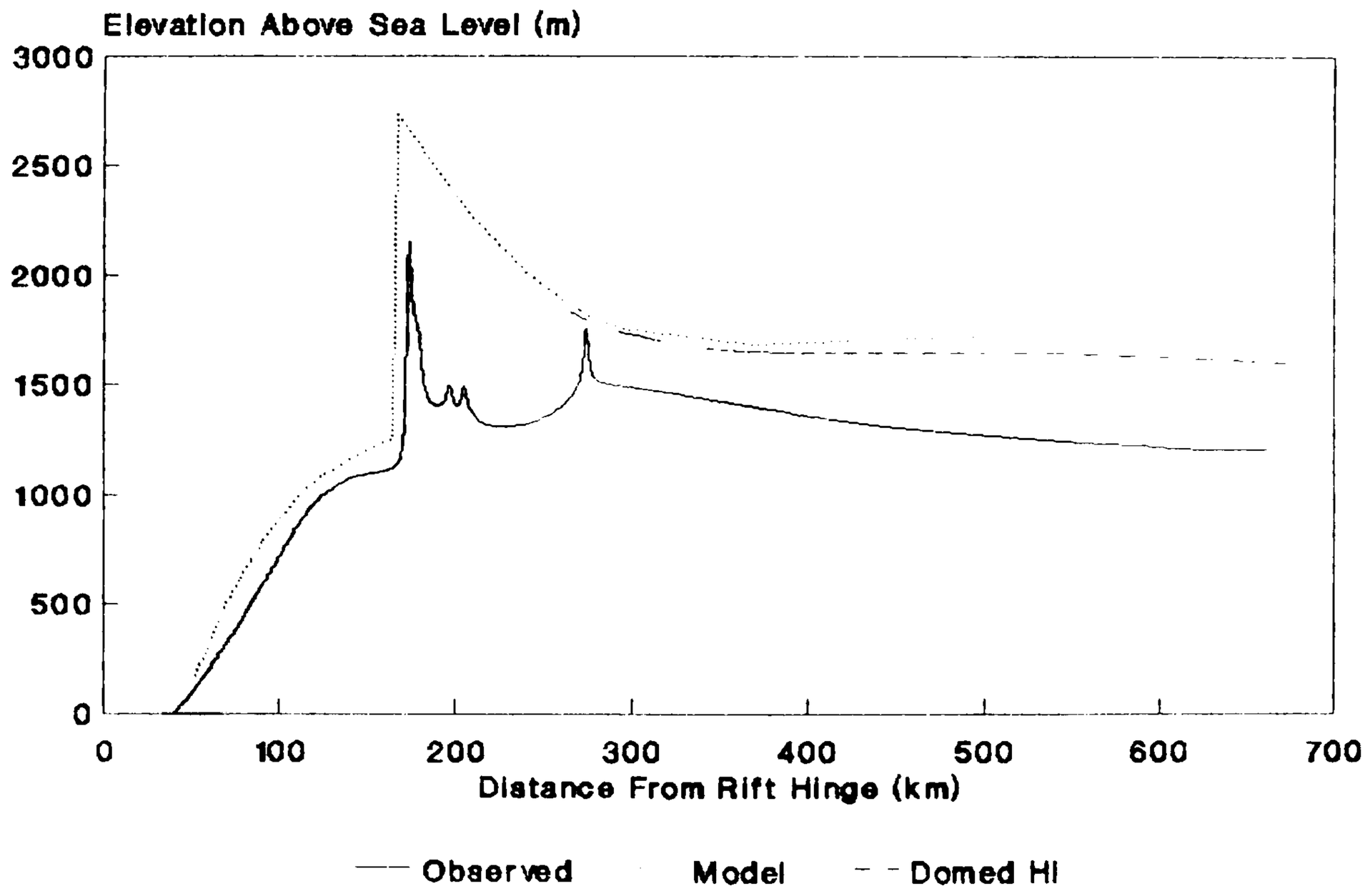

Fig. 7.22. Revised modelled fit for profile ERO. See Fig. 7.20 for details.

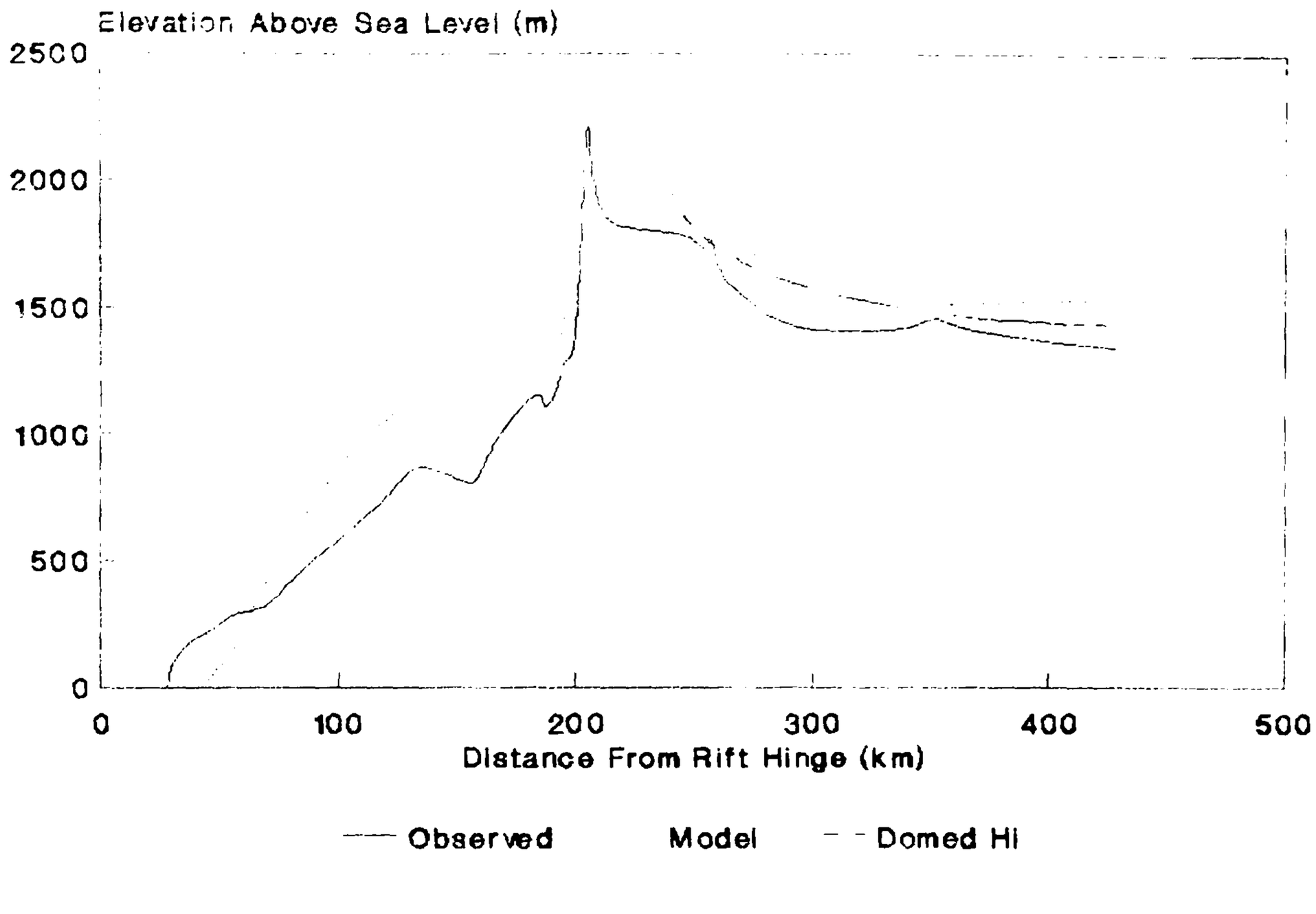

Fig. 7.23. Revised modelled fit for profile GAM. See Fig. 7.20 for details.

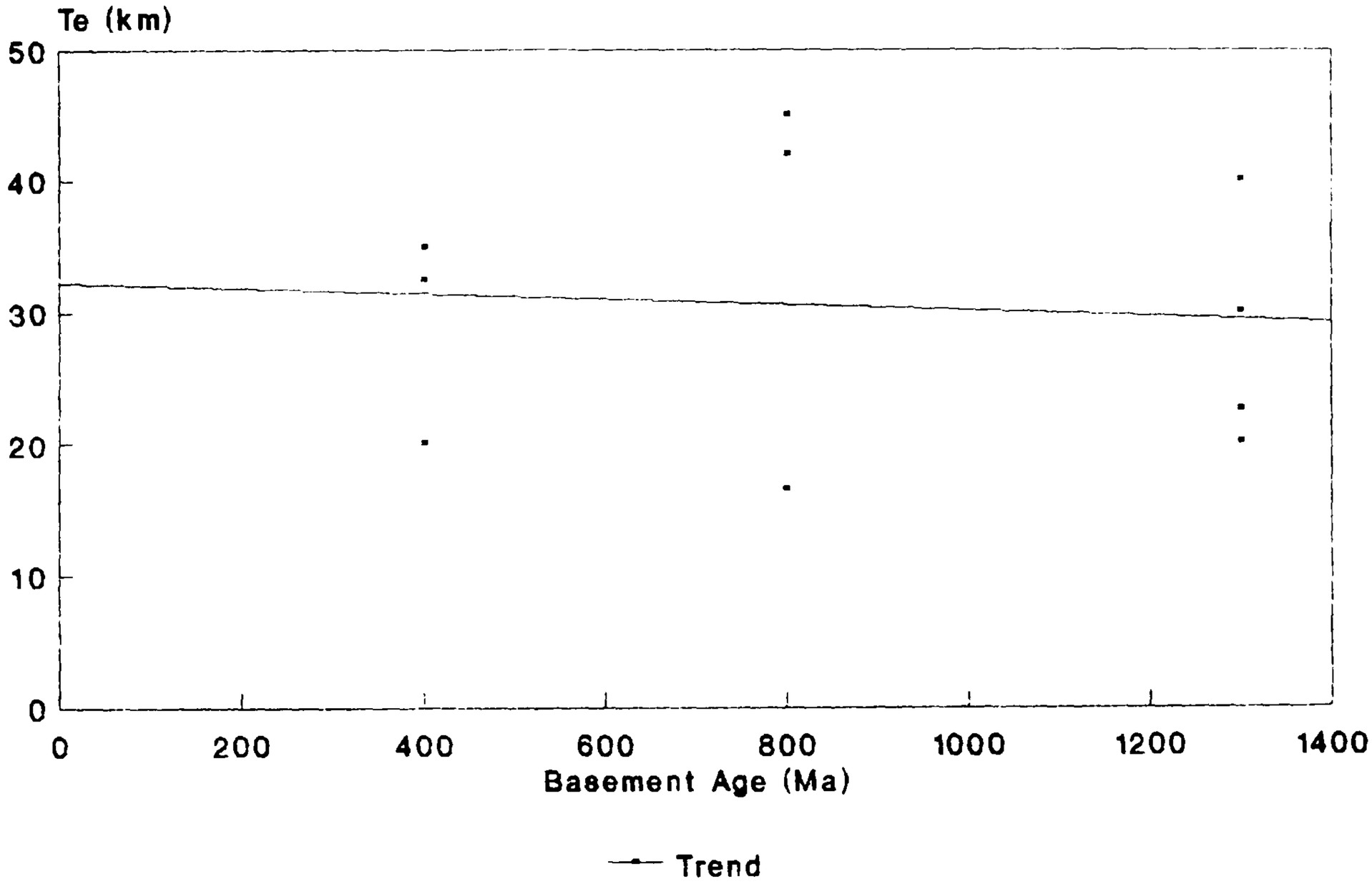

Fig. 7.24. Plot of the best modelled fit T_e versus approximate basement age for each profile in Fig. 7.1. Data from Fig. 7.2 and Fig. 2.2.

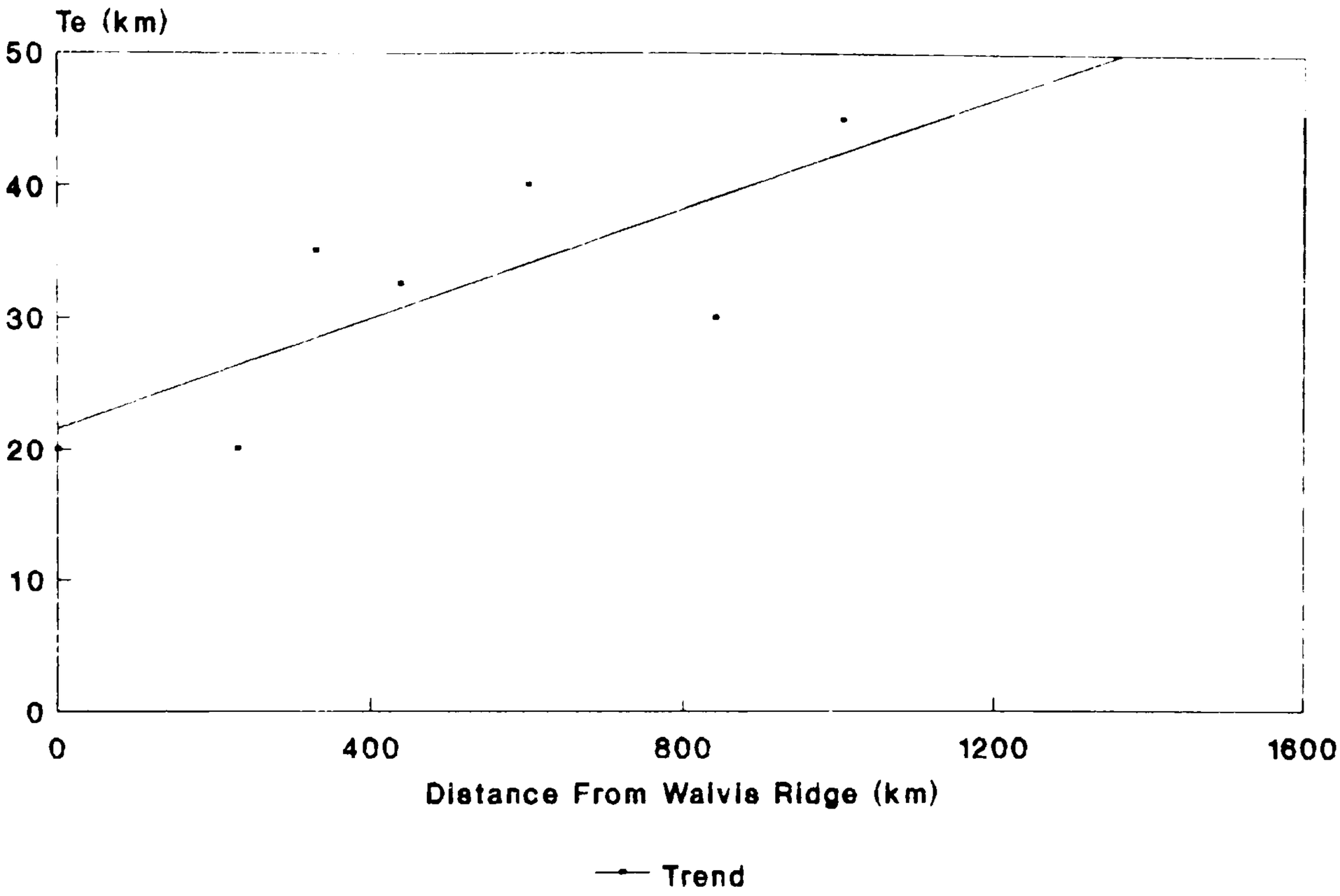

Fig. 7.25. Plot of the best modelled fit T_e versus distance from the Walvis Ridge, which coincides with the centre of the postulated mantle plume of White and McKenzie (1989) (see Fig. 7.18 for discussion). Data from Fig. 7.2 and Fig. 7.18.

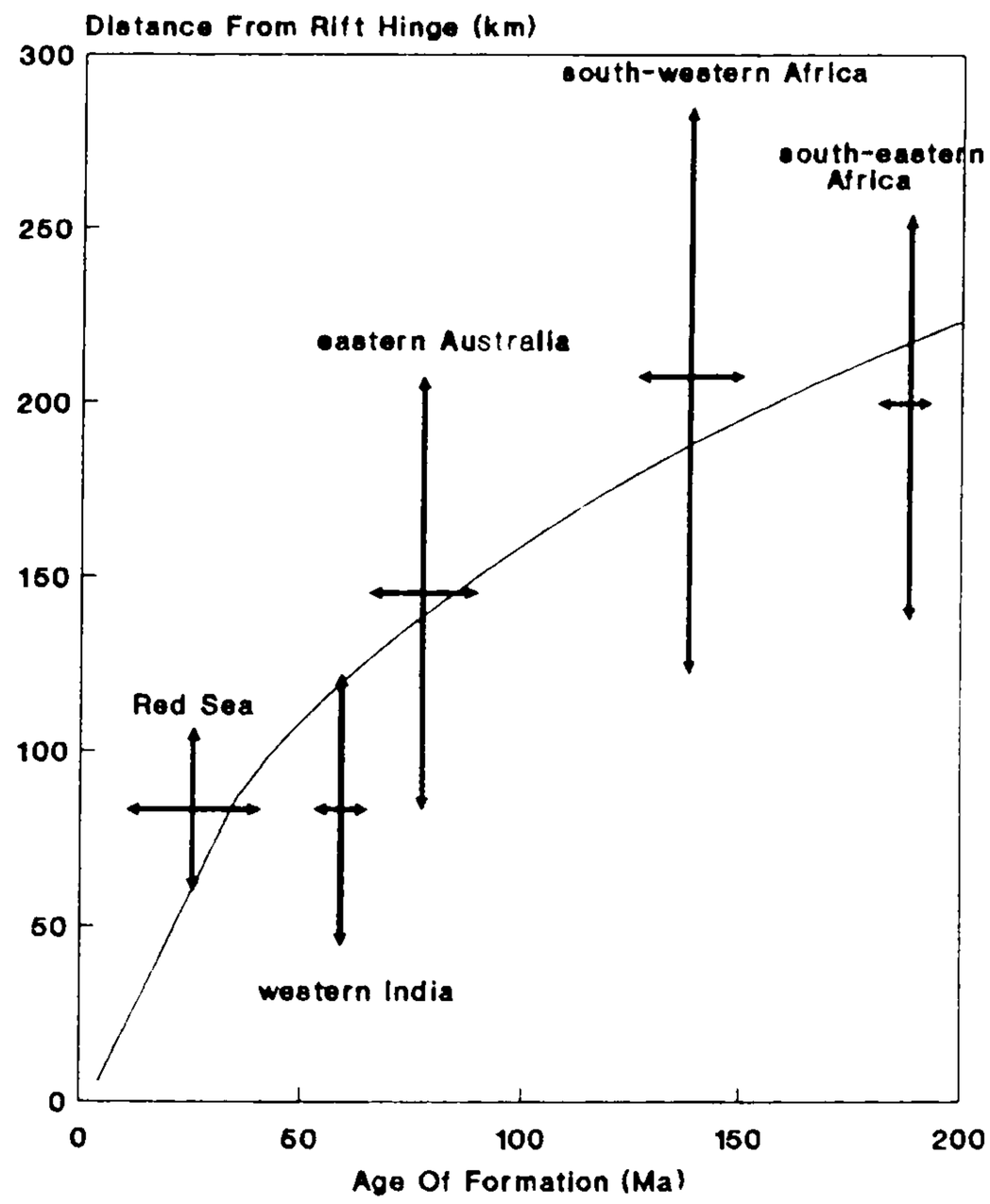

Fig. 7.26. Plot of the distance of the Great Escarpment from the rift hinge versus age of formation for different passive margins. Data from Fig. 7.1; Karner and Watts, 1982; Ollier, 1985; Ollier and Marker, 1985; Bohannon, 1987; White and McKenzie, 1989).

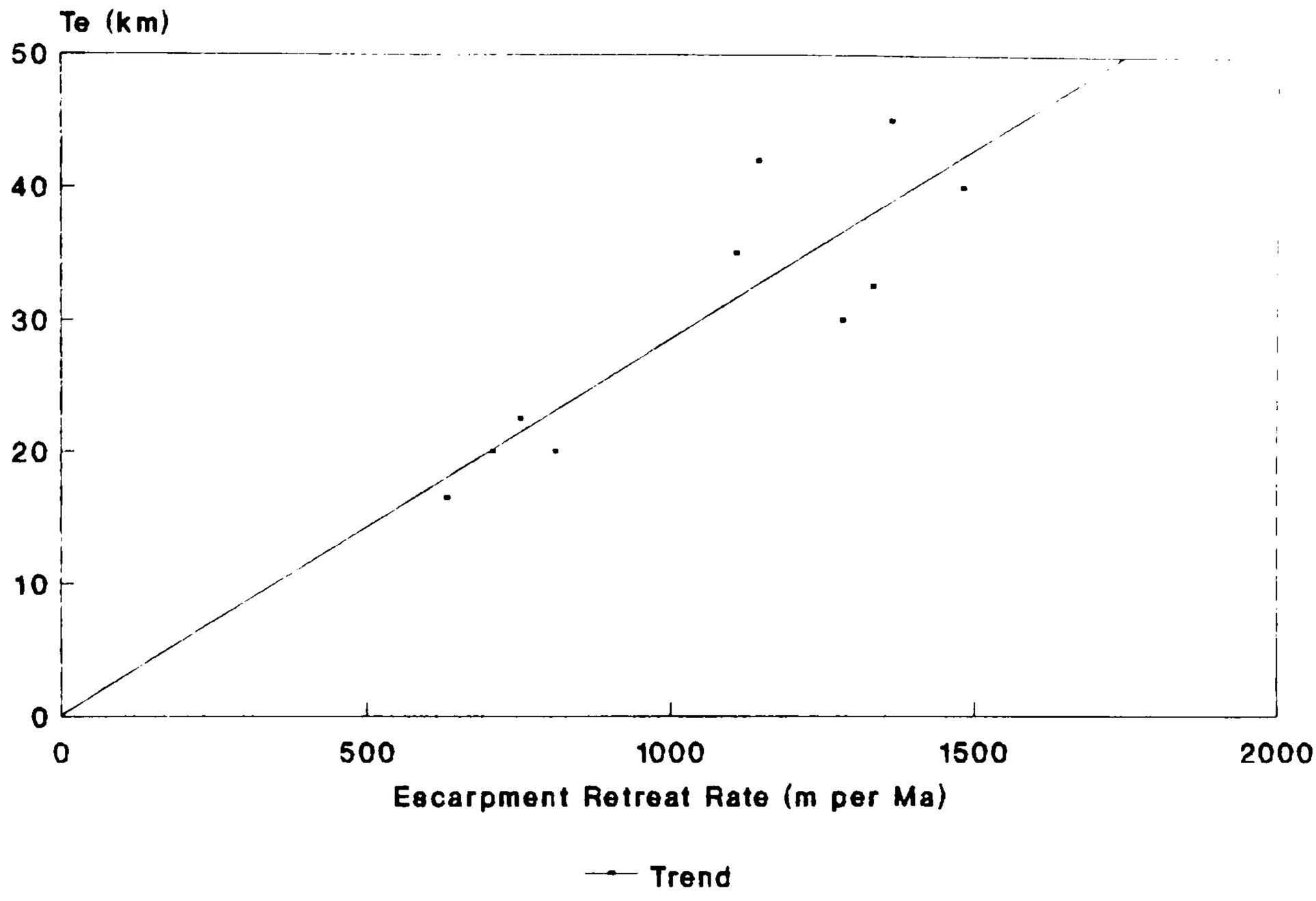

Fig. 7.27. Plot of the best modelled fit T_e versus Escarpment retreat rate (SRR) for the topographic profiles in Fig. 7.1. Data from Fig. 7.2.

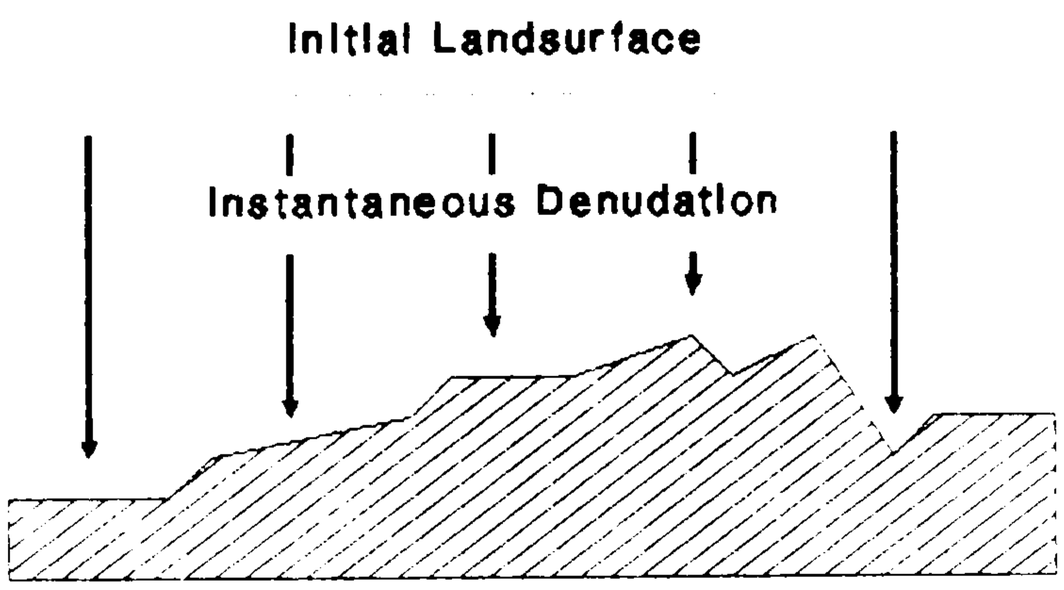

Fig. 7.28. Instantaneous down-wearing denudational model of landform evolution (model 2). The initial landsurface is effectively reduced to its final configuration instantaneously, although this is achieved by several steps since isostatic rebound is invoked as denuded material is removed.

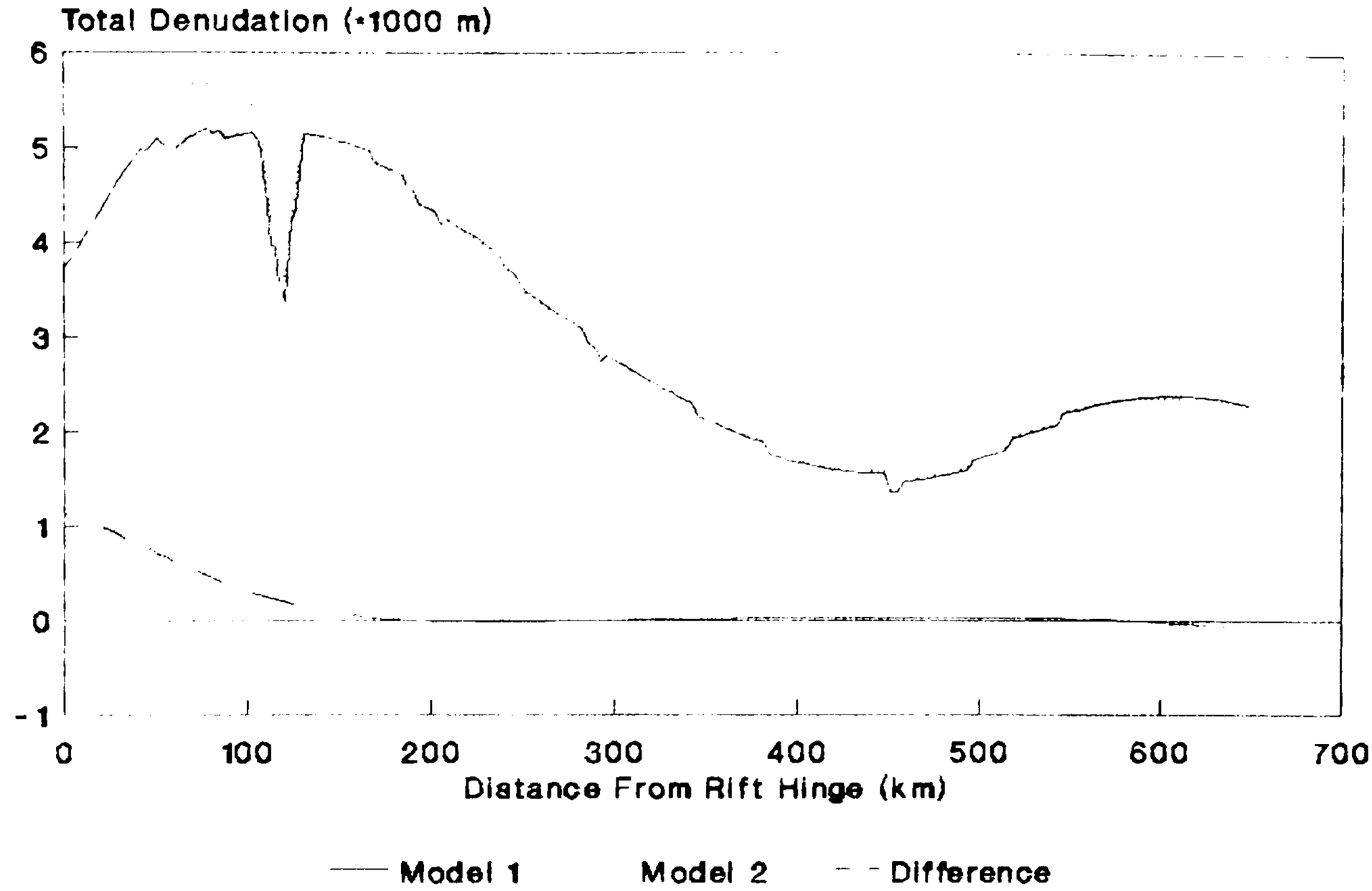

Fig. 7.29. Comparison of the total denudation calculated for the escarpment retreat (model 1) and the instantaneous down-wearing (model 2) models of landform evolution for profile BRA. Both models have the same initial topographic configuration and the final solutions coincide with the observed topography. Flexural model parameters as in Fig. 7.2. Denudation model parameters for the escarpment retreat model as in Fig. 7.2.

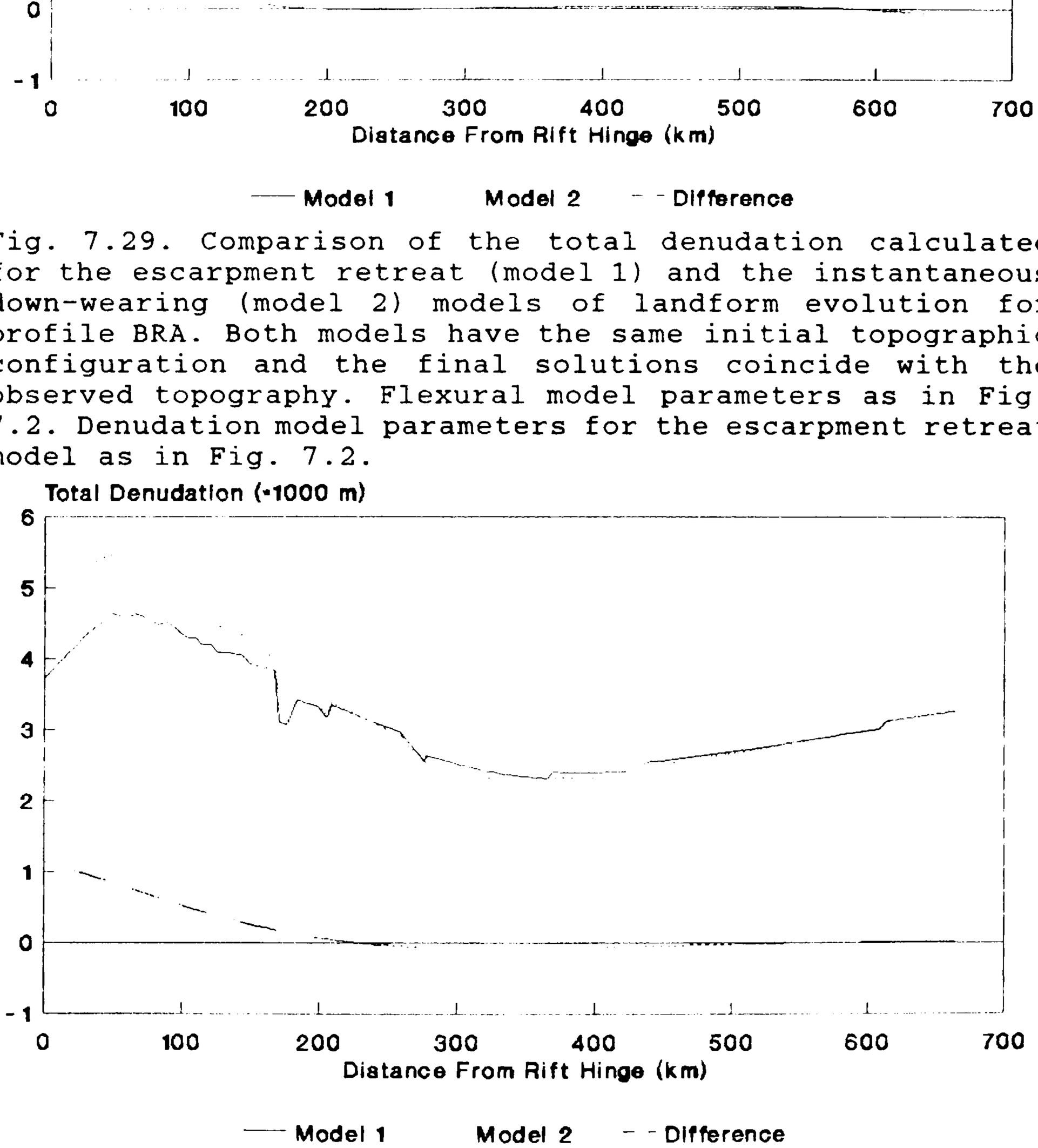

Fig. 7.30. Comparison of the total denudation calculated for the escarpment retreat (model 1) and the instantaneous down-wearing (model 2) models of landform evolution for profile ERO. See Fig. 7.29 for details.

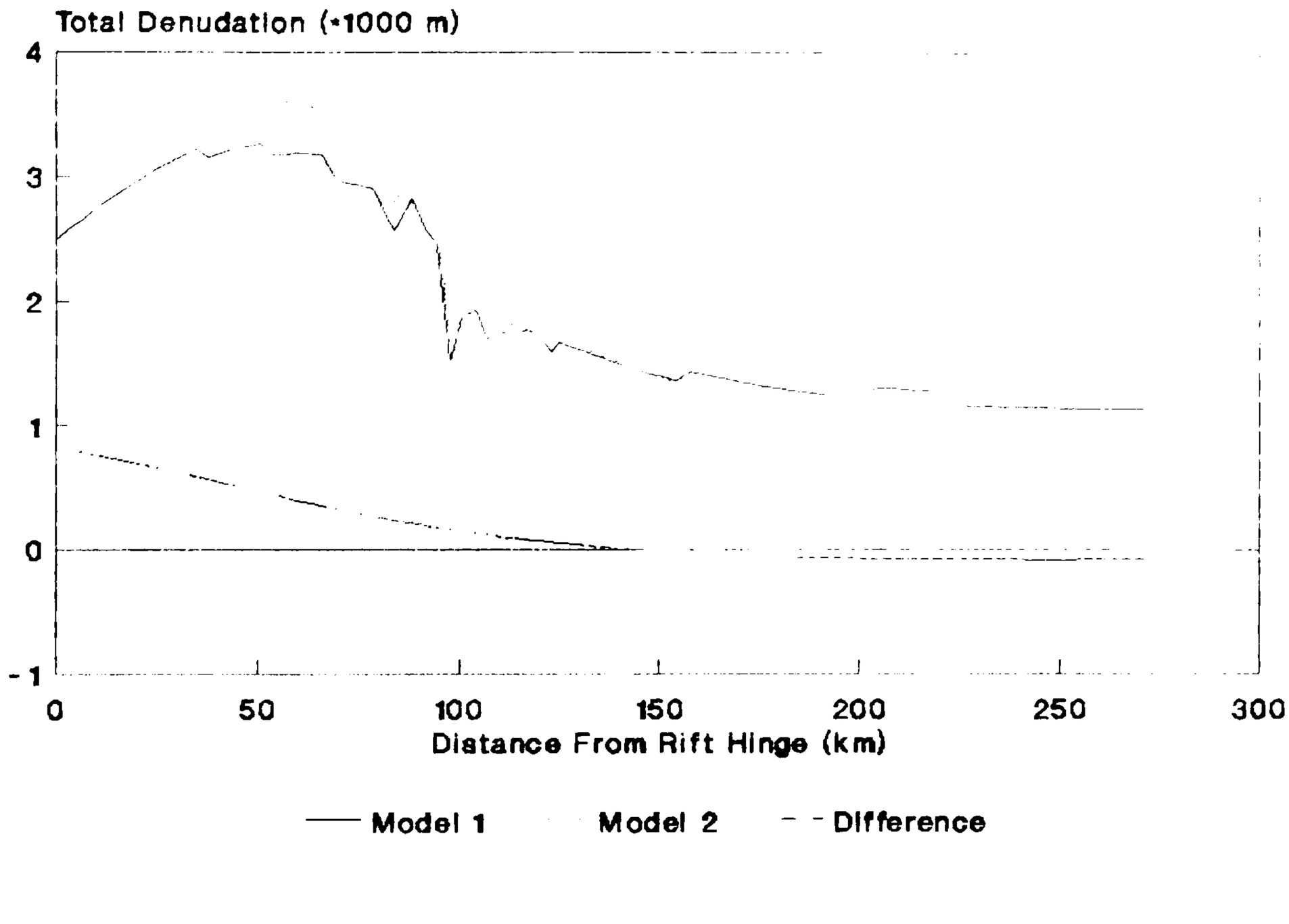

Fig. 7.31. Comparison of the total denudation calculated for the escarpment retreat (model 1) and the instantaneous down-wearing (model 2) models of landform evolution for profile ROO. See Fig. 7.29 for details.

8 CONCLUSIONS

8.1 Introduction

This chapter will briefly present the findings of this thesis and discuss their implications for aspects of geodynamic theory.

8.2 The Application of Numerical Models to Geodynamics

The principal research method used in this study has been the application of a numerical model to the geodynamics of landform evolution on passive margins, in particular south-western Africa. In this case a morphotectonic model quantifying onshore denudation/ offshore sedimentation, coupled to an isostatic component, has been formulated.

The theory concerning the isostatic response of the lithosphere to loading events is relatively well understood from gravity and load studies. The work of others has been employed in this aspect of the research reported here. Because any evolving landsurface is constantly being irrevocably changed by denudational processes the real challenge has been the formulation of a denudational model applicable to the evolution of high-elevation passive margins. The factors controlling denudation in such an environment, and over such long time scales (10^6 a), are not well constrained. Therefore, a conceptual denudational model has been developed, with reference to the dynamics of contemporary systems, and the morphological constraints

provided by the south-west African rifted margin. This model has been calibrated with reference to offshore sedimentation in the adjacent rift basins and assumptions concerning the drainage evolution of the rifted margin.

This modelling approach contains two sets of unknown model parameters, namely those concerned with the isostatic component and the initial topographic configuration of the model. Both of these are, however, constrained with reference to other studies and are varied in order to give the best modelled fit given the other calibrated denudational model parameters.

The necessary weakness of this approach is that it assumes that the conceptual denudational model accurately describes the system under consideration. This is a problematic assumption in any numerical model which attempts to reduce the complexity of a real system to a simple series of model parameters and associated mathematical formulae. Has the system been realistically parameterised? It should be emphasised that any numerical model does not represent reality but merely attempts to replicate it in a simplified way that can be processed by a computer program or summarised by analytical equations. Because of this, the calculations concerning the evolution of geodynamic systems, and especially the implications from such studies, should be treated with caution.

Does this, therefore, imply that in this case the application of a numerical model to the problem of the landscape evolution of passive margins has no validity?

Some of the aspects of the denudational model presented in this thesis cannot, at present, be directly tested and corroborated since the detailed denudational chronology of the margin is unknown due to post-rift denudation. The application of apatite fission track analysis has been used to infer denudation histories, but the technique has yet to be refined enough to provide an analytical tool where predictions can be made with any degree of certainty. However, in this study the morphotectonic model, which has been developed within a rigid geological framework, has been able to corroborate other models of geodynamic processes which directly affect the surface of the Earth. For example the probable influence of magmatic crustal underplating in determining the topographic configuration of the study area during the break up of Gondwana. This gives a high degree of confidence that the model is able to replicate elements of reality.

Therefore, the application of numerical models to geodynamic systems can provide valuable information to test ideas and constrain possible interpretations of existing data. However, the researcher in this field must always be aware of the limitations of the models that are formulated and try, whenever possible, to test them within a comprehensive geodynamic framework.

8.3 Morphotectonic Model of Passive Margin Evolution

8.3.1 Model Parameters

Current quantitative geodynamic models of rifted

margin evolution have been reviewed in chapter 3 and those applicable to the geomorphological evolution of passive margins have been discussed. This indicates that dynamic models of rifting can affect the morphological evolution of rifted margins. However, their consequences are localised to the region immediately surrounding the rift and, especially in the case of thermal effects, are most important in the early evolution (<60 Ma after formation) of the margin. Magmatic underplating models, while able to create broad topographic swells, cannot account for the origin of marginal topographic upwarps which have a different scale and form.

It is postulated that the geomorphological evolution of high-elevation passive margins, especially those that are mature, is principally controlled by the link between the mass transfer of material denuded from the continental landmass to the adjacent rift basins and isostasy. The quantitative morphotectonic model presented in this thesis has been formulated in terms of both theory and concepts. The theory of isostasy is well documented while the conceptual denudational model which has been formulated is an original contribution in the subject area.

8.3.2 Application to South-Western Africa

The morphotectonic model of passive margin evolution presented in this thesis has been formulated with reference to south-western Africa. It has been demonstrated that since the break up of Gondwana more material has been

denuded from the coastal fringes than the continental interior. Given this spatial variation in total denudation across the margin, which has also been recorded across other margins such as eastern Australia and western Brazil, and assuming that isostatic compensation occurs flexurally, then the creation of a marginal topographic upwarp is inevitable.

Given the assumptions of the model and the constraints provided by data from the south-west African rifted margin, the results indicate that the offshore evolution of the Cape sedimentary basin has not significantly affected the final topographic solution of the modelled profile. In general the early landscape evolution of the margin has been most affected by depression of the coastal region during offshore sedimentation in narrow, deep syn-rift basins which are located adjacent to the rift hinge. The thermal subsidence basins often extend beyond the syn-rift depocentres but are usually thinner in extent. The results of the model suggest that onshore flexural deformation associated with this loading phase is relatively minor with comparison to the isostatic uplift due to denudation. Therefore, a simplified model, which only considers the link between denudation and isostasy has been applied to the post-Gondwana landscape evolution of south-western Africa.

The two terrane flexural rigidity model, which takes account of the different physical properties of rifted and unrifted continental lithosphere, is not critical in

determining the final topographic solution of the model. For the best modelled fit using the two terrane isostatic model a lower rigidity for rifted continental lithosphere has been assumed. The calibrated values of T_e are consistent with other studies. The effect of changing the flexural rigidity of the model is to change the distribution of isostatically generated uplift due to denudation, and for the simple model coupling denudation and isostasy a constant rigidity has been assumed.

The simple model is able to replicate the features of some of the topographic profiles under consideration in this study. The mismatch between most of the observed and calculated topographic profiles is probably attributable to enhanced denudation rates associated with the incision of major drainage systems. In view of this hypothesis the denudation residual between observed and calculated topographic profiles has been qualitatively compared to the present stream magnitude across each profile. This analysis indicates that at least some of the difference between calculated and observed topography is probably due to fluvial incision. Further development of the model will require more detailed denudational chronology data, but any analysis will be hampered by the absence of geological and structural data of denuded regions. This point is crucial since it has been shown in chapter 4 that bedrock structure has a critical control on landform development in south-western Africa.

8.3.3 Model Implications

8.3.3.1 Geomorphology of Passive Margins

The generation of marginal topographic upwarps as a consequence of differential denudational unloading probably occurs progressively as the Great Escarpment retreats from the rift hinge. The quantitative morphotectonic model indicates that marginal upwarps reach their maximum elevation ≈100 Ma after rifting which may account for the deflection of drainage systems away from many mature rifted margins. If rates of surface uplift are high enough in the coastal region then the establishment of fully integrated external drainage networks may not occur until a significant time after rifting and margin formation. Indeed, in the case of south-western Africa there is evidence from the offshore stratigraphic record of a lag of ≈50 Ma between rifting and the establishment of a major focused sediment input into the rifted margin basin. Where drainage systems do breach a marginal upwarp, the isostatically generated surface uplift will tend to maintain a significant change in channel gradient.

The quantitative morphotectonic model indicates that marginal upwarps develop progressively from the time of continental margin formation. This is contrary to the cyclical surface uplift framework of landscape evolution proposed by previous geomorphological analyses of southern Africa. These studies envisage punctuated surface uplift throughout the evolution of the margin, but current tectonic models for both inter-plate and intra-plate

settings cannot readily account for this framework. Recent models of passive margin development suggest that maximum active tectonic uplift generated by magmatic underplating, thermal perturbations or mechanical unloading linked to lithospheric extension involves a single major event associated with continental rifting. Thus, the absence of any obvious cyclical surface uplift model applicable to inter-plate and intra-plate tectonic regions indicates that the geomorphic and sedimentological evidence on which the identification of episodic surface uplift has been based perhaps deserves more rigorous appraisal. Although erosion surface sequences are ubiquitous on the Gondwana continents many, if not all, appear to be subject to direct structural control. As a consequence, the vertical separation of such erosion surfaces cannot be taken as unambiguous evidence of discrete episodes of surface uplift initiating relative falls in base level.

The comparison of scarp retreat and instantaneous down-wearing models of landscape evolution, given the same initial and final topography, generally indicates that different spatial/temporal patterns of denudation do not greatly affect the total accumulative denudation profile of the model. Therefore, an independent quantitative technique for assessing denudational chronology is required in order to rigorously test the conceptual denudation model presented in this thesis and further develop it. Apatite fission track analysis has much potential in this respect although this has yet to be realised.

A syn-rift topographic profile, parallel to the south-west African margin, has been deduced by the application of the quantitative morphotectonic model. This suggests the probable importance of magmatic crustal underplating in elevating the region into an approximately domal topographic feature at around the time of rifting. Therefore, the drainage at this time was probably radial in nature, directed away from the dome centre. Prior to underplating, the region was probably an area of low relief near to sea level.

The analysis of escarpment location, with respect to the rift hinge, on high-elevation passive margins of different ages of formation, indicate that rates of escarpment retreat tend to decrease as the margins age. This suggests that new, lower, base levels initiated during rifting quickly cause fluvial incision of the rift-flanks giving high rates of escarpment retreat. As the margin evolves denudational processes operating on the landsurface tend towards a graded quasi-equilibrium and escarpment retreat rates decrease.

8.3.3.2 Sedimentation on Passive Margins

The presence of a marginal topographic upwarp on high-elevation passive margins acts as a barrier to sediment transport from continental interiors to the offshore sedimentary basins. The persistence of such a barrier throughout the evolution of the margin suggests that patterns of offshore sedimentation are likely to be

controlled by a dual drainage system comprising numerous small aggressively eroding coastal catchments and widely spaced outlets of large basins draining continental interiors well into the mature rifted margin phase. It has been suggested that the nature of sediment sources are an important factor in determining the distribution of different sediment facies within rifted margin basins. Thus, geomorphology has much to offer the study of sedimentology. The location of fluvial outlets from large continental interior catchments is dependent upon fluvial incision remaining at the same rate, or greater, than the isostatically driven uplift associated with differential denudation unloading. This suggests that the location of major fluvial outlets may change in time as rocks more susceptible to denudation are uncovered, but with a different spatial distribution.

8.3.3.3 Geodynamics of Passive Margins

The application of the morphotectonic model of passive margin evolution to south-western Africa has enabled the syn-rift topography of this region of Gondwana to be approximated. With reference to the geological framework of the region the major mechanisms controlling the origin of its topography have been determined.

The correspondence of a domal topographic feature with the postulated location of a mantle plume indicates the probable importance of magmatic crustal underplating in permanently uplifting the region and determining the syn-

rift drainage of the margin. With respect to present sea level this mechanism has probably accounted for ≈1.5 km of surface uplift at the centre of the dome in response to the underplating of ≈10.5 km of relatively buoyant magmatic material.

In the southern part of the study area the influence of the Cape Orogeny in the early Triassic has been instrumental in elevating the landsurface. The calculated syn-rift elevation for this area is ≈1.7 km which compares with a postulated value of up to ≈4.2 km for the original height of this orogenic belt. This indicates that denudation has significantly reduced the amplitude of the Cape Mountains, probably depositing much of the denuded material in the adjacent Karoo sedimentary basin, before the break up of Gondwana.

The post-rift landscape evolution of south-western Africa has been dominated by the link between denudation and its isostatic response. It has been shown that a marginal topographic upwarp, which has influenced the drainage and sedimentological evolution of the margin, has developed in response to the differential unloading if the lithosphere responds flexurally. This has been due to the development of a new denudational regime after rifting, probably due to the creation of new, lower, base levels.

Variations in the effective elastic thickness of the lithosphere (T_e) along the south-west African rifted margin have been considered. The analysis indicates that the thermal anomaly associated with a mantle plume in this area

≈120 Ma BP has probably reset the thermal age of the lithosphere. Near to the centre of the plume the T_e of the lithosphere has probably been lowered by this effect. From the strong linear relationship between T_e and escarpment location on the ten profiles modelled across the study area, it is suggested that the morphological evolution of high-elevation rifted margins is influenced by the flexural properties of the lithosphere. This may be as the graded response of denudational processes to flexural isostatic uplift.

The flexural coupling of rifted and unrifted lithosphere has been investigated with a variable rigidity isostatic component in the morphotectonic model. It has been determined that the flexural properties of rifted continental lithosphere do not greatly influence the morphological evolution of south-western Africa. Since onshore denudation and offshore sedimentation create a couple around the rift hinge it may be expected that brittle failure of the lithosphere will be concentrated in this region. Modelling has shown this to be the case. However, the degree of failure is not enough to significantly change the flexural properties of the lithosphere.

8.4 Concluding Remarks

This study has considered aspects of the morphotectonic evolution of passive continental margins, in particular the landscape evolution of south-western Africa

since the break up of Gondwana. This has been conducted by the application of a conceptual denudation model coupled to a theoretical model of isostatic compensation.

Perhaps the most important conclusion that has arisen is that the formulation and application of conceptual and theoretical numerical models of geodynamic processes can provide valuable insight into the evolution and implications of those processes. However, this is only the case when such models are constructed and tested, wherever possible, within a comprehensive geological framework of reference.

Geomorphology, with its readily observable and quantifiable processes, has the potential of being a powerful analytical tool with which to test and constrain models of geodynamic processes which influence the surface of the Earth.

REFERENCES

Ahnert, F. 1970. Functional relationships between denudation, relief and uplift in large mid-latitude drainage basins, American Journal of Science, 268, 243-263.

Ahnert, F. 1973. Coslop2 - a comprehensive model program for simulating slope profile development, Geocombulletin, 8, 99-121.

Anderson, R.S. and Humphrey, N.F. 1989. Interaction of weathering and transport processes in the evolution of arid landscapes, Quantitative Dynamic Stratigraphy, Cross, T.A. (Editor), Prentice Hall, 349-361.

Ashwal, L.D. and Burke, K. 1989. African lithospheric structure, volcanism, and topography, Earth and Planetary Science Letters, 96, 8-14.

Bally, A.W. and Snelson, S. 1980. Realms of subsidence, in A.D. Miall, (Ed.), Facts and principles of world petroleum occurrence, Canadian Society of Petroleum Geology Memoir, 6, 9-94.

Bally, A.W., Watts, A.B., Grow, J.A., Manspeizer, W., Bernoulli, D., Schreiber, C. and Hunt, J.M. 1981. Geology of passive continental margins: history, structure and sedimentologic record (with special emphasis on the Atlantic margin), for the AAPG eastern section meeting and Atlantic margin energy conference, American Association of Petroleum Geologists Education course note series, 19.

Barton, P. and Wood, R. 1984. Tectonic evolution of the North Sea basin: Crustal stretching and subsidence, Royal Astronomical Society Geophysical Journal, 79, 987-1022.

Beaumont, C., Keen, C.E. and Boutilier, R. 1982. A comparison of foreland and rift margin sedimentary basins, Philosophical Transactions of the Royal Society of London, A 305, 295-317.

Bechtel, T.D., Forsyth, D.W., Sharpton, V.L. and Grieve, R.A.F. 1990. Variations in effective elastic thickness of the North American lithosphere, Nature, 343, 636-638.

Bills, B.G. and May, G.M. 1987. Lake Bonneville: Constraints on lithospheric thickness and upper mantle viscosity from Isostatic warping of Bonneville, Provo, and Gilbert stage shorelines, Journal of Geophysical Research, 92, 11493-11508.

Bohannon, R.G. 1987. Tectonic configuration of the western Arabian continental margin, southern Red Sea, Tectonics, 5, 477-499.

Bohannon, R.G., Naeser, C.W., Schmidt, D.L., and Zimmermann, R.A. 1989. The timing of uplift, volcanism, and rifting peripheral to the Red Sea: a case for passive rifting?, Journal of Geophysical Research, 94, 1683-1701.

Bond, G.C. and Kominz, M.A. 1988. Evolution of thought on passive continental margins from the origin of geosynclinal theory (≈1860) to the present. Geological

Society of America Bulletin, 100, 1909-1933.

Bott, M.H.P. and Kusznir, N.J. 1984. The origin of tectonic stress in the lithosphere, Tectonophysics, 105, 1-13.

Braun, J. and Beaumont, C. 1989. A physical explanation of the relation between flank uplifts and the breakup unconformity at rifted continental margins, Geology, 17, 760-764.

Brown, R.W., Rust, D.J., Summerfield, M.A., Gleadow, A.J.W. and De Wit, M.C.J. 1990. An early cretaceous phase of accelerated erosion on the south-western margin of Africa: evidence from apatite fission track analysis and the offshore record, Nuclear Tracks and Radiation Measurement, 17, 339-350.

Buck, W.R. 1986. Small-scale convection induced by passive rifting: the cause for uplift of rift shoulders, Earth and Planetary Science Letters, 77, 362-72.

Buck, W.R., Martinez, F., Steckler, M.S. and Cochran, J.R. 1988. Thermal consequences of lithospheric extension: pure and simple, Tectonics, 7, 213-234.

Byerlee, J. 1978. Friction of rocks, Pure and Applied Geophysics, 116, 615-626.

Carson, M.A. and Kirkby, M.J. 1972. Hillslope Form and Process, Cambridge University Press, Cambridge.

Chorley, R.J., Schumm, S.A. and Sugden, D.E. 1984. Geomorphology, Methuen, London.

Cox, K.G. 1970. Tectonics and vulcanism of the Karoo period and their bearing on the postulated fragmentation of Gondawanaland, in African Magmatism and Tectonics,

Oliver and Boyd, Edinburgh, 211-235.

Cox, K.G. 1972. The Karoo volcanic cycle, Journal of the Geological Society of London, **128**, 311-336.

Cox, K.G. 1978. Flood basalts, subduction and the break up of Gondwanaland, Nature, **274**, 47-49.

Cox, K.G. 1989. The role of mantle plumes in the development of continental drainage patterns, Nature, **342**, 873-877.

Creer, K.M. 1965. Palaeomagnetic data from the Gondwanic continents, Philosophical Transactions of the Royal Society of London, **A258**, 27-40.

Culling, W.E.H. 1965. Theory of erosion on soil-covered slopes, Journal of Geology, **73**, 230-254.

Dalziel, I.W.D., Storey, B.C., Garrett, S.W., Grunow, A.M., Herrod, L.D.B. and Pankhurst, R.J. 1987. Extensional tectonics and the fragmentation of Gondwanaland, Continental Extensional Tectonics, Geological Society Special Publication, **28**, 433-441.

Deffontaines, B. 1991. Drainage network analysis: a useful tool to evidence the France morphotectonic features, Terra abstracts, 3, 349.

De Swardt, A.M.J. and Bennet, G. 1974. Structural and physiographic development of Natal since the late Jurassic, Transactions of the Geological Society of South Africa, **77**, 309-322.

De Wit, M.J. 1986. What the oldest rocks say, in: Workshop on the Earth as a planet, Lunar Planetary Institute Technical Report, **86-08**, 14-17.

Dietz, R.s and Holden, J.C. 1970. Reconstruction of Pangaea: breakup and dispersion of continents, Permian to present, Journal of Geophysical Research, 75, 39-53.

Dingle, R.V. 1973. Mesozoic palaeogeography of the southern Cape, South Africa, Palaeogeography, Palaeoclimatology and Palaeoecology, 13, 203-213.

Dingle, R.V. and Scrutton, R.A. 1974. Continental breakup and the development of post-Palaeozoic sedimentary basins around southern Africa. Bulletin of the Geological Society of America, 85, 1467-1474.

Dingle, R.V., Siesser, W.G. and Newton, A.R. 1983. Mesozoic and Tertiary Geology of Southern Africa, A. A. Balkema, Rotterdam.

Donnelly, T.W. 1982. Worldwide continental denudation and climatic deterioration during the late Tertiary: evidence from deep-sea sediments, Geology, 10, 451-454.

Du Toit, A.L. 1937. Our Wandering Continents, An Hypothesis of Continental Drifting, Oliver and Boyd, Edinburgh, 366.

Eales, H.V., Marsh, J.S. and Cox, K.G. 1984. The Karoo igneous province: an introduction, Special Publication of the Geological Society of South Africa, 13, 1-26.

Ebinger, C.J., Bechtel, T.D., Forsyth, D.W. and Bowin, C.O. 1989. Effective elastic plate thickness beneath the east African and Afar plateaus and dynamic compensation of the uplifts. Journal of Geophysical

Research, 94, 2883-2901.

Etheridge, M.A., Symonds, P.A. and Lister, G.S. 1990. Application of the detachment model to reconstruction of conjugate passive margins, American Association of Petroleum Geologists Memoir, 46, 23-40.

Fernandez, L.M. and Guzman, J.A. 1979. Seismic history of southern Africa, Geological Survey of South Africa Seismologic Series 9, 38.

Fitch, F.J. and Miller, J.A. 1984. Dating Karoo igneous rocks by the conventional K-Ar and 40Ar/39Ar age spectrum methods, petrogenesis of the volcanic rocks of the Karoo province, Special Publication of the Geological Society of South Africa, 13.

Forsyth, D.W. 1985. Subsurface loading and estimates of the flexural rigidity of continental lithosphere, Journal of Geophysical Research, 90, 12623-12632.

Gerrard, I. and Smith, G.C. 1980. Post Palaeozoic succession and structure of the southwestern African continental margin, American Association of Petroleum Geologists Memoir, 34, 49-74.

Gilchrist, A.R. and Summerfield, M.A. 1990. Differential denudation and flexural isostasy in formation of rifted-margin upwarps, Nature, 346, 739-742.

Gilchrist, A.R. and Summerfield, M.A. Denudation, Isostasy and Landscape Evolution, Earth Surface Processes and Landforms, (in press).

Gilluly, J. 1955. Geologic contrasts between continents and ocean basins, Geological Society of America Special

Paper 62, 561-590.

Green, P.F., Duddy, I.R., Laslett, G.M., Hegarty, K.A., Gleadow, A.J.W. and Lovering, J.F. 1989. Thermal annealing of fission tracks in apatite, Chemical Geology (Isotope Geoscience Section), 79, 155-182.

Gunn, R. 1943. A quantitative evaluation of the influence of the lithosphere on the anomalies of gravity, Journal of the Franklin Institute, 236, 373-396.

Gunn, R. 1949. Isostasy - extended, Journal of Geology, 57, 263-279.

Gurnis, M. 1988. Large-scale mantle convection and the aggregation and dispersal of super-continents, Nature, 332, 695-699.

Hack, J.T. 1975. Dynamic equilibrium and landscape evolution, in Theory of Landform Development, Binghamton New York State University of New York Publications in Geomorphology, 87-102.

Hack, J.T. 1979. Rock control and Tectonism- their importance in shaping the Appalachian highlands, U.S. Geological Survey Professional Paper, 1126-B, B1-B17.

Halbich, I.W. 1983. A tectogenesis of the Cape Fold Belt, in Geodynamics of the Cape Fold Belt, Geological Society of South Africa Special Publication.

Halbich, I.W., Fitch, F.J. and Miller, J.A. 1983. Dating the Cape Orogeny, in Geodynamics of the Cape Fold Belt, Geological Society of South Africa Special Publication.

Hartnady, C.J.H. 1985. Uplift, faulting, seismicity,

thermal spring and possible incipient volcanic activity in the Lesotho-Natal region, SE Africa: the Quathlamba hot spot hypothesis, Tectonics, 4, 371-377.

Hartnady, C.J.H. 1989. Seismicity and plate boundary evolution in southeastern Africa, Unpublished manuscript.

Haxby, W.F. and Turcotte, D.L. 1976. Stresses induced by the addition or removal of overburden and associated thermal effects, Geology, 181-184.

Hill, R.S. 1972. The geology of the northern Algoa basin, Port Elizabeth, Unpublished M.Sc. thesis, University of Stellenbosch, South Africa.

Holmes, A. 1965. Principles of Physical Geology, 2nd edn, Nelson, London.

Karner, G.D. and Watts, A.B. 1982. On isostasy at Atlantic-type passive margins, Journal of Geophysical Research, 87, 2923-2948.

Karner, G.D., Steckler, M.S. and Thorne, J.A. 1983. Long-term thermo-mechanical properties of the continental lithosphere, Nature, 304, 250-253.

Kent, P.E. 1977. The Mesozoic development of aseismic continental margins, Journal of the Geological Society of London, 134, 1-18.

King, L.C. 1955. Pediplanation and Isostasy: An example from South Africa, Quarterly Journal of the Geological Society, 111, 353-359.

King, L.C. 1967. The morphology of the Earth (2 edn), Olivier and Boyd, Edinburgh.

Kirkby, M.J. 1971. Hillslope process-response models based on the continuity equation, Slope form and process, Brunsden, D (Editor), Institute of British Geographers Special Publication 3, 15-30.

Kirkby, M.J. 1986. A two-dimensional simulation model for slope and stream evolution, in A.D. Abrahams (ed), Hillslope Processes, 203-222.

Kusznir, N.J. and Karner, G.D. 1985. Dependence of the flexural rigidity of the continental lithosphere on rheology and temperature, Nature, 316, 138-142.

Kusznir, N.J., Karner, G.D. and Egan, S. 1987. Geometric, thermal and isostatic consequences of detachments in continental lithosphere extension and basin formation, Canadian Society of Petroleum Geologists, **Memoir 12**, 185-203.

Kusznir, N.J. and Egan, S.S. 1989. Simple-shear and pure-shear models of extensional sedimentary basin formation: application to the Jeanne d'Arc basin, grand banks of Newfoundland, American Association of Petroleum Geologists Memoir, **46**, 305-322.

Kusznir, N.J., Marsden, G. and Egan, S.S. 1990. A flexural cantilever simple-shear/pure-shear model of continental lithosphere extension: applications to the Jeanne D'Arc basin, Grand Banks and Viking Graben, North Sea, from Roberts, A.M., Yielding, G. and Freeman, B. (eds), The Geometry of Normal Faults, Geological Society Special Publication, **56**, 41-60.

Lambeck, K. and Stephenson, R. 1986. The post-palaeozoic

uplift history of south-east Australia, Australian Journal of Earth Sciences, 33, 253-270.

Langbein, W.B. and Schumm, S.A. 1958. Yield of sediment in relation to mean annual precipitation, American Geophysical Union Transactions, 39, 1076-1084.

Larson, R.L. and Ladd, J.W. 1973. Evidence for the opening of the south Atlantic in the early Cretaceous, Nature, 246, 209- 212.

Larson, R.L. and Hilde, T.W. 1975. A revised time scale of magnetic reversals for the early Cretaceous, Late Jurassic, Journal of Geophysical Research, 80, 2586-2594.

Latin, D. and White, N. 1990. Generating melt during lithospheric extension: pure shear vs. simple shear, Geology, 18, 327-331.

Lawver, L.A., Sclater, J.G. and Meinke, L. 1985. Mesozoic and Cenozoic reconstructions of the south Atlantic, Tectonophysics, 114, 233-254.

Lister, G.S., Etheridge, M.A. and Symonds, P.A. 1986. Detachment faulting and the evolution of passive continental margins, Geology, 14, 246-250.

Lock, B.E. 1980. Flat-plate subduction and the Cape Fold Belt of South Africa, Geology, 8, 35-39.

Marsden, G., Yielding, G., Roberts, A.M. and Kusznir, N.J. 1990. Application of a flexural cantilever simple-shear/pure-shear model of continental lithosphere extension to the formation of the northern North Sea basin, Tectonic Evolution of the North Sea Rifts,

Blundell, D.J. and Gibbs, A.D. (Editors), Clarendon Press, Oxford.

Martin, A.K. 1987. Comparison of sedimentation rates in the Natal Valley, south-west Indian Ocean, with modern sediment yields in east coast rivers of Southern Africa, South African Journal of Science, 83, 716-724.

McKenzie, D.P. and Bowin, C. 1976. The relationship between bathymetry and gravity in the Atlantic Ocean, Journal of Geophysical Research, 81, 1903-1915.

McKenzie, D.P. 1978. Some remarks on the development of sedimentary basins, Earth and Planetary Science letters, 40, 25-32.

McKenzie, D.P. 1984. A possible mechanism for epeirogenic uplift, Nature, 307, 616-618.

McKenzie, D.P. and Bickle, M.J. 1988. The volume and composition of melt generated by extension of the lithosphere, Journal of Petrology, 29, 625-679.

Meissner, R. and Strehlau, J. 1982. Limits of stresses in continental crusts and their relation to the depth-frequency distribution of shallow earthquakes, Tectonics, 1, 73-89.

Moon, B.P. and Selby, M.J. 1983. Rock mass strength and scarp forms in southern Africa, Geografiska Annaler, 65A, 135-145.

Moore, A.E. 1976. Controls of post-Gondwanaland alkaline volcanism in southern Africa, Earth and Planetary Science Letters, 31, 291-296.

Moore, M.E., Gleadow, A.J.W. and Lovering, J.F. 1986.

Thermal evolution of rifted continental margins: new evidence from fission tracks in basement apatites from southeastern Australia, Earth and Planetary Science Letters, 78, 255-270.

Morgan, W.J. 1983. Hot spot tracks and the early rifting of the Atlantic, Tectonophysics, 94, 123-139.

Mörner, N.A. (Ed.) 1980. Earth Rheology, Isostasy and Eustasy, Wiley, Chichester.

Moretti, I. and Turcotte, D.L. 1985. A model for erosion, sedimentation, and flexure with application to New Caledonia, Journal of Geodynamics, 3, 155-168.

Moretti,I. and Chenet, P.Y. 1987. The evolution of the Suez rift: a combination of stretching and secondary convection, Tectonophysics, 133, 229-234.

Nadai, A. 1963. Theory of Flow and Fracture of Solids, McGraw-Hill, New York.

Newton, A.R. 1980. Intraplate nature of the Cape Fold Belt, South African Journal of Science, 76, 272-273.

Nisbet, E.G. 1982. Komatiites, (Eds Arndt, N.T. and Nisbet, E.G.), chapter 29, Allen and Unwin, London.

Nunn, J.A. and Sleep, N.H. 1984. Thermal contraction and flexure of intra-cratonic basins: A three-dimensional study of the Michigan Basin, Royal Astronomical Society Geophysical Journal, 76, 587-635.

Nunn, J.A. and Aires, J.R. 1988. Gravity anomalies and flexure of the lithosphere at the middle Amazon basin, Brazil, Journal of Geophysical Research, 93, 415-428.

Oberlander, T.M. 1989. Slope and pediment systems, In

Thomas, D.S.G. (Ed), Arid Zone Geomorphology, Belhaven Press, London, 56-84.

Oelofsen, B.W. 1987. The biostratigraphy and fossils of the Whitehill and Irati shale formations of the Karoo and Parana basins, Gondwana Six: Stratigraphy, Sedimentology and Palaeontology, Geophysical Monograph **41**, 131-138.

Ohmori, H. 1983. Characteristics of the erosion rate in the Japanese mountains from the viewpoint of climatic geomorphology, Zeit. Geomorph. Suppl, **46**, 1-14.

Ollier, C.D. 1985. Morphotectonics of continental margins with great escarpments, Tectonic Geomorphology, Allen and Unwin, Boston, 3-25.

Ollier, C.D. and Marker, M.E. 1985. The great escarpment of southern Africa, Zeit. Geomorph. Suppl, **54**, 37-56.

Parsons, A.J. 1988. Hillslope Form, Routledge, London and New York.

Partridge, T.C. and Maud, R.R. 1987. Geomorphic evolution of southern Africa since the Mesozoic, South African Journal of Geology, **90**, 179-208.

Partridge, T.C. and Maud, R.R. 1988. The geomorphic evolution of southern Africa: a comparative review, Geomorphological Studies in southern Africa, Balkema, Rotterdam.

Peltier, W.R. and Andrews, J.T. 1976. Glacio-isostatic adjustment I: The forward problem, Geophysical Journal of the Royal Astronomical Society, **46**, 605-646.

Pinet, P. and Souriau, M. 1988. Continental erosion and

large scale relief, Tectonics, 7, 563-582.

Pretorius, D.A. 1979. The crustal architecture of southern Africa, Geological Society of South Africa (Annex), 82, 1-60.

Pugh, J.C. 1955. Isostatic readjustment in the theory of pediplanation, Quarterly Journal of the Geological Society, 111, 361-369.

Reading, H.G. and Orton, G.J. 1991. Sediment calibre: A control in facies models with special reference to deep sea depositional systems, In Muller, D.W., McKenzie, J.A. and Weissert, H. (Eds), Controversies in Modern Geology, Academic Press, 85-111.

Rogers,A.W. 1920. Geological Survey and its aims: and a discussion on the origin of the Great Escarpment, Transactions of the Geological Society of South Africa, 23, 19-23.

Rooseboom, A. and von M. Harmse, H.J. 1979. Changes in the sediment load of the Orange River during the period 1929-1969, International Association of Hydrology Scientific Publications, 128, 459-470.

Royden, I. and Keen, C.E. 1980. Rifting process and thermal evolution of the continental margin of eastern Canada determined from subsidence curves, Earth and Planetary Science Letters, 51, 343-361.

Rust, D.J. and Summerfield, M.A. 1990. Isopach and borehole data as indicators of rifted margin evolution in southwestern Africa, Marine and Petroleum Geology, 7, 277-287.

Ryan, P.J. 1967. Stratigraphic and palaeocurrent analysis of the Ecca Series and lowermost Beaufort beds in the Karoo basin of South Africa, Unpublished Ph.D, Witwatersrand, Johannesburg, South Africa.

Schmidt, K. 1989. The significance of scarp retreat for cenozoic landform evolution on the Colorado plateau, U.S.A., Earth Surfaces Processes and Landforms, 14, 93-105.

Schumm, S.A. 1963. The disparity between present rates of denudation and orogeny, United States Geological Survey Professional Paper, 454-H.

Schumm, S.A. 1977. The Fluvial System, Wiley, New York.

Sclater, J.G. and Christie, P.A.F. 1980. Continental Stretching: An explanation of the post-Mid-Cretaceous subsidence of the central North Sea Basin. Journal of Geophysical Research, 85, 3711-3739.

Sclater, J.G., Jaupart, C. and Galson, D. 1980. The heat flow through oceanic and continental crust and the heat loss of the Earth, Reviews in Geophysics and Space Physics, 18, 269-311.

Scrutton, R.A. 1973. The age relationship of igneous activity and continental breakup, Geology Magazine, 110, 227-234.

Scrutton, R.A. 1976. Continental breakup and deep crustal structure at the margins of southern Africa, Annals of the Brazilian Academy of Science, 48 (supplement), 275-286.

Selby, M.J. 1985. Earth's Changing Surface: An Introduction

to Geomorphology, Clarendon Press, Oxford.

Shreve, R.L. 1966. Statistical law of stream numbers, Journal of Geology, **74**, 17-37.

Siedner, G., and Mitchell, J.G. 1976. Episodic Mesozoic volcanism in Namibia and Brazil: a K-Ar isochron study bearing on the opening of the south Atlantic, Earth and Planetary Science Letters, **30**, 292-303.

Siesser, W.G. and Dingle, R.V. 1981. Tertiary sea-level movements around southern Africa, Journal of Geology, **89**, 523-536.

Simpson, E.S.W., Sclater, G.J., Parsons, B., Norton, I. and Meinke, 1. 1979. Mesozoic magnetic lineations in the Mozambique basin, Earth and Planetary Science Letters, **43**, 260-264.

Smith, A.G. 1982. Late Cenozoic uplift of stable continents in a reference frame fixed to South America, Nature, **296**, 400-404.

Speight, J.G. 1987. Minimal post-Permian tectonism and erosion south of the Sydney basin, The Age of Landforms in Eastern Australia: Technical Memo, **87/2**, 61-65, (CSIRO Division of Water and Land Resources, Canberra, 1987).

Steckler, M.S. 1985. Uplift and extension at the Gulf of Suez: indications of induced mantle convection, Nature, 317, 135-139.

Steckler, M.S. 1990. The role of the thermal-mechanical structure of the lithosphere in the formation of sedimentary basins, in Cross, T.A. (Editor),

Quantitative Dynamic Stratigraphy, Prentice-Hall, Englewood Cliffs, 89-112.

Stephenson, R. 1984. Flexural models of continental lithosphere based on the long-term erosional decay of topography, Geophysical Journal of the Royal Astrological Society, 77, 385-413.

Summerfield, M.A. 1981. Macroscale Geomorphology, Area, 13, 3-8.

Summerfield, M.A. 1985. Plate tectonics and landscape development on the African continent, Tectonic Geomorphology, Allen and Unwin, Boston, 27-51.

Summerfield, M.A. 1988. Global tectonics and landform development, Progress in Physical Geography, 12, 389-404.

Summerfield, M.A. 1989. Tectonic geomorphology: convergent plate boundaries, passive margins and super-continent cycles, Progress in Physical Geography, 13, 431-441.

Summerfield, M.A. 1991a. Global Geomorphology, Longman, London and Wiley, New York, 537.

Summerfield, M.A. 1991b. Sub-aerial denudation of passive margins: regional elevation versus local relief models, Earth and Planetary Science Letters, 102, 460-469.

Tankard, A.J. and Hobday, D.K. 1979. Sedimentation patterns in Early Palaeozoic tensional failed arms: The Table Mountain Group of southern Africa, Geological Society of America Congress Abstract.

Tankard, A.J., Jackson, M.P.A., Eriksson, K.A., Hobday,

D.K., Hunter, D.R. and Minter, W.E.L. 1982. Crustal Evolution of Southern Africa, 3.8 Billion Years of Earth History, Springer-Verlag, Berlin.

Theron, J.N. 1962. On the nature of the Cape folding in the district of Willowmore, Cape Province, University of Stellenbosch Annals, A37, 347-424.

Thiessen, R., Burke, K. and Kidd, W.S.F. 1979. African hot spots and their relation to the underlying mantle, Geology, 7, 263-266.

Thomas, D.S.G. and Shaw, P.A. 1987. The deposition and development of the Kalahari group sediments, central southern Africa, unpublished manuscript.

Turcotte, D.L. and Schubert, G. 1982. Geodynamics: Applications of Continuum Physics to Geological Problems, Wiley, New York.

Vail, P.R., Mitchum, R.M. Jr and Thompson, S.III. 1977. Seismic stratigraphy and global changes of sea level, part 4: global cycles of relative changes of sea level. In Payton, C.E. (ed), Seismic Stratigraphy - applications to hydrocarbon exploration, American Association of Petroleum Geologists Memoir, 26, 83-97.

Van Hinte, J.E. 1976a. A Cretaceous timescale, Bulletin of the American Association of Petroleum Geologists, 60, 269-287.

Van Hinte, J.E. 1976b. A Jurassic timescale, Bulletin of the American Association of Petroleum Geologists, 60, 489-497.

Walcott, R.I. 1970a. Isostatic response to crustal loading

in Canada, Canadian Journal of Earth Sciences, 1, 716-727.

Walcott, R.I. 1970b. Flexural rigidity, thickness, and viscosity of the lithosphere, Journal of Geophysical Research, 75, 3941-3954.

Ward, J.D., Seely, M.K. and Lancaster, N. 1983. On the antiquity of the Namib, South African Journal of Science, 79, 175-183.

Watts, A.B., Cochran, J.R. and Selzer, G. 1975. Gravity anomalies and flexure of the lithosphere: A 3-D study of the Great Meteor seamount, N.E. Atlantic, **Journal of Geophysical Research**, **80**, 1391-1398.

Watts, A.B. 1978. An analysis of isostasy in the world's oceans, 1, Hawaiian-Emperor seamount chain, Journal of Geophysical Research, 83, 5989-6004.

Watts, A.B. 1982. Tectonic subsidence, flexure and global changes of sea-level, Nature, 297, 469-474.

Watts, A.B., Karner, G.D. and Steckler, M.S. 1982. Lithospheric flexure and the evolution of sedimentary basins, Philosophical Transactions of the Royal Society of London, A 305, 249-281.

Weissel, J.K. and Karner, G.D. 1989. Flexural uplift of rift flanks due to mechanical unloading of the lithosphere during extension, Journal of Geophysical Research, 94, 13919-13950.

Wellman, P. 1987. Eastern highlands of Australia; their uplift and erosion, Journal of Australian Geology and Geophysics, 10, 277-286.

Wernicke, B. 1981. Insights from Basin and Range surface geology for the process of large-scale divergence of

the continental lithosphere (abstract), Papers presented to the Conference on Processes of Planetary Rifting, Lunar and Planetary Institute, Houston, Texas, Contribution 457, 90-92.

Wernicke, B. 1985. Uniform-sense normal simple shear of the continental lithosphere, Canadian Journal of Earth Sciences, 22, 108-125.

White, N. and McKenzie, D.P. 1988. Formation of the "steers head" geometry of sedimentary basins by differential stretching of the crust and mantle, Geology, 16, 250-253.

White, R.S. and McKenzie, D.P. 1989. Magmatism at rift zones: the generation of volcanic continental margins and flood basalts, Journal of Geophysical Research, 94, 7685-7729.

Whitten, D.G.A. and Brooks, J.R.V. 1972. The Penguin dictionary of geology, Penguin, Harmondsworth, England.

Winter, H. and Venter, J.J. 1970. Lithostratigraphic correlation of recent deep boreholes in the Karoo-Cape sequence, Proceedings of the Second Gondwana Symposium, South Africa, 395-408.

Young, R.W. 1985. Waterfalls: form and process, Zeit. Geomorph. Suppl, 55, 81-95.

Zuber, M.T., Bechtel, T.D. and Forsyth, D.W. 1989. Effective elastic thickness of the lithosphere and mechanisms of isostatic compensation in Australia. Journal of Geophysical Research, 94, 9353-9367.

APPENDIX 1 – ABBREVIATIONS

The following abbreviations are in general use and have been used in the text.

a	annum
AFTA	apatite fission track analysis
BP	before present
Fig.	figure
kbar	kilobar
ka	thousand years
km	kilometre
m	metre
Ma	million years
T_e	effective elastic thickness
≈	is approximately equal to

APPENDIX 2 – PUBLISHED PAPERS

This appendix includes two papers which contain elements of the work embodied in this thesis. The first paper has already been published in Nature and the second is in press in Earth Surface Processes and Landforms.

Reprinted from Nature, Vol. 346, No. 6286, pp. 739–742. 23rd August, 1990

Differential denudation and flexural isostasy in formation of rifted-margin upwarps

A. R. Gilchrist*† & M. A. Summerfield†‡

* Department of Earth Sciences, University of Liverpool, PO Box 147, Liverpool L69 3BX, UK
† Macrogeomorphology Research Group, Department of Geography, University of Edinburgh, Edinburgh EH8 9XP, UK

MARGINAL upwarps are common features of rifted continental margins[1,2], but tectonic models of the evolution of rifted margins have not adequately explained their form, or their persistence along some margins more than 100 Myr after continental rupture. Marginal upwarps not only significantly influence the geomorphological evolution of rifted margins and their adjacent continental interiors, but are also important in determining patterns of offshore sedimentation. Here we show that the contrast in denudation rates between the evolving coastal flanks of rifted margins and their interior hinterlands can promote significant marginal upwarps if the lithosphere responds flexurally to the resulting differential unloading[2,3]. Using data for the western margin of southern Africa, we demonstrate that upwarps of 600 m with respect to the adjacent continental interior can be generated by this process independently of the mechanics of rifting.

Although the morphology of rifted continental margins is highly variable, two main types of mature rifted margin (>60 Myr old) can be identified: (1) low-lying margins, such as southern Australia, which rise gradually from the coast to a low interior plain (low-elevation rifted margins); (2) steeply rising margins in which the coast is commonly separated from an often relatively high continental interior by a single major escarpment which has retreated inland[1] (high-elevation rifted margins). A typical feature of high-elevation rifted margins, such as those of southwestern Africa, eastern Brazil and eastern Australia, is the gradual decline in mean elevation inland of the escarpment, or series of escarpments (Fig. 1*a*). This gives rise to a rim of high terrain, or marginal upwarp, typically 300–900 m high and 50–300 km wide which separates the coast from the adjacent continental interior.

Marginal upwarps are also characteristic of young rifted margins, and in this setting they are usually referred to as rift-flank uplifts. Several models have been proposed to explain their development. Thermal effects[4,5] are time-dependent and decay with a time constant of ~60 Myr (ref. 6) and are therefore not applicable to upwarps associated with mature margins. Other models, including the regional compensation of lithospheric unloading[7,8] and depth-dependent extension[9,10] during rifting can generate some residual rift-flank surface uplift, but in each case its amplitude is reduced by sediment loading within the rift. More generally, marginal upwarps along mature rifted margins cannot be adequately explained by models based on dynamic models of rifting because the axis of maximum surface uplift along most mature rifted margins is now located 100 km or more from the hinge line marking the boundary between rifted and unrifted continental lithosphere. Underplating models[11] alone are also incapable of accounting for marginal upwarps because the domal uplifts generated by underplating create broad topographic swells of significantly greater extent than those characteristic of mature rifted margins[12]. Our proposed mechanism for the creation of marginal upwarps on mature rifted margins focuses on the isostatic response of the lithosphere to the contrasting rates of denudation that prevail on the coastal and inland flanks of the marked topographic discontinuity present along high-elevation rifted margins. The fact that such a discontinuity is found on both young rifted margins (such as those bordering the Red Sea[13]) and mature rifted margins indicates that it is a persistent feature of margin evolution.

Before rifting, the topography of supercontinents is probably one of predominantly low local relief owing to prolonged denudation, although regional elevation may be relatively high in areas remote from pre-rifting coastlines where local channel gradients, and hence rates of denudation, are low. In addition, underplating associated with rifting may generate a regionally extensive increase in elevation along some rifted margins soon after rifting begins[12]. Continental rupture will create significantly lower base levels along newly formed high-elevation rifted margins, and consequently two distinct denudational systems will be established, separated by a retreating major escarpment. This is illustrated by the western margin of southern Africa where the high local relief along the coast associated with high slope and channel gradients promotes relatively high denudation rates, whereas the very low local relief inland of the Great Escarpment gives rise to low denudation rates, although the regional elevation is relatively high (generally >1,000 m) (Fig. 1*b*). Along this margin the prominence of the escarpment is locally emphasized by the strong lithological control exerted by certain units in the Karoo sequence.

This denudational model is supported by several kinds of evidence. The overall depth of post-rifting denudation averaged over all Atlantic-draining catchments in southern Africa has been estimated to be ~1,800 m on the basis of offshore sediment volume data[14]. Apatite fission-track data indicate upwards of 2.5 km of post-rifting denudation along the margin[15] and therefore denudation rates in the interior must have been significantly lower. Fission-track analyses from other rifted margins also indicate significant post-rifting denudation oceanward of their escarpments[13,16]. Furthermore, given the former greater westward extent of the Karoo Basin[17], the exposure of older Karoo strata and basement rocks along the western margin of southern Africa also indicates significant depths of erosion, whereas the preservation of younger Karoo sediments and Cenozoic weathering profiles indicates generally low rates of post-rifting denudation in the interior.

We have modelled the denudation of two terrain types characterized by high and low local relief and separated by a moving boundary. The present mean local relief, based on 10-min areas (~18 × 18 km), of the coastal catchments south of the mouth of the Orange River is 456 m, whereas that of the interior Orange catchment is 191 m. Given the linear relationship between mean local relief and denudation rate[18], this indicates that the present mean denudation rate of the coastal catchments is ~2.4 times that of the interior. Given the morphological constraints provided by the present topography and the significantly greater depths of post-rifting denudation along the coast we have assumed that this differential has been maintained since rifting of the Cape Basin (~150 Myr ago)[19]. We have modelled the Great Escarpment as retreating from the hinge line to its present location at a constant rate of 667 m Myr^{-1} (equivalent to a denudation rate of 900 m Myr^{-1}). The size of the coastal catchments has been assumed to have increased linearly from zero at the time of rifting to a present area of 686×10^3 km^3 as the Great Escarpment retreated, whereas the total Atlantic-draining area has been assumed to have remained constant at 1.6×10^6 km^2. Although there is some evidence that the drainage of the interior of southern Africa was not integrated with Atlantic drainage until some time after rifting[2,14], we have adopted the simplest interpretation in view of the uncertainty of the detailed drainage history. In any case the presence of internal drainage in the initial post-rifting phase whould have enhanced the differential denudation that we are modelling. Estimating the mean depth of denudation to be 1,800 m for all Atlantic-draining catchments, the mean denudation rates for the coastal and interior Orange catchments are estimated to be 16.5 m Myr^{-1} and 6.9 m Myr^{-1}, respectively. At the coastal boundary the topography is graded to sea level as the escarpment retreats.

‡ To whom correspondence should be addressed.

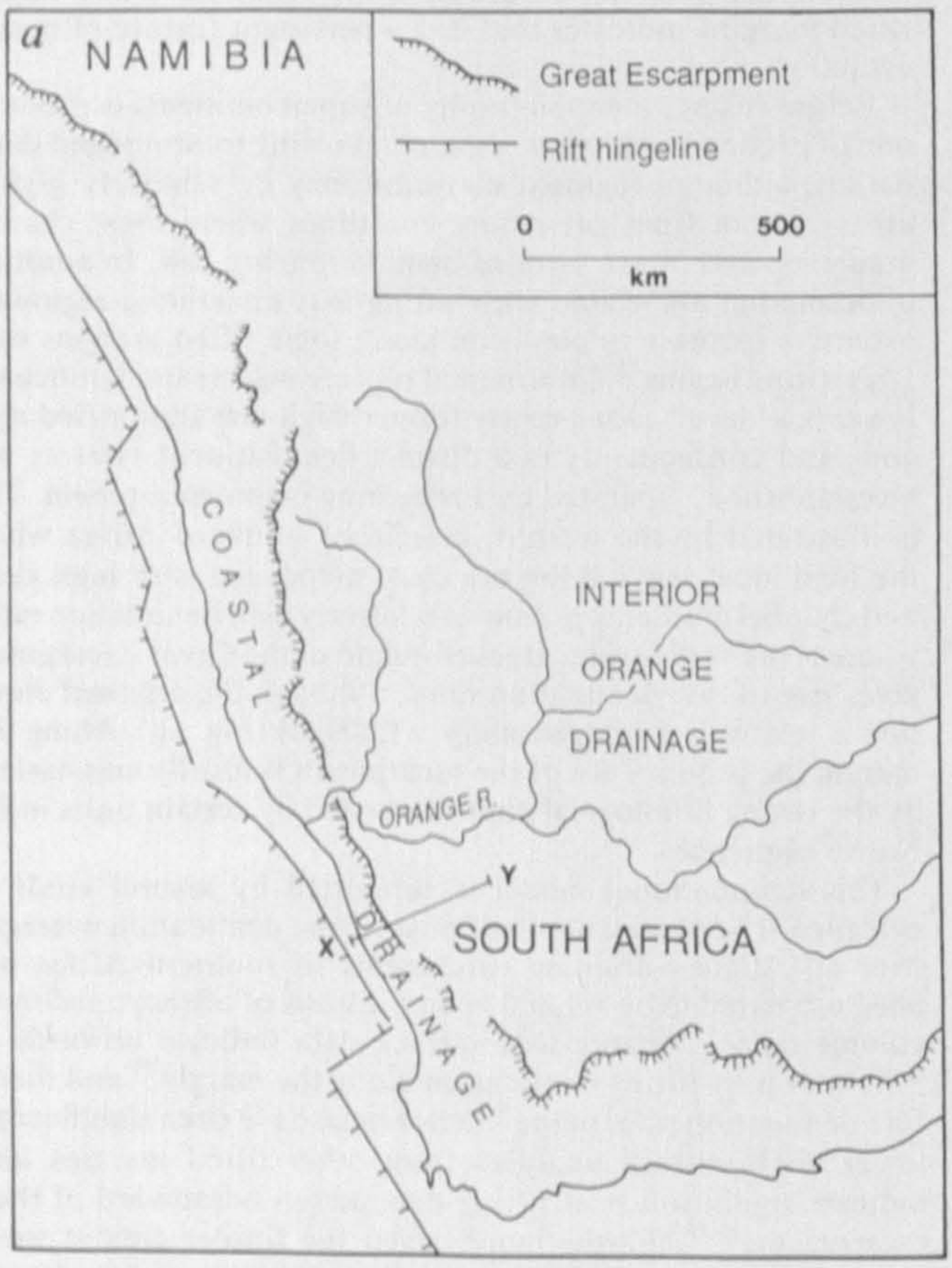

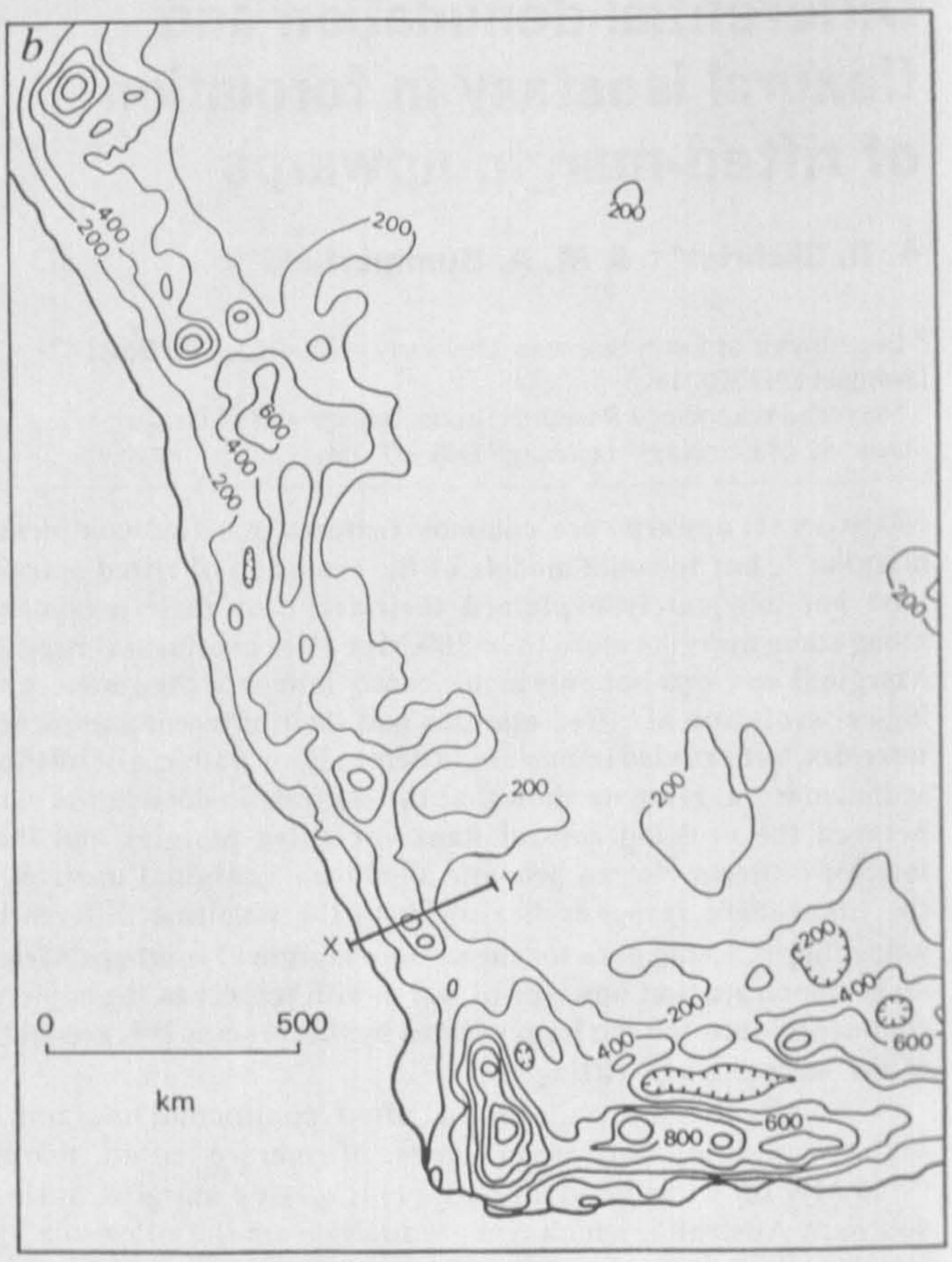

FIG. 1 Major morphological features (*a*) and variations in local relief (*b*) along the western margin of southern Africa. Local relief (maximum − minimum elevation) contours (m) have been generalized from local relief values derived from the 10-min digital topographic data set from the National Geophysical Data Center, Boulder, Colorado. The modelled topographic profile illustrated in Fig. 2 is shown by X–Y line on both maps.

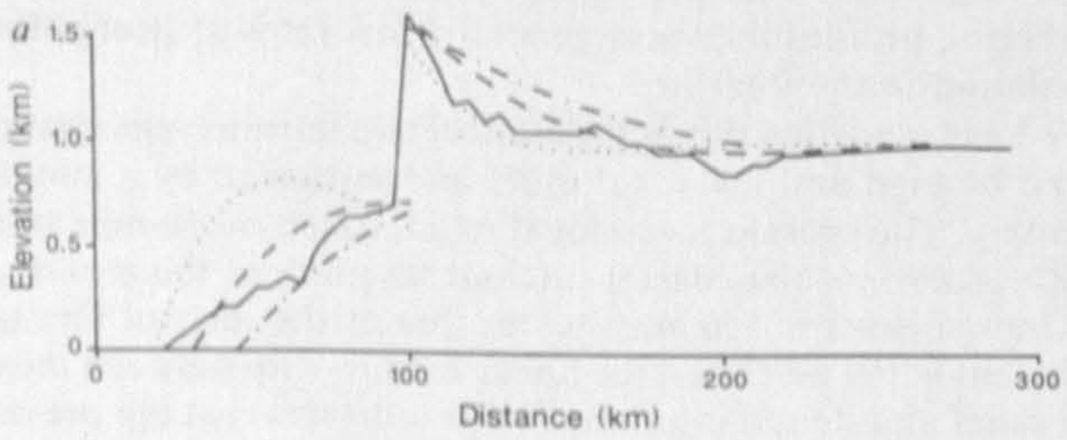

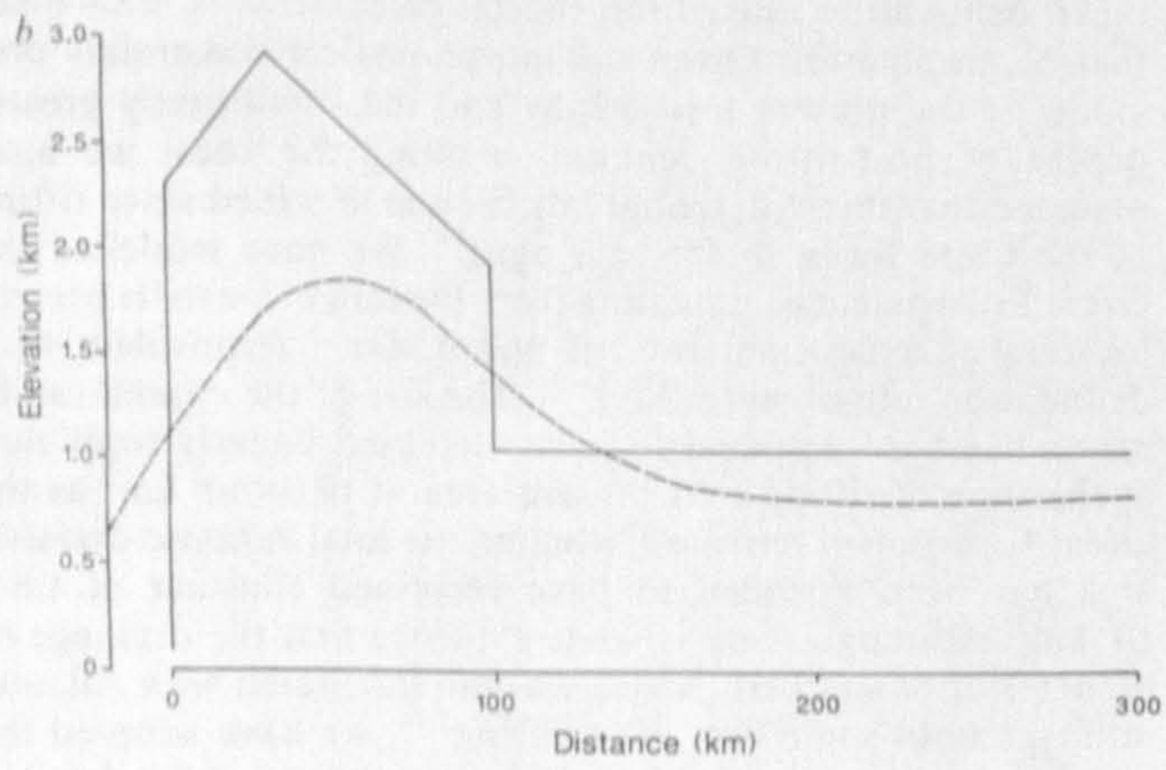

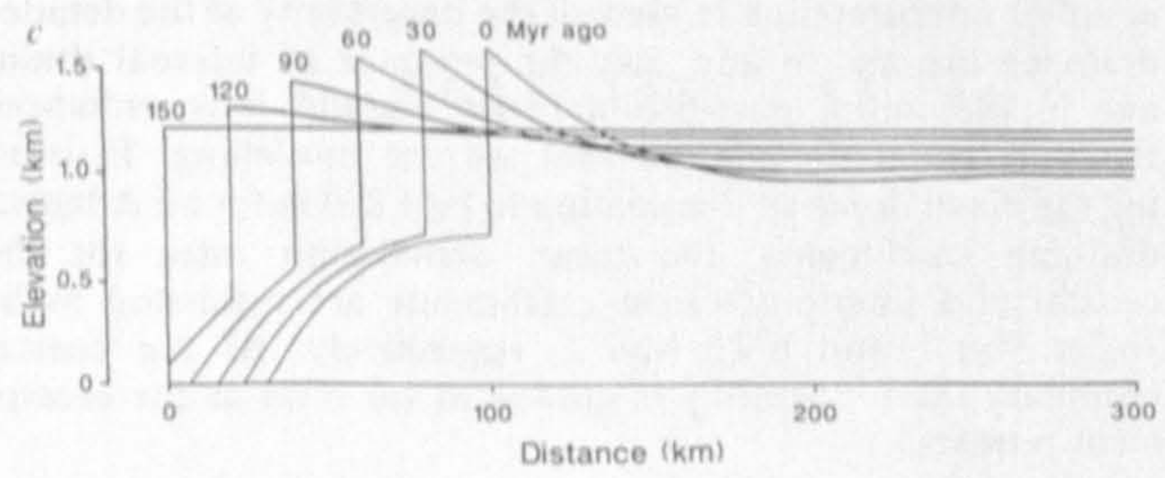

◀ FIG. 2 *a*, Calculated topographic profiles for various T_e values (dotted line, $T_e = 7.5$ km; dashed line, $T_e = 15.0$ km; dashed–dotted line, $T_e = 22.5$ km) compared with a typical topographic profile (solid line) across the western margin of southern Africa. *b*, Total denudation (solid line) and total flexural uplift (dashed line) of the margin. *c*, Evolution of the calculated profiles for $T_e = 15$ km. Profile location (X–Y) is indicated on Fig. 1. Zero on horizontal axes indicates location of hinge line. Flexural model parameters were $E = 1 \times 10^{11}$ N m^{-2}, $\nu = 0.25$, $g = 9.81$ m s^{-2}, $\rho_m = 3{,}300$ kg m^{-3}.

In previous attempts to assess the isostatic response to denudational unloading it has either been assumed that denudation rates are linearly proportional to mean regional elevation[20,21], or that denudation follows a simple diffusion equation in which it is assumed that flux of regolith is proportional to the slope gradient[22]. Neither approach provides a valid basis for modelling denudation rates on high-elevation rifted margins. The relationship between regional elevation and denudation rate does not apply because on high-elevation rifted margins low local relief (low slope and channel gradients) prevails on the high interior inland of the escarpment, whereas high local relief typifies the lower elevation terrain on its oceanward flank. Although the diffusion equation may be applicable to homogeneous, regolith-mantled hillslopes[23] it is not capable of modelling regional-scale topography characterized by marked lithological control.

The precise pre-rifting elevation of southern Africa is unknown; nevertheless, taking the mean elevation of present-day Atlantic-draining catchments of ~930 m and the depth of post-rifting denudation of 1,800 m, the mean pre-rifting elevation of the region of Atlantic-draining catchments can be estimated by reloading the material represented by offshore sediment thickness (d) and allowing for adjustment by Airy isostasy. The pre-rifting elevation will have been higher than present elevation by h, where $h = d(\rho_m - \rho_c)/\rho_m$. For a crustal density ρ_c of 2,800 kg m^{-3} and mantle density ρ_m of 3,300 kg m^{-3} the mean pre-rifting elevation of the Atlantic-draining catchment area is

estimated to have been ~1,200 m. In this simple model we have ignored surface uplift associated with the thermo-mechanical evolution of the margin because it would be substantially compensated by sediment loading offshore. To assess specifically the development of the marginal upwarp, the initial topography is assumed to be a block terminating at the rift hinge line.

The isostatic response to denudational unloading has been modelled assuming a thin elastic plate of constant thickness overlying an inviscid fluid according to

$$\frac{\partial^2}{\partial x^2}\left(D\frac{\partial^2 w}{\partial x^2}\right)+(\rho_m-\rho_i)gw=l(x)$$

where w is the vertical flexure, D is the flexural rigidity, ρ_m is the mantle density, ρ_i is the flexure infill density (in this case air), g is the acceleration due to gravity, and $l(x)$ is the denudational load as a function of x (ref. 24). Flexural rigidity is given by

$$D=\frac{ET_e^3}{12(1-\nu^2)}$$

where E is Young's modulus, T_e is the effective elastic thickness of the lithosphere and ν is Poisson's ratio. Vertical flexure was calculated in the wavenumber domain from

$$W(k)=R(k)\cdot L(k)$$

where $R(k)$ is the isostatic response function so that

$$R(k)=\frac{1}{(\rho_m-\rho_i)g+Dk^4}$$

$W(k)$ and $L(k)$ are the Fourier transforms of $w(x)$ and $l(x)$ and k is wavenumber given by $k=2\pi/\lambda$ where λ is the wavelength.

Figure 2*a* shows topographic profiles calculated using different T_e values compared with a typical profile across the western margin of southern Africa (Fig. 1). The elastic thickness of the highly faulted lithosphere below the Cape Basin has been estimated at 5–10 km (ref. 25) whereas that of the cratonic interior is thought to be 64–90 km (ref. 26). Our best fit of 15 km is therefore consistent with this range of values given the intermediate location of the topographic profile between these two types of flexural terrane. In the region of the escarpment our model generates a maximum of ~600 m of surface uplift with respect to the slowly eroding continental interior and closely replicates the characteristic curved profile of the marginal upwarp. Given the spatial variation in total denudation (Fig. 2*b*) (which has also been recorded on other rifted margins[27]), and assuming that compensation to unloading occurs flexurally, the creation of a marginal upwarp is inevitable. Varying the T_e changes the distribution of the upwarped region but the zone of maximum surface uplift remains in approximately the same position. The mismatch between modelled ($T_e=15$) and actual profile on the inland flank of the upwarp is probably attributable to enhanced rates of denudation in this zone associated with back-cutting tributary drainage systems, which have not been incorporated into the model. The evolution of the marginal upwarp as the escarpment retreats is shown in Fig. 2*c*.

The generation of marginal upwarps as a result of differential denudational unloading not only explains their presence along mature rifted margins but also has important geomorphological and sedimentological implications. The presence of marginal upwarps up to 100 Myr or more after rifting may account for the deflection of drainage systems away from many mature rifted margins[2,12,28]. The persistence of such a barrier to sediment transport across high-elevation rifted margins suggests that patterns of offshore deposition are likely to be controlled by a dual drainage system comprising numerous small aggressively eroding coastal catchments and widely spaced outlets of large basins draining continental interiors well into the mature rifted margin stage. Where drainage systems breach a marginal upwarp, the isostatically generated uplift will maintain a significant change in channel gradient (such as the Augrabies Falls on the Orange River). Moreover, the predicted inland migration of the axes of marginal upwarps in response to escarpment retreat has implications for existing denudation and surface uplift chronologies for the Gondwana continents[29]. Further development of our model requires an assessment of the role of denudational unloading along other rifted margins and the more detailed incorporation of apatite fission-track data which, in southwestern Africa at least, indicate significant denudation inland of the present escarpment shortly after rifting during the Early Cretaceous[15]. □

Received 13 February; accepted 29 June 1990.

1. Ollier, C. D. (ed.) *Z. Geomorph. Suppl.* **54** (1985).
2. Summerfield, M. A. in *Tectonic Geomorphology* (eds Morisawa, M. & Hack, J. T.) 27–51 (Allen & Unwin, Boston, 1985).
3. Thomas, M. F. & Summerfield, M. A. in *Int. Geomorph. 1985, Proc. 1st Int. Conf. on Geomorphology* (eds Gardiner, V. *et al.*) 935–956 (Wiley, Chichester, 1987).
4. Buck, W. R. *Earth planet. Sci. Lett.* **77,** 362–372 (1986).
5. Buck, W. R., Martinez, F., Steckler, M. S. & Cochran, J. R. *Tectonics* **7,** 213–234 (1988).
6. McKenzie, D. P. *Nature* **307,** 616–618 (1984).
7. Braun, J. & Beaumont, C. *Geology* **17,** 760–764 (1989).
8. Weissel, J. K. & Karner, G. D. *J. geophys. Res.* **94,** 13919–13950 (1989).
9. Royden, L. & Keen, C. E. *Earth planet. Sci. Lett.* **51,** 343–361 (1980).
10. White, N. & McKenzie, D. P. *Geology* **16,** 250–253 (1988).
11. White, R. S. & McKenzie, D. P. *J. geophys. Res.* **94,** 7685–7729 (1989).
12. Cox, K. G. *Nature* **342,** 873–877 (1989).
13. Bohannon, R. G., Naeser, C. W., Schmidt, D. L. & Zimmermann, R. A. *J. geophys. Res.* **94,** 1683–1701 (1989).
14. Rust, D. J. & Summerfield, M. A. *Mar. Petrol Geol.* (in the press).
15. Brown, R. W., Rust, D. J., Summerfield, M. A., Gleadow, A. J. W. & De Wit, M. C. J. *Nucl. Tracks* (in the press).
16. Moore, M. E., Gleadow, A. J. W. & Lovering, J. F. *Earth planet. Sci. Lett.* **78,** 255–270 (1986).
17. Oelofsen, B. W. *Geophys. Monogr.* **41,** 131–138 (1987).
18. Ahnert, F. *Am. J. Sci.* **268,** 243–263 (1970).
19. Gerrard, I. & Smith, G. C. *Am. Ass. Petrol. Geol. Mem.* **34,** 49–74 (1980).
20. Stephenson, R. *Geophys. J. R. astr. Soc.* **77,** 385–413 (1984).
21. Lambeck, K. & Stephenson, R. *Aust. J. Earth Sci.* **33,** 253–270 (1986).
22. Moretti, I. & Turcotte, D. L. *J. Geodyn.* **3,** 155–168 (1985).
23. Culling, W. E. H. *J. Geol.* **73,** 230–254 (1965).
24. Nadai, A. *Theory of Flow and Fracture of Solids* (McGraw-Hill, New York, 1963).
25. Karner, G. D. & Watts, A. B. *J. geophys. Res.* **87,** 2923–2948 (1982).
26. Ebinger, C. J., Bechtel, T. D., Forsyth, D. W. & Bowin, C. O. *J. geophys. Res.* **94,** 2883–2901 (1989).
27. Speight, J. G. in *The Age of Landforms in Eastern Australia: Tech. Memo. 87/2* **61**–65 (CSIRO Div. Water and Land Resources, Canberra, 1987).
28. Summerfield, M. A. *Area* **13,** 3–8 (1981).
29. Partidge, T. C. & Maud, R. R. *S. Afr. J. Geol.* **90,** 179–208 (1987).

ACKNOWLEDGEMENTS. We thank N. J. Kusznir and D. J. Rust for discussions. This work was supported by NERC. M.A.S. thanks the Royal Society of Edinburgh for a Support Research Fellowship.

DENUDATION, ISOSTASY AND LANDSCAPE EVOLUTION

A.R. Gilchrist[1,2] and M.A. Summerfield[1*]

1 Macrogeomorphology Research Group, Department of Geography, University of Edinburgh, Edinburgh EH8 9XP

2 Department of Earth Sciences, University of Liverpool, Liverpool L69 3BX

* To whom correspondence should be addressed

ABSTRACT

The idea that the isostatic response to progressive denudational unloading can be episodic over cyclic time scales is widely cited in the geomorphological literature. We demonstrate, however, that this notion, which has been regarded as a possible mechanism of widespread landscape rejuvenation, is based on a fundamental misunderstanding of the principles of flexural isostasy. Rather than a discontinuous response, in cases where the half-width of the applied load is greater than a few tens of kilometres the lithosphere experiences a continuous compensation which is dependent upon the wavelength of the applied load rather than upon a lateral, or vertical, threshold of unloading which has to be exceeded before isostatic recovery is initiated. Although a flexural isostatic response cannot account for episodic uplift during a denudational cycle, it can explain the growth and persistence of significant marginal upwarps along passive margins across which there is a marked contrast in denudation rates. Such marginal upwarps, in turn, probably play a critical role in the long-term evolution of drainage systems and landscapes in adjacent continental hinterlands.

KEY WORDS Denudation Isostasy Flexural isostasy Landscape evolution Passive margins

INTRODUCTION

Isostasy is the mechanism through which the lithosphere responds to applied loads in order to attain hydrostatic equilibrium. Although its effects can be ignored in mass transfer calculations at the scale of small catchment studies, at the macroscale of regional denudation isostatic restoring forces are an integral part of the mass transfer system. It has, for instance, long been acknowledged that the isostatic response to denudational unloading significantly increases the time required to reduce the mean elevation of a landscape by a specific amount (Gilluly, 1955; Schumm, 1963, 1977; Holmes, 1965; Ahnert, 1970). Moreover, the temporal and spatial characteristics of isostatically induced landsurface deformation in response to ice sheet unloading and lake desiccation have themselves provided important data for the estimation of sub-lithospheric mantle properties (Peltier and Andrews, 1976; Mörner, 1980; Bills and May, 1987).

Although geomorphologists have been aware of the potential significance of isostasy in studies of long-term landform development, the geomorphological literature reveals a fundamental misunderstanding of the way in which the lithosphere responds to applied loads at the temporal and spatial scales relevant to landscape evolution. In particular, the notion that isostatic uplift in response to continuous denudation over cyclic time scales (10^7 a) is episodic in nature has become firmly established in the literature. The aims of this paper are to demonstrate how the concept of isostasy has been misunderstood in relation to landscape evolution, to outline a model of isostasy that is applicable to large-scale, long-term denudational

unloading, and briefly to assess some of the implications of this model for landscape evolution.

CONVENTIONAL APPLICATIONS OF CONCEPTS OF ISOSTASY TO LANDSCAPE EVOLUTION

The significance for models of landscape evolution of supposedly discontinuous isostatic adjustment to denudational unloading was first systematically considered in the co-published papers by King (1955) and Pugh (1955) in the context of escarpment retreat from passive margins. King (1955) argued that the retreat of escarpments from the coastlines of Africa initiated by the break-up of Gondwana would have resulted in unloading of the crust along the coastal hinterlands coupled with crustal loading by sediment offshore. The isostatic response should thus hinge about this coastal zone with uplift inland and subsidence offshore. Noting that the marginal upwarp which characterizes much of the coastal hinterland of Africa is around 400 km wide, and that the fringing continental shelf is about 80 km in width, King (1955) pointed out that the total span of the zone affected by isostatic adjustment is approximately the same as the estimate of 480 km by Gunn (1949) "for the length of the circumferential arc that cannot be rigidly supported by the earth's crust for more than a limited period". On the basis of this understanding of Gunn's discussion of the principles of isostasy King concluded that isostatic recovery only commences once a threshold distance of escarpment retreat of some hundreds of kilometres has occurred, and that, consequently, a sequence of erosion cycles could be generated by this episodic isostatic response. Pugh

(1955) similarly interpreted Gunn's summary of isostasy to mean that isostatic recovery was delayed until a significant critical width of denudation had occurred, and both authors correlated the hypothetical elevations of erosion surfaces subject to episodic isostatic uplift with the actual altitude of erosion surfaces in Africa assumed to be associated with distinct denudational cycles.

Subsequently, Carson and Kirkby (1972) reiterated this interpretation of isostatic adjustment to escarpment retreat and, following Pugh (1955), asserted that whereas the isostatic response to vertical lowering of a landscape (as in Davisian peneplanation) will be almost immediate, there is a threshold of several hundred kilometres of lateral denudation (associated with escarpment retreat) before isostatic adjustment occurs. Recently, in a detailed assessment of landscape development in southern Africa supporting episodic post-Gondwana surface uplift parallel to the continental margin, Partridge and Maud (1987) have concluded that "any workable model [of surface uplift] must involve an episodic, isostatic response both to the recession of the Great Escarpment on the one hand and to concomitant sedimentation of the continental shelf on the other" Futhermore, they suggest that their hypothesized Late Pliocene surface uplift of up to 900 m may be attributable in part to a delayed isostatic response to the load imbalance between onshore denudation and offshore deposition created during the 'African' cycle of erosion which was terminated at the end of the Early Miocene.

Although different in some respects to the interpretations of King (1955) and Pugh (1955), the idea of episodic isostatic

uplift is also pervasive in the influential contributions by S.A. Schumm to the problem of long-term landscape development (Schumm, 1963, 1975, 1979). Again referring to Gunn's summary of the principle's of isostasy, Schumm (1963) has concluded that the strength of the crust must be exceeded by a certain depth of denudation "before isostatic adjustment can occur". Noting that there is a lag between pulses of rapid ice sheet melting and the associated isostatic uplift, he has suggested that isostatic adjustment to denudation in orogenic belts will also be episodic although the time scales are in fact vastly different in the two cases. Schumm (1963) cites a figure of 2000 a for glacio-isostasy but his diagrammatic representation of the isostatic response to denudation (Fig. 3, p. H11) indicates a lag in isostatic uplift of 1.5 to 2 Ma during which time a depth of around 900 m of rock is eroded. Schumm (1963) makes it clear that he sees the strength of the crust as being positively related to the length of time before isostatic adjustment to denudation occurs.

The notion of episodic isostatic uplift in response to long-term denudational unloading has now become widely accepted by the geomorphological community, as is illustrated by its inclusion in widely used text books (Chorley et al., 1984; Selby, 1985). The idea, however, is based on a fundamental misunderstanding of the principles of isostasy as outlined by Gunn (1949) and elaborated by later workers.

MODELS OF ISOSTASY APPLICABLE TO LANDSCAPE EVOLUTION

The seminal review by Gunn (1949) was focussed specifically on a model of isostasy involving a strong elastic lithosphere supported by weak underlying mantle. Referred to as the theory of 'isobaric equilibrium' by Gunn, this model, which has subsequently become known as flexural isostasy, treats local 'Airy' isostasy as a special case where the lithosphere has no rigidity when subject to a vertical load.

More recent work has, in fact, led to the development of two distinct flexural models describing deformation of the lithosphere during loading (denudation representing a negative load). The elastic model, as outlined by Gunn (1949), assumes that the lithosphere can be represented by an elastic lithospheric plate overlying an inviscid asthenosphere where the response to a single loading event is instantaneous and therefore does not exhibit time-dependent behaviour. By contrast, in the Maxwell viscoelastic model the lithosphere behaves elastically at short time scales but deforms as a viscous fluid over long periods of time (Walcott, 1970). As demonstrated by the response of the lithosphere to the unloading of ice sheets and evaporation of lakes, time-dependent behaviour is only relevant at time scales of the order of 10^4 -10^5 a. Consequently, for changes in load, such as that associated with long-term denudation, which occur over much longer time spans in excess of 10^5 a, the elastic model of flexural isostasy is adequate for predicting the response of the lithosphere to loading events (Karner et al., 1983).

The elastic model represents the response to an applied load in terms of the elastic bending resistance of the lithosphere and the buoyancy forces acting upon it, and can be expressed by the equation:

∂ = partial derivative
ω = omega
ρ = rho

$$\frac{\partial^2}{\partial x^2}\left(\frac{D\,\partial^2 \omega}{\partial x^2}\right) + (\rho_m - \rho_i)\, g\, \omega = l(x)$$

where ω is vertical flexure, D is flexural rigidity, ρ_m is mantle density, ρ_i is flexure infill density, g is acceleration due to gravity and $l(x)$ is the load as a function of x (Nadai, 1963). Thus, on application of a load, flexural deformation extends beyond the load boundaries due to the elastic bending resistance of the lithosphere and the load is said to be regionally compensated (Fig. 1A). The spatial distribution of the flexural response is dependent on the flexural rigidity (D) of the elastic plate where

ν = nu

$$D = \frac{E\,T_e^{\,3}}{12(1-\nu^2)}$$

and E is Young's modulus, T_e is the effective elastic thickness of the lithosphere and ν is Poisson's ratio. For progressively higher flexural rigidities an applied load is compensated over a greater area. The Airy model is thus simply a special case of the elastic model where the flexural rigidity of the lithosphere is assumed to be zero and the applied load is therefore totally compensated locally due to the displacement of the immediately underlying asthenosphere (Fig. 1B).

The degree of load compensation (C) is defined as the ratio of the deflection of the lithosphere to its maximum, or hydrostatic, deflection (Turcotte and Schubert, 1982). It relates the flexural deformation of the lithosphere to the applied periodic

λ - lambda

load of wavelength λ , and is given by

ρ = rho
π = pi
λ = lambda

$$C = \frac{\rho_m - \rho_i}{\rho_m - \rho_i + \frac{D}{g}\left(\frac{2\pi}{\lambda}\right)^4}$$

When C = 1.0 the load is compensated locally according to the Airy isostatic model (Fig. 1B) and when C = 0 the isostatic system behaves rigidly and the load is supported by the lateral strength of the lithosphere (Fig. 1C). Between these two extremes loads are compensated both by elastic bending resistances and by buoyancy forces.

ν = nu

The elastic plate model parameters of Gunn (1949) ($E = 1.2 \times 10^{11}$ N m^{-2}, T_e = 50 km, $\nu = 0.25$, $\rho_m = 3100$ kg m^{-3}, $\rho_i = 0$ kg m^{-3} and g = 9.8 m s^{-2}) yield the compensation function shown in Figure 2.

λ = lambda

This illustrates that for a T_e value of 50 km an applied periodic load is 50% compensated (C = 0.5) when $\lambda \sim 500$ km. Periodic loads of greater wavelength are only partially supported by the rigidity of the lithosphere whereas shorter wavelength loads are substantially supported. Beyond loads with half-widths of a few tens of kilometres there is consequently a continuous spatial variation in the degree of load compensation dependent on the wavelength of the applied load and not, as suggested by King (1955) and Pugh (1955), a significant lateral threshold, or, as proposed by Schumm (1963), a vertical threshold, of unloading before isostatic readjustment is initiated.

Varying the elastic thickness of the lithosphere changes the form of the compensation function, and thus the isostatic response to

a loading event (Figure 2). For a T_e of 20 km an applied periodic load is 50 per cent compensated (C = 0.5) when $\lambda \sim 250$ km, whereas $\lambda \sim 575$ km for a similarly compensated load with a T_e of 60 km. Recently, the wide variation in the effective elastic thickness of continental lithosphere has become appreciated; T_e values in Africa, for instance, range from an estimated 5-10 km for the rifted lithosphere below the Cape Basin in south-western Africa (Karner and Watts, 1982) to 64-90 km in the cratonic interior (Ebinger et al., 1989). Similarly, in North America the effective elastic thickness of the lithosphere varies from a minimum of ~4 km in the Basin and Range Province to ~128 km in the cratonic core of the continent (Bechtel et al., 1990).

Isostatic compensation is only episodic on the time scale of small, individual crustal displacements along faults in response to progressive loading, and exhibits lags in response to applied loads only on the time scale of sub-lithosperic mantle flow, that is over periods of the order of 10^4-10^5 a. Over the time scale of landscape evolution isostatic compensation occurs continuously, but in a manner dependent on the relationship between flexural rigidity (characterized by effective elastic thickness) and the wavelength of applied loads.

IMPLICATIONS FOR MODELS OF LANDSCAPE DEVELOPMENT

Rejection of the idea of temporally discontinuous isostatic compensation in lagged response to either progressive vertical or lateral denudation has important implications for models of long-term landscape evolution. The most obvious relate to attempts to explain cases of apparent episodic surface uplift of landsurfaces

in terms of a discontinuous isostatic response to progressive denudational unloading (King, 1955; Partridge and Maud, 1987; Pugh, 1955; Schumm, 1963, 1977, 1979). Although the rejection of long-term, discontinuous isostatic uplift does not, of course, rule out active tectonic mechanisms as an explanation of the pulsed uplift of landsurfaces, current tectonic models for both inter-plate and intra-plate settings cannot readily account for the kind of long-term episodic uplift envisaged by some workers. Present understanding of active tectonic processes is not such as to exclude totally the possibility of punctuated uplift, but, for passive margins at least, recent models suggest that maximum active tectonic uplift generated by magmatic underplating, thermal perturbations, or mechanical unloading linked to extension (Summerfield, 1988, 1989; Weissel and Karner, 1989; White and McKenzie, 1989; Steckler, 1990) involves a single major event associated with continental rupture.

The lack of any obvious episodic mechanism of active tectonic uplift that could be applicable to both interplate and intraplate environments suggests that the geomorphic and sedimentological evidence on which the identification of episodic surface uplift has been based perhaps deserves more rigorous appraisal. Although erosion surface sequences are ubiquitous on the Gondwana continents many, if not all, appear to be subject to direct structural control, or to indirect control through the creation of local base levels. Consequently, the vertical separation of such erosion surfaces cannot be taken as unambiguous evidence of discrete episodes of surface uplift initiating relative falls in base level. Furthermore, in the contrasting tectonic setting of

the central Southern Alps, New Zealand, where there is apparently a steady-state topography, crustal uplift (Summerfield, 1991, p. 371) seems to have been relatively constant over the past 2 Ma years at least, with rates for the Late Quaternary (Bull and Cooper, 1986) determined from the altitude of elevated uneroded marine terraces being similar to those over the longer term estimated from apparent K-Ar ages of outcrop samples (Adams, 1981). It is also relevant to note that the recent recognition that denudation rates are in approximate equilibrium with crustal uplift rates in the central Southern Alps (Adams, 1985; Whitehouse, 1988), and in at least some other active orogenic belts (Summerfield, 1991), challenges Schumm's assertion that rates of uplift in such tectonic settings are several times maximum rates of denudation (Schumm, 1963). This observation is important because the supposed discrepancy between rates of crustal uplift and denudation in orogenic belts has been seen as necessitating rapid, episodic uplift in order for this difference in rates to be reconciled over the long term with observed topography.

Although it is necessary to reject the episodic model of isostatic compensation, the continuous flexure of passive margins in response to progressive denudational unloading during their post-rifting evolution has important implications for long-term landscape development. For instance, it has recently been demonstrated that retreat of the Great Escarpment on the high-elevation passive margin of south-western Africa has produced a short-wavelength denudational load sufficient to generate a significant marginal upwarp with an amplitude of several hundred metres (Gilchrist and Summerfield, 1990). Such

upwarps are characteristic features of both juvenile and mature (>60 Ma) high-elevation passive margins (Ollier, 1985; Summerfield, 1985) and various models have been proposed to explain their development (Steckler, 1990; Summerfield, 1988). Thermal effects (Buck, 1986; Buck et al., 1988), which, it has been proposed, can account for the rift-flank uplifts of young margins, are time-dependent and decay with a time constant of ~60 Ma (McKenzie, 1984). Depth-dependent extension (Royden and Keen, 1980; White and McKenzie, 1989) and the regional compensation of lithospheric unloading (Braun and Beaumont, 1989; Weissel and Karner, 1989) during rifting are capable of generating some residual surface uplift along rift flanks but its amplitude is significantly reduced by within-rift sediment loading. More generally, models based on the dynamics of rifting cannot provide an adequate explanation of marginal upwarps along mature, as opposed to young, rifted margins because in most cases the axis of maximum uplift in the former is now located at least 100 km from the hinge line representing the boundary between rifted and unrifted lithosphere. Although underplating models (White and Mckenzie, 1989) provide an attractive explanation for the long wavelength domal form and high mean elevation of some mature rifted margins and their hinterlands, they do not account for the short wavelength marginal upwarps which also characterize these margins. Since thermal and rift-related mechanical effects cannot explain marginal upwarps on mature margins now located well inland of the rift hinge line, flexural isostasy appears to be the only mechanism capable of generating and sustaining these features. Rather than promoting episodic uplift, modelling of the development of marginal upwarps indicates that they develop

progressively from the time of continental margin formation and, for the western margin of southern Africa at least, do not attain their maximum amplitude until around 100 Ma after rifting.

The persistence of marginal upwarps along elevated passive margins has important implications for the way drainage systems evolve in the hinterlands of such margins (Summerfield, 1985, 1991). If rates of crustal uplift along the axes of marginal upwarps are sufficiently high then the establishment of fully integrated external drainage networks may well not occur until a significant time after continental rifting and margin formation. Indeed there is evidence from the offshore sedimentary record for south-western Africa for a lag of more than 50 Ma between rifting and the establishment of a major focussed sediment input into the margin (Rust and Summerfield, 1990). The implications for drainage evolution of non-episodic flexural isostasy along high-elevation passive margins in turn requires a thorough re-evaluation of the application of cyclic concepts to landscape evolution in the hinterlands of such margins.

CONCLUSIONS

We have shown that models of long-term landscape development incorporating episodic isostatic uplift in response to progressive denudational unloading rest on an erroneous interpretation of the way in which the lithosphere responds over geological time to an applied load. Rather than pulsed isostatic uplift resulting from the discontinuous adjustment of the lithosphere to a continuous applied load, there is a continuous spatial variation in the degree of load compensation depending on

the applied load wavelength. Consequently, distinct denudational cycles arising from episodic uplift cannot be attributed to the discontinuous response of the lithosphere to progressive denudational unloading. The flexural response of the lithosphere, however, does play a critical role in long-term landscape evolution since, for example, the differential denudation experienced across great escarpments along passive margins can generate a persistant marginal upwarp which may significantly influence drainage development for 100 Ma or more after continental rupture.

ACKNOWLEDGEMENTS

This work was supported by the Natural Environment Research Council through grant number GR3/6693 to M.A.S. and a research studentship jointly supervised by M.A.S. and Professor N.J. Kusznir and to A.R.G. M.A.S. is also grateful to the Royal Society of Edinburgh for a Support Research Fellowship.

REFERENCES

Adams, C.J. 1981. 'Uplift rates and thermal structure in the Alpine Fault Zone and Alpine Schists, Southern Alps, New Zealand', Geological Society Special Publication, 9, 211-222.

Adams, J. 1985. 'Large-scale tectonic geomorphology of the Southern Alps, New Zealand', in Morisawa, M. and Hack, J.T. (Eds), Tectonic Geomorphology, Allen and Unwin, Boston, 105-128.

Ahnert, F. 1970. 'Functional relationships between denudation, relief and uplift in large mid-latitude drainage basins, American Journal of Science, 268, 243-263.

Bechtel, T.D., Forsyth, D.W., Sharpton, V.L. and Grieve, R.A.F. 1990. 'Variations in effective elastic thickness of the North American lithosphere', Nature, 343, 636-638.

Bills, B.G. and May, G.M. 1987. 'Lake Bonneville: Constraints on lithospheric thickness and upper mantle viscosity from isostatic warping of Bonneville, Provo, and Gilbert stage shorelines', Journal of Geophysical Research, 92, 11493-11508.

Buck, W.G. 1986. 'Small-scale convection induced by passive rifting: the cause for uplift of rift shoulders', Earth and Planetary Science Letters 77, 362-372.

Buck, W.G., Martinez, F., Steckler, M.S. and Cochran, J.R. 1988. 'Thermal consequences of lithospheric extension: pure and simple', Tectonics 7, 213-234.

Bull, W.B. and Cooper, A.F. 1986. 'Uplifted marine terraces along the Alpine Fault, New Zealand, Science, 234, 1225-1228.

Carson, M.A. and Kirkby, M.J. 1972. Hillslope Form and Process, Cambridge University Press, Cambridge, 475pp.

Chorley, R.J., Schumm, S.A. and Sugden, D.E. 1984. Geomorphology, Methuen, London, 605pp.

Ebinger, C.J., Bechtel, T.D., Forsyth, D.W. and Bowin, C.O. 1989. 'Effective elastic plate thickness beneath the East African and Afar Plateaus and dynamic compensation of the uplifts', Journal of Geophysical Research 94, 2883-2901.

Gilchrist, A.R. and Summerfield, M.A. 1990. 'Differential denudation and flexural isostasy in formation of rifted-margin upwarps', Nature, 346, 739-742.

Gilluly, J. 1955. 'Geologic contrasts between continents and ocean basins', Geological Society of America Special Paper 62, 561-590.

Gunn, R. 1949. 'Isostasy - extended', Journal of Geology, 57, 263-279.

Holmes, A. 1965. Principles of Physical Geology, 2nd edn, Nelson, London, 1288pp.

Karner, G.D., Steckler, M.S. and Thorne, J.A. 1983. 'Long-term thermo-mechanical properties of the continental lithosphere', Nature, 304, 250-253.

Karner, G.D. and Watts, A.B. 1982. 'On isostasy at Atlantic-type continental margins', Journal of Geophysical Research 87, 2923-2948.

King, L.C. 1955. 'Pediplanation and isostasy: An example from South Africa', Quarterly Journal of the Geological Society, 111,

353-359.

McKenzie, D. 1984. 'A possible mechanism for epeirogenic uplift', Nature 307, 616-618.

Mörner, N-A. (Ed.) 1980. Earth Rheology, Isostasy and Eustasy, Wiley, Chichester, 599pp.

Nadai, A. 1963. Theory of Flow and Fracture of Solids, McGraw-Hill, New York.

Ollier, C.D. (Ed.) 1985. 'Morphotectonics of Passive Continental Margins', Zeitschrift für Geomorphologie Supplementband, 54.

Partridge, T.C. and Maud, R.R. 1987. 'Geomorphic evolution of southern Africa since the Mesozoic', South African Journal of Geology, 90, 179-208.

Peltier, W.R. and Andrews, J.T. 1976. 'Glacio-isostatic adjustment I: The forward problem', Geophysical Journal of the Royal Astronomical Society, 46, 605-646.

Pugh, J.C. 1955. 'Isostatic readjustment in the theory of pediplanation', Quarterly Journal of the Geological Society, 111, 361-369.

Royden, L. and Keen, C.E. 1980. 'Rifting processes and thermal evolution of the continental margin of eastern Canada determined from subsidence curves', Earth and Planetary Science Letters 51, 343-361.

Rust, D.J. and Summerfield, M.A. 1990. 'Isopach and borehole data as indicators of rifted margin evolution in southwestern Africa', Marine and Petroleum Geology, 7, 277-287.

Schumm, S.A. 1963. 'The disparity between present rates of denudation and orogeny', United States Geological Survey Professional Paper, 454-H.

Schumm, S.A. 1977. The Fluvial System, Wiley, New York, 338pp.

Schumm, S.A. 1979. 'Geomorphic thresholds: the concept and its applications', Transactions, Institute of British Geographers, NS 4, 485-515.

Selby, M.J. 1985. Earth's Changing Surface: An Introduction to Geomorphology, Clarendon Press, Oxford, 607pp.

Steckler, M.S. 1990. 'The role of the thermal-mechanical structure of the lithosphere in the formation of sedimentary basins', in Cross, T.A. (Ed.), Quantitative Dynamic Stratigraphy, Prentice-Hall, Englewood Cliffs, 89-112.

Summerfield, M.A. 1985. 'Plate tectonics and landscape development on the African continent', in Morisawa, M. and Hack, J.T. (Ed.), Tectonic Geomorphology, Allen and Unwin, Boston, 27-51.

Summerfield, M.A. 1988. 'Global tectonics and landform

development', Progress in Physical Geography, 12, 389-404.

Summerfield, M.A. 1989. 'Tectonic geomorphology: convergent plate boundaries, passive continental margins and supercontinent cycles', Progress in Physical Geography 13, 431-441.

Summerfield, M.A. 1991. Global Geomorphology, Longman, London and Wiley, New York, 537pp.

Turcotte, D.L. and Schubert, G. 1982. Geodynamics: Applications of Continuum Physics to Geological Problems, Wiley, New York, 450pp.

Walcott, R.I. 1970. 'Flexural rigidity, thickness, and viscosity of the lithosphere', Journal of Geophysical Research, 75, 3941-3954.

Weissel, J.K. and Karner, G.D. 1989. 'Flexural uplift of rift flanks due to mechanical unloading of the lithosphere during extension', Journal of Geophysical Research 94, 13919-13950.

White, R. and McKenzie, D. 1989. 'Magmatism at rift zones: The generation of volcanic continental margins and flood basalts', Journal of Geophysical Research, 94, 7685-7729.

Whitehouse, I.E. 1988. 'Geomorphology of the central Southern Alps, New Zealand: the interaction of plate collision and atmospheric circulation', Zeitschrift fur Geomorphologie Supplementband, 69, 105-116.

FIGURE CAPTIONS

Figure 1 Schematic representations of the response to an applied load of an elastic lithosphere with finite rigidity (A), no lateral rigidity (B), and infinite rigidity (C). Note that denudation is represented by a negative load.

Figure 2 Compensation functions of an elastic lithosphere for a range of effective elastic thicknesses (T_e) and variable wavelength loading. Model parameters are given in the text. The curve for T_e = 50 km illustrates the model presented by Gunn (1949).

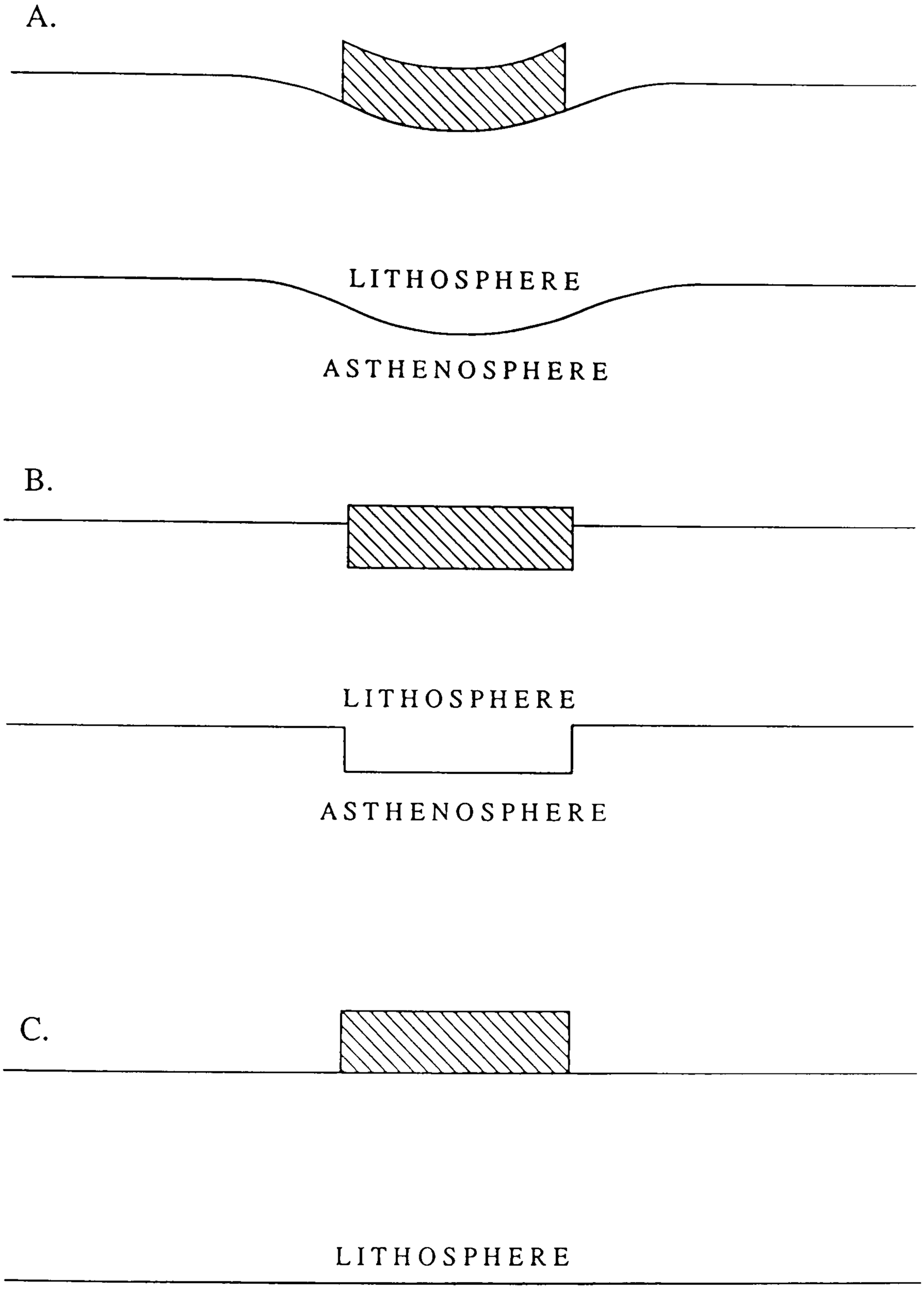

Gilchrist and Summerfield Fig. 1

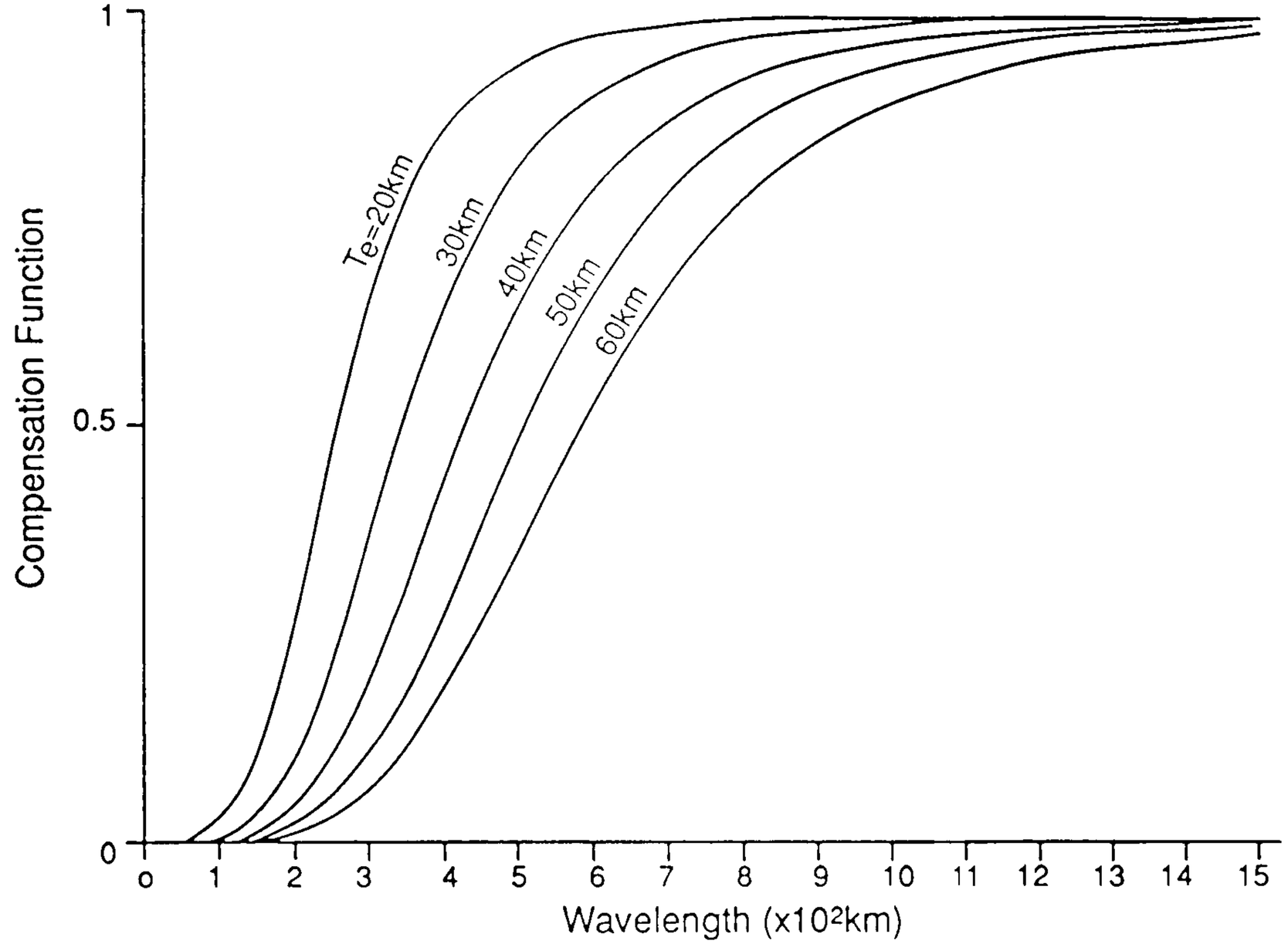
Compensation Function
1
0.5
0
Te=20km
30km
40km
50km
60km
0
1
2
3
4
5
6
7
8
9
10
11
12
13
14
15
Wavelength (x10²km)

Fig. 2